Engineering cholera toxin for the targeted delivery of oligonucleotides

Darren Christopher Machin

Submitted in accordance with requirements for the degree of

Doctor of Philosophy

The University of Leeds

School of Chemistry

September 2016

The candidate confirms that the work submitted is his own and that appropriate credit has been given where reference has been made to the work of others.

Acknowledgements

I would like to express great and sincere thanks to my supervisors, Andrew Macdonald, Ben Andrews, Bruce Turnbull and Mike Webb, for the huge amount of support, guidance and encouragement they have provided throughout my project. To Mike and Bruce go particular thanks, for giving me the opportunity to be here in the first place, for convincing me everything was going fine really, and for their great patience with my pushing of report deadlines. I truly appreciate everything you've done for me.

Working in lab 1.49 has been a pleasure. Thank you to Arthur, Chadamas, Clare, Dan, Dana, Diana, Gemma, Heather, Ivona, James R, James W, Jess, Kat, Kristian, Laura, Ludwig, Matt, Phil, Tom B, Tom M and Zoe for an excellent four years. I have enjoyed (almost) every minute. I also recognise the contribution of Old Bar to the last four years.

Special thanks go to James Ross for teaching me molecular biology, and to Chris Wasson for teaching me tissue culture, your expertise has been invaluable. To Dan Williamson for being a chemist so I didn't have to, I cannot thank you enough. I am grateful to Gemma Wildsmith for teaching me to use the AKTA, and helping me stare at it when it misbehaved. I would also like to thank Iain Manfield for teaching me to use the iTC200, Sally Boxall for microscope training and assistance, and Zoe Arnott, Matt Balmforth, Jess Haigh, Tom Branson and Tom McAllister for providing various useful materials. And of course, anyone who offered advice or a shoulder.

I would not be here (figuratively and literally) without my family, who have provided me with so much help and support to me get through university, and continue to maintain at least a semblance of pride in the fact I'm still in education and aiming for my third degree at the age of 29. I couldn't ask for better than you.

I would not have been able to write my thesis without the support of Grace Roberts. She made sure I was fed when I was too busy to feed myself, provided me with sweets and generally kept me emotionally balanced. I largely have her to thank for coming away from my writing desk with my sanity intact.

Finally, I would like to thank Chris Kirkham for graciously allowing me to put a roof over his head for a year and Matt Balmforth for charitably allowing me to be his chauffeur to the climbing wall; your generosity knows no bounds.

Abstract

Half of the 20 best-selling prescription drugs of 2014 were large biologic therapeutics, however to date there have only been two licensed non-aptamer oligonucleotide drugs. Oligonucleotides have proven highly successful at modification of gene expression in the laboratory, but the lack of a robust delivery vehicle has largely prevented their transferal to clinical use. That role could be filled by cholera toxin, a protein produced by *Vibrio cholerae*, responsible for the diarrhoeal symptoms of cholera infection. Cholera toxin targets cells presenting GM1 ganglioside on their surface for endocytosis and carries a toxic payload to the endoplasmic reticulum (ER) by retrograde translocation. Several non-toxic variants of cholera toxin have been produced which are capable of carrying a cargo into cells, but to date it has not been tested for oligonucleotide delivery.

The non-toxic subunit of cholera toxin responsible for endocytosis, CTB, was expressed in the absence of the toxic A subunit. CTB was site-specifically labelled with fluorescein using sortase A and shown to carry the payload into Vero cells. The endocytic pathway was able to be altered through modification of the protein sequence. Subsequently, a short RNA duplex was delivered to different locations in Vero cells by two subtly different CTB variants. Several strategies were then trialled to promote oligonucleotide release from CTB and export to the cytosol. While oligonucleotides conjugated via a disulfide bond were released in the ER, and a short hydrophobic peptide mediated export of an oligonucleotide-CTB complex from the ER, a combination of both was not observed.

This study showed CTB has the potential to function as an effective delivery vehicle for therapeutic oligonucleotides, but also that there remains work to do and are hurdles to overcome to achieve this goal. It provides a platform for the development of CTB, or other similar proteins, for clinical use.

Abbreviations

2′-MOE	2′-methoxyethyl
2xYT	2 × yeast tryptone
Aβ	Amyloid-β
Ab	Antibody
ADP	Adenosine diphosphate
AF	Alexa fluor
APS	Ammonium persulfate
ARF6	Adenosine diphosphate-ribosylation factor 6
ATP	Adenosine triphosphate
BCN	Bicyclononyne
BG	Benzylguanine
bp	Base pairs
cAMP	Cyclic adenosine monophosphate
CBD	Chitin binding domain
CDK	Cyclin-dependent kinase
CIP	Calf intestinal alkaline phosphatase
CMV	Cytomegalovirus
COPI	Coat protein complex I
CPP	Cell penetrating peptide
CT	Cholera toxin
CTA	Cholera toxin A subunit
CTB	Cholera toxin B subunit
DMD	Duchenne muscular dystrophy
DMEM	Dulbecco’s modified Eagle medium
DMSO	Dimethylsulfoxide
ds	Double-stranded

DTA	Diphtheria toxin A subunit
EDC	1-ethyl-3-(3-dimethylaminopropyl)carbodiimide
EGFP	Enhanced green fluorescent protein
EM	Electron microscopy
EMP	Exponential megapriming polymerase chain reaction
Eps	Extracellular protein secretion
eq	Equivalents
ER	Endoplasmic reticulum
ERAD	Endoplasmic reticulum-associated degradation
FACS	Fluorescence-activated cell sorting
FdsRNA	Fluorescein-double-stranded RNA conjugate
FITC	Fluorescein isothiocyanate
FISH	Fluorescence *in situ* hybridisation
FPLC	Fast protein liquid chromatography
GABA	γ-aminobutyric acid
Gal	Galactose
GalNAc	N-acetyl galactosamine
GAr	Glycine-alanine repeat
GFP	Green fluorescent protein
Glc	Glucose
GM1os	GM1 oligosaccharide
GSK	GlaxoSmithKline
HA	Hemagglutinin
HIV	Human immunodeficiency virus
HPLC	High performance liquid chromatography
HRP	Horseradish peroxidase
HSV	Herpes simplex virus
I654	Human β-globin intron 2 with C654T mutation

IF	Immunofluorescence
IPTG	Isopropyl β-D-1-thiogalactopyranoside
ITC	Isothermal titration calorimetry
LSCM	Laser scanning confocal microscopy
LB	Lysogeny broth
LC	Liquid chromatography
LTB	Heat-labile enterotoxin
LNA	Locked nucleic acid
MBP	Maltose binding protein
MEM	Minimum essential media
MMT	Monomethoxytrityl
mRNA	Messenger RNA
MS	Mass spectrometry
MTT	3-(4,5-dimethylthiazol-2-yl)-2,5-diphenyltetrazolium bromide
NeuNAc	N-acetyl neuraminidate
NHS	N-hydroxy succinimide
nt	Nucleotide
PAGE	Polyacrylamide gel electrophoresis
PBS	Phosphate-buffered saline
PBST	Phosphate-buffered saline with Tween-20
PCR	Polymerase chain reaction
PDI	Protein disulfide isomerase
PNA	Peptide nucleic acid
RISC	RNA-induced silencing complex
RNAi	RNA interference
RNase	Ribonuclease
SDM	Site-directed mutagenesis
SDS	Sodium dodecyl sulfate

SEC	Size exclusion chromatography
siRNA	Short interfering RNA
SPAAC	Strain-promoted alkyne-azide cycloaddition
SrtA	Sortase A
ss	Single-stranded
STB	Shiga toxin B subunit
TBS	Tris-buffered saline
TBST	Tris-buffered saline with Tween-20
TEV	Tobacco etch virus
TGN	Trans-Golgi network
wt	Wild type

Contents

Chapter 1: Introduction

1. Background

The wide range of experimental therapeutics currently in development have the potential to treat a wide range of diseases with currently unmet treatment needs. However, for many of these, efficient delivery remains a significant challenge and has blocked their application in a clinical setting. RNA interference (RNAi) technology is a classic example of the difficulties involved in transferring promising therapies from the laboratory to clinical use. This technique involves the use of short RNAs which can induce post-transcriptional gene-silencing of disease-relevant genes, thereby down-regulating the disease phenotype[1]. This technique has been extensively studied and trialled to great success *in vivo* in the laboratory[2-4], but as yet has not been transferred to the clinic. One of the major factors blocking the transfer of RNAi to the clinic is how to specifically target particular cells in the complex environment of the body[4,5]. RNAi is not an isolated case; there are multiple examples of gene therapy[6,7], cancer therapy[8,9], antiviral treatments[2,10] and others where efficacy could be improved, side-effects negated, or even the therapy made clinically viable, by improvements in delivery methods.

This current gap in targeted therapeutic delivery could potentially be filled by cholera toxin (CT). Secreted by *Vibrio cholerae* and responsible for the classic diarrhoeal symptoms of cholera[11,12], this protein has the capability to enter cells that display its receptor, GM1 ganglioside, on their surface[11-13]. Better still, the toxin can be separated into two distinct subunits with exclusive functions; one subunit is responsible for toxicity, and the other for host cell recognition and entry, functioning independently to the toxic subunit[11-13]. If this protein could be harnessed for the delivery of molecules to target cells, new avenues of potential treatments and therapies could be opened up. It is the aim of this study to elucidate the mechanism by which the CT binding subunit (CTB) functions in the absence of the toxic subunit (CTA), with a view to determining if it could function as an efficient vector for targeted oligonucleotide delivery.

1.1. Cholera toxin

1.1.1. Discovery and history

Cholera toxin is an enzymatically-active hexameric protein produced by the bacterium *Vibrio cholerae*, and is the causative agent of the extensive diarrhoeal symptoms typical of *V. cholerae* infection[11,12]. It was first discovered in 1959 that cell-free filtrates of *V. cholerae* could induce cholera-like symptoms[14], and ten years later the toxin was isolated for the first time[15]. Shortly afterwards, CT was shown to be comprised of two subunits; a 58 kDa homopentamer subunit and a 28 kDa subunit[16]. At the same time, GM1 ganglioside was identified as the receptor for CT at the cell surface[17]. The high-resolution structure of the 58 kDa B subunit pentamer in complex with GM1 was solved by X-ray crystallography in 1994, at a resolution of 2.2 Å[18], followed by structures of the un-complexed B pentamer (2.4 Å resolution)[19] and the holotoxin (2.5 Å resolution)[20] in 1995. Subsequent refinements yielded improved structural detail, up to a 1.90 Å resolution structure of the holotoxin[21] and a 1.25 Å resolution structure of the pentameric B subunit in complex with GM1[22].

1.1.2. Structure and organisation

The 28 kDa subunit of CT is the catalytically-active (A) subunit, while the 58 kDa homopentameric (B) subunit is responsible host cell recognition through receptor binding (figure 1.1). The B subunit consists of five identical protomers arranged in a ring. The binding sites for the CT cell surface receptor, GM1 ganglioside (figure 1.2A), are located at the interfaces between each protomer, close to the N-termini, and incorporate a single Gly residue from neighbouring protomers[22] (figure 1.2B and C). The A subunit consists of two separate domains, A1 and A2. The A2 domain consists of a long α-helix anchored in the centre of the B subunit ring, with the C-terminus extending marginally from the surface of the binding face and the N-terminus extending out above the non-binding face. The A2 domain possesses a C-terminal KDEL signal sequence (figure 1.1), associated with targeting and retention of the protein to the endoplasmic reticulum (ER)[23]. The toxic A1 domain, an NAD-dependent ADP-ribosyltransferase[24], is linked to the complex via a disulfide bond from its C-terminal region to the N-terminal region of the A2 domain (figure 1.1).

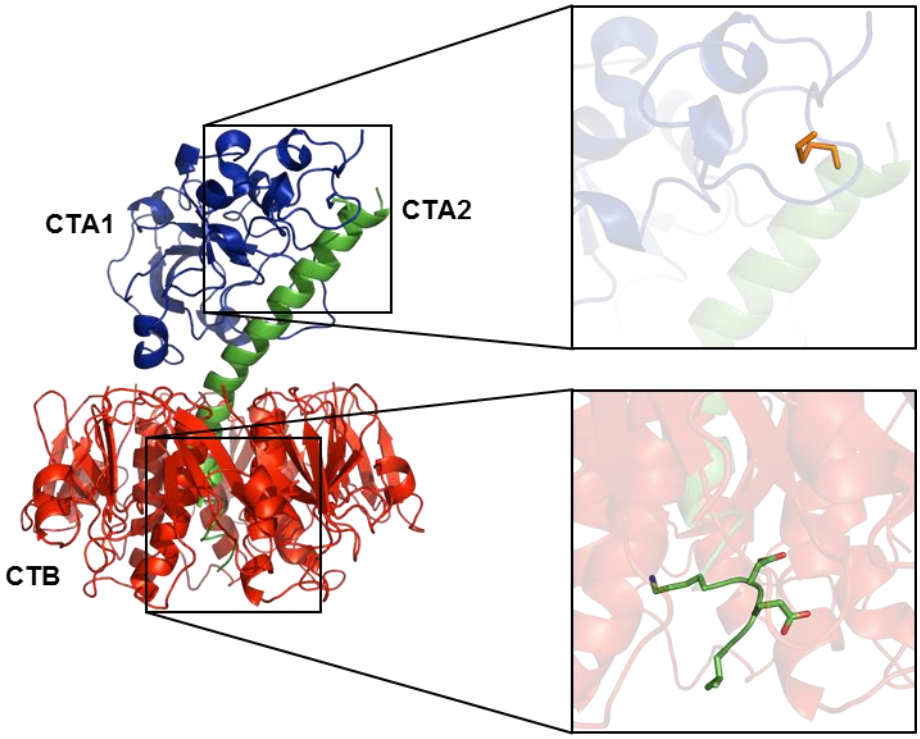

Figure 1.1. Structure of cholera toxin Crystal structure of CT. CTA1 is shown in blue, CTA2 in green and CTB in red. The A1-A2 disulfide bond (upper window, orange) and A2 C-terminal KDEL signal sequence (lower window, green) are highlighted. PDB ref. 1XTC.

1.1.3. Toxin formation

Both CT subunits are expressed with an N-terminal periplasmic leader sequence (MVKIIFVFFIFLSSFSYA for CTA, MIKLKFGVFFTVLLSSAYAHG for CTB), resulting in immediate secretion of the newly synthesised, unfolded polypeptides into the periplasm through the Sec secretion system[25,26]. The subunits fold and the toxin assembles in the periplasm, prior to extracellular secretion[27]. The A subunit is synthesised as a single polypeptide chain with a disulfide bond between residues Cys187 and Cys199. The B subunit is synthesised as individual polypeptides, which subsequently assemble into a non-covalently linked homopentamer in the periplasm, mediated by hydrophobic interactions between the individual CTB polypeptide units[13,28]. An intramolecular disulfide bond is formed between Cys9 and Cys86 within the protomers[18,29], which along with Trp88 are crucial in maintaining the tertiary and quaternary structure of CTB[29]. Formation of the holotoxin occurs in tandem with CTB pentamer formation[30]. The A2 domain interacts strongly with hydrophilic residues in the lower region of the CTB pore, and in particular with hydrophobic residues in the upper region of the pore, with these interactions providing the driving force to favour holotoxin formation over pentamer

formation alone[28,31]. CTA requires CTB for secretion and biological action[27], but CTB is highly stable and capable of being secreted and initiating endocytosis separate to CTA[28].

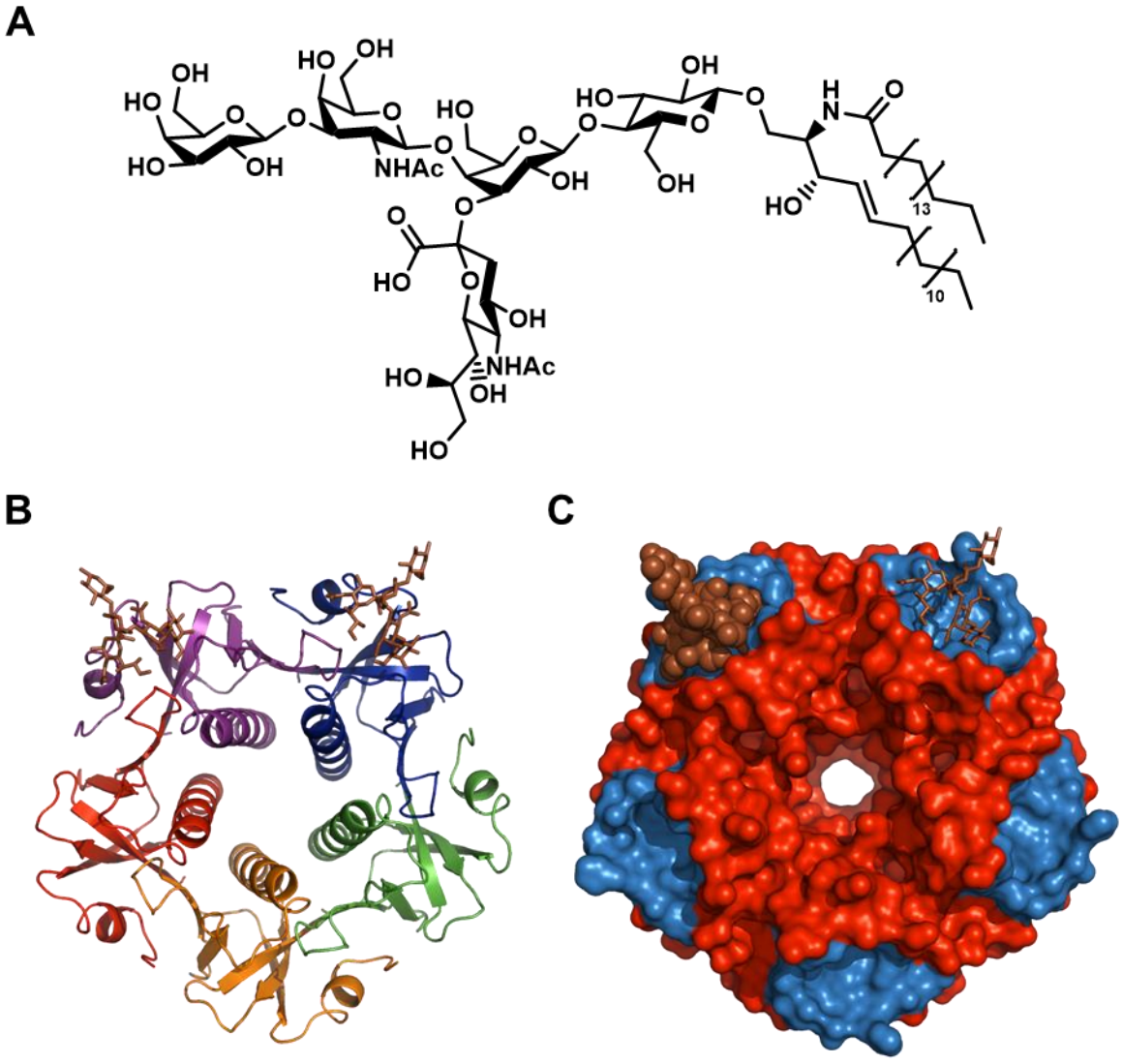

Figure 1.2. Cholera toxin GM1 binding A. Structure of GM1 ganglioside. B. Crystal structure of the binding face of CTB in complex with GM1 oligosaccharide (brown). Each protomer is shown in a different colour for distinguishment. C. Crystal structure of the binding surface of CTB (red) in complex with GM1 (brown). GM1 binding sites are highlighted (blue). In both cases, three of the complexed GM1 oligosaccharides have been removed for clarity. PDB ref. 3CHB.

1.1.4. Toxin secretion

Following assembly in the periplasm, CT is secreted across the outer membrane via the type II secretion system[32,33]. This system is common to all Gram-negative bacteria and is responsible for transporting secreted proteins from the periplasmic space to the extracellular environment[33]. In *V. cholerae*, this process involves a complex of several

identified individual protein components (figure 1.3), termed Eps (extracellular protein secretion) C-M and S[32,34]. CT is extruded to the extracellular space through the outer membrane complex, consisting primarily of EpsD, which forms a pore in the outer membrane[33,35], along with EpsS. While the exact mechanism is not fully understood, the holotoxin is believed to be transported through the action of a pseudopilus consisting mainly of EpsG, along with EpsH-K at its tip, which acts as a piston to push the toxin through the pore[34,35]. The energy for secretion is believed to be provided by EpsE, a cytoplasmic ATPase[34], which is connected to the pseudopilus and pore proteins by the inner membrane platform, consisting of EpsC, EpsF, EpsL and EpsM[33,34]. Following toxin secretion, the A subunit polypeptide chain undergoes host serine protease-mediated cleavage between Arg194 and Ser195[36,37], resulting in two separate domains connected via a disulfide bond.

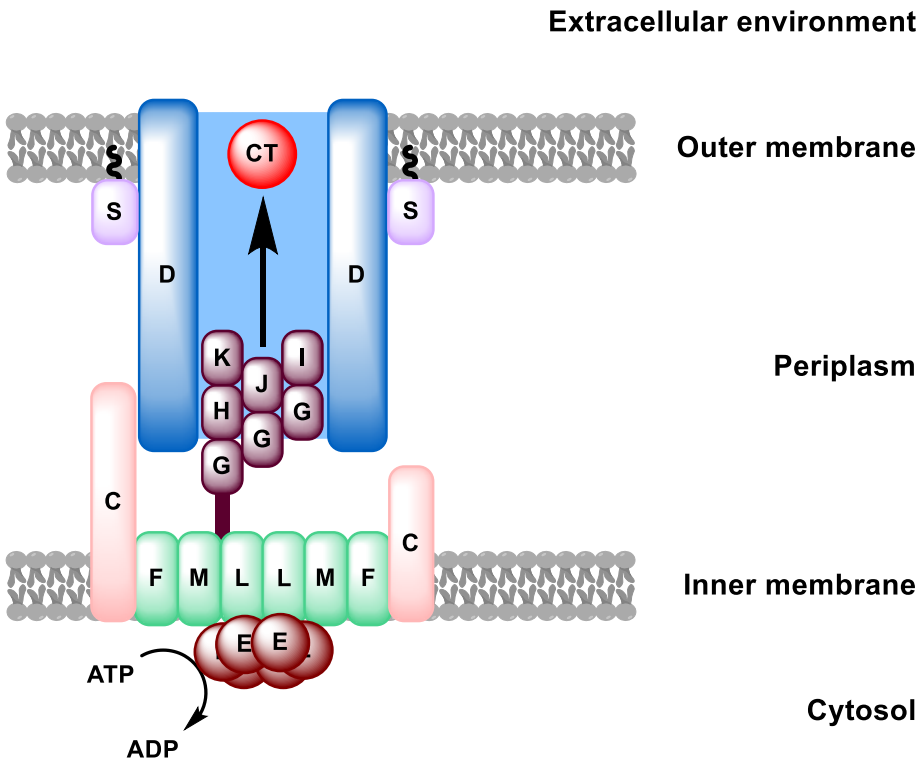

Figure 1.3. Type II secretion system Schematic representation of the *V. cholera* type II secretion protein complex. Single letters represent Eps proteins.

1.1.5. Receptor binding

CT must initially recognise and gain entry to its target cells to exhibit its native biological function. This involves CTB binding to its cell surface receptor, GM1 ganglioside. The

crystal structure of CTB in complex with GM1 has been solved to a resolution of 1.25 Å[18,22]. From this data, it has been determined that the oligosaccharide domain of GM1 interacts with the binding sites in a bivalent manner; the terminal β-D-galactose (Gal) and N-acetyl-β-D-galactosamine (GalNAc) branch forms one arm of the interaction, while the N-acetyl-α-neuraminidate (NeuNAc) branch forms the other[18,22,38]. The majority of the binding interactions between the oligosaccharide and the protein occur through the Gal and NeuNAc residues, with a smaller contribution provided by the GalNAc residue[18,38,39]; these residues provide 39%, 43% and 17% of the buried surface intermolecular contacts[18], respectively, with Gal and NeuNAc contributing 54% and 44% of the intrinsic binding energy[38]. The glucose (Glc) and branching Gal residues do not form interactions with CTB.

The oligosaccharide is held in place largely through hydrogen bonding, both directly with CTB amino acids and through tightly bound water molecules[18,22,40] (figure 1.4). All of the binding site residues responsible for interacting with the oligosaccharide belong to a single protomer, with the exception of a backbone amine contribution from Gly33, which belongs to an adjacent protomer[18,22]. On GM1 binding, Gal forms a hydrophobic stacking interaction with Trp88[18], in addition to extensive hydrogen bonds directly with Glu51, Gln56, Gln61, Asn90 and Lys91, and with water molecules co-ordinated to His13, Asn14, Gln56 and Gln61[18,22,38]. The Gal-binding region of the binding site in CTB contains a flexible loop comprising residues 51-60, allowing free entry to the binding site[40]. Upon GM1 binding, this loop becomes rigidly ordered, held tight by intermolecular hydrogen bonds between the loop and Gal/GalNAc as well as intramolecular interactions, helping to secure the pentasaccharide[40] (figure 1.5). NeuNAc forms hydrogen bonds directly with Glu11 and His13, in addition to water molecules co-ordinated to Glu11, His13, Gly33, Gln56, Gln61 and Trp88[18,22,38]. GalNAc forms a hydrogen bond directly with Gln56, as well as with a water molecule co-ordinated with Gln56 and Gln61[18,22,38]. It also forms a stabilising intermolecular interaction with NeuNAc[18,22,38]. These combined interactions result in an unusually high receptor affinity compared to other lectins, with a K_d in the low nM range[18,38].

Both Gly33 and Trp88 are critical binding residues, and mutation of either has been shown to abolish GM1 binding[29,41]. The specificity for GM1 over other gangliosides is believed to be conferred largely by His13, the only binding site residue not conserved between CT and the closely related *E. coli*-derived heat-labile enterotoxin[18] (LTB).

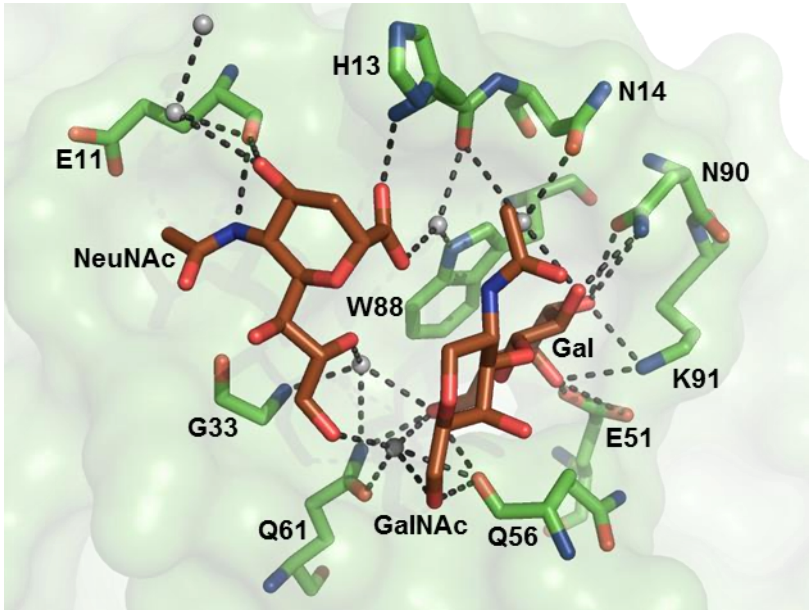

Figure 1.4. GM1 binding to CTB Crystal structure of GM1 bound to CTB, showing critical binding residues. Residues belonging to CTB are shown in green, and GM1 in brown, with oxygen and nitrogen atoms represented by red and blue, respectively. Bound water molecules are represented by grey spheres, and hydrogen bond interactions by dashed lines. The Glc and branching Gal residues, which do not interact with the binding site, have been removed for clarity. PDB ref. 3CHB.

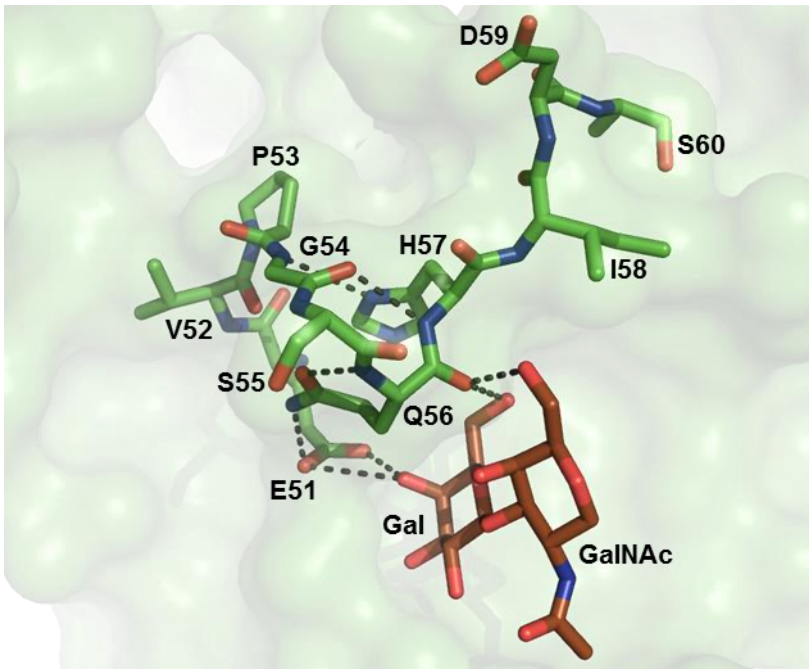

Figure 1.5. Terminal galactose binding region Crystal structure showing the interactions between the terminal Galβ(1-3)GalNAc of GM1 and the flexible loop formed by residues 51-60 of CTB. Residues belonging to CTB are shown in green, and GM1 in brown, with oxygen and nitrogen atoms represented by red and blue, respectively. Hydrogen bond interactions by dashed lines. PDB ref. 3CHB.

1.1.6. Endocytosis

A general overview of CT endocytosis and retrograde transport is shown in figure 1.6. Cell entry is achieved through CTB binding to GM1 ganglioside, displayed on the cell surface of the intestinal epithelial cells, with high affinity and specificity[38,42]. Toxin uptake is heavily dependent on cell surface GM1 levels[43]. GM1 is found predominantly in lipid rafts, and it is thought that these formations are important for internalisation of the holotoxin[42,44], supported by the fact that cholera toxin can be used as a marker for lipid rafts[45]. This is possibly because toxin uptake is dependent on cholesterol, shown as cholesterol chelation reversibly inhibits endocytosis[46], and cholesterol is predominantly found in lipid rafts.

The exact mechanism of endocytosis is not fully understood, as there is disagreement as to exactly how CT enters cells. The toxin has been reported to enter the host cell through several different mechanisms following GM1 binding. Some studies have reported that CT is internalised by clathrin-dependent mechanisms. An electron microscopy (EM) study showed exposure to CT caused formation of clathrin-coated pits but not caveolae[47], while inhibition of clathrin-mediated endocytosis by various means decreased CT uptake by up to 60%[48]. Knockdown of clathrin by siRNA also decreased CT uptake, while up-regulating caveolin had no effect[49]. However, it should be noted that in these last two cases, CT uptake was not totally negated. Other studies have reported CT uptake is caveolae-dependent. CT and caveolae have been shown to co-localise by EM[50], and CT endocytosis has been shown to be sensitive to caveolae inhibitors[43]. The use of inducible caveolin and various endocytosis pathway inhibitors showed CT preferentially utilised caveolae-dependent mechanisms[51], although this study also suggested clathrin-dependent mechanism could also be utilised in the absence of caveolin, albeit less efficiently. There are contrasting reports that CT endocytosis relies on mechanisms which are both clathrin- and caveolae-independent; inhibition of either pathway by expression of non-functional mutant proteins did not affect CT uptake and blocking both simultaneously still resulted in CT-mediated cell toxicity[52], while endocytosis in cells expressing or lacking caveolin was identical[53]. One study found that flotillin co-accumulated with CT within clathrin- and caveolae-independent endocytic intermediates, and that siRNA knockdown inhibited CT uptake[54], suggesting a completely separate endocytic mechanism. Uptake has been reported to be at least partially dependent on dynamin, a protein associated with microtubules and endocytic membrane budding. Dynamin depletion[55] or mutations[56] have been shown to decrease CT endocytosis, although dynamin-independence has also been

reported[52] and non-functional dynamin does not negate endocytosis[57]. Taken together, these studies illustrate that CT is likely capable of utilising several different endocytosis mechanisms and no single pathway is absolutely required. Cell type and species may also be factors in determining which endocytic mechanism is favoured, as 15 different cell lines derived from human, monkey, pig, dog, rat, and hamster sources were used to conduct these studies,

The exact mechanism by which binding induces internalisation is also currently unknown. CTB has five GM1 binding sites, but it has been shown through CT chimeras of wt and non-binding subunits that only a single GM1 binding site is necessary for endocytosis[58,59], in this case occurring through exploitation of endogenous lipid-sorting pathways[58-60]. However, multivalent receptor binding increased both endocytosis efficiency and toxin activity[58,59]. This suggests multivalency may have evolved later to improve endocytosis efficiency. It is possible that multivalent binding to GM1 embedded in lipid raft domains, which are significantly more tightly packed and well-ordered than the rest of the plasma membrane[61], could initiate endocytosis by induction of membrane curvature through remodelling the structure and organisation of the lipid rafts[62,63]. However, to date this has not been directly observed and remains a purely speculative hypothesis.

Following initial internalisation, CT is transported from the plasma membrane to its eventual destination, the endoplasmic reticulum (ER), via a Golgi-dependent retrograde transport pathway. The whole of the transport process is thought to be heavily dependent on the actin cytoskeleton[42,55], as inhibitors of actin filament assembly block transport to the ER. CT is known to travel directly from the early endosome to the trans-Golgi network (TGN)[64,65] and enter by vesicle docking[13], bypassing the Golgi apparatus[64,65], as disruption of the Golgi apparatus but not the TGN allows CT to reach the ER. This process requires syntaxins 5, 6 and 16[55,66,67], SNARE proteins which support retrograde transport from the early endosome to the TGN[66,67]. The toxin is subsequently transported to the ER via a coat protein complex I (COPI)-independent pathway[23,42,64]. Unlike the process of COPI-mediated retrograde transport from the Golgi apparatus to the rough ER[68], including the transport of species containing a C-terminal KDEL[69], COPI-coated vesicles are not involved in transport of CT to the ER, as dispersal of COPI to the cytosol does not prevent CT transport to the ER[64]. The C-terminal KDEL signal sequence of CTA2 has been shown to be unnecessary for targeting the protein complex to the ER[23,42], through mutation of the KDEL sequence and dispersal of the KDEL receptor protein, but rather promotes ER retention through dynamic recycling between the Golgi apparatus and the

ER[13,42]. It appears that the transport pathway utilised by CT is not a complete physiological pathway but is distinct to the toxin[13,55]; it possibly hijacks different aspects of various physiological pathways.

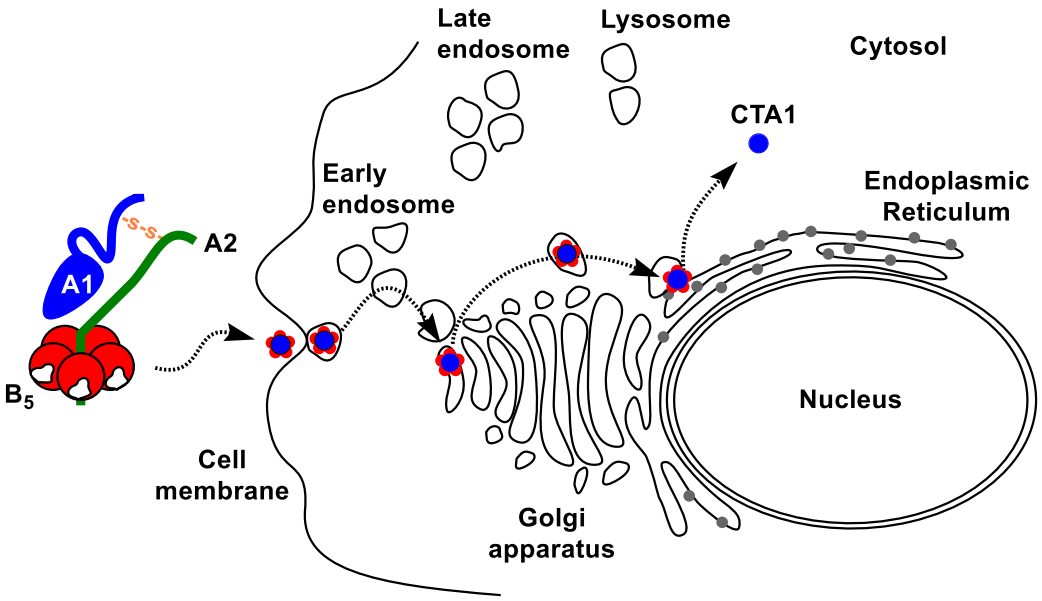

Figure 1.6. Overview of the cholera toxin trafficking pathway CTB is shown in red, CTA1 in blue and CTA2 in green. Figure reproduced and adapted with permission from M. Webb.

1.1.7. Toxic action

Once the intact holotoxin has reached the ER, CTA1 is released from the complex. In the redox environment of the ER lumen, the redox-dependent protein disulfide isomerase (PDI) chaperone recognises the A subunit and reduces the disulfide bond[37,70], with glutathione, present in high concentrations in the ER[71], acting as the electron donor[70,72]. This process partially unfolds CTA1 at the C-terminus[37,73], as CTA1 is unstable when not in complex with the rest of the holotoxin[73,74]. CTA1 is then exported to the cytosol of the host cell through the hijacking of the ER-associated degradation (ERAD) pathway[74,75], masquerading as a misfolded protein through its inherent instability and exposure of hydrophobic residues[74,75]. Ero1, an ER oxidase enzyme, releases CTA1 from PDI through oxidation of the PDI-CTA1 complex, forming a complex with CTA1 in the process[76]. CTA1 is released from Ero1 on association of the Ero1-CTA1 complex with the protein-channelling Sec61 translocon and is exported from the ER lumen to the cytosol through Sec61[76-78].

In the cytosol, rapid refolding of CTA1 occurs to prevent degradation[74,79]. This process is mediated by binding to CTA1 of ADP-ribosylation factor 6 (ARF6), stabilising CTA[73,74]. The lack exposed of Lys residues present in the stabilised CTA1 allow it to avoid ubiquitination and subsequent degradation by the proteasome[79,80]. At this stage, a signalling cascade is triggered. Binding of CTA1 to ARF6 causes conformational changes to CTA1, allowing the NAD^+ cofactor to bind in the active site[81]. This complex catalyses G-protein α-subunit ADP-ribosylation, preventing GTP inactivation by hydrolysis[11,12]. Consequently, adenylate cyclase activity is up-regulated, resulting in a huge increase in intracellular cAMP levels[11,12]. Increased cAMP increases protein kinase A activation, which increases activation of the cystic fibrosis transmembrane conductance regulator protein channel and results in a massive efflux of chloride ions[11,12]. This causes secretion of water and other ions into the intestinal lumen, resulting in extreme cases in the loss of up to 20 L of fluid per day[11], the signature symptom of cholera infection.

1.2. Modifications to cholera toxin

Numerous studies have been conducted aimed at modifying cholera toxin. Modifications have been made to all subunits of CT, as both holotoxin and isolated CTB, in an attempt to adapt the protein for non-native functions. The primary uses for these protein chimeras have been as cell trafficking probes and immune-stimulating adjuvants.

1.2.1. Holotoxin modifications

The desire to probe the cellular transport mechanisms of CT have been the driving force behind many modifications made to the A1, A2 and B_5 domains of the holotoxin. CTA1 bearing a C-terminal recognition motif has been enzymatically labelled using sortase A (SrtA)[82], a bacterial transpeptidase enzyme for attaching virulence factors to the cell wall[83] (discussed in full in chapter 3). The protein was labelled with a short biotinylated peptide containing a glycosylation site, and was used to probe toxin entry to the ER[82]. Subsequently, the same method was used to conjugate the toxic A subunit of diphtheria toxin (DTA) to the C-terminus of CTA1 (figure 1.7) to form a cytolethal delivery system, resulting in the identification of host cell factors critical for intoxication through a genetic screen of knockdown mutations[82]. Holotoxin bearing a CTA1 domain incorporating genetically encoded N-terminal or C-terminal 21 residue peptide extensions showed the N-terminal extension caused rapid degradation in the cytosol, while the C-terminal extension was tolerated[79]. This provided insight into the mechanism by which CTA1

evades degradation in the cytosol. Additionally, the CTA1 and CTB domains were separately chemically labelled to probe retrotranslocation of the holotoxin[84]. CTB was labelled non-specifically at exposed amine groups using N-hydroxysuccinimide (NHS) ester-functionalised Cy5, protected, and then CTA1 labelled with Cy2 (presumably non-specifically, though the authors do not state the mechanism of functional groups involved)[84].

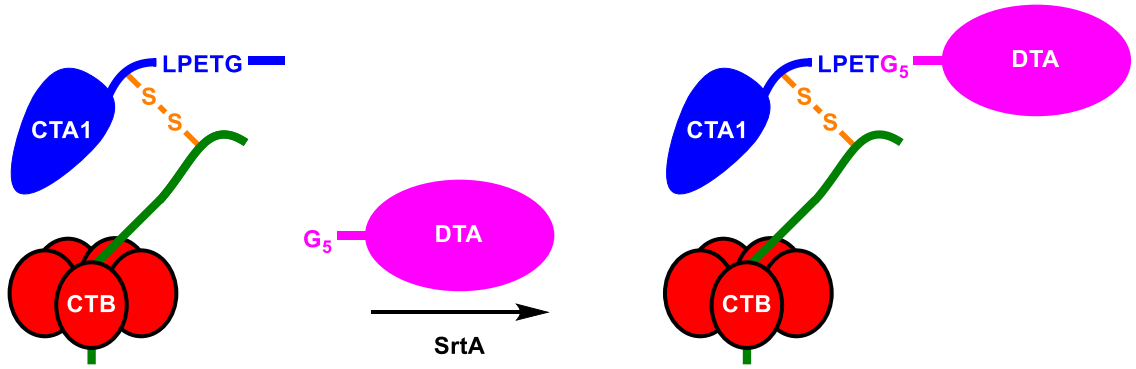

Figure 1.7. Cytolethal chimeric cholera holotoxin formation SrtA-mediated ligation to couple DTA bearing an N-terminal penta-Gly to CTA1 through a C-terminal LPETG SrtA recognition motif.

One particularly intricate study of CTB GM1 binding and endocytosis produced holotoxin chimeras with defined numbers of native GM1 binding sites by mixing expression of wt CTB with non-binding G33D mutants[59]. The CTB subunits also contained genetically-encoded C-terminal 34 residue peptides including a glycosylation site and a sulfation site, to detect entry to the ER and Golgi apparatus, respectively. The study found that a single native binding site was sufficient to induce endocytosis, although multivalency increased endocytosis efficiency[59].

In addition to probing retrotranslocation, holotoxin modifications have been made for immunogenic purposes. Holotoxin-like chimeras have been generated through genetically-encoded N-terminal fusions of CTA2 to GFP[25,85], RFP[25], alkaline phosphatase[86], maltose binding protein[86] (MBP) and β-lactamase[86]. In all cases, biological function and immunogenicity were retained both for the non-native fusion protein and CTB.

1.2.2. CTB-based fusion proteins

For reasons of safety, as well as labelling potential per protein complex, it is preferable to avoid use of the A subunit and focus on the isolated B subunit. A diverse number of genetically-encoded peptide fusion modifications have been made to CTB in the absence of CTA, primarily for immunogenic research. A CTB N-terminal fusion with a 15 residue epitope of *Streptococcus* glucosyltransferase B was shown to retain B subunit structure and function, and caused an immunogenic response against the fusion peptide[87]. However, N-terminal peptide extensions of increasing length (8, 12, 24 residues) were later found to increasingly ablate GM1 affinity and oral immunogenicity[88]. There is a paucity of further studies involving CTB N-terminal fusions, implying this is not an effective method for modification.

There are many examples of CTB C-terminal fusion proteins. Genetically incorporated fusions of a 15 residue insulin epitope[89], or the full insulin protein[90], to the C-terminus of CTB administered nasally[89] and orally[90] both resulted in a tolerogenic response to the antigen. Similarly, oral administration of a fusion of a 53 residue peptide, consisting of three repeats of a glutamate decarboxylase epitope, to the C-terminus of CTB induced tolerance in diabetes models, observed through decreased pancreatic islet inflammation[91].

In addition to inducing a tolerogenic response, CTB C-terminal fusions have also been used to illicit an immune response for vaccination purposes. A C-terminal fusion with a 42 residue amyloid-β (Aβ) peptide, expressed in silkworm pupae, resulted in protection against Alzheimer's disease in models, observed through decreased Aβ deposition in the brain and improved memory function[92]. Impressively, CTB has been expressed in algal chloroplasts with a C-terminal fusion of the entire VP1 protein (approximately 30 kDa) from foot-and-mouth disease virus, whilst retaining GM1 binding and VP1 immunogenicity[93]. CTB has also been expressed with a C-terminal fusion of the fimbria 2 protein (approximately 24 kDa) from *Bordetella pertussis*[94]. Pentameric structure and GM1 binding were retained, and immunisation resulted in protection from *Pertussis* infection through a mixed T-helper cell response[94].

Separate to immunogenic purposes, CTB C-terminal fusions have also been designed with specific treatments in mind. A C-terminal fusion with the YVAD tetrapeptide, known to inhibit caspase-1 activation, was expressed in, and secreted from, *Lactobacillus casei*[95]. This is significant, as *L. casei* is able to be delivered live to the intestine through oral ingestion[95], and so has implications for inflammatory diseases of the intestine, the natural target of CTB.

1.2.3. Non-specific chemical modification of CTB

Chemical modification has the potential for functionalisation with a greater number of highly diverse molecules compared with fusion proteins. CTB has been chemically modified in a large number of studies. CTB-Alexa fluor (AF) conjugates are commercially available (Thermo-Fisher) and have been used as lipid raft markers[45,96] and neural tracers[97,98]. Additionally, CTB conjugates with AFs and horseradish peroxidase (HRP) have been used to probe endocytosis mechanisms[53]. However, the company does not specify the conjugation method.

Perhaps the simplest method of chemical modification of CTB is through non-specific labelling of exposed amines with active ester functional groups. This method of labelling has largely been adapted to produce CTB-based endocytic and retrotranslocation probes. Non-specific conjugations of AF-NHS ester to CTB resulted in labelled protein for which GM1 binding and cell trafficking were unaffected[52]. CTB has been non-specifically labelled with carboxylate-functionalised quantum dots at exposed amine groups by 1-ethyl-3-(3-dimethylaminopropyl)carbodiimide (EDC)-mediated conjugation[99] (figure 1.8), involving an active ester intermediate. Both protein-dye conjugates were used as endocytic probes[52,99]. CTB-carbon dot conjugates were produced through non-specific labelling of CTB with carbon dot-HNS ester conjugates[100]. The protein-dye conjugate produced, which was used as a neural tracer, was non-toxic and displayed high photoluminescence and photostability[100].

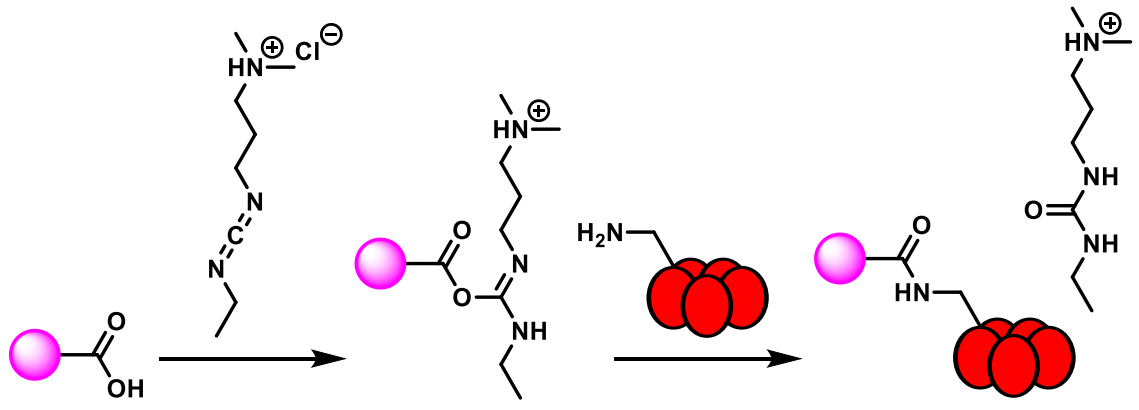

Figure 1.8. EDC-mediated conjugation CTB (red) is coupled to carboxylate-functionalised quantum dots (magenta) through EDC-mediated functionalisation of the carboxylate to form as active ester, which labels exposed Lys residues.

In addition to the above adaptations, which all involve direct visualisation of the CTB probe, CTB has been used for the development of an intricate assay for indirect detection of retrotranslocation to the ER or the cytosol, termed SNAP-trap[55] (figure 1.9). Cells were transfected with a vector containing a SNAP-tag reporter protein gene, targeted to either the ER or the cytosol. The SNAP-tag protein covalently and irreversibly binds benzylguanine (BG) through an exposed Cys residue[55,101], so proteins carrying the BG group will be labelled with SNAP-tag on entry to the ER or cytosol. CTB was non-specifically labelled with BG-NHS ester, and using ER-targeted SNAP-tag it was discovered that CTB transport to the ER was dependent on dynamin-2 and syntaxin-5[55].

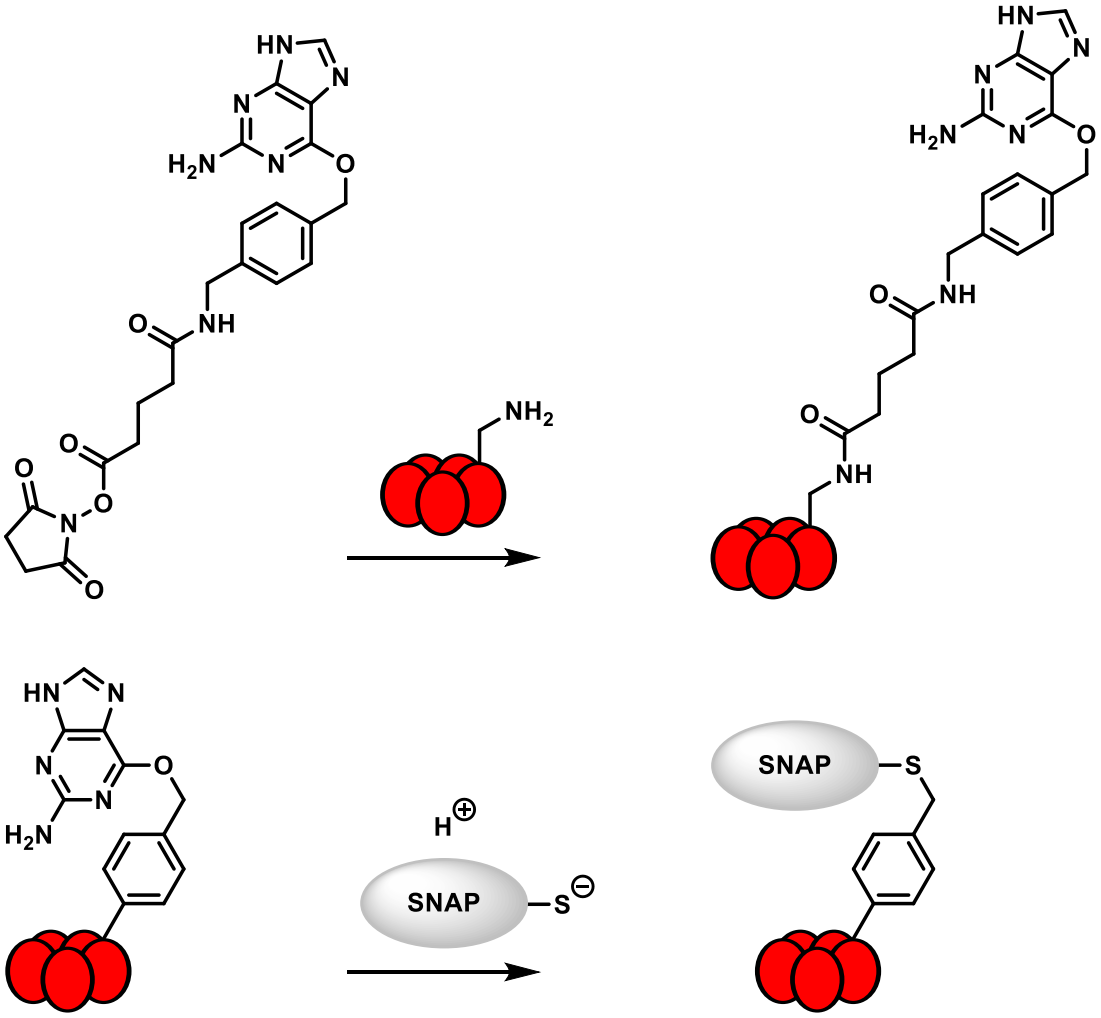

Figure 1.9. SNAP-trap CTB (red) is labelled with BG-NHS ester at exposed Lys residues. CTB-BG, on encountering the SNAP-tag protein (grey) in the ER or cytosol, is covalently labelled with SNAP-tag.

CTB has also been non-specifically chemically labelled for immunogenic purposes. CTB was non-specifically thiolated with 3-(2-pyridyldithio)propionate NHS ester, and subsequently conjugated to maleimide-modified liposomes through thioether formation[102]. In this instance, CTB both retained biological activity and acted as an adjuvant. Non-specifically thiolated CTB has also been coupled to a similarly-labelled *Streptococcal* antigenic peptide by disulfide formation, with oral administration evoking a strong antibody response[103]. One particular immunogenic example of note involved the conjugation of norcocaine to CTB. Initially developed with BSA and subsequently applied to CTB, succinimyl-norcocaine was non-specifically conjugated to exposed Lys residues of CTB through an *in situ* active ester intermediate[104,105]. The CTB-norcocaine conjugate was investigated as a vaccine against cocaine addiction[105], and recently underwent phase II clinical trials[106], with mixed results; while the vaccine was shown to be safe, the benefits seen in earlier investigations were not repeatable to the same degree.

1.2.4. Site-specific chemical modification of CTB

The previously described methods of chemical conjugation, while effective, do not offer the same level of control and reproducibility as site-specific methods. Two methods of site-specific labelling of CTB have been reported, both at the N-terminus. The first is enzymatic, involving SrtA. A CTB variant containing a genetically-encoded N-terminal oligo-Gly was site-specifically labelled with peptides containing the SrtA recognition motif (LPXTG) and modified with fluorescein or biotin[107]. The reaction efficiency was improved by replacement of terminal Gly residue of the SrtA recognition motif with a methyl ester; contrary to Gly, methanol cannot act as a substrate for the reverse reaction[107] (figure 1.10). Labelled CTB was shown to assemble correctly and retained GM1 binding.

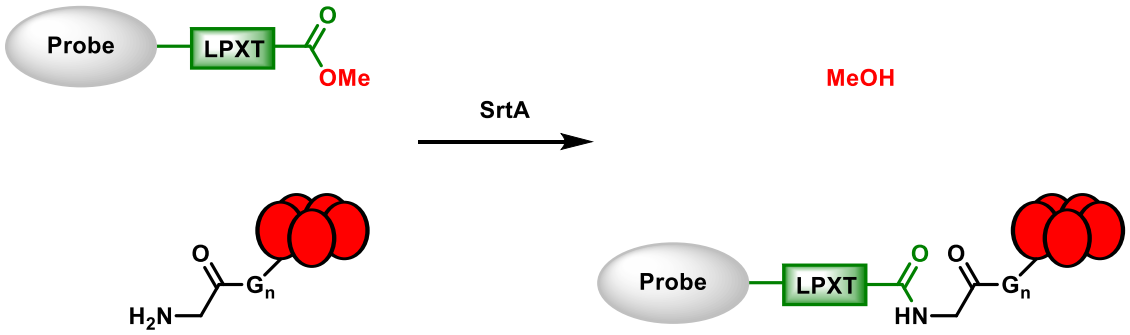

Figure 1.10. Efficient N-terminal SrtA-mediated ligation SrtA is used to ligate a probe (grey) conjugated to a methoxy-modified SrtA recognition peptide (LPRT; green) to an N-terminal oligo-Gly extension on CTB (red). The MeOH product is not a substrate for the reverse reaction.

The second method for site-specific labelling of CTB involves oxidation of an N-terminal Thr to an aldehyde using sodium periodate, followed by attachment of a species containing an aminooxy functional group by oximation[108,109], a one-pot reaction termed oxime ligation. By this method, CTB (which naturally contains an N-terminal Thr) was site-specifically, N-terminally labelled with five aminooxy-peptides, each containing five Ser residues linked to main-chain Lys residues through their amino side-chains. These were subsequently labelled with a separate aminooxy peptide by oxime ligation[116], forming a multiply branched complex. This method was adapted for conjugation of synthetic aminooxy antigenic peptides based on hemagglutinin (HA) from influenza virus, forming a CTB-based five-branched structure containing 25 copies of the antigenic peptide in total[109] (figure 1.11). This peptide even displayed increased avidity for GM1.

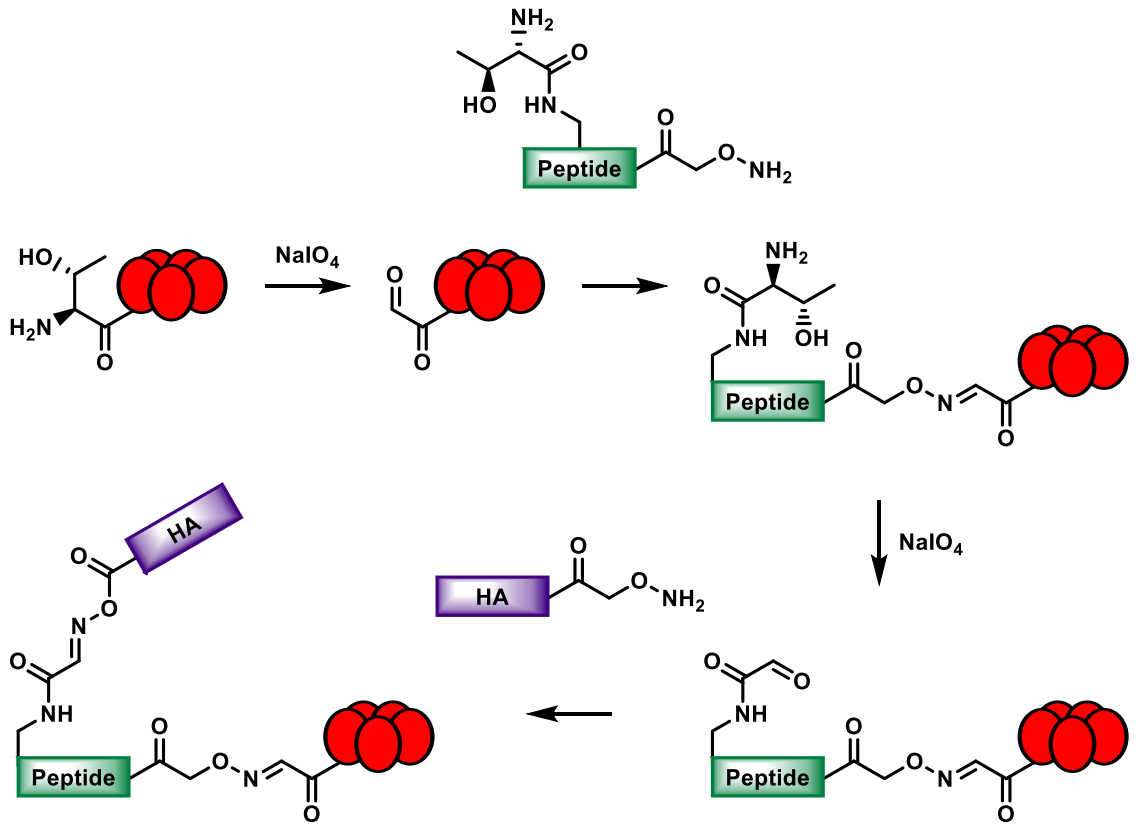

Figure 1.11. Oxime ligation The N-terminal Thr of CTB (red) is oxidised with sodium periodate and conjugated to an aminooxy-functionalised peptide (green) by oximation. Five Ser residues conjugated to Lys side-chains from the aminooxy-peptide are then oxidised and conjugated to an aminooxy-functionalised antigenic peptide from influenza HA, forming a branched structure with 25 antigenic peptides for presentation.

The utility of oxime ligation was recently demonstrated through the creation of a pentavalent inhibitor of CT[41]. A non-binding W88E CTB mutant was used as a scaffold, as the N-termini extend from the binding face at regular intervals. Aminooxy-functionalised GM1 with a long, flexible linker between was conjugated to the N-terminus of CTB by oxime ligation (figure 1.12). The resultant neoglycoprotein displayed an IC_{50} of 104 pM for CTB, the most potent multivalent inhibitor reported to date[41].

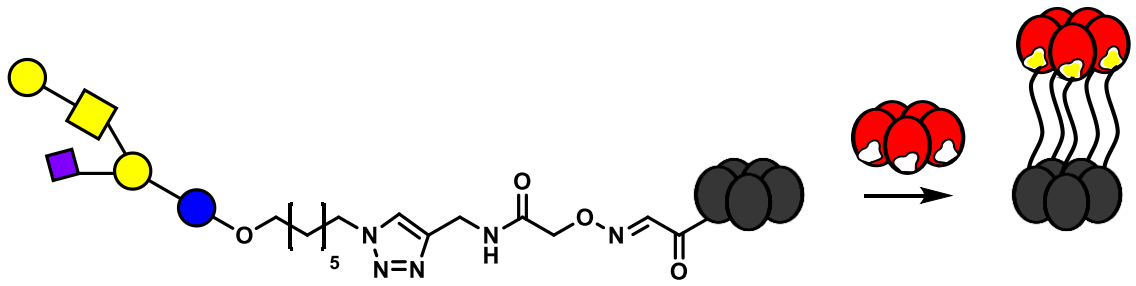

Figure 1.12. A pentavalent CTB inhibitor based on a CTB scaffold GM1 conjugated to a flexible aminooxy-functionalised linker is ligated to the N-terminal Thr residues of the non-binding CTB mutant W88E (grey) by oxime ligation, resulting in a pentavalent inhibitor of CTB (red).

1.2.5. Cholera toxin homologue modifications

In addition to CT modifications, several useful and potentially applicable modifications have been made to homologous AB_5 proteins. Shiga toxin B subunit (STB), a homologue of CTB derived from *Shigella dysenteriae*, has been modified with a genetically-encoded C-terminal peptide extension consisting of a glycosylation site, a sulfation site and a KDEL ER retention sequence[110]. This protein was used to probe the effect of a KDEL sequence on retrograde transport. It was determined that the protein reaches the ER, is removed to the Golgi apparatus and is subsequently dynamically recycled from the Golgi apparatus back to the ER[110]. This protein was later adapted for the study of endosome-Golgi transport[66]. In addition, LTB, sharing 80% sequence similarity with CTB[111], has been modified with a genetically-encoded 14 residue C-terminal fusion with the antigenic Pk peptide tag[112]. This was used to make a large complex with an antibody and a separate, secondary antigen. The complex retained GM1 binding and produced an immunogenic reaction[112]. The Pk tag was further modified to contain a Cys residue and successfully expressed (though with reduced yield), after which a maleimide-functionalised HRP was conjugated, which provoked a HRP-specific immune response[113].

1.3. Oligonucleotide therapies

1.3.1. Background

Large biologic therapeutics is a rapidly growing area of pharmaceutical research. Drugs of this category represent half of the 20 best-selling prescription drugs of 2014, including the top two, with global sales totalling almost US $71 billion[114]. Biopharmaceuticals tend to offer higher specificity and lower cytotoxicity than their small molecule counterparts, so they are attractive to the pharmaceutical industry. Oligonucleotide-based therapies have the potential to treat many genetic disorders and pathogenic diseases through pre-translation alteration of gene expression[3,115,116]. However, despite a huge amount of research into oligonucleotide-based therapies[3,115,116], to date there are only two licensed non-aptamer oligonucleotide-based drugs; fomiversen[117] and mipomersen[118]. Poor efficacy, *in vivo* stability and bioavailability have in the past prevented large-scale transfer of oligonucleotide-based drugs to the clinic. Oligonucleotide efficacy and stability have both been vastly improved[3,119,120], but while progress has been made in oligonucleotide delivery, poor bioavailability remains a significant stumbling block[121-123].

1.3.2. Synthetic oligonucleotides

The immune system has evolved a number of mechanisms for the recognition and destruction of oligonucleotides as a protection against pathogenic infections[3,116,120]. As a result, native oligonucleotides are inherently unstable *in vivo*. For oligonucleotides to survive long enough to exhibit a physiological effect, they must be protected from recognition and degradation by nucleases. Several modifications to the chemical structure of the nucleotides have been shown to increase *in vivo* half-lives through increased nuclease resistance[3,116,120]. In addition, many of these modifications have been reported to improve target binding through the forced adoption of favourable conformations for hybridisation[3,116,120].

These chemical alterations primarily involve modifications at the ribose 2′ carbon, modifications to the phosphodiester backbone, and alternative scaffolds to ribose. Examples of 2′ modifications include replacement of the 2′-hydroxyl group of native RNA (figure 1.13A) with a 2′-methoxy group[124-126] (2′-OMe; figure 1.13B), a 2′-methoxyethyl group[124,126,127] (2′-MOE; figure 1.13C), and cyclisation of the ribose 2′ oxygen with the 4′ carbon (figure 1.13D), termed locked nucleic acids[128,129] (LNA). Phosphodiester backbone modifications include phosphorothioates (figure 1.13E), in which a non-bridging oxygen is replaced with a sulfur[124,125,130], and phosphorodiamidates (figure 1.13F), in which a non-bridging oxygen is replaced with a neutral dimethylamine

group[124,131]. In addition, the ribose sugar can be replaced with a morpholine ring[124,131,132], termed morpholino oligomers (figure 1.13G), or the whole sugar phosphate backbone can be replaced with repeating N-(2-aminoethyl)-glycine units connected by peptide bonds, termed peptide nucleic acids[124,133,134] (figure 1.13H). Many of these modifications can also be combined to improve stability or increase target binding; 2′-OMe, 2′-MOE and LNA oligomers with phosphorothioate backbones are common, as well as morpholino oligomers with phosphorodiamidate backbones[124,127,131,135].

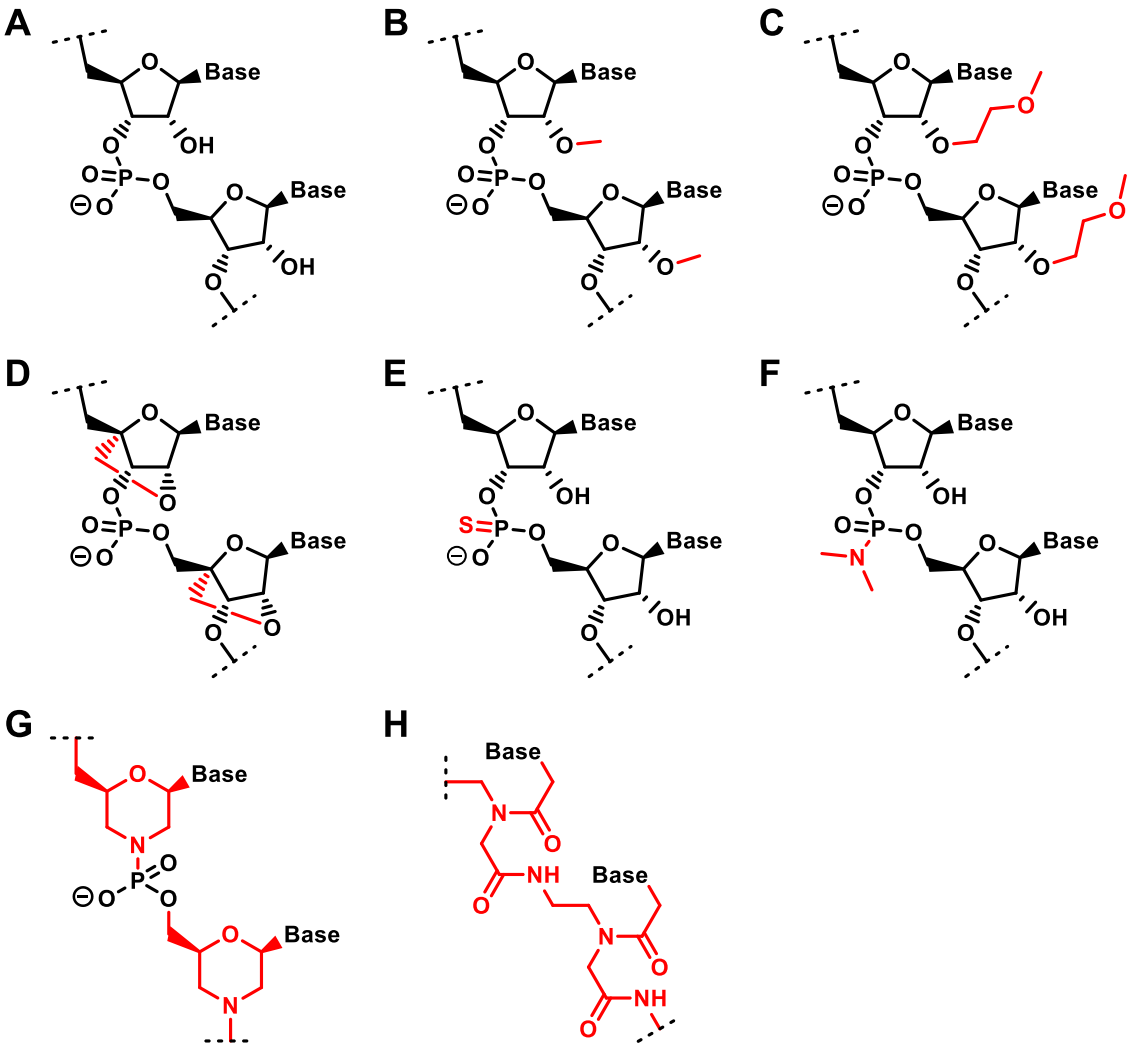

Figure 1.13. Oligonucleotide chemical modifications for improved function Summary of popular oligonucleotide chemical modifications for improved stability and efficacy *in vivo*. A. Native structure of RNA. B. 2′-methoxy ribose modification. C. 2′-methoxyethyl ribose modification. D. Locked nucleic acid, with the ribose 2′ oxygen cyclised to the 4′ carbon bridged. E. Phosphorothioate backbone modification. F. Phosphorodiamidate backbone modification. G. Morpholino oligomer, with a morpholine ring replacement of the ribose. G. Peptide-nucleic acid, with the sugar-phosphate backbone replaced by N-(2-aminoethyl)-glycine linked by peptide bonds. All deviations from native structure are highlighted in red.

1.3.3. Mechanism of action

Oligonucleotides have been studied extensively as potential therapeutic molecules. The most widely applicable function is pre-translational repair or knockdown of faulty proteins associated with disease states. Methods for messenger RNA (mRNA) manipulation include RNAi, gapmer oligonucleotides, steric blocking oligonucleotides and splice-altering oligonucleotides (figure 1.14).

1.3.3.1. RNAi: Perhaps the most recognisable example is RNAi, which involves manipulation of a natural mechanism. The RNAi pathway is a eukaryotic pathogen defence mechanism whereby the enzyme Dicer cleaves double-stranded RNA (dsRNA) into short fragments of approximately 20 nucleotides[136,137] (nt), termed short interfering RNA (siRNA). These siRNAs associate with the RNA-induced silencing complex (RISC), where the coding strand (passenger strand) is degraded[138,139]. The non-coding strand, or guide strand, is incorporated into the endonuclease argonaute, the catalytic component of the RISC[140-142]. Hybridisation of the guide strand to complementary mRNA results in argonaute-mediated cleavage of the mRNA, downregulating protein expression[141-143]. This process has been exploited *in vitro* and *in vivo* through the introduction of synthetic siRNA homologous to a region of mRNA targeted for degradation[4,116,144]. The siRNA interacts with the RISC to promote cleavage of mRNA, severely decreasing protein expression. These synthetic siRNAs will tolerate extensive chemical modifications to the passenger strand, but modifications to the guide strand must be kept minimal to ensure interaction with the RISC[3,145].

1.3.3.2. Gapmer oligonucleotides: Gapmer oligonucleotides are short, single-stranded (ss) antisense RNAs of approximately 20 nt. The ~ 5 nt at each end are chemically modified at both the phosphodiester backbone (usually phosphorothioate) and the ribose 2′ position, conferring cellular exonuclease resistance[3,115,116]. The central region is modified only at the phosphodiester backbone, increasing stability of the oligonucleotide while creating a gap (hence the term gapmer) of 2′-unmodified RNA of ~ 10 nt[3,115,116]. On hybridisation to complementary mRNA, the unmodified gap is recognised as ds RNA and cleaved by ribonuclease (RNase) H prior to translation[3,115,116], downregulating protein expression.

1.3.3.3. Steric blocking oligonucleotides: In addition to oligonucleotides which promote cleavage, some translation-suppressing oligonucleotides function through steric inhibition. These oligonucleotides are heavily modified so as to be highly resistant to degradation. On hybridisation with complementary mRNA, a degradation-resistant duplex is formed which sterically blocks ribosome binding and translation[3,134,146], downregulating protein expression.

1.3.3.4. Splice altering oligonucleotides: Steric blocking antisense oligonucleotides have also been adapted for manipulation of protein sequence at the pre-mRNA level. These heavily modified oligonucleotides are complementary to regions of pre-mRNA recognised by the spliceosome, the complex responsible for the removal of introns from pre-mRNA prior to mRNA formation[147]. These oligonucleotides form a stable, degradation-resistant duplex at splice sites, preventing spliceosome interaction[3,124] and altering the sequence of the mature mRNA. Splice-altering oligonucleotides have been used both to restore native sequence by preventing recognition of aberrant splice sites[135,148], and for removal of faulty exons through preventing native splice site recognition[149-151], restoring functional protein in both cases.

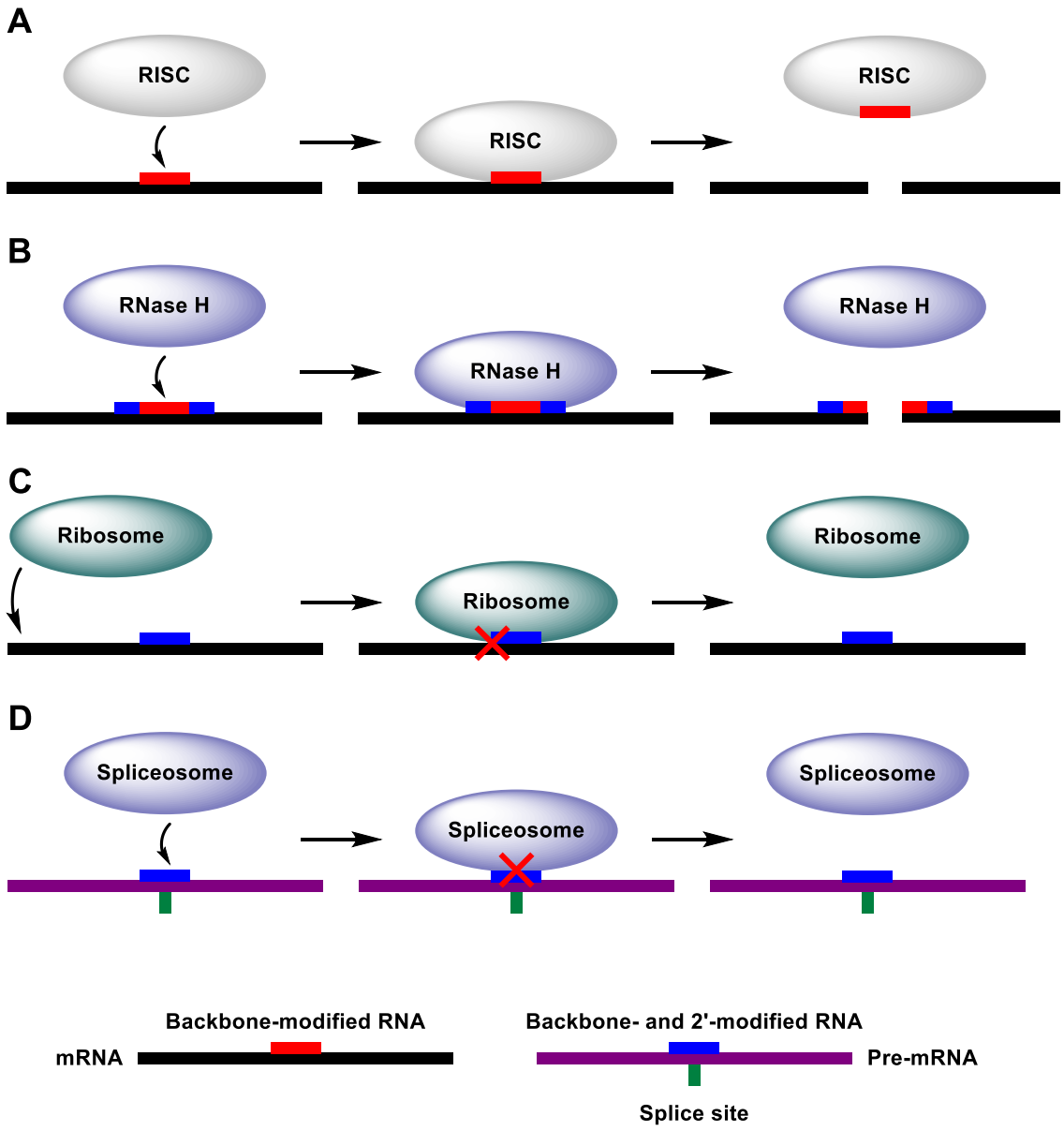

Figure 1.14. Oligonucleotide-mediated pre-translational modification of gene expression Schematic representation of pre-translational modification of gene expression using A. siRNA, B. gapmer oligonucleotides, C. steric blocking oligonucleotides, and D. alternative splicing oligonucleotides.

1.3.4. Delivery methods

Effective delivery remains the major stumbling block in the transferral of oligonucleotides from laboratory to clinical use. Their size and charge prevent them crossing the cell membrane barrier, and as a result they display poor bioavailability[152,153]. Native oligonucleotides also lack a means for cell-specific targeting, important for increasing efficacy and reducing side-effects. Several methods have been trialled for improving bioavailability, primarily through chemical modification and encapsulation.

1.3.4.1. Gymnotic delivery: Some success has been achieved through local gymnotic (naked) delivery of oligonucleotides, particularly to locally restricted regions such as the eye[3,116]. However, systemic gymnotic delivery has generally fared poorly. Tissue uptake is often poor, non-specific and unpredictable, and can lead to a build-up of oligonucleotides in the liver and kidneys, damaging those ograns[154-156]. In addition to these problems, modifications which improve functionality *in vitro* often do not confer a matching improvement on systemic *in vivo* delivery[151]. Certain chemical modifications can improve the systemic bioavailability of oligonucleotides. Phosphorothioate backbone modifications have been shown to mildly improve bioavailability through increasing serum lifetime[157]. Oligonucleotide conjugation to hydrophobic molecules including lipids[158], cholesterol[157] and vitamin E[159] have also been shown to improve oligonucleotide delivery *in vitro* and *in vivo*. However, these do not improve target specificity and delivery vectors have been shown to be generally superior.

1.3.4.2. Peptide-mediated delivery: Certain short, positively charged peptides possess the ability to cross the cell membrane barrier[153,160], termed cell-penetrating peptides (CPP). While there is some debate over the exact mechanism by which they enter cells, there is a general consensus that it occurs through endocytosis[161], initiated by their interaction with anionic glycosaminoglycans[153]. Covalently attached CPPs have been reported to mediate transport of a range of macromolecules into cells, including oligonucleotides[162-164]. Delivery and activity of a non-functional PNA oligomer has been reported to be rescued through addition of a tetra-Lys peptide[135]. Cytotoxicity is usually not observed at concentrations required for efficient payload delivery[165] and they do not tend to elicit a host immune response[153], distinct advantages over other delivery methods. However, CPPs are susceptible to phagocytic clearance from the circulatory system[121] and often display poor *in vivo* stability and non-specific distribution[166], in addition to suffering in many cases from endosomal entrapment[153].

1.3.4.3. Viral vectors: Viral vectors make an attractive choice for nucleic acid delivery, as they have evolved mechanisms to efficiently deliver genetic material into cells for replication. They have the advantages of high transfection efficiency and target specificity[122] whilst protecting the nucleic acids within the capsid from clearance or degradation. Viral expression of short therapeutic oligonucleotides has shown some promise *in vitro*[167,168], while oligonucleotide-based anti-cancer treatments delivered with adenovirus have had some success *in vivo*[168,169]. However, despite the fact that pathogenic genes are removed, safety concerns remain. Clinical trials involving viral delivery systems have been linked with the development of cancer due to viral genome integration[170,171]. In addition, they have high potential to cause a host immune response, putting the host at risk and increasing the chances of resistance developing and rejection of the treatment.

1.3.4.4. Liposomal delivery: Liposomes represent the most widely utilised method for oligonucleotide delivery[121,122]. Liposomes mimic the arrangement of the lipid bilayer, forming vesicle-like structures with an aqueous internal compartment[172,173], presenting a permeability barrier which protects internally encapsulated molecules[172,173]. Nucleic acid delivery is usually achieved using cationic liposomes[174-176]. These promote complex formation with nucleic acids, termed lipoplexes, through electrostatic interactions with the cationic polar head groups. They possess a net positively charged exterior surface, which promotes interaction with the cell membrane and cell entry through endocytosis[121,123]. Liposomes have been shown to hugely alter the pharmacokinetic profile of nucleic acids *in vivo*, in general inducing longer circulatory half-lives and lowed distribution[121,177]. Liposomes have been shown to mediate successful *in vivo* delivery of oligonucleotides for treatment of hypercholesterolemia[178], ocular inflammation[179], viral infections including herpes[180] and ebola[181], chronic pain[182], arthritis[183] and various forms of cancer[184-186]. However, there are drawbacks with this delivery method. Liposomes tend to accumulate in the liver[121,178]. While this makes liver disease a prime therapy target, it can also result in toxicity[178]. Aside from this, cationic liposomes are generally cytotoxic[187-189] and susceptible to phagocytic clearance from the circulatory system[121]. In addition, cell entry by endocytosis has been linked with endosomal entrapment[121,123], decreasing bioavailability and increasing the potential of an immune response through exposure to Toll-like receptors[190,191]; sequences which elicit an innate immune response on liposomal delivery have avoided this when expressed in the cells[192] or gymnotically

introduced[193]. Clearly, further study is required to find solutions to these problems before liposomal vectors could be considered for clinical use.

1.3.4.5. Polymers: Polymeric vectors for oligonucleotide delivery are not as widely studied as lipid-based vectors, and thus have not progressed to the same level[121]. They are attractive as they are highly biocompatible, relatively easy to produce and have high potential for modification[123,194]. Polymeric vectors for oligonucleotide delivery come in two major classes for oligonucleotide delivery; polymer micelles and polyplexes (figure 1.15). Polymer micelles are self-assembling structures comprised of amphiphilic polymers, containing a hydrophilic domain for aqueous interaction, a hydrophobic domain to mediate self-assembly and a cationic domain to promote oligonucleotide interaction and encapsulation[123,194]. They may also be coated with neutral shielding polymers, such as PEG, to improve immune evasion and circulation half-lives[195,196]. Polyplexes are gel-like complexes of cationic polymers and oligonucleotides, complexed through surface adsorption mediated by electrostatic interactions[123,194]. Cationic polymers in general provide excellent transfection efficiency[197,198]. They enter cells through endocytosis. Although the exact mechanism is not fully understood, it has been linked to both scavenger receptor recognition[197,199] and the cholesterol trafficking system[200]. Polymeric vectors commonly contain many protonatable amine groups allowing them to act as a proton sponge, promoting endosomal disruption and high transfection efficiency[121,198]. They have been used to mediate successful *in vivo* oligonucleotide delivery for the treatment of ischemia[201], viral infection[202], alopecia[203] and various cancers[204,205]. It is of note that the first instance of siRNA-cancer treatment in humans also involved a polymeric carrier[206]. However, the cationic nature of the polymers has been linked to immunogencitiy and cytotoxicity[122,123,207], possibly due to impairment of mitochondrial function[208], as well as promotion of non-specific interactions leading to off-target effects and circulation clearance[198,209]. Clearance of polymeric nanoparticles from the circulatory system tends to be relatively rapid, mediated by interactions with plasma proteins and phagocytic recognition[198,210]. This can lead to accumulation in the liver[210,211] and potential liver toxicity. Efforts have been made to improve polymeric vectors. These include decreased cytotoxicity through use of biodegradable polymers[212], increased bioavailability trough incorporation of shielding molecules[213] and CPPs[214,215], and improved specificity through decoration with targeting molecules[213,216]. However, no major breakthroughs have yet been made and further work is required before polymeric vectors can be considered viable for routine clinical use.

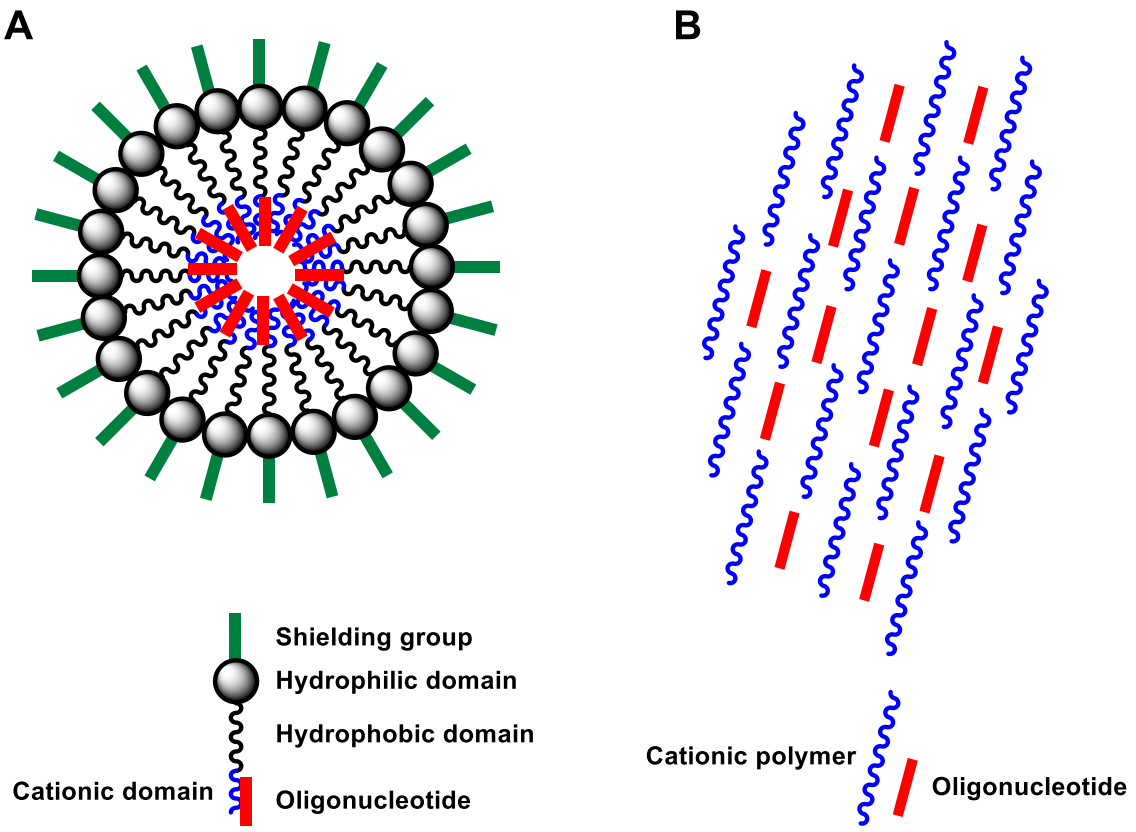

Figure 1.15 Polymer-based vectors Schematic representation of A. polymer micelle, and B. polyplex oligonucleotide delivery vectors.

1.3.5. Therapeutic oligonucleotides

Many of these oligonucleotide varieties have been tested in clinical trials, with varying degrees of success. Two non-aptamer oligonucleotide drugs are currently licensed for clinical use. One, fomiversen[117], is a 2′-OMe phosphorothioate gamper antisense oligonucleotide targeting the IE2 protein of cytomegalovirus (CMV) for treatment of CMV-induced retinitis in immunocompromised patients. The second and more recent, mipomersen[118], is a 2′-MOE phosphorothioate gapmer antisense oligonucleotide targeting apolipoprotein B100, a protein expressed in the liver and linked with production of low density lipoprotein cholesterol, for treatment of hypercholesterolemia. Other oligonucleotides are currently in clinical trials for diseases including hepatitis C infection, deep vein thrombosis and spinal muscular atrophy[121]. However, many more have produced disappointing results in late stage clinical trials, including oligonucleotides targeted against Duchenne muscular dystrophy, prostate cancer, macular degeneration,

breast cancer, melanoma and myeloma[3,121], while fomiversen has been discontinued by the manufacturer[3]. It is clear further research is required for oligonucleotides to fulfil their immense therapeutic promise, and development of a robust, targeted delivery system would represent a huge stride forward in this regard.

1.4. Project outline

The ability of cholera toxin to be labelled with various macromolecules for cell delivery has been demonstrated. However, there has been no attempt to engineer the non-toxic B subunit for oligonucleotide conjugation and delivery, macromolecules which currently lack a robust delivery method. The aim of this study was to determine the suitability of CTB as a vector for targeted delivery of therapeutic oligonucleotides. The primary objective was to develop a robust method for labelling CTB, and to determine the behaviour of the labelled protein in mammalian cells. If found suitable, an oligonucleotide payload would be attached and cellular behaviour investigated, with a view towards release of the oligonucleotide payload for a therapeutic action (figure 1.16).

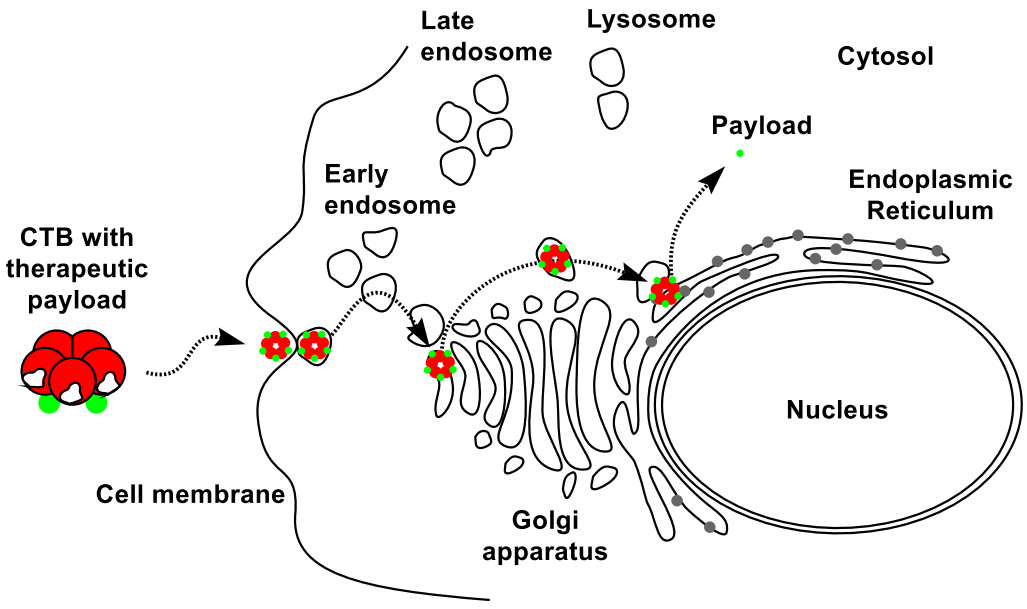

Figure 1.16. CTB-mediated targeted oligonucleotide delivery Schematic representation of the delivery and release of a therapeutic oligonucleotide payload to mammalian cells.

Chapter 2: Materials and methods

2.1. Introduction to core techniques

2.1.1. Assembly PCR

During this study, a range of modified CTB variants were generated, in order to vary the position at which labels were attached, the identity of the labels themselves, and the biological action of the protein. Assembly PCR (or polymerase cycling assembly) provided the method by which most of the genes required for protein expression were produced. An overview of the process is provided in figure 2.1. It is similar in principle to standard PCR, but differs in the provision of the template strand. Rather than providing a single whole template strand, the template is comprised of several short oligonucleotide sequences of approximately 70 base pairs (bp), alternating between sense and antisense, which overlap by approximately 20 bp at each end. An excess of shorter "terminal" forward and reverse primers, complementary to the 5′ ends of the sense and antisense strands, are also present. The oligonucleotide "parts" act as primers, and on assembly (due to the overlap of complementary sequences) are extended to the end of the adjacent oligonucleotide. The extended parts continue to assemble and become extended in a stepwise manner over subsequent PCR cycles, eventually providing a full template for the terminal primers[217,218]. At this stage, the whole gene is exponentially amplified, in a similar manner to standard PCR. This technique takes advantage of the relative ease of synthesising short oligonucleotide sequences chemically; it allows large gene libraries to be created in a short space of time, as mutants can be created with several different mutations at various different positions in the same gene in a single "one pot" reaction.

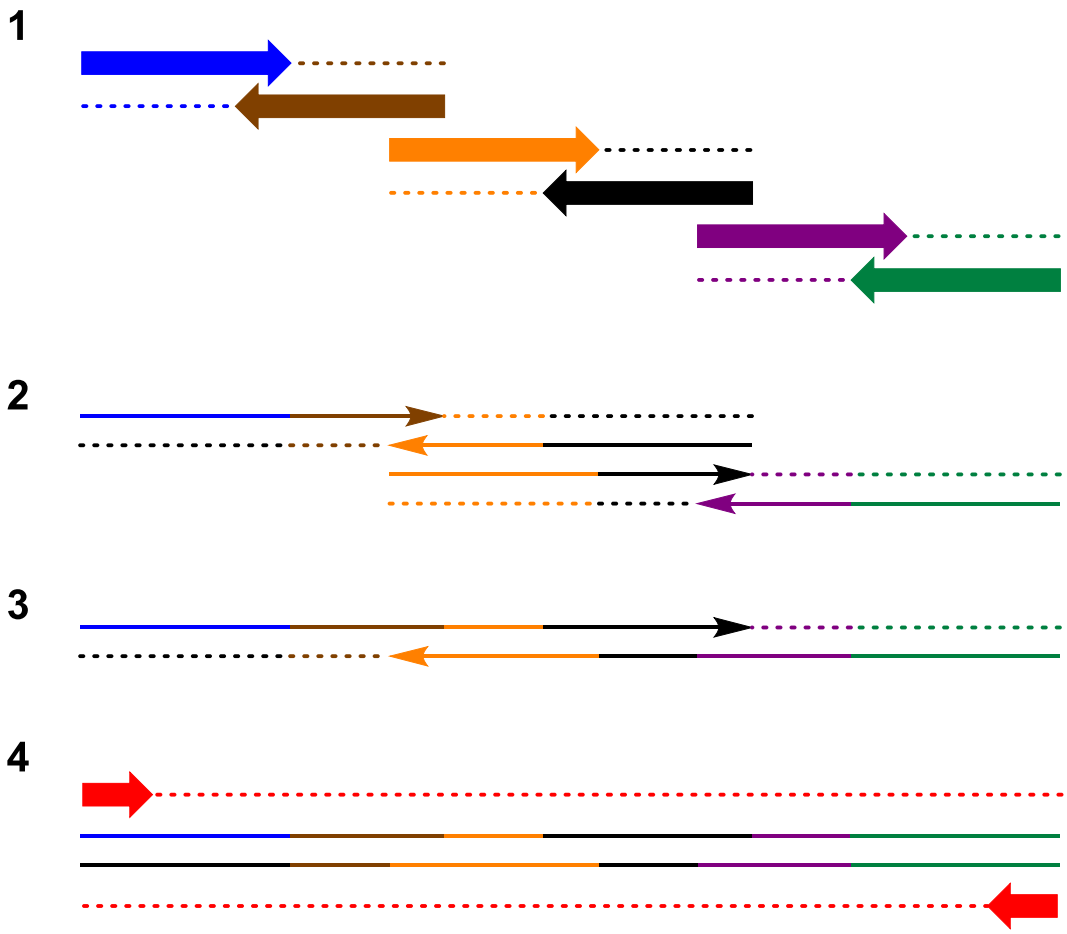

Figure 2.1. Overview of assembly PCR 1. Each of the six colours – blue, brown, orange, black, purple and green – represent a different section of the target gene. These short, overlapping oligonucleotide "parts" (single-coloured arrows) assemble due to their overlapping lengths of complementary sequence, and are extended (dotted lines) through the action of DNA polymerase. 2. and 3. The newly extended parts (multi-coloured arrows) assemble due to their overlapping lengths of complementary sequence, and are extended (dotted lines) through the action of DNA polymerase. 4. The full gene sequence has been produced during subsequent PCR cycles. The shorter "terminal" primers (red arrows) anneal to the 5′ ends of the sense and antisense strands and are extended (dotted red lines) through the action of DNA polymerase, resulting in exponential amplification of the full target gene.

2.1.2. Exponential megapriming PCR (EMP)

It was occasionally necessary to insert a length of DNA into a plasmid without the use of restriction enzymes, due both to the lack of restriction sites in the required position on the plasmid, and the desire to avoid insertion of extra nucleotides which would cause codon shifts or undesirable amino acid insertions in the gene. For this purpose, EMP was the chosen cloning method. An overview of the process is provided in figure 2.2. A region of a plasmid in which DNA insertion is desired is first identified, after which a "megaprimer" is produced. To create the megaprimer, the DNA to be inserted into the plasmid is used as a template for a PCR reaction, using a standard forward primer (F1; complementary to the 5′ end of the antisense strand of the template). However, the reverse primer (R1; complementary to the 3′ end of the sense strand of the template) used contains a 5′ overhang which is complementary to the region of the plasmid immediately downstream of the desired insertion site, with the overhang region having similar properties to a standard primer. The megaprimer is then used as a forward primer in a second PCR reaction, with the plasmid as a template and a reverse primer (R2) complementary to the region of the plasmid immediately upstream of the desired insertion site. This creates linear DNA with the insert incorporated into the plasmid at the 5′ end. The final round of PCR involves exponential amplification of the linear insert-plasmid hybrid using the forward primer F1 and reverse primer R2. Following this, the PCR product can be purified and subsequently cyclised, through 5′ phosphorylation by polynucleotide kinase (PNK) and ligation with T4 DNA ligase, in order to improve transformation efficiency.

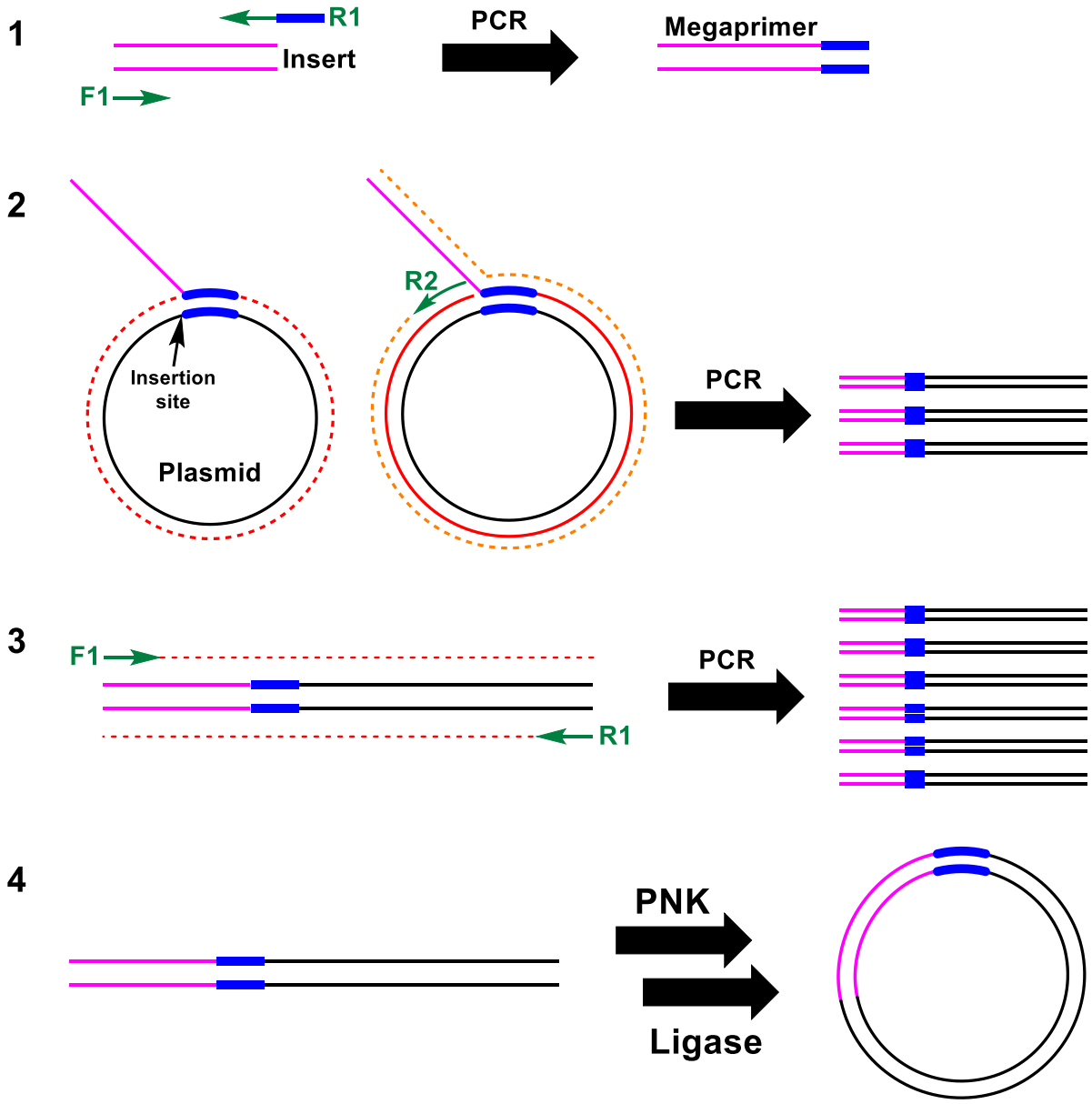

Figure 2.2. Overview of exponential megapriming PCR cloning 1. The insert (pink) is amplified by PCR with primers F1 (green) and R1 (green/blue) to produce the megaprimer, containing a 3′ overhang (blue) complementary to the region of the plasmid immediately downstream of the insertion site. 2. The plasmid (black) is used as a PCR template with the megaprimer (pink/blue; extension in red) and primer R2 (green; extension in orange) to produce linear insert-plasmid hybrid DNA. 3. The insert-plasmid hybrid DNA is amplified by PCR using primers F1 and R1 (both green). 4. The linear PCR product in cyclised with polynucleotide kinase and T4 DNA ligase, resulting in circular plasmid DNA containing the insert in the desired location ready for transformation.

2.1.3. Isothermal titration calorimetry

This highly sensitive technique allows for the measurement of the thermodynamic parameters of binding interactions in solution. The enthalpy change (ΔH), association constant (K_a) and stoichiometry of a reaction (N) can be directly measured, while dissociation constant (K_d) can be derived from the reciprocal of K_a, and change in Gibbs free energy (ΔG) and entropy (ΔS) can be derived from these measurements[219,220] using the following equation;

$$\Delta G = -RT\ln K_a = \Delta H - T\Delta S$$[219]

where R = gas constant (8.314 J mol^{-1} K^{-1}) , and T = absolute temperature (K). These measurements are determined through changes in temperature due to the interaction occurring. A calorimeter consists of two cells, a reference and a sample cell. The reference cell contains a known volume of liquid (water or buffer), while the sample cell contains a known volume and concentration of the macromolecule being investigated. A constant power is supplied to the reference cell, and the sample cell is equilibrated to a similar temperature using a measurable amount of power[219,220]. An excess concentration of ligand is titrated into the sample cell in known volumes, resulting in a temperature change in the sample cell due to the reaction occurring inside. A feedback loop causes a change in the power heating the sample cell in order to re-equilibrate it with the reference cell; less input for an exothermic event, more input for an endothermic event[219,220]. With increasing titrations, the necessary input required for re-equilibration will change as the number of available binding sites for the ligand in the sample cell decreases. Measurements consist of the change in power to the sample cell required for re-equilibration, plotted vs time, and the integrals of these peaks (ΔH of individual titrations) can be plotted vs the molar ratio of ligand:macromolecule in order to obtain a binding curve, from which can be derived overall ΔH, K_a and N for the reaction[219,220].

2.1.4. Microscopy

2.1.4.1 Fluorescence microscopy: This technique exploits the properties of fluorophores in order to detect the fluorescence they emit at a specific wavelength. Each individual fluorophore possesses excitation and emission spectra; continuous spectra of electromagnetic wavelengths at which the fluorophore absorbs and emits energy. Electrons in the fluorophore absorb energy at wavelengths within its excitation spectrum, resulting in excitation to a higher energy state. As these electrons relax back to their ground state, energy is emitted within the emission spectrum in the form of a photon. The photon emitted is of a lower energy than that initially absorbed, and hence of a longer wavelength. This difference is termed the Stokes shift[221]. This is the principle exploited by fluorescence microscopy. Photons from a light source, usually a laser, are passed through an excitation filter which selects for a desired wavelength. These then pass through a chromatic beam splitter, reflecting the shorter wavelength photons through the objective lens, focusing the beam on the sample. This excites the fluorophores, and the longer wavelength photons they emit pass through the chromatic beam splitter and emission filter to the detector, ensuring only photons of the desired wavelength are detected[221]. A schematic representation of the process is shown in figure 2.3.

2.1.4.2. Confocal microscopy: Confocal microscopy functions using similar principles to standard fluorescence microscopy, but with the addition of a pinhole between the beam splitter and the detector for the purpose of increased resolution (figure 2.4). The pinhole results in detection of light from a specific depth of the sample only, as only light originating from a specific distance is correctly focused such that it is able to pass through the pinhole; contaminating photons from different depths within the sample are not correctly focused and thus cannot pass through the pinhole. The resulting images are produced at a higher resolution and with reduced noise[222].

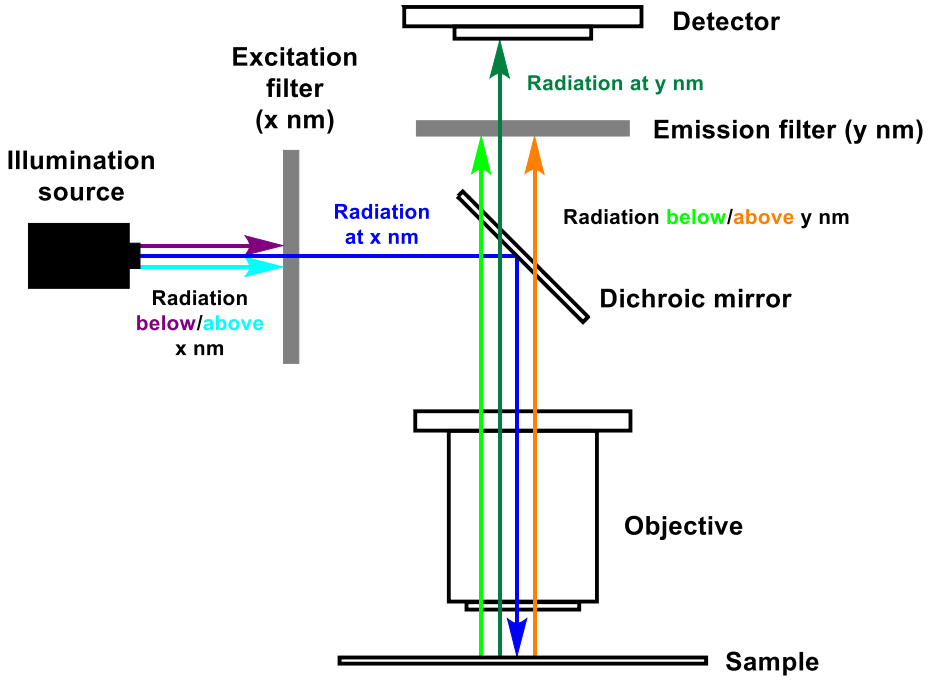

Figure 2.3. Schematic representation of fluorescence microscopy Photons from a source are passed through the excitation filter, restricting the beam to a set wavelength range (x nm) by absorbing wavelengths outside the range (purple and light blue arrows). Photons of the desired wavelength (dark blue arrow) are reflected by the dichroic mirror and focused by the objective onto the sample. Fluorophores in the sample become excited and emit photons of a longer wavelength. The beam is focused by the objective, passes through the dichroic mirror, and photons of the desired wavelength range (y nm) pass through the emission filter to the detector for processing (dark green arrow), while those of undesirable wavelengths are absorbed (light green and orange arrows).

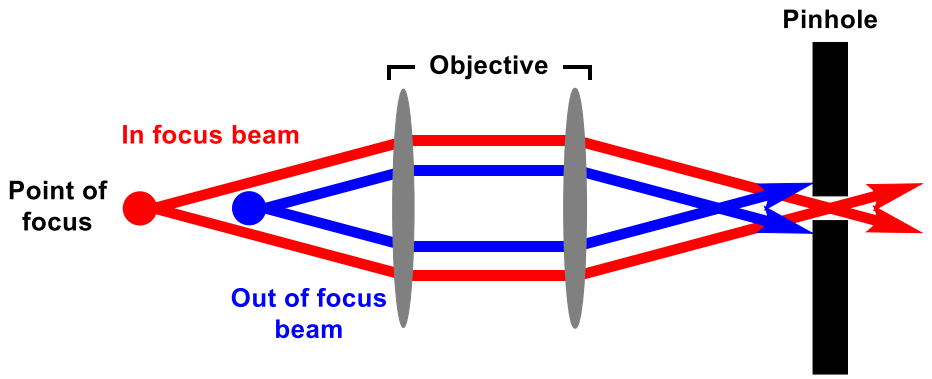

Figure 2.4. Schematic representation of focusing in confocal microscopy Photons emitted from the desired depth (red arrow) are focused correctly by the objective such that they are able to pass through the pinhole, while photons emitted from an undesired depth (blue arrow) are not focused correctly and thus cannot pass through the pinhole.

2.2. Source of reagents and instrumentation

Analytical grade reagents were obtained from Sigma Aldrich, Fisher Scientific, Alfa Aesar and VWR International. Water was purified using an ELGA PURLAB Classic purifier. Oligonucleotides were obtained from Integrated DNA Technologies. Enzymes, buffers, reagents and DNA standard ladders for molecular biology were obtained from New England Biolabs. QIAprep spin Miniprep, Plasmid Plus Midi, QIAquick gel extraction and QIAquick PCR purification kits for DNA extraction and purification were obtained from Qiagen. Bacterial cultures were grown using an ISF1-X shaker incubator (Kuhner). Centrifugation was performed using the Avanti J30-I (Beckman Coulter), Pico 17 and Fresco 21 centrifuges (Thermo Scientific). Ni-NTA agarose resin was obtained from Qiagen. Lactose-agarose resin was obtained from Sigma Aldrich. FPLC was performed with an AKTA Purifier (GE Healthcare). Protein molecular weight markers were obtained from New England Biolabs. Gels were imaged and analysed using a Universal Hood II gel documentation system (BioRad). LC-MS analysis of proteins and peptides was performed using an HCTultra (Bruker Daltonics). Oligonucleotide synthesis was performed using an AKTA Oligopilot Plus (GE Healthcare Life Sciences). Oligonucleotide purification and desalting were performed using an AKTA Purifier (GE Healthcare Life Sciences). Oligonucleotide lyophilisation was performed using a ModulyoD freeze dryer (Thermo Scientific). Oligonucleotides were characterised using an Agilent 1100 series HPLC system (Agilent Technologies) and a Finnigan LTQ LC-MS (Thermo Scientific). Cell culture media and serum was obtained from Sigma Aldrich, serum-free media from Gibco, and other cell culture reagents obtained from Lonza. Mammalian cells were incubated in a MCO-18AIC(UV) CO_2 incubator (Sanyo) and experimentation carried out in an Airstream class II biological safety cabinet (ESCO). Cell viability experiments were analysed with a PowerWave XS2 plate reader (BioTek Instruments). Cells were imaged using an Imager Z2 LSM880 upright confocal microscope (Zeiss).

2.3. Common buffers, solutions and media

Buffers, solutions and media were produced in-house unless otherwise stated.

2 × yeast-tryptone (2xYT) growth medium – 1.6% (*w/v*) tryptone, 1% (*w/v*) yeast extract, 0.5% (*w/v*) NaCl

Agarose gel electrophoresis loading buffer – 2.5% (*w/v*) Ficoll 400, 11 mM ethylenediaminetetraacetic acid (EDTA), 3.3 mM Tris-HCl, 0.017% (*w/v*) SDS, 0.15% (*w/v*) Orange G

Buffer BB (Qiagen) – Exact composition confidential

Buffer ETR (Qiagen) – Exact composition confidential

Buffer N3 (Qiagen) – 4.2 M guanidine-HCl, 0.9 M KAc

Buffer QG (Qiagen) – 20 mM Tris-HCl (pH 6.6), 5.5 M guanidine thiocyanate

Buffer P1 (Qiagen) – 50 mM Tris-HCl (pH 8.0), 10 mM EDTA, 100 μg mL^{-1} RNase A, 0.1% (*v/v)* LyseBlue

Buffer P2 (Qiagen) – 200 mM NaOH, 1% (*w/v*) SDS

Buffer PB (Qiagen) – 5.0 M guanidine-HCl, 30% (*v/v*) isopropanol

Buffer PE (Qiagen) – 10 mM Tris (pH 7.5), 80% (*v/v*) ethanol

Buffer S3 (Qiagen) – Exact composition confidential

CutSmart buffer (NEB) – 50 mM CH_3CO_2K, 20 mM Tris-acetate, 10 mM $Mg(CH_3COO)_2$, 100 μg mL^{-1} BSA (pH 7.9)

HEPES buffer – 50 mM HEPES, 200 mM NaCl, 5 mM $CaCl_2$ (pH 7.5)

Immunofluorescence antibody dilution buffer - 137 mM NaCl, 3 mM KCl, 8 mM Na_2HPO_4, 1.5 mM KH_2PO_4, 0.1% (*v/v*) Tween 20, 1% (*w/v*) BSA (pH 7.3)

Immunofluorescence blocking buffer - 137 mM NaCl, 3 mM KCl, 8 mM Na_2HPO_4, 1.5 mM KH_2PO_4, 0.1% (*v/v*) Tween 20, 1% (*w/v*) BSA, 300 mM glycine (pH 7.3)

Immunofluorescence/FISH permeabilization buffer - 137 mM NaCl, 3 mM KCl, 8 mM Na_2HPO_4, 1.5 mM KH_2PO_4, 0.5% (*v/v*) Triton X-100 (pH 7.3)

Ligase buffer (NEB) – 50 mM Tris-HCl, 10 mM $MgCl_2$, 10 mM dithiothreitol (DTT), 1 mM ATP (pH 7.5)

LB growth medium (Fisher) – 1% (*w/v*) tryptone, 0.5% (*w/v*) yeast extract, 1% (*w/v*) NaCl

NEBuffer 2 (NEB) – 50 mM NaCl, 10 mM Tris.HCl, 10 mM $MgCl_2$, 1 mM DTT (pH 7.9)

Pfu buffer – 20 mM Tris HCl, 10 mM KCl, 10 mM $(NH_4)_2SO_4$, 0.1-4 mM $MgSO_4$, 1% (*v/v*) Triton X-100, 1 mg mL^{-1} BSA (pH 8.8)

Phosphate-buffered saline (PBS)– 137 mM NaCl, 3 mM KCl, 8 mM Na_2HPO_4, 1.5 mM KH_2PO_4 (pH 7.3)

Phosphate-buffered saline-Tween 20 (PBST) - 137 mM NaCl, 3 mM KCl, 8 mM Na_2HPO_4, 1.5 mM KH_2PO_4, 0.1% (*v/v*) Tween 20 (pH 7.3)

SDS-PAGE loading buffer – 50 mM Tris-HCl (pH 6.8), 2% (*w/v*) SDS, 10% (*v/v*) glycerol, 100 mM DTT, 12.5 mM EDTA, 0.02% (*w/v*) bromophenol blue

SDS-PAGE running buffer – 25 mM Tris, 192 mM glycine, 0.1% (*w/v*) SDS

SDS-PAGE separating gel (12%) – 380 mM Tris (pH 8.8), 12% (*w/v*) acrylamide, 0.32% (*w/v*) bis-acrylamide, 0.1% (*w/v*) SDS, 0.1% (*w/v*) ammonium persulfate, 0.01% (*v/v*) tetramethylethylenediamine (TEMED)

SDS-PAGE stacking gel (5%) – 95 mM Tris (pH 6.8), 5% (*w/v*) acrylamide, 0.13% (*w/v*) bis-acrylamide, 0.1% (*w/v*) SDS, 0.1% (*w/v*) ammonium persulfate, 0.02% (*v/v*) TEMED

Saline-sodium citrate (SSC) buffer – 150 mM NaCl, 15 mM sodium citrate (pH 7.0)

Tris-acetate-EDTA (TAE) buffer – 40 mM Tris, 20 mM acetic acid, 1 mM EDTA

ULTRAhyb Ultrasensitive hybridization buffer (Ambion) – Exact composition confidential

2.4. Standard protocols

2.4.1. Molecular biology

2.4.1.1. Oligonucleotide design: Oligonucleotide sequences for assembly PCR were designed based on information from the Assembly PCR Oligo Maker programme[223] (http://www.yorku.ca/pjohnson/AssemblyPCRoligomaker.html), and their properties calculated and confirmed for purpose using the OligoCalc programme[224] (http://biotools.nubic.northwestern.edu/OligoCalc.html), except where they were already available in the lab (designed by J. Ross).

2.4.1.2. Assembly PCR: The template for assembly PCR was provided by short oligonucleotide "parts" covering the whole gene sequence, with alternating complementarity to the sense and antisense strands, and terminal overlapping regions of sequence complementarity to allow assembly. The PCR reaction mix (50 μL total) consisted of the relevant parts (10 nM each) and terminal forward and reverse primers (2 μM each), dNTPs (250 μM each) and *Pwo* polymerase (0.01 U μL^{-1}, where 1 U = the amount required to catalyse the incorporation of 10 nmol dNTPs into acid insoluble material in 30 min at 75 °C) in Pfu buffer ([$MgSO_4$] dependent on reaction). See section 2.4 for a list of oligonucleotides. The thermocycler programme used is described in table 2.1.

Step	Temperature (°C)	Time (s)	Number of cycles
1. Initial denaturing	95	30	1
2.1. Denaturing	95	30	30
2.2. Annealing	Dependent on primer T_m	30	
2.3. Elongation	72	Dependent on template length (500 bp min^{-1})	
3. Final elongation	72	Dependent on template length (> cycle elongation)	1

Table 2.1. Thermocycler programme for assembly PCR

2.4.1.3. PCR: Similar to assembly PCR above, but the template was provided by a whole gene sequence (10 nM) in place of the parts.

2.4.1.4. Restriction digest: Both the insert (10 µL in 20 µL total CutSmart buffer) and vector (20 µL in 40 µL total CutSmart buffer) were digested for 1 h at 37 °C with the relevant restriction enzymes (amount (U) dependent on [DNA], where 1 U = the amount required to completely digest 1 µg DNA in a 50 µL reaction in 60 min at 37 °C). The vector digestion also contained calf intestinal alkaline phosphatase (CIP; 10 U, where 1 U = the amount required to completely hydrolyse 1 µmol p-nitrophenyl phosphate in a 1 mL reaction in 1 min at 37 °C) to prevent re-annealing. All CTB variants were produced with a 5′ SphI site and a 3′ PstI site, thus these enzymes were used to digest these and the pSAB2.2 vector in all cases.

2.4.1.5. Ligation: A 5:1 molar ratio of digested insert:digested vector (total of 50 ng digested vector) was ligated for 30 min at room temperature in the presence of T4 DNA ligase (40 U μL^{-1}; where 1 U = the amount required to give 50% ligation of HindIII fragments of 0.12 µM λ DNA in a 20 µL reaction in 30 min at 16 °C) in ligase buffer (10 µL total volume).

2.4.1.6. Transformation by heatshock: Plasmid DNA (1 µL pure plasmid DNA or 2 µL impure manipulated DNA) was used to transform 10 µL *E. coli* XL10-Gold ultracompetent cells (for plasmid cloning) or *E. coli* C41(DE3) pRARE2 competent cells

(for protein expression) by heatshock; incubation at 4 °C for 30 min, 42 °C for 45 s, and 4 °C for 5 min. Transformation products were added to 1 mL pre-warmed (37 °C) LB and incubated for 1 h at 37 °C. These were then plated (100 μL for pure plasmid DNA, entire cell population concentrated to 200 μL otherwise) on LB agar (1.5% (*w/v*)) containing the relevant antibiotic (100 μg mL^{-1} ampicillin or 50 μg mL^{-1} kanamycin) and incubated at 37 °C overnight.

2.4.1.7. Site-directed mutagenesis:[225,226] The protocol was based on the QuikChange site-directed mutagenesis protocol (Stratagene). Template DNA was provided by the plasmid requiring mutation. The PCR reaction mix (50 μL total) consisted of 50 ng plasmid DNA template, 125 ng each of the forward and reverse primers, dNTPs (500 μM each) and *Pwo* polymerase (0.05 U μL^{-1}) in Pfu buffer (2 mM $MgSO_4$). Primers were designed based on the QuikChange protocol recommendations; 25-45 bp, ≥ 40% GC content, primers terminating in one or more G/C base, $T_m \geq 78$ °C. Primer T_m was calculated using the following formula:

$$T_m = 81.5 + 0.41\,(\%\,GC) - \frac{675}{N} - \%\,\text{mismatch}$$

where % GC and % mismatch are integers.

The thermocycler programme used is described in table 2.2.

Following thermocycling, DpnI (10 U, where 1 U = the amount required to digest 1 μg of *dam* methylated pBR322 DNA in 1 h at 37 °C in 50 μL) was added to the PCR reaction and incubated for 1 h at 37 °C in order to digest genomic methylated DNA. Samples taken before and after DpnI treatment were analysed by agarose gel electrophoresis (section 2.4.3), and the DpnI treated PCR reaction mix used to transform *E. coli* XL10 by heatshock (section 2.4.1.6).

Step	Temperature (°C)	Time (s)	Number of cycles
1. Initial denaturing	95	30	1
2.1. Denaturing	95	30	20
2.2. Annealing	55	60	
2.3. Elongation	72	Dependent on plasmid size (500 bp min^{-1})	
3. Final elongation	72	Dependent on plasmid size (> cycle elongation)	1

Table 2.2. Thermocycler programme used for site-directed mutagenesis

2.4.1.8. Exponential megapriming PCR:[227] The EMP megaprimer was produced by PCR (section 2.4.1.3), using a forward primer complementary to the 5' end of the desired insert, and a reverse primer complementary to the 3' end of the desired insert, containing a 5' extension complementary to the region immediately downstream of the insertion site. The megaprimer was purified by gel extraction (section 2.4.4) and inserted into the target vector by PCR (similar cycle and reaction composition to site-directed mutagenesis (section 2.4.1.7), except the annealing temperature was dependent on the primer T_m, and 5% (*v/v*) dimethylsulfoxide (DMSO) was included), using the forward primer from the first step and a reverse primer complementary to the region of the plasmid immediately upstream of the insertion site. The plasmid (containing the insert) was amplified by PCR (section 2.4.1.3) using 1 μL of the product from the previous step as template and the same primers. Amplified product was purified by PCR cleanup and used to transform *E. coli* XL10-Gold ultracompetent cells by heatshock (section 2.4.1.6).

2.4.2. Determination of DNA concentration

All DNA concentrations (ng μL^{-1}) were determined by spectrophotometry at 260 nm and calculated using the formula:

$$[\mathrm{DNA}] = 50 \times \mathrm{A}_{260}$$

2.4.3. Agarose gel electrophoresis

Gels of 1-2% (*w*/*v*) agarose in TAE buffer were prepared, depending on the expected size of the DNA fragments to be analysed; 1% for plasmid DNA, 1.6% for fragments up to 1.5 kb, 1.2% for samples containing both. Ethidium bromide was added to the gels (0.003% (*v*/*v*)) for DNA visualisation. DNA samples were mixed with loading buffer prior to sample loading, and the gels run at 100 V in TAE buffer. Gels were visualised by UV illumination in the gel documentation system.

2.4.4. Purification of digested plasmid DNA (gel extraction)

Digested plasmid DNA was purified using a QIAquick gel extraction kit, following the manufacturer-recommended protocol. All centrifugation steps took place at 17,000 × *g* at room temperature. The gel generated from an agarose gel electrophoresis experiment was illuminated with UV light, and the target band excised from the gel using a scalpel. Buffer QG (3 gel volumes) was added at 50 °C to dissolve the agarose. Isopropanol (1 gel volume) was added for increased DNA yield, and the solution passed through a silica membrane by centrifugation for 1 min, to which DNA is adsorbed but RNA, protein and metabolites may pass through. The membrane was washed by centrifugation for 1 min with buffer PE (750 μL) to remove salts, before a further 1 min centrifugation to remove residual ethanol. DNA was then eluted in water (30 μL) by centrifugation for 1 min.

2.4.5. Purification of PCR product from reaction mixture (PCR cleanup)

DNA from a PCR reaction was purified using a modified QIAquick gel extraction protocol. All centrifugation steps took place at 17,000 × *g* at room temperature. Buffer QG (10 volumes) was added to the PCR reaction mix and the solution passed through a silica membrane by centrifugation for 1 min, to which DNA is adsorbed. The membrane was washed by centrifugation for 2 × 1 min with buffer PE (750 μL) to remove salts, and DNA eluted in water (30 μL) by centrifugation for 1 min.

2.4.6. Small-scale plasmid DNA extraction from bacteria (Miniprep)

Plasmid DNA was extracted from small-scale bacterial cultures (5 mL growth medium) using a QIAprep spin Miniprep kit, following the manufacturer-recommended protocol. All centrifugation steps took place at 17,000 × *g* at room temperature unless otherwise stated. Bacterial cells were cultured overnight in 2xYT (5 mL) containing the relevant antibiotic. Cells were pelleted from cultures by centrifugation at 4600 × *g* for 10 min at 20 °C, growth medium discarded, and the cells resuspended in buffer P1 (250 μL). Buffer P2 (250 μL) was added to lyse the bacterial cells by alkaline lysis[228], followed by buffer N3 (350 μL) to neutralise the suspension and adjust to high salt binding conditions. The

precipitate (SDS, genomic DNA and cell debris) was pelleted by centrifugation for 10 min, and the supernatant passed through a silica membrane by centrifugation for 1 min, to which the DNA was adsorbed. The membrane was washed by centrifugation for 1 min with buffer PB (500 μL) to remove endonucleases, and centrifugation for 2 × 1 min with buffer PE (750 μL) to remove salts, before the DNA was eluted in water (60 μL) by centrifugation for 1 min.

2.4.6. Medium-scale plasmid DNA extraction from bacteria (Midiprep)

Plasmid DNA was extracted from medium-scale bacterial cultures (35 mL growth medium) using a Plasmid Plus Midi kit (Qiagen), following the manufacturer-recommended protocol. All centrifugation steps took place at 17,000 × *g* at room temperature unless otherwise stated. Bacterial cells were cultured overnight in LB (35 mL) containing the relevant antibiotic. Cells were pelleted from cultures by centrifugation at 4600 × *g* for 10 min at 20 °C, growth medium discarded, and the cells resuspended in buffer P1 (4 mL). Buffer P2 (4 mL) was added to lyse the bacterial cells by alkaline lysis[228], followed by buffer S3 (4 mL) to neutralise the suspension. The lysate was incubated at room temperature for 10 min before filtration to remove the precipitate. Buffer BB (2 mL) was added to adjust the lysate to high salt binding conditions, and the solution passed through a silica membrane, to which the DNA was adsorbed, using a vacuum manifold at approximately 300 mbar. The membrane was washed using the vacuum manifold with buffer ETR (700 μL) to remove endotoxins, followed by buffer PE (700 μL) to remove salts. Residual ethanol was removed by centrifugation for 1 min, before the DNA was eluted in water (200 μL) by centrifugation for 1 min.

2.4.7. Protein overexpression

2.4.7.1. Inoculation and growth of bacterial cultures: Transformation of *E. coli* C41(DE3) pRARE2 cells (10 μL) took place (as described in section 2.4.1.6) with plasmid DNA (1 μL) extracted by Miniprep (as described in section 2.4.6). Single colonies were transferred from the plate and used to inoculate 5 mL LB with the relevant antibiotic, which was incubated at 37 °C with aeration (200 rpm) overnight. Samples of these cultures (1.5 mL) were used to inoculate 500 mL LB in 2 L flasks with the relevant antibiotic, which was incubated at 37 °C with aeration (200 rpm).

2.4.7.2. Induction of protein overexpression: Once the 500 mL cultures reached OD_{600} value of 0.6-0.8, protein overexpression was induced with isopropyl β-D-1-thiogalactopyranoside (IPTG; 0.5 mM), and the cultures incubated overnight at 25 °C with aeration (200 rpm).

2.4.8. Protein purification

2.4.8.1. Protein extraction from growth medium: The induced 500 mL cultures were centrifuged at 10,000 × *g* for 10 min at 4 °C to pellet the cells. Pellets were discarded, 57% (*w/v)* ammonium sulfate added slowly to the supernatant, and the mixture incubated at 4 °C overnight in order to precipitate the protein. The suspension was centrifuged at 17,696 × *g* for 1 h at 4 °C to pellet the protein. The supernatant was discarded, and each pellet resuspended by agitation in 10 mL lysis buffer. The resuspended protein was vacuum-filtered (0.8 μm) prior to further purification.

2.4.8.2. Protein extraction from cells: The induced 500 mL cultures were centrifuged at 10,000 × *g* for 10 min at 4 °C to pellet the cells. The growth medium was discarded and the cell pellets resuspended in lysis buffer containing cOmplete EDTA-free protease inhibitor cocktail (Roche) where this would not interfere with the function of expressed protein. Cells were lysed 30 kPsi using a cell disruptor (Constant Systems), and cell debris precipitated by centrifugation at 35,000 × *g* for 45 min at 4 °C. The supernatant was syringe-filtered (0.45 μm) prior to further purification.

2.4.8.3. Ni-NTA affinity chromatography purification: The protein sample was passed through a Ni-NTA column, pre-equilibrated with lysis buffer (HEPES buffer containing 10 mM imidazole). The column was washed with 25 mL wash buffer (HEPES buffer containing 25 mM imidazole). The protein was eluted with 30 mL elution buffer (HEPES buffer containing 250 mM imidazole) and collected in 5 mL fractions.

2.4.8.4. Lactose affinity chromatography purification: The protein sample was passed through a lactose column pre-equilibrated with HEPES buffer. The column was washed with 25 mL HEPES buffer, and the protein eluted with 30 mL HEPES buffer containing 300 mM lactose and collected in 5 mL fractions.

2.4.8.5. Fast protein liquid chromatography (FPLC) purification: Following initial purification steps, protein was further purified by size exclusion chromatography (SEC) using an AKTA Purifier (GE Healthcare) automated system. All purifications were carried out at 4 °C. Depending on size, protein was purified large-scale (for example following *E. coli* protein expression) using a HiLoad Superdex 200 26/60 prep grade column (GE Healthcare) or a HiLoad Superdex 75 16/60 prep grade column (GE Healthcare), both with an injection volume of 1.5 mL and a flow rate of 1 mL min^{-1}. Purification was followed by A_{280}. Purified product was collected in 5 mL fractions in 14 mL disposable culture tubes (VWR) using a Frac-950 (GE Healthcare) fraction collector.

Small-scale purification (for example following protein labelling reactions) and analytical SEC was carried out using a Superdex 200 10/300 GL column (GE Healthcare), with an injection volume of 400 µL and a flow rate of 250 µL min^{-1}. Purification was analysed by absorbance (280 nm for protein, 260 nm for RNA, 488 nm for fluorescein). For purifications, product was collected in 500 µL fractions in MASTERBLOCK 96-well deep well microplates (Greiner Bio-One). Fractions were not collected for analytical SEC.

2.4.9. Determination of protein concentration

Protein concentration (M) was determined by spectrophotometric analysis at 280 nm of the protein, using a molar extinction coefficient (ε) provided by the ProtParam tool (ExPASy; http://web.expasy.org/protparam/), and calculated using the following formula:

$$[\text{Protein}] = \frac{A_{280}}{\varepsilon}$$

Where proteins were labelled, [protein] and labelling efficiency were determined by spectrophotometry at 280 nm (protein) and the absorption maximum for the relevant dye, using the following formulae (information obtained from Thermo Scientific; https://tools.thermofisher.com/content/sfs/brochures/TR0031-Calc-FP-ratios.pdf):

$$[\text{Protein}] = \frac{A_{280} - A_{max} \times CF}{\varepsilon}\ ;\quad \text{dye:protein ratio} = \frac{A_{max}}{\varepsilon' \times [\text{protein}]}$$

A_{280} = absorbance at 280 nm, A_{max} = absorbance at absorption maximum of the dye, ε = protein molar extinction coefficient, ε′ = dye molar extinction coefficient, CF = correction factor (specific to the dye).

2.4.10. SDS-PAGE

Gels of 12% (*w/v*) acrylamide (37.5:1 acrylamide:bis-acrylamide) were prepared. Protein samples were mixed with loading buffer prior to sample loading, and the gels run at 180 V in running buffer. Gels were stained with Instant Blue until protein bands were clearly visible, background staining removed with water, and visualised by transillumination using the gel documentation system, except for visualisation of fluorescent protein labelling, when they were visualised by UV illumination prior to staining.

2.4.11. SrtA-mediated protein labelling

The protein containing an N-terminal poly-Gly motif was incubated with 3 eq depsipeptide in the presence of 20 mol% SrtA at 37 °C with agitation (200 rpm). Where fluorophores were present, the reaction was undertaken in darkness. The reaction was quenched after 3 h by flash freezing at -196 °C.

2.4.12. Isothermal titration calorimetry

ITC was carried out using a MicroCal iTC200 System (GE Healthcare Life Sciences). A total of 202.8 μL protein was loaded into the sample cell, and 38.5 μL ligand added into the sample cell over 20 injections; 1 × 0.5 μL over a duration of 1 s, 19 × 2 μL over a duration of 4 s, with 120 s recovery between injections. Buffers were matched prior to ITC by dialysis. Titrations of buffer into buffer and ligand into buffer were carried out as controls. Data was fitted using NITPIC[229], thermodynamic parameters calculated using SEDPHAT, and presented using GUSSI (NIH).

2.4.13. Cell culture experimentation

2.4.13.1. Passage of cells: Cells were grown in DMEM (containing 4500 mg L^{-1} glucose, L-glutamine, sodium pyruvate, sodium bicarbonate and pyridoxine; Sigma Aldrich) containing 10% (*v/v*) foetal bovine serum (FBS; Lonza) and 250 U mL^{-1} (each) penicillin/streptomycin (pen/strep; Lonza) in T-75 cell culture flasks (Sarstedt) at 37 °C with 5% CO_2. Once cells had reached approximately 90% confluency, growth medium was removed and the cells washed with 10 mL PBS. Cells were detached from the flask surface by treatment with 2 mL trypsin (0.25% *w/v*) at 37 °C with 5% CO_2 for 5 min, and the trypsin deactivated by addition of 8 mL fresh DMEM + FBS/pen/strep. This was removed, leaving the desired volume in the flask, and 12 mL fresh DMEM + FBS/pen/strep was added. Cells were then grown at 37 °C with 5% CO_2.

2.4.13.2. Cell seeding: During passage, unused cells were retained for seeding. Cells were counted in a 10 μL sample of the suspension using a BS1000 Improved Neubauer haemocytometer (Hawksley) and the number multiplied by 10^4 to determine the number of cells mL^{-1} suspension. The relevant volume of cell suspension was added to DMEM + FBS/pen/strep in the concentration and volume required by the plate in use (see table 2.3), with glass coverslips if required. These were incubated at 37 °C with 5% CO_2.

Plate size	Cells seeded per well	DMEM volume per well (mL)
12-well	1.2×10^5	1.0
24-well	8.0×10^4	0.5
96-well	1.0×10^4	0.1

Table 2.3. Cell seeding number and media volume for tissue culture experiments

2.4.13.3. Liposomal transfection: At cell confluency of approximately 50%, growth medium was removed, cells were washed with 1 mL PBS, and fresh serum-free minimum essential medium (Opti-MEM; containing L-pyruvate; Gibco) was added. Per 1 mL to be transfected, 1 µL NanoJuice core transfection reagent and 1.5 µL NanoJuice booster transfection reagent were mixed in 40 µL Opti-MEM and incubated for 5 min at room temperature. DNA (500 ng) was added to the reagent, which was incubated for 15 min at room temperature before cell treatment. Transfecting cells were incubated for 4 h at 37 °C with 5% CO_2, before media containing transfection reagent was removed. Cells were washed with 1 mL PBS, and fresh DMEM + FBS/pen/strep was added. Cells were then incubated for 20 h at 37 °C with 5% CO_2 prior to fixation.

2.4.13.4. Treatment of cells with protein: At cell confluency of approximately 60-80%, growth medium was removed, cells were washed with 1 mL PBS, and fresh DMEM + FBS/pen/strep added. The protein being tested was added to the desired concentration, and the plate was incubated for the desired time of the experiment at 37 °C with 5% CO_2.

2.4.13.5. Cell fixation: Growth medium was removed and cells washed with 2 × 1 mL PBS, before fixation by treatment with 1 mL paraformaldehyde (4% *v/v*) in PBS for 10 min at room temperature. Cells were washed with 2 × 1 mL PBS and stored short-term in PBS at 4 °C prior to further treatment.

2.4.13.6. Fluorescence in situ hybridization (FISH): Where this technique was required in addition to immunofluorescence, it was performed prior to antibody staining due to the harsh nature of the hybridization buffer. Cell membranes were permeabilised with 0.5 mL Triton-X 100 (0.5% *v/v*) in PBS for 5 min at room temperature. Cells were washed twice with 1 mL PBS and once with 1 mL 2 × SSC buffer for 10 min at room temperature. Cells were treated with 500 µL fluorescent oligonucleotide probe (bis-rhodamine complement RNA; 250 µg mL^{-1}) in ULTRAhyb Ultrasensitive hybridization buffer (Ambion) at 42 °C for 20 h. Cells were washed twice with 2 × SSC buffer, once with 0.5 × SSC buffer and once with PBS for 10 min at room temperature, and stored short-term in PBS at 4 °C.

2.4.13.7. Antibody staining: Cell membranes were permeabilised with 0.5 mL Triton-X 100 (0.5% *v/v*) in PBS for 5 min at room temperature. Cells were washed with 3 × 1 mL PBS for 5 min at room temperature, and non-specific protein binding was blocked by treatment with blocking buffer (1% BSA (*w/v*), 300 mM glycine in PBST) for 1 h at room temperature. Blocking buffer was removed and cells treated with primary antibody diluted in 1% (*w/v*) BSA in PBST at 4 °C overnight. Cells were washed with 3 × 1 mL PBS for 5 min and treated with secondary antibody diluted in 1% (*w/v*) BSA in PBST for 1 h at room temperature. Antibody details and staining conditions are described in table 2.4.

Primary antibodies

Recognises	Species	Supplier	Dilution	Incubation time	Incubation temperature (°C)
CTB	Rabbit	Sigma Aldrich (C3062)	10,000	Overnight	4
RCAS1 (Golgi)	Rabbit	Cell Signalling Technology (D2B6N)	100	Overnight	4
PDI (ER)	Rabbit	Cell Signalling Technology (C81H6)	100	Overnight	4
Calnexin (ER)	Rabbit	Cell Signalling Technology (C5C9)	50	Overnight	4
LAMP1 (lysosome)	Rabbit	Cell Signalling Technology (D2D11)	100	Overnight	4

Secondary antibodies

Recognises	Species	Supplier	Conjugate dye	Dilution	Incubation time (h)	Incubation temperature
Rabbit (CTB)	Donkey	Invitrogen (A-21206)	Alexa Fluor 488	1000	1	Room
Rabbit (CTB)	Donkey	Invitrogen (A-31572)	Alexa Fluor 555	1000	1	Room
Rabbit (organelle markers)	Goat	Invitrogen (A-11034)	Alexa Fluor 488	500	1	Room
Rabbit (organelle markers)	Chicken	Invitrogen (A-21442)	Alexa Fluor 594	500	1	Room

Table 2.4. Antibody details and staining conditions for fixed cells

2.4.13.8. Slide preparation: Coverslips were mounted on microscope slides using 12 µL (12-well plate) or 6 µL (24 –well plate) ProLong Gold antifade mountant with DAPI (Invitrogen), set overnight in darkness at room temperature, and sealed with nail varnish.

2.4.13.9. Visualisation by confocal microscopy: Mounted cells were visualised with an Axio Imager Z2 LSM880 upright confocal microscope (Zeiss) equipped with Diode 405 m, Argon 458/488/514 nm, DPSS 561 nm and HeNe 633 nm lasers and a GaAsp detector with fully tunable emission detection. Emission filter parameters for multiple fluorophore imaging were designed using the Fluorescence SpectraViewer tool (Thermo Scientific). Images were processed using Zen lite 2.3 software (Zeiss).

2.4.13.10. MTT cell viability assay: Cells were seeded in 96-well plates at 1×10^4 cells per well in 100 µL DMEM + FBS/pen/strep, and incubated overnight at 37 °C with 5% CO_2. Growth medium was removed and the cells were treated with the desired molecule or protein in 100 µL DMEM + FBS/pen/strep for the desired time at 37 °C with 5% CO_2. Growth medium was removed and 100 µL 3-(4,5-dimethylthiazol-2-yl)-2,5-diphenyltetrazolium bromide (MTT; 1 mg mL^{-1}) in Opti-MEM was added per well. The cells were incubated at 37 °C with 5% CO_2 in darkness for 30 min. MTT reagent was discarded, and 100 µL DMSO was added for 10 min with agitation (60 rpm) at room temperature to dissolve the insoluble violet crystals formed due to reduction of the MTT reagent. Assay results were taken by absorbance at 570 nm using a PowerWave XS2 plate reader (BioTek Instruments) run with Gen5 version 1.07 software (BioTek Instruments). Experiments were conducted in triplicate, with wells containing no cells used as a blank, 2 µM staurosporine used as the cell death control and mock treated cells used as the positive viability control.

2.4.14. Oligonucleotide synthesis

Oligonucleotides were synthesised by solid phase synthesis using an AKTA Oligopilot Plus 10 (GE Healthcare). Synthesis was begun with an Oligosynt 2′-OMe RNA 30 column (minimum 30 µM scale; GE Healthcare) of the relevant base. Removal of the 5′ monomethoxytrityl (MMT) protecting group was performed by treatment with dichloroacetic acid (3% *v/v*) in toluene, leaving a free 5′ hydroxyl group. Three equivalents of the relevant nucleoside phosphoramidite (Thermo Scientific) in acetonitrile was added; either 2′-OMe A phosphoramidite (Bz protecting group), 2′-OMe C phosphoramidite (Ac protecting group), 2′-OMe G phosphoramidite (iBu protecting group) or 2′-OMe U phosphoramidite. These nucleoside phosphoramidites were activated using 0.5 M 5-ethylthio-1H-tetrazole in acetonitrile and coupled to the previous

nucleoside phosphoramidite for 15 min, forming a phosphite triester linkage. Sulfation of the phosphate moiety to form a phosphorothioate was carried out using 0.2 M phenylacetyl disulfide in 3-methylpyridine/acetonitrile (1:1 (*v/v*)), before the unreacted OH groups were capped using a mixture of N-methylimidazole (20% (*v/v*)) in acetonitrile, acetic anhydride (40% (*v/v*)) in acetonitrile and 2,6-lutidine (60% (*v/v*)) in acetonitrile, in order to prevent erroneous sequence elongation. Between each step, the solid support was washed with diethylamine/acetonitrile (20:80 (*v/v*)). Following synthesis, an amino amidite (5′-MMT-amino-modifier C6-CE phosphoramidite; Link Technologies) was reacted with the final nucleoside phosphoramidite.

2.4.15. Oligonucleotide extraction and purification

2.4.15.1. Resin cleavage: The synthesised oligonucleotides were cleaved from the solid support and side-chain deprotected with saturated aqueous ammonia overnight at 55 °C. Crude oligonucleotide was removed from the column by cooling to 4 °C and washing with 50% aqueous EtOH (20mL) followed by water (10 mL).

2.4.1.2. Trityl deprotection: The aqueous ammonia and EtOH mixture from resin cleavage was removed by evaporation under reduced pressure. Aqueous acetic acid (2% (*v/v*)) was added to remove the 5′-MMT protecting group, and the reaction followed by HPLC to completion.

2.4.15.3. Purification: The deprotected oligonucleotide solution was basified with 2 M NaOH to pH > 7. Oligonucleotides were purified by ion exchange using an AKTA Purifier with a HiScale 16 anion exchange column (GE Healthcare) and eluted with a basic NaCl gradient up to 3 M. Oligonucleotides were then desalted using an AKTA purifier with a HiScale 50 gel filtration column (GE Healthcare) and lyophilised with a ModulyoD freeze dryer (Thermo Scientific).

2.4.15.4. Analysis: Oligonucleotides were dissolved in 15 mM aqueous hexyl ammonium acetate (HAA) and analysed for purity with an Agilent 1100 series HPLC system (Agilent Technologies) and identity confirmed by LC-MS with a Finnigan LTQ mass spectrometer (Thermo Scientific).

2.4.16. Temperature-resolved spectrophotometry of oligonucleotides

Oligonucleotides to be tested were mixed in equimolar concentrations in water, denatured at 95 °C for 30 s and cooled to room temperature to ensure full annealing. The A_{260} of the samples was recorded every 1 min as they were heated from 10-80 °C, at a rate of 0.2 °C min^{-1}, using a Cary series UV-Vis spectrophotometer (Agilent Technologies).

2.4.17. Labelling protein with oligonucleotides

2.4.17.1. Labelling by SPAAC: Where duplex oligonucleotides were required, the 5′-azido oligonucleotide to be conjugated was first incubated with the oligonucleotide to be hybridised in HEPES buffer at 95 °C for 30 s and cooled to room temperature. The CTB variant to be labelled, functionalised with a BCN-depsipeptide (labelled by SrtA-mediated ligation as described in section 2.3.11), was incubated with an excess of 5′-azido-nucleotide overnight at room temperature in HEPES buffer, and the reaction quenched by flash freezing at -196 °C. Where fluorophores were present, the reaction was undertaken in darkness.

2.4.17.2. Labelling by disulfide formation: The Cys-containing CTB variant to be labelled was incubated in HEPES buffer with an excess of 5′-pyridylthio oligonucleotide for 2 h at room temperature, and the reaction quenched by flash freezing at -196 °C.

2.4.18. Determination of oligonucleotide-labelled protein concentration

The concentration of purified protein labelled with the fluorescent dsRNA was determined spectrophotometrically. As the absorbance at 494 nm is not affected by either the RNA or the protein and is caused by fluorescein only, concentration of the fluorescein was determined using the A_{494} and $\varepsilon = 68{,}000\ M^{-1}\ cm^{-1}$ (Thermo Scientific). This was assumed equal to the concentration of dsRNA. An A_{260} value of 1 = 3.47 μM dsRNA for the specific sequence and modifications of the dsRNA used (OligoCalc), which allowed the A_{260} due to RNA to be determined. Using correction factors of 0.3 for the fluorescein group (Thermo Scientific) and 0.51 for the RNA (determined experimentally) and subtracting these values from the A_{280}, the A_{280} value related to the protein was determined. Protein concentration and labelling efficiency was then calculated (as described in section 2.4.9). Where the RNA-labelled protein did not contain a fluorophore, concentration was determined by densitometry, performed using Quantity One 1-D analysis software (Bio-Rad), of SDS-PAGE Coomassie-stained bands compared to standards of a known concentration.

2.5. Synthetic experimental

2.5.1. 5′-fluorescein skipper RNA synthesis

2.5.1.1. Oligonucleotide synthesis

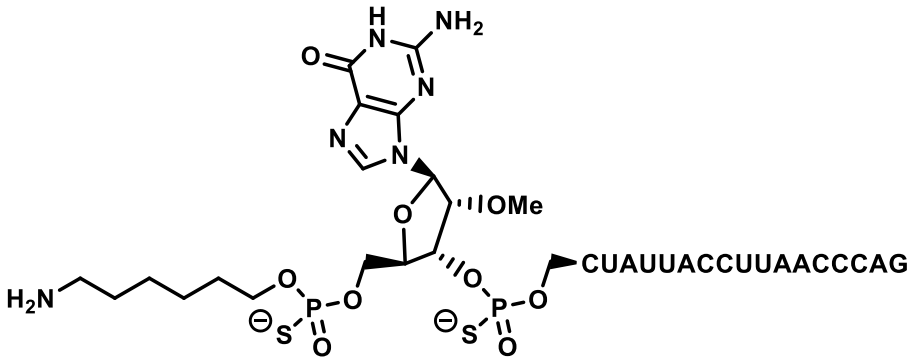

A 2′-OMe phosphorothioate oligonucleotide with a 5′-amino modifier, of sequence 5′-H_2N-GCUAUUACCUUAACCCAG-3′, was synthesised by solid phase synthesis (section 2.4.14). The crude product was removed from the resin, deprotected, purified by ion exchange and desalted (section 2.4.15). The 5′-amino skipper RNA was isolated as a white solid lyophilisate (58 mg, 25% yield). Purity was determined as 96% by HPLC. Identity was confirmed by LC-MS, with a detected mass of 6357.4 Da (6357.2 Da expected).

2.5.1.2. Fluorescein conjugation

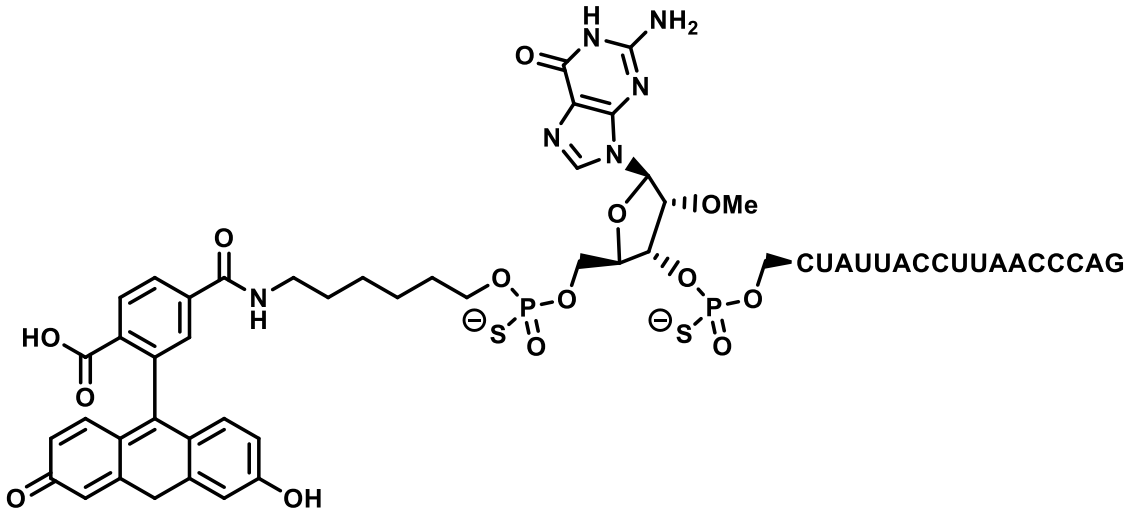

The 5′-amino skipper RNA (21 mg, 1.3 mM, 2.3 mL total reaction volume) was reacted with 6-carboxyfluorescein NHS ester (5 mg, 3.4 eq) in 0.1 M phosphate buffer with 25% (*v/v*) DMSO (pH 8.5) for 1 h at room temperature. The crude product was purified by desalting. The 5′-fluorescein skipper RNA was isolated as a yellow lyophilisate (19 mg,

86% yield). Purity was determined as 94% by HPLC. Identity was confirmed by LC-MS, with a detected mass of 6716.0 Da (6715.5 Da expected).

2.5.2. 5′-azido complement RNA synthesis

2.5.2.1. Oligonucleotide synthesis

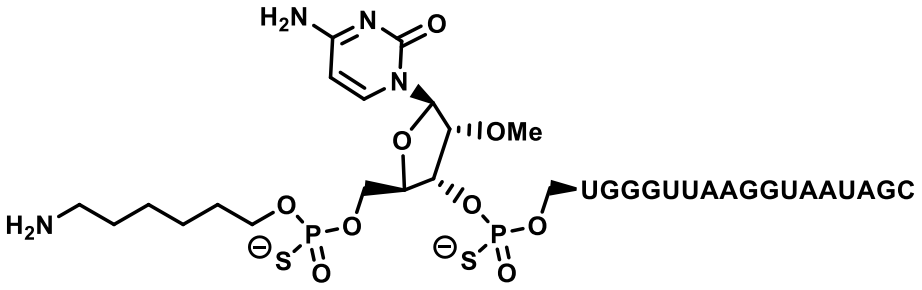

A 2′-OMe phosphorothioate oligonucleotide with a 5′-amino modifier, of sequence 5′-H_2N-CUGGGUUAAGGUAAUAGC-3′ was synthesised by solid phase synthesis (section 2.4.14) The crude product was removed from the resin, deprotected, purified by ion exchange and desalted (section 2.4.15). The 5′-amino complement RNA was isolated as a white solid lyophilisate (42 mg, 20% yield). Purity was determined as 96% by HPLC. Identity was confirmed by LC-MS, with a detected mass of 6516.4 Da (6517.3 Da expected).

2.5.2.2. Azide conjugation

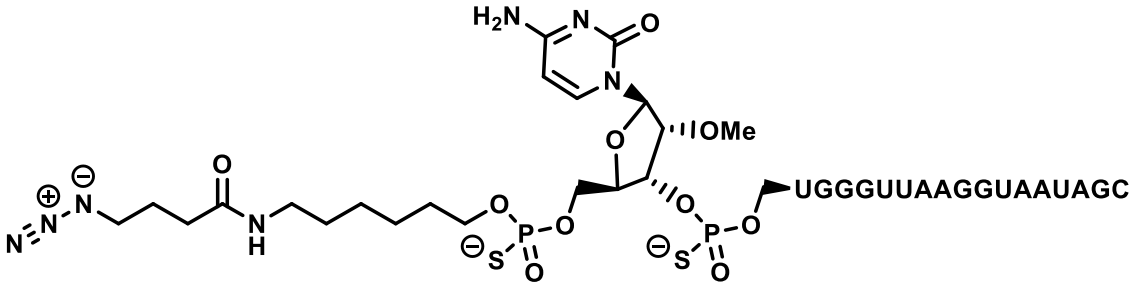

The 5′-amino complement RNA (21 mg, 1.3 mM, 2.3 mL total reaction volume) was stirred with azidobutyrate NHS ester (3.4 mg, 5 eq) in 0.1 M phosphate buffer with 25% (*v/v*) DMSO (pH 8.5) for 1 h at room temperature. The crude product was purified by desalting. The 5′-azido complement RNA was isolated as a white solid lyophilisate (18 mg, 84% yield). Purity was determined as 94% by HPLC. Identity was confirmed by LC-MS, with a detected mass of 6627.8 Da (6628.4 Da expected).

2.5.3. 5′-pyridylthio skipper RNA synthesis

2.5.3.1. Oligonucleotide synthesis

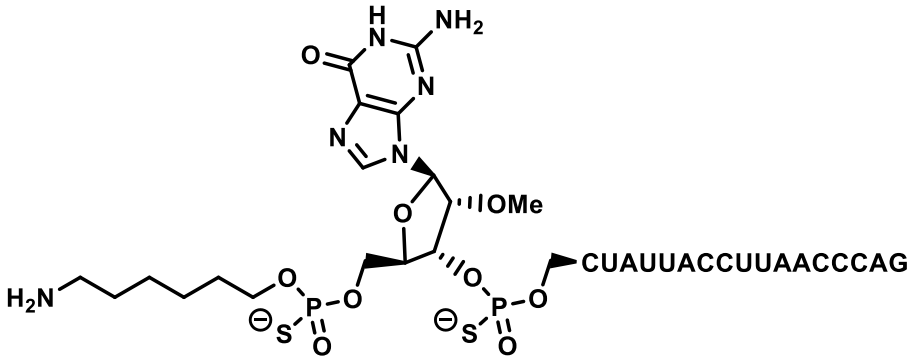

A 2′-OMe phosphorothioate oligonucleotide with a 5′-amino modifier, of sequence 5′-H_2N-GCUAUUACCUUAACCCAG-3′, was synthesised by solid phase synthesis (section 2.4.14). The crude product was removed from the resin, deprotected, purified by ion exchange and desalted (section 2.4.15). The 5′-amino skipper RNA was isolated as a white solid lyophilisate (85 mg, 42% yield). Purity was determined as 96% by HPLC. Identity was confirmed by LC-MS, with a detected mass of 6356.8 Da (6357.2 Da expected).

2.5.3.2. Pyridylthio conjugation

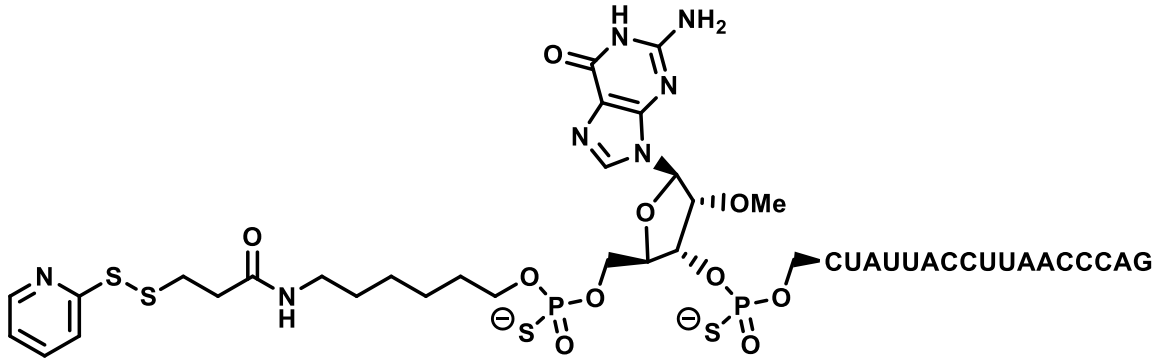

The 5′-amino skipper RNA (15 mg, 1.1 mM, 2 mL total reaction volume) was stirred with 3-(2-pyridyldithio)propionic acid NHS ester (2.1 mg, 3 eq) in 0.1 M phosphate buffer with 10% (*v/v*) DMSO (pH 8.5) for 1 h at room temperature. The crude product was purified by desalting. The 5′-pyridylthio skipper RNA was isolated as a white solid lyophilisate (13 mg, 86% yield). Purity was determined as 87% by HPLC. Identity was confirmed by LC-MS, with a detected mass of 6553.6 Da (6554.5 Da expected), and 6444.7 Da (6445.3 Da expected) on reduction with 5 mM DTT.

2.5.4. Bis-fluorescein complement RNA synthesis

2.5.4.1. Oligonucleotide synthesis

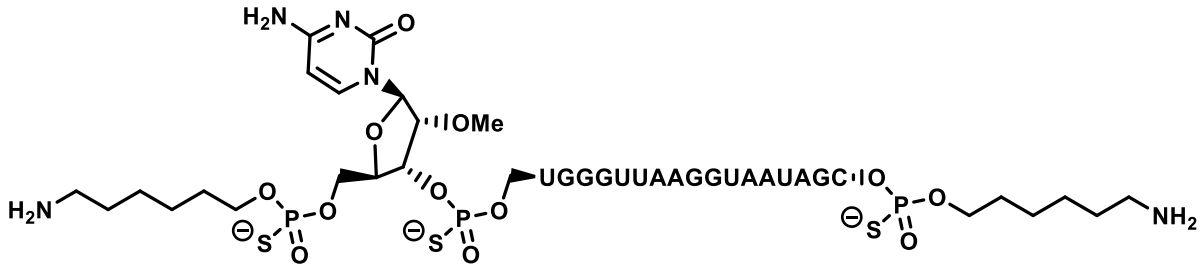

A 2′-OMe phosphorothioate oligonucleotide with 5′- and 3′-amino modifiers, of sequence 5′-H_2N-CUGGGUUAAGGUAAUAGC-NH_2-3′, was synthesised by solid phase synthesis (section 2.4.14). The crude product was removed from the resin, deprotected, purified by ion exchange and desalted (section 2.4.15). The bis-amino skipper RNA was isolated as a white solid lyophilisate (108 mg). Purity was determined as 76% by HPLC, deemed insufficient. The product was further purified by preparatory HPLC in 15 mM aqueous HAA, followed by ion exchange, and desalted. The bis-amino skipper RNA was isolated as a white solid lyophilisate (42 mg, 20% yield). Purity was determined as 99% by HPLC. Identity was confirmed by LC-MS, with a detected mass of 6356.8 Da (6357.2 Da expected).

2.5.4.2. Fluorescein conjugation

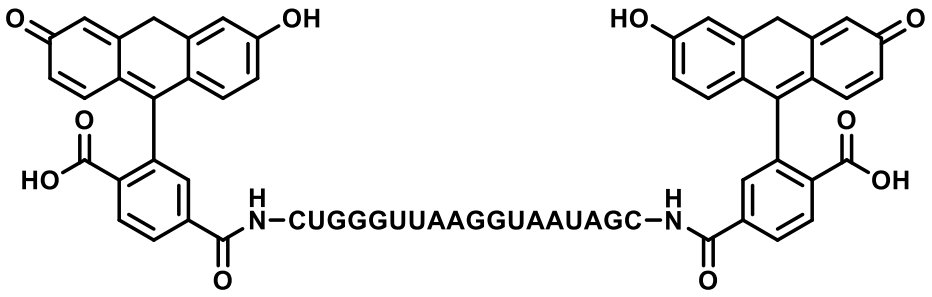

The bis-amino complement RNA (21 mg, 2.9 mM, 2 mL total reaction volume) was stirred in darkness with 6-carboxyfluorescein NHS ester (8.9 mg, 6 eq; 3 eq per NH_2) in 0.1 M phosphate buffer with 10% (*v/v*) DMSO (pH 8.5) for 1 h at room temperature. The crude product was purified by desalting. The bis-fluorescein complement RNA was isolated as a yellow solid lyophilisate (12 mg, 51% yield). Purity was determined as 83% by HPLC, with a further 9% identified as the mono-labelled species. Identity was confirmed by LC-MS, with a detected mass of 7428.7 Da (7429.1 Da expected), along with a minor species of 7070.2 Da (7070.8 Da expected).

2.5.5. Bis-rhodamine complement RNA synthesis

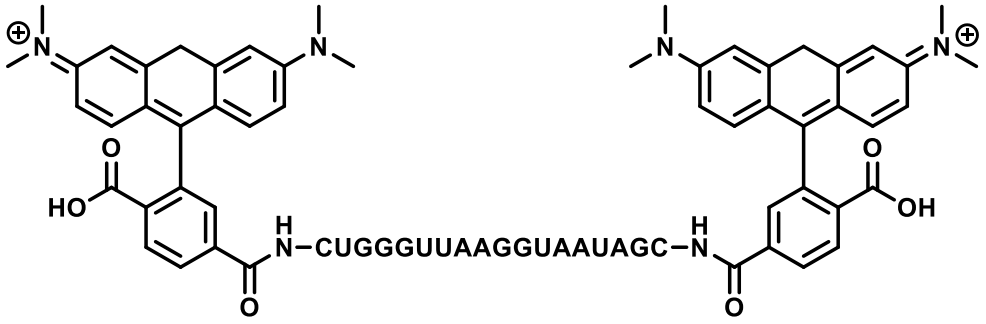

Bis-amino complement RNA (section 2.5.4; 21 mg, 2.9 mM, 2 mL total reaction volume) was stirred in darkness with 6-carboxytetramethylrhodamine NHS ester (9.9 mg, 6 eq; 3 eq per NH_2) in 0.1 M phosphate buffer with 10% (*v/v*) DMSO (pH 8.5) for 1 h at room temperature. The crude product was purified by desalting. The bis-rhodamine complement RNA was isolated as a purple solid lyophilisate (21 mg, 87% yield). Purity was determined as 93% by HPLC. Identity was confirmed by LC-MS, with a detected mass of 7536.7 Da (7539.4 Da expected).

2.5.6. 5′-azido 11mer complement RNA synthesis

2.5.6.1. Oligonucleotide synthesis

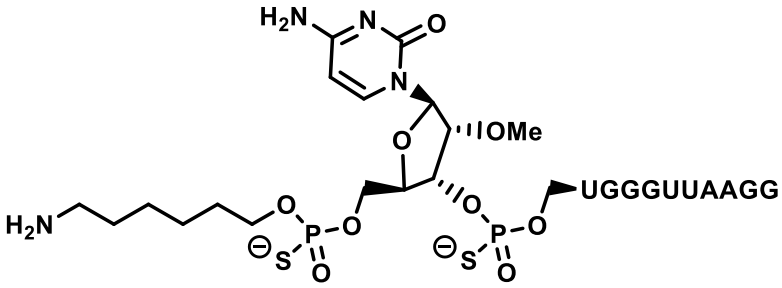

A 2′-OMe phosphorothioate oligonucleotide with a 5′-amino modifier, of sequence 5′-H_2N-CUGGGUUAAGG-3′, was synthesised by solid phase synthesis (section 2.4.14) The crude product was removed from the resin, deprotected, purified by ion exchange and desalted (section 2.4.15). The 5′-amino complement RNA was isolated as a white solid lyophilisate (48 mg, 37% yield). Purity was determined as 97% by HPLC. Identity was confirmed by LC-MS, with a detected mass of 4055.7 Da (4056.3 Da expected).

2.5.6.2. Azide conjugation

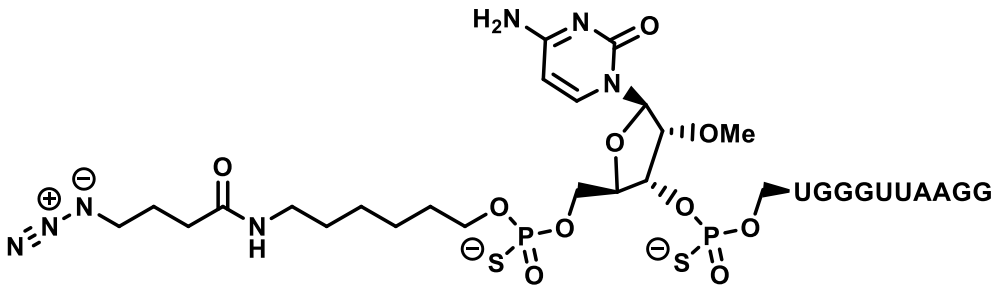

The 5′-amino 11mer complement RNA (35 mg, 4.1 mM, 2 mL reaction volume) was stirred with azidobutyrate NHS ester (5.6 mg, 3 eq) in 0.1 M phosphate buffer with 10% (*v/v*) DMSO (pH 8.5) for 1 h at room temperature. The crude product was purified by desalting. The 5′-azido 11mer complement RNA was isolated as a white solid lyophilisate (24 mg, 67% yield). Purity was determined as 94% by HPLC. Identity was confirmed by LC-MS, with a detected mass of 4167.0 Da (4167.4 Da expected).

2.5.7. 5′-azido complement RNA synthesis

2.5.7.1. Oligonucleotide synthesis

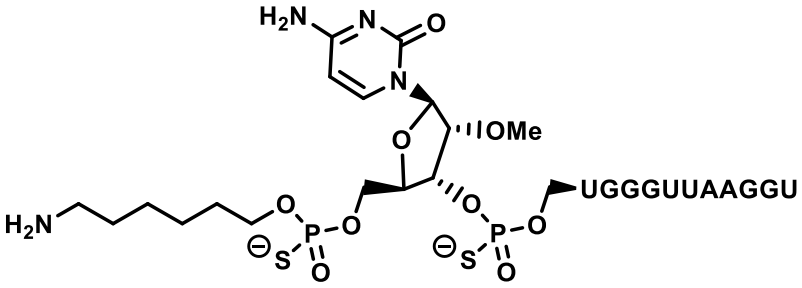

A 2′-OMe phosphorothioate oligonucleotide with a 5′-amino modifier, of sequence 5′-H_2N-CUGGGUUAAGGU-3′, was synthesised by solid phase synthesis (section 2.4.14) The crude product was removed from the resin, deprotected, purified by ion exchange and desalted (section 2.4.15). The 5′-amino complement RNA was isolated as a white solid lyophilisate (55 mg, 40% yield). Purity was determined as 97% by HPLC. Identity was confirmed by LC-MS, with a detected mass of 4392.0 Da (4392.6 Da expected).

2.5.7.2. Azide conjugation

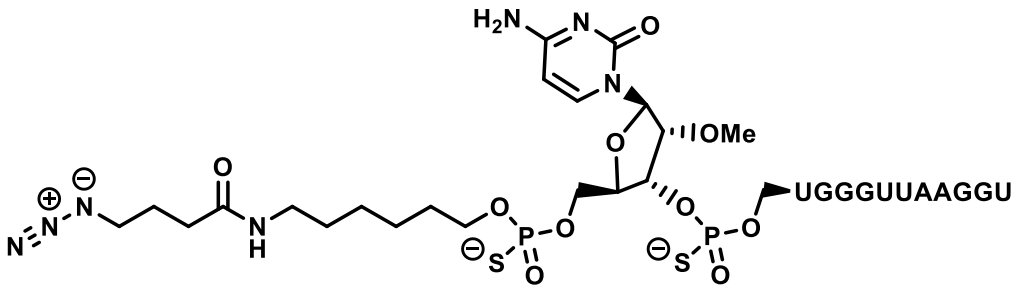

The 5′-amino 12mer complement RNA (40 mg, 4.3 mM, 2 mL reaction volume) was stirred with azidobutyrate NHS ester (5.6 mg, 3 eq) in 0.1 M phosphate buffer with 10% (*v/v*) DMSO (pH 8.5) for 1 h at room temperature. The crude product was purified by desalting. The 5′-azido 12mer complement RNA was isolated as a white solid lyophilisate (34 mg, 84% yield). Purity was determined as 97% by HPLC. Identity was confirmed by LC-MS, with a detected mass of 4503.0 Da (4503.7 Da expected).

2.5.8. 5′-azido 13mer complement RNA

2.5.8.1. Oligonucleotide synthesis

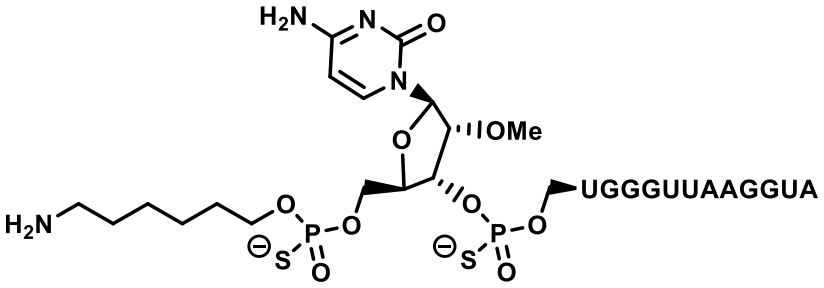

A 2′-OMe phosphorothioate oligonucleotide with a 5′-amino modifier, of sequence 5′-H_2N-CUGGGUUAAGGUA-3′, was synthesised by solid phase synthesis (section 2.4.14) The crude product was removed from the resin, deprotected, purified by ion exchange and desalted (section 2.4.15). The 5′-amino complement RNA was isolated as a white solid lyophilisate (38 mg, 25% yield). Purity was determined as 97% by HPLC. Identity was confirmed by LC-MS, with a detected mass of 4751.3 Da (4751.9 Da expected).

2.5.8.2. Azide conjugation

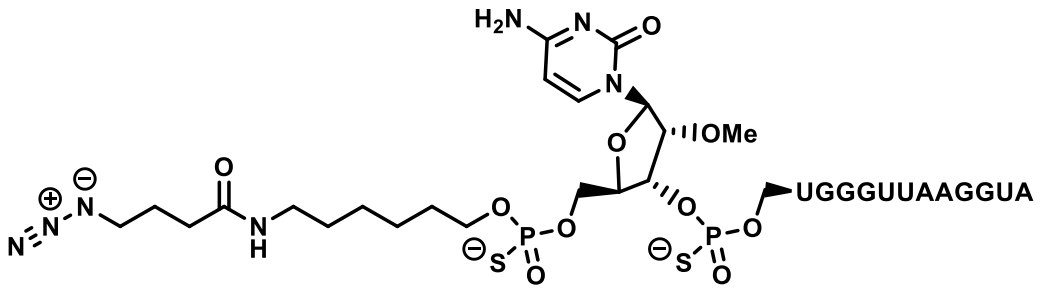

The 5′-amino 11mer complement RNA (30 mg, 3.0 mM, 2 mL reaction volume) was stirred with azidobutyrate NHS ester (4.1 mg, 3 eq) in 0.1 M phosphate buffer with 10% (*v/v*) DMSO (pH 8.5) for 1 h at room temperature. The crude product was purified by desalting. The 5′-azido 11mer complement RNA was isolated as a white solid lyophilisate (24 mg, 78% yield). Purity was determined as 93% by HPLC. Identity was confirmed by LC-MS, with a detected mass of 4862.7 Da (4863.0 Da expected).

2.5.9. 5′-BCN skipper RNA synthesis

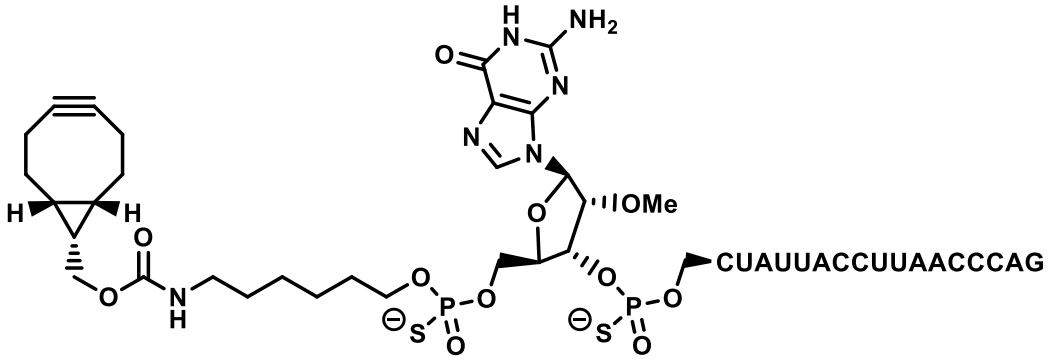

Previously synthesised 5′-amino skipper RNA (section 2.5.3; 70.5 mg, 3.4 mM, 3 mL total reaction volume) was stirred with bicyclonon-4-yn-9-ylmethyl N-succinimidyl carbonate (9.1 mg, 3 eq) in 0.1 M phosphate buffer with 10% (*v/v*) DMSO (pH 8.5) for 1 h at room temperature. The crude product was purified by desalting, and 113 mg product isolated of insufficient purity. The product was further purified by preparatory HPLC in 15 mM aqueous HAA, followed by ion exchange, and desalted. The 5′-BCN skipper RNA was isolated as a white solid lyophilisate (30 mg, 41% yield). Purity was determined as 92% by HPLC. Identity was confirmed by LC-MS, with a detected mass of 6533.0 Da (6533.4 Da expected).

2.5.10. 5′-peptide skipper RNA synthesis

Peptides for oligonucleotide conjugation were provided by Cambridge Research Biochemicals with standard amino acids except for an L-azidolysine (K(N_3)) at either the N-terminus or C-terminus for functionality.

2.5.10.1. CTApep-skipper RNA

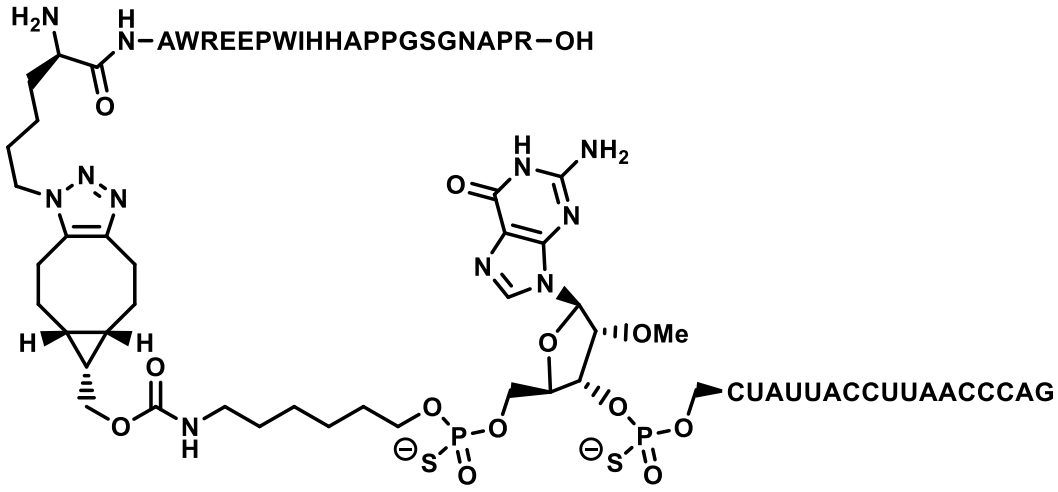

5′-BCN skipper RNA (section 2.5.8; 7.5 mg, 1.2 mM, 900 µL total reaction volume) was stirred with N-terminal K(N_3) modified peptide (3.1 mg, 1.2 eq), of sequence H_2N-K(N_3)-AWREEPWIHHAPPGSGNAPR-OH, in 0.1 M phosphate buffer with 10% (*v/v*) DMSO (pH 8.5) overnight at room temperature. The crude product was purified by desalting. The CTApep-skipper RNA was isolated as a white solid lyophilisate (8.7 mg, 87% yield). Purity was determined as 90% by HPLC. Identity was confirmed by LC-MS, with a detected mass of 8951.7 Da (8951.0 Da expected).

2.5.10.2. NLSpep-skipper RNA

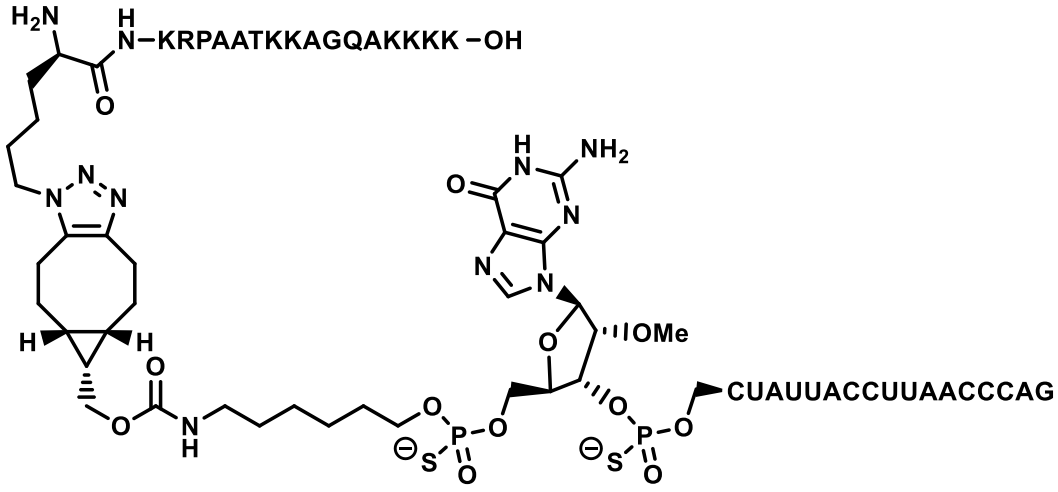

5′-BCN skipper RNA (section 2.5.8; 7.5 mg, 1.2 mM, 900 µL total reaction volume) was stirred with N-terminal K(N_3) modified peptide (2.5 mg, 1.2 eq), of sequence H_2N-K(N_3)-KRPAATKKAGQAKKKK-OH, in 0.1 M phosphate buffer with 10% (*v/v*) DMSO (pH 8.5) overnight at room temperature. The crude product was purified by desalting. The NLSpep-skipper RNA was isolated as a white solid lyophilisate (8.0 mg, 84% yield). Purity was unable to be determined by HPLC post-purification, although a pre-purification product purity of 82% was determined. Identity was confirmed by LC-MS, with single peak detected of mass of 8426.3 Da (8426.2 Da expected).

2.5.10.3. UNSpep-skipper RNA

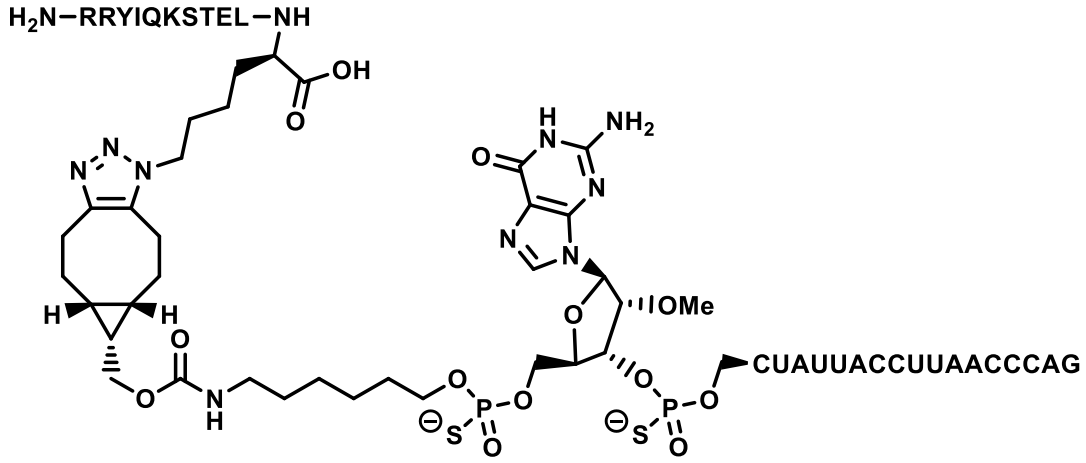

5′-BCN skipper RNA (section 2.5.8; 7.5 mg, 1.2 mM, 900 µL total reaction volume) was stirred with C-terminal K(N_3) modified peptide (1.9 mg, 1.2 eq), of sequence H_2N-RRYIQKSTEL-K(N_3)-OH, in 0.1 M phosphate buffer with 10% (*v/v*) DMSO (pH 8.5) overnight at room temperature. The crude product was purified by desalting. The UNSpep-skipper RNA was isolated as a white solid lyophilisate (8.1 mg, 89% yield). Purity was determined as 91% by HPLC. Identity was confirmed by LC-MS, with a detected mass of 7979.6 Da (7978.6 Da expected).

2.5.10.4. LACpep-skipper RNA

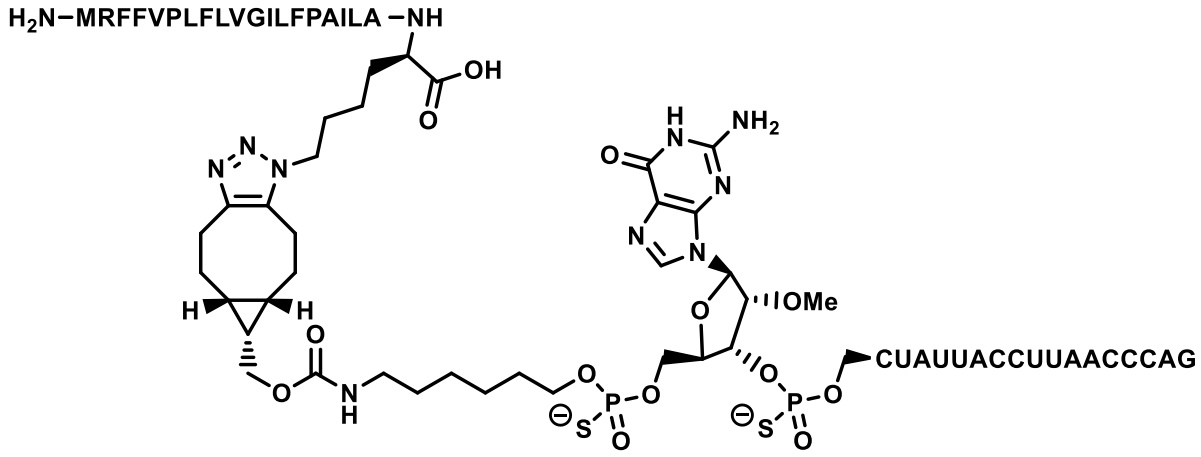

5′-BCN skipper RNA (section 2.5.8; 7.5 mg, 1.2 mM, 900 µL total reaction volume) was stirred with N-terminal K(N_3) modified peptide (3 mg, 1.2 eq), of sequence H_2N-MRFFVPLFLVGILFPAILA-K(N_3)-OH, in 0.1 M phosphate buffer with 10% (*v/v*) DMSO (pH 8.5) overnight at room temperature. The peptide did not fully dissolve under these conditions, and as a result the reaction was 30% complete as determined by HPLC. The reaction was allowed to proceed for 24 h at 40 °C with an additional 0.3 eq peptide and 720 µL DMSO (to 50% (*v/v*)). The reaction remained incomplete and the peptide still not fully dissolved, so an additional 945 µL DMSO (to 76% (*v/v*)) was added and the reaction allowed to proceed overnight at 40 °C to completion. The crude product was purified by desalting. The CTApep-skipper RNA was isolated as a white solid lyophilisate (8.4 mg, 84% yield). Purity was determined as 82% by HPLC. Identity was confirmed by LC-MS, with a detected mass of 8850.9 Da (8849.6 Da expected).

Chapter 3: Modification of CTB for cellular payload delivery

The suitability of CTB for use as a vector for targeted cellular delivery of macromolecules was investigated. Initially, the behaviour of the CTB in the absence of CTA was probed. This chapter outlines the design, production and purification of two CTB variants, both capable of site-specific labelling by SrtA-mediated ligation but with different organelle targeting. The labelling, characterisation and endocytic pathway of both are discussed.

3.1. Introduction

Functional CTB has previously been expressed and purified in the absence of CTA, primarily from various *E. coli* strains[18,88,91,230-233] and *Vibrio* species[234-239], along with examples in other bacteria including several *Lactobacillus* strains[240], *Bacillus brevis*[241] and *Brevibacillus choshinensis*[89]. Expression has even been reported in non-bacterial vectors including yeast[242], plant[243-245] and insect[246] cells. Yield estimates and were greatest from expression in *E. coli* and *Vibrio* cells, ranging from 1 mg[233] to 1.2 g[231] pure protein isolated per 1 L cultured cells, depending on the expression system. Protein was reported to have been isolated from whole cell lysate[18,91,230-233,235], periplasmic isolate[88,231] and growth medium[231,235-239], with the highest yields reported where protein was isolated from the growth medium. Taking into consideration yield, ease of handling and safety, CTB variants were expressed in *E. coli* cells and extracted and purified from the growth medium.

To test CTB as a potential drug delivery vector with the greatest level of control, a site-specific method of protein labelling was required. Several methods were considered and rejected. For example, the addition of a non-native Cys residue in a surface loop to be labelled with a maleimide was rejected due to the possibility of formation of non-native disulfide bonds with one of the other two Cys residues native to the protein. Genetic incorporation of non-canonical amino acids into CTB was also rejected on the grounds of reduced yield, increased complexity and possible structural destabilisation. Modification at either the N-terminus or C-terminus presented the most promising options, as both are

surface-exposed[22] and less likely to cause structural disruption than modification of an internal residue. However, previous C-terminal modifications have been shown to destabilise the pentameric quaternary structure[247], while N-terminal modifications have resulted in reduced GM1 binding[88], so in either case the resultant labelled protein would require careful characterisation to determine suitability.

Enzymatic labelling of CTB represents a generally specific, rapid and mild method for conjugation. Sortase A has been widely used to modify proteins. SrtA is a transpeptidase expressed by *Staphylococcus aureus* for the attachment of proteins to the cell wall[83,248-250]. The native enzyme recognises proteins containing the conserved amino acid sequence LPXTG (where X = any amino acid) and cleaves the peptide bond between the Thr and Gly, reversibly ligating the Thr to peptidoglycans bearing an N-terminal oligo-Gly[83,248-250] (figure 3.1). This procedure can be modified for recombinant protein modification, primarily to the C-terminus[45,82,107,251-258], though examples exist of N-terminal modification[82,107,258]. Common modifications include attachment of small molecules such as biotin[45,82,253,256,259] fluorophores[107,253,256,259] and azides[259]. Other examples include protein labelling with lipids[254,257], cholesterol[254] and PEG[252], protein-protein conjugation[82], and protein immobilisation to solid supports[251,252] and sensor chips[255]. In addition to *in vitro* labelling in solution, SrtA-mediated labelling has also been applied to complex cell lysates[253] and the surfaces of liposomes[257] and live cells[253,256,259], highlighting the versatility of the procedure. However, the common theme with all of these applications is that the reversible nature of the reaction renders labelling inefficient, requiring high SrtA concentrations and large reagent excesses to promote greater than 50% product formation.

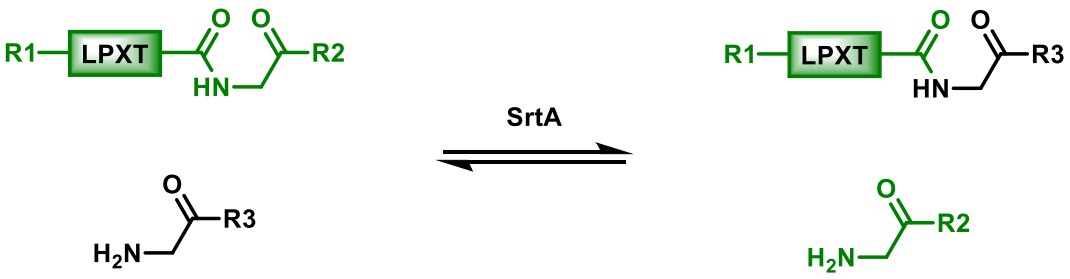

Figure 3.1. SrtA-mediated ligation Reaction scheme describing native SrtA-mediated ligation of a species bearing a LPXTG recognition motif (green; R1 = NH_2 or any amino acid, R2 = OH or any amino acid) to a species bearing an N-terminal Gly (black; R3 = any amino acid).

A number of attempts have been made to improve SrtA-mediated labelling efficiency. Dialysis has been used to remove the Gly cleaved by SrtA from the reaction, preventing its use as a substrate for the reverse reaction[260]. Replacing the terminal Gly of the SrtA recognition motif with a methyl ester results in the formation of methanol following cleavage, which does not act as a substrate for the reverse reaction[107]. The use of LPXTGGHG as a SrtA recognition motif results in the release of GGHG following cleavage, which can be sequestered using Ni^{2+} and prevented from participating in the reverse reaction[258]. However, while all of these methods improved labelling efficiency, they still required large excesses of reagent and high SrtA concentrations. The most successful method was developed recently, enabling efficient, site-specific labelling of an oligo-Gly motif at the N-terminus of proteins[261] (figure 3.1B). This method involves the use of a depsipeptide substrate, whereby the amide of the peptide bond between the Thr and Gly is replaced with an ester[261]. The product of the depsipeptide cleavage cannot act as a substrate for the reverse reaction as the lone pairs of the more electronegative oxygen atom are less readily available for nucleophilic attack of the Thr carbonyl, allowing near-quantitative labelling with relatively low reagent and SrtA concentrations[261]. This was chosen as the method for labelling CTB.

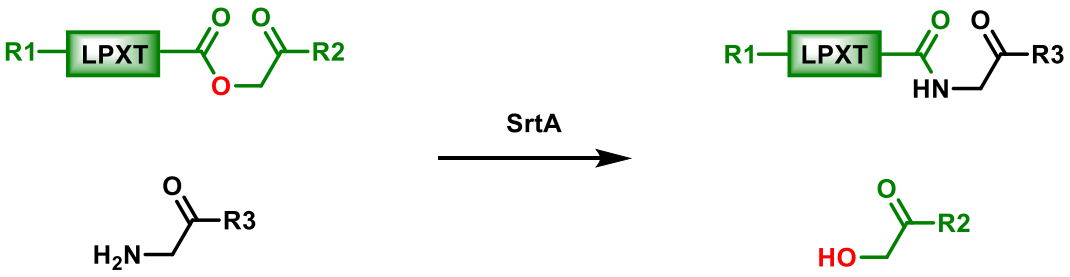

Figure 3.2. Efficient N-terminal SrtA-mediated ligation Reaction scheme describing efficient labelling of a species bearing an N-terminal Gly (black; R3 = any amino acid) with a depsipeptide containing the LPXTG SrtA recognition motif (green; R1 = NH_2 or any amino acid, R2 = OH or any amino acid).

3.2. Generation of a CTB variant for N-terminal labelling

3.2.1. Creation of an expression construct

Existing CTB expression constructs produce mature protein containing an N-terminal Ala or Thr residue. A variant of CTB was required which was compatible SrtA-mediated ligation. CTB containing an N-terminal tri-Gly has been shown to be readily labelled by SrtA[107]. A CTB variant was designed encoding an N-terminal tri-Gly (GGG) extension,

with 5′ SphI and 3′ PstI restriction sites for vector insertion, and the coding sequence produced by assembly PCR. A band was detected at approximately 350 bp, in good agreement with the expected fragment size (351 bp), along with minor impurities. The crude product was amplified and purified by PCR using the same terminal primers (figure 3.3A). The GGG-CTB insert was subcloned with SphI and PstI into the pSAB2.2 plasmid (J. Ross; figure 3.3B); derived from the commercially available pMAL-p5X plasmid, modified by addition of the CTB leader sequence for periplasmic expression and removal of the *MalE* gene coding for maltose binding protein. Successful cloning confirmed by DNA sequencing.

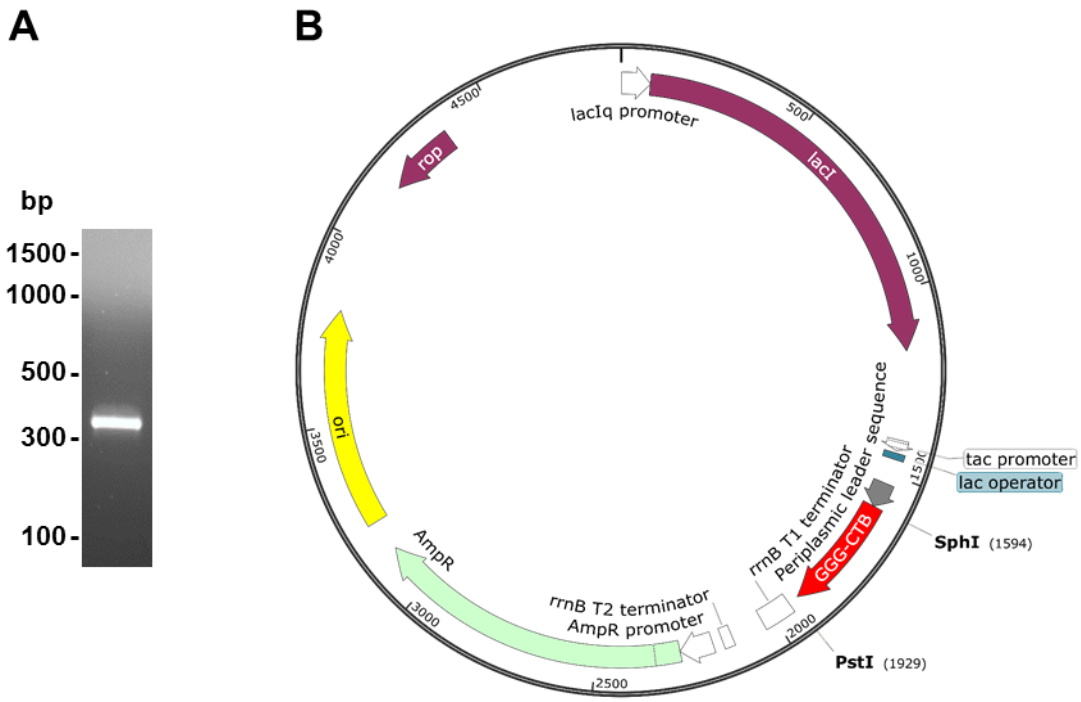

Figure 3.3. Production of a GGG-CTB expression vector A. Agarose gel analysis of the purified GGG-CTB coding sequence, produced by assembly PCR. B. Plasmid map of GGG-CTB (red) inserted into pSAB2.2, highlighting the leader sequence (grey), SphI and PstI restriction sites, and other important features of the plasmid. Plasmid map generated with SnapGene Viewer software version 3.1.4.

3.2.2. Protein expression and purification

GGG-CTB was expressed in *E. coli* C41(DE3) cells by IPTG induction at 25 °C overnight. The overexpressed protein was isolated from the growth medium by ammonium sulfate precipitation and purified by Ni^{2+} affinity chromatography. This method was chosen, despite the lack of a His-tag on the protein, as the surface-exposed His13 and His94 residues have been found to promote Ni^{2+} coordination[262], acting in a similar fashion to a His-tag in the pentameric protein to allow immobilisation[262]. CTB was identified by SDS-PAGE (figure 3.4A); the protein is sufficiently stable to remain pentameric under SDS-PAGE denaturing conditions, and required heating at 95 °C for denaturation and dissociation into the protomer. Interestingly, the GGG-CTB pentamer did not migrate consistent with its MW (~ 59 kDa). Intense protein bands of approximately 48 kDa appeared in the elution fractions, which were identified as CTB as they were replaced by a band of approximately 12 kDa on denaturation. This is presumably due to CTB remaining folded and relatively compact, therefore behaving like a denatured protein of lower molecular weight (MW). Remaining impurities following Ni^{2+} affinity chromatography were removed by SEC (figure 3.4B). The identity of the protein was confirmed by LC-MS; a protomer mass of 11814.0 Da was detected (11,813.8 Da calculated). Approximately 5 mg pure protein was isolated per 1 L cultured cells.

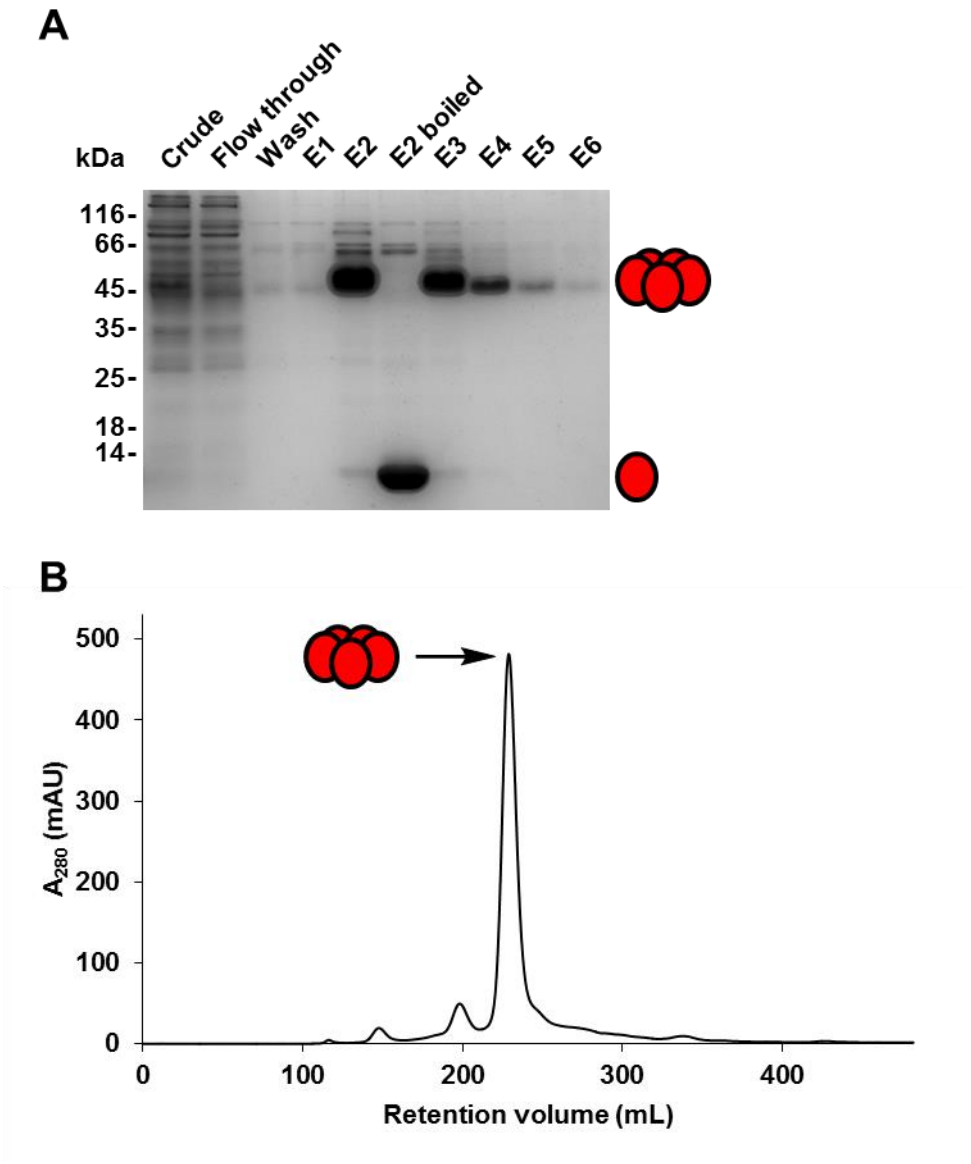

Figure 3.4. Purification and analysis of GGG-CTB A. SDS-PAGE analysis of GGG-CTB purification by Ni^{2+} affinity chromatography. GGG-CTB as pentamer and dissociated protomer are indicated. B. A_{280} trace from SEC purification of Ni^{2+}-purified GGG-CTB, with the desired protein peak indicated.

3.2.3. Site-specific labelling of GGG-CTB with fluorescein

CTB was labelled with a depsipeptide (LPEToGG; o represents the ester bond between residues) following the method developed by Williamson *et al.*[261] for efficient SrtA-mediated N-terminal labelling of proteins. The depsipeptide was modified at the Leu amine with a gamma-aminobutyric acid (GABA) linker conjugated to fluorescein isothiocyanate (FITC) (D. Williamson; figure 3.5).

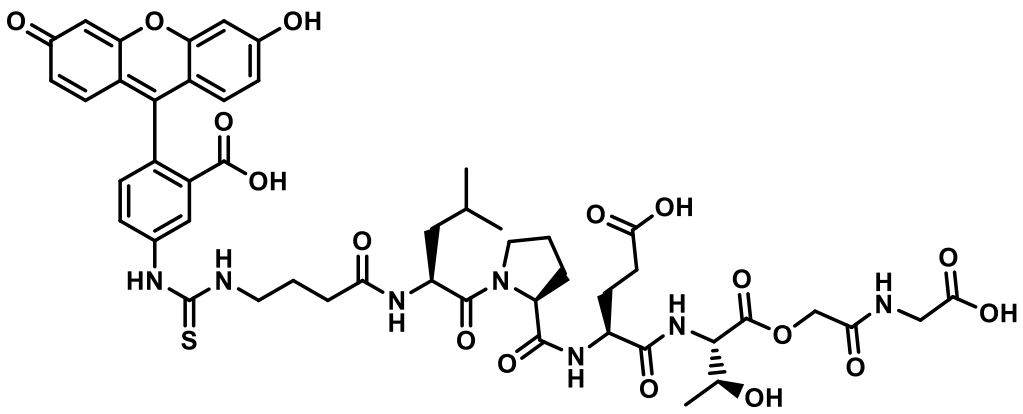

Figure 3.5. FITC-depsipeptide structure The LPEToGG depsipeptide substrate with FITC conjugated to the N-terminus via a GABA linker.

GGG-CTB (120 μM) in HEPES buffer was labelled with 3 eq FITC-depsipeptide with 20 mol% SrtA for 3 h at 37 °C. SDS-PAGE analysis (figure 3.6A) showed the pentamer split into two bands, both of increased MW compared to unlabelled CTB, following labelling. On denaturation, there was a clear shift of the protomer band (~ 14 kDa) compared to the unlabelled protomer (~ 12 kDa). Tellingly, fluorescent bands consistent with the increased MW bands appeared fluorescent under UV illumination following labelling, confirming the conjugation of FITC to the protein. FITC-CTB was purified by lactose affinity chromatography and concentrated, and successful labelling was confirmed by LC-MS (figure 3.6B), with a mass of 12728.4 Da detected (12729.4 Da calculated). Relative intensities of the denatured protein bands indicated labelling efficiency of approximately 90%, consistent with the LC-MS (figure 3.6B), where some unlabelled protein was detected in the FITC-CTB sample. Pure FITC-CTB was isolated at 77 μM (800 μL), giving 62% protein recovery and 56% yield of labelled protein.

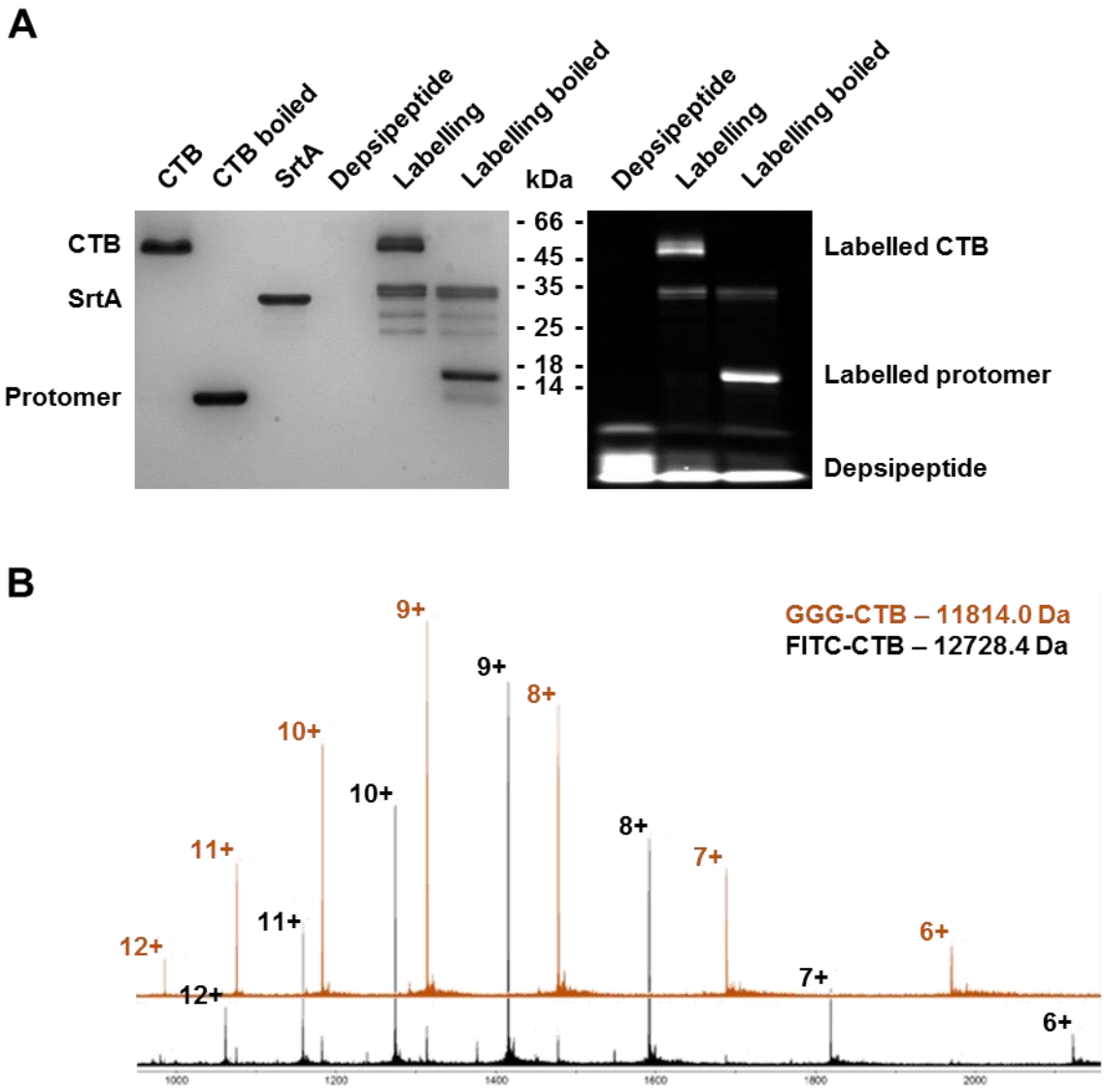

Figure 3.6. SrtA-mediated CTB labelling A. Coomassie-stained (left) and UV illuminated (right) SDS-PAGE analysis SrtA-mediated labelling of CTB with FITC-depsipeptide. B. Overlaid LC-MS comparing FITC-CTB (black) with unlabelled CTB (orange).

3.3. Functional characterisation of labelled CTB

3.3.1. Isothermal titration calorimetry to determine GM1 binding

Labelling of GGG-CTB with the FITC-depsipeptide generated a pentameric protein of which 90% of the protomers were extended by seven additional residues plus a relatively bulky, hydrophobic group. Moreover, these were attached to the N-terminus of CTB, which lies adjacent to the GM1 binding site, oriented towards the cell surface (figure 3.7). It was therefore possible labelling could have a detrimental effect on GM1 binding and endocytosis.

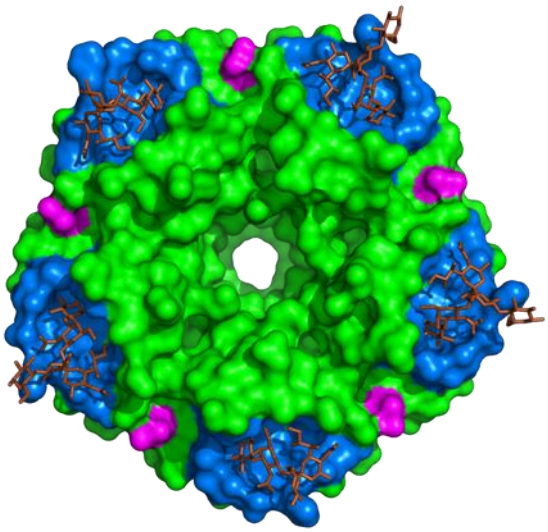

Figure 3.7. CTB N-termini CTB at 1.25 Å resolution, viewed from the binding face. The N-termini are shown in magenta, the binding sites in blue and GM1 oligosaccharide ligands in brown (PDB ref. 3CHB).

The affinity of FITC-CTB for GM1 was assayed by isothermal titration calorimetry (ITC). For solubility reasons, it was impractical to use GM1 ganglioside. The titration was therefore carried out using GM1 oligosaccharide (GM1os), in which the sphingosine and stearic acid tails had been enzymatically removed (T. Branson). GM1os was titrated against wt CTB, GGG-CTB and FITC-CTB (figure 3.8; data summarised in table 3.1). All three proteins bound GM1os with an approximate stoichiometry of 1 GM1os residue per binding site. While the N-terminal GGG extension had little effect on GM1os binding, N-terminal conjugation of the FITC-depsipeptide resulted in an approximate six-fold decrease in the affinity of CTB for GM1os. This was unsurprising, due to the position of the N-termini relative to the binding sites. The labels may have introduced steric hindrance, inhibiting GM1os access to the binding sites. Parts of the FITC-depsipeptide, particularly the hydrophobic fluorophore, may also have formed weak interactions with the exposed surface of the binding sites, inhibiting GM1os binding. Critically however, FITC-CTB retained a relatively high affinity for GM1os.

Protein	[Protein] (μM)	[GM1os] (μM)	K_d (nM)	N
wt CTB	12.5	90	60 ± 34	0.93 ± 0.02
GGG-CTB	12.5	90	90 ± 30	0.93 ± 0.02
FITC-CTB	5	50	358 ± 97	1.08 ± 0.03

Table 3.1. Summary of ITC to assay modified CTB binding to GM1os

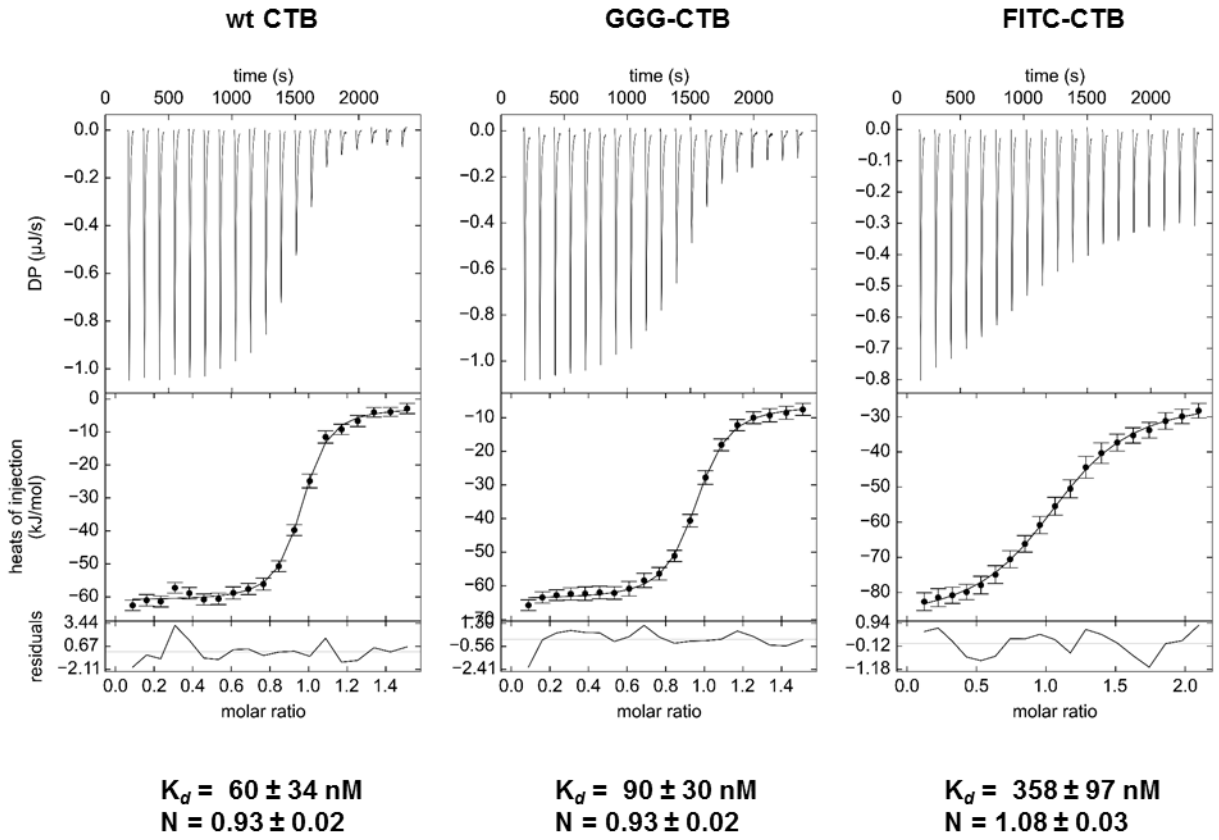

Figure 3.8. ITC of GM1os titrated into wt CTB, GGG-CTB and FITC-CTB Titration of GM1os into wt CTB (left), GGG-CTB (centre), and FITC-CTB (right). Each plot shows the baseline-adjusted raw thermogram (upper), the fitted integral data (middle) and the residual error of the fitting (lower).

It should be noted, however, that this is an imperfect model system for GM1-mediated cell binding. GM1 gangliosides are anchored in the cell membrane, with the oligosaccharide presented on the surface, and so are held in a single plane and orientation, while the GM1os used for ITC are in solution and tumble freely. Steric hindrance provided by the depsipeptide label could act as a barrier between the cell surface and the lower face of the protein, preventing the immobilised GM1 reaching the CTB binding sites, which ITC is unable to account for. Conversely, cell surface GM1 binding could increase the effective avidity, tethering CTB to the membrane and bringing the other binding sites into more favourable orientations for further binding in a pseudo-cooperative effect, which again ITC is unable to account for.

3.3.2. Cellular uptake of labelled CTB

Effective endocytosis of FITC-CTB into metazoan cells was assayed. Vero cells, isolated from the kidney of African green monkeys[263], were chosen for endocytosis trials. They are relatively easy to handle, requiring no specific special treatment[263], naturally display GM1 on their surface[264] and provide an adequate model for human cells due to the close relationship between humans and primates. Additionally, there are several examples of CT-based endocytosis experiments using Vero cells[72,264-266]. Initially, Vero cells were incubated with FITC-CTB (2 μg mL^{-1} protein) in DMEM at 37 °C with 5% CO_2 and fixed with PFA after 24 h. The cells were stained with a rabbit anti-CTB primary antibody (Ab) followed by an anti-rabbit Alexa Fluor (AF) 555-conjugated secondary Ab, to ensure the label remained attached to the protein post-transfection and thus FITC staining was consistent with protein location. The cells were mounted in ProLong Gold Antifade mounting reagent with DAPI, allowing nuclei detection, and viewed by laser scanning confocal microscopy (LSCM; figure 3.9). The FITC and AF555 stains showed excellent co-localisation, indicating FITC remained attached to CTB following endocytosis. No AF555 staining was detected in mock treated cells.

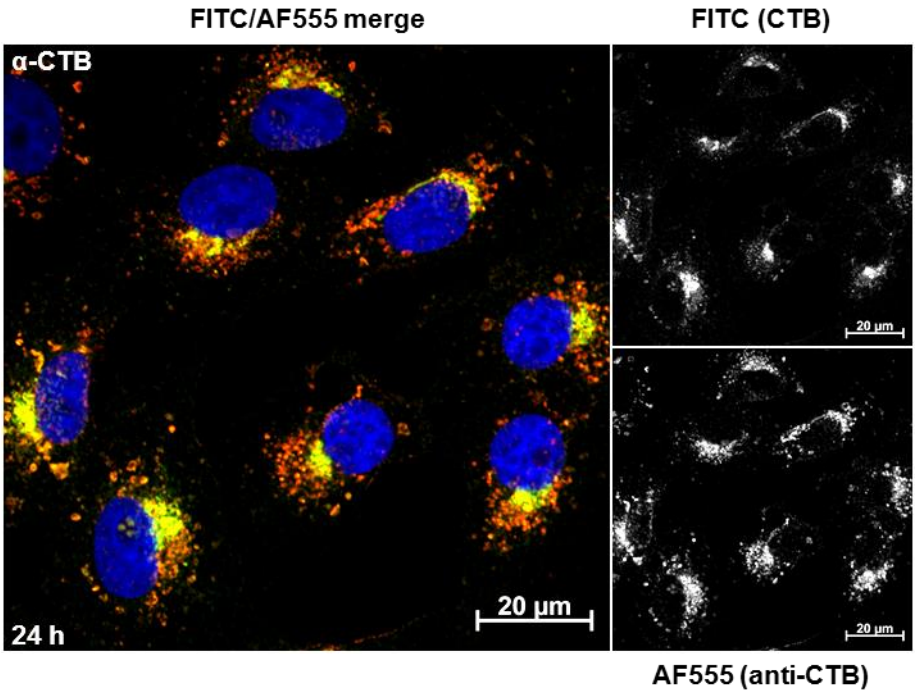

Figure 3.9. Vero cell incubation with FITC-CTB and anti-CTB co-staining LSCM imaging of Vero cells incubated with FITC-CTB (2 μg mL^{-1} protein), fixed after 2 h and stained with anti-CTB primary and AF594-conjugate secondary antibodies. The panel shows a false-colour merged image (left) of FITC (CTB; green), AF594 (α-CTB; red) and DAPI (nuclei; blue), in addition to individual green (FITC; upper right) and red (AF594; lower right) channels.

Subsequently, Vero cells were incubated with either FITC-CTB (2 μg mL^{-1} protein) or an equivalent concentration of FITC-depsipeptide under similar conditions over 24 h, and fixed after 15 min, 30 min, 1 h, 2 h, 6 h and 24 h. The cells were mounted in ProLong Gold Antifade mounting reagent with DAPI and viewed by LSCM (figure 3.10). FITC staining was undetectable in cells treated with the Depsipeptide, but was detectable within the cells treated with FITC-CTB at all time points. The staining was generally seen to become increasingly defined over time. This indicated the protein was not free in the cytosol, which would result in non-discrete, uniform staining across the cells, but was localised in organelles or other vesicular structures. From 1 h, the discrete foci spread throughout the cytoplasm decreased, with staining localised increasingly intensely to small, discrete clumps immediately adjacent to the nuclei, consistent with the morphology of the Golgi apparatus. After 24 h, staining with this morphology was almost exclusively detected.

To confirm the identity of the organelle, Vero cells were incubated with FITC-CTB (2 μg mL^{-1} protein) for 24 h and co-stained for RCAS1, a transmembrane protein localised to the Golgi with a role in protein glycosylation[267], with an anti-RCAS1 primary Ab to detect the Golgi apparatus. The primary Ab was stained with an AF594-conjugated secondary Ab, and mounted with DAPI. LSCM (figure 3.11) showed excellent morphological match and co-localisation between FITC-CTB and the Golgi, confirming localisation to this organelle over 24 h. These results are consistent with current knowledge of the CT retrograde transport. CTB would be expected to follow the native endocytic pathway of the holotoxin to the trans-Golgi[13,64], as the B subunit is exclusively responsible for GM1 binding and endocytosis[29,42]. However, as CTB lacks the KDEL ER retention sequence present on the CTA2 domain, it should not be targeted for retention in the ER, and would be expected to either build up in the Golgi or be degraded in the lysosome. The presence of intense, localised staining after 24 h, which had increased in intensity leading to that time point, indicated the former was occurring, with little evidence of lysosomal degradation.

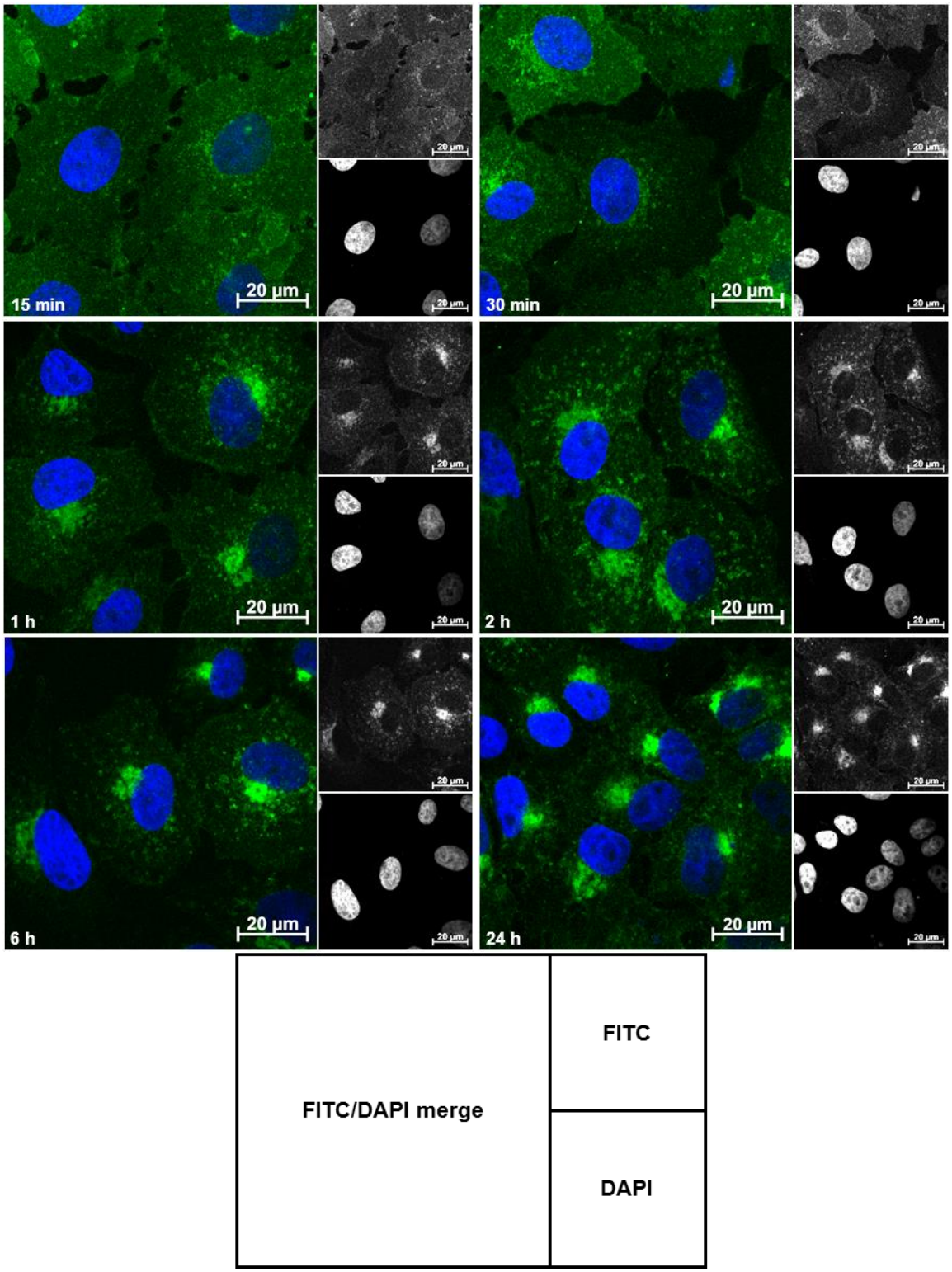

Figure 3.10. Time course of Vero cell incubation with FITC-CTB LSCM imaging of Vero cells incubated with FITC-CTB (2 µg mL^{-1} protein) and fixed after 15 min, 30 min, 1 h, 2 h, 6 h or 24 h. Each panel shows a false-colour merged image (left) of FITC (CTB; green) and DAPI (nuclei; blue), in addition to individual green (FITC; upper right) and blue (DAPI; lower right) channels.

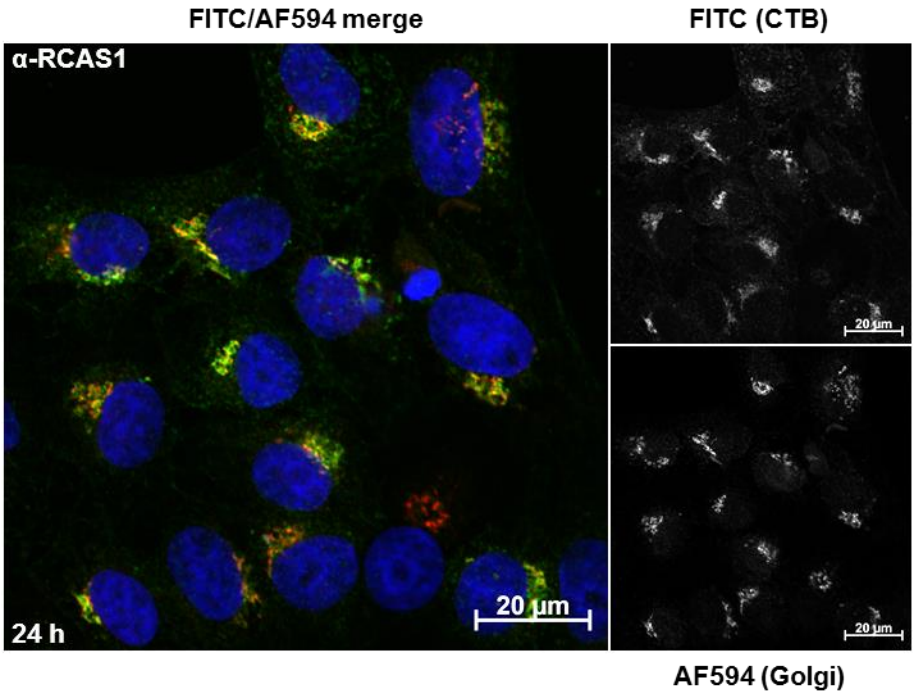

Figure 3.11. Golgi co-staining of FITC-CTB treated Vero cells LSCM imaging of Vero cells incubated with FITC-CTB (2 µg mL^{-1} protein) for 24 h and co-stained for the Golgi apparatus with anti-RCAS1 primary Ab and AF594-conjugated secondary Ab; the panel shows a false-colour merged image (left) of FITC (CTB; green), AF594 (Golgi; red) and DAPI (nuclei; blue), in addition to individual green (FITC; upper right) and red (AF594; lower right) channels.

3.4. A CTB variant for alternative organelle targeting

3.4.1. Design

While CTB built up in the Golgi, the native holotoxin is transported to the ER, a more desirable location for CTB in terms of therapeutic action. The C-terminal KDEL present on CTA2 in the holotoxin has been shown to promote efficient retrotranslocation to the ER[23]. In an attempt to mimic this, a CTB variant was designed possessing both an N-terminal GGG for SrtA labelling and a C-terminal KDEL ER retention sequence (hereafter termed CTB-KDEL). Despite the difference in position and orientation of the C-termini between CTB and CTA2, the addition of the C-terminal KDEL would hopefully promote retrograde transport of CTB to the ER. The B subunit of Shiga toxin from *Shigella dysenteriae* has been shown to be targeted to the ER on addition of a C-terminal KDEL[110], which suggested the same would be true of CTB due to the positional similarity of the C-termini in both proteins[268].

3.4.2. Expression and purification of CTB-KDEL

The CTB-KDEL DNA coding sequence was produced by assembly PCR and subcloned into pSAB2.2 using SphI and PstI restriction endonucleases. The protein was expressed from this plasmid in *E. coli* C41(DE3) cells by IPTG induction overnight at 25 °C, and extracted from the growth medium by ammonium sulfate precipitation. The protein was initially purified by Ni^{2+} affinity chromatography. SDS-PAGE analysis (figure 3.12A) showed intense protein bands of approximately 45 kDa present in the elution fractions, which was replaced with a band of approximately 12 kDa on denaturation, indicating CTB. The remaining impurities following Ni^{2+} affinity chromatography were removed by SEC (figure 3.12B). This resulted in a major A_{280} peak at approximately 220 mL, which was identified as CTB-KDEL by SDS-PAGE (figure 5.5C) and LC-MS, with a protomer mass of 13299.3 Da detected (13300.0 Da calculated). Approximately 4 mg pure protein was isolated per 1 L cultured cells, a good yield when compared to GGG-CTB, particularly given that C-terminal modifications can cause pentameric instability[247].

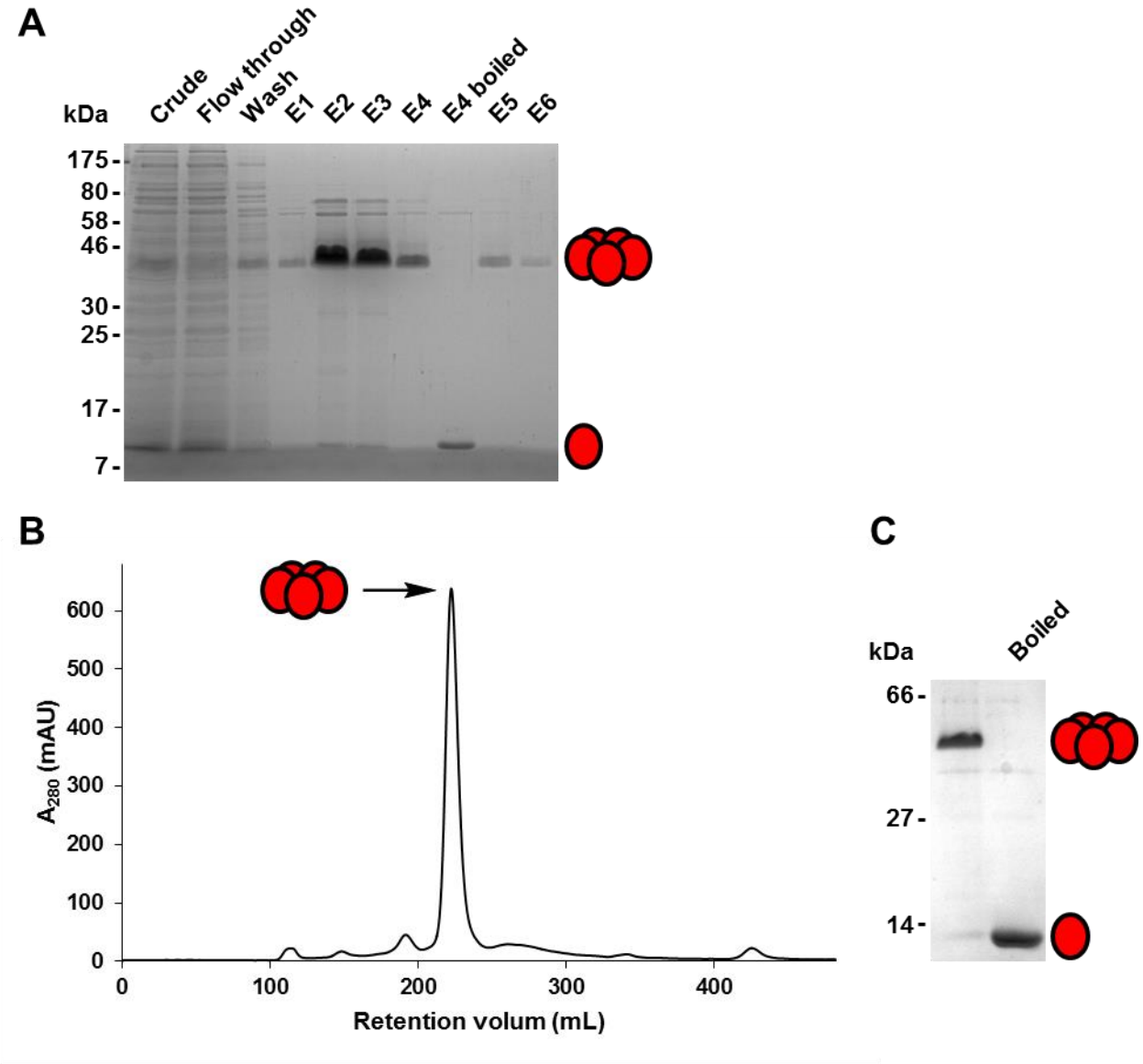

Figure 3.12. Purification of CTB-KDEL A. SDS-PAGE analysis of CTB-KDEL purification by Ni^{2+} affinity chromatography. GGG-CTB as pentamer and dissociated protomer are indicated. B. A_{280} trace from SEC purification of Ni^{2+}-purified CTB-KDEL, with the desired protein peak indicated. C. SDS-PAGE analysis of the indicated CTB-KDEL peak.

3.4.3. Site-specific labelling of GGG-CTB-KDEL with fluorescein

CTB-KDEL (100 μM) in HEPES buffer was site-specifically labelled at the N-terminus with 3 eq FITC-depsipeptide with 20 mol% SrtA for 3 h at 37 °C. SDS-PAGE analysis (figure 3.13A) showed the pentamer split into several bands of increased MW compared to unlabelled CTB following labelling. On denaturation, a protomer band (~ 14 kDa) appeared of increased MW compared to the unlabelled protomer (~ 12 kDa). The bands attributed to the both labelled pentamer and labelled protomer appeared fluorescent under UV illumination, confirming FITC conjugation. FITC-CTB-KDEL was purified by

lactose affinity chromatography and concentrated, and successful labelling was confirmed by LC-MS (figure 3.13B), with a mass of 13216.9 Da detected (13215.6 Da calculated). Relative intensities of the denatured protein bands indicated labelling efficiency of approximately 80%. Pure FITC-CTB-KDEL was isolated at 85 µM (700 µL), giving 70% protein recovery and 60% yield of labelled protein.

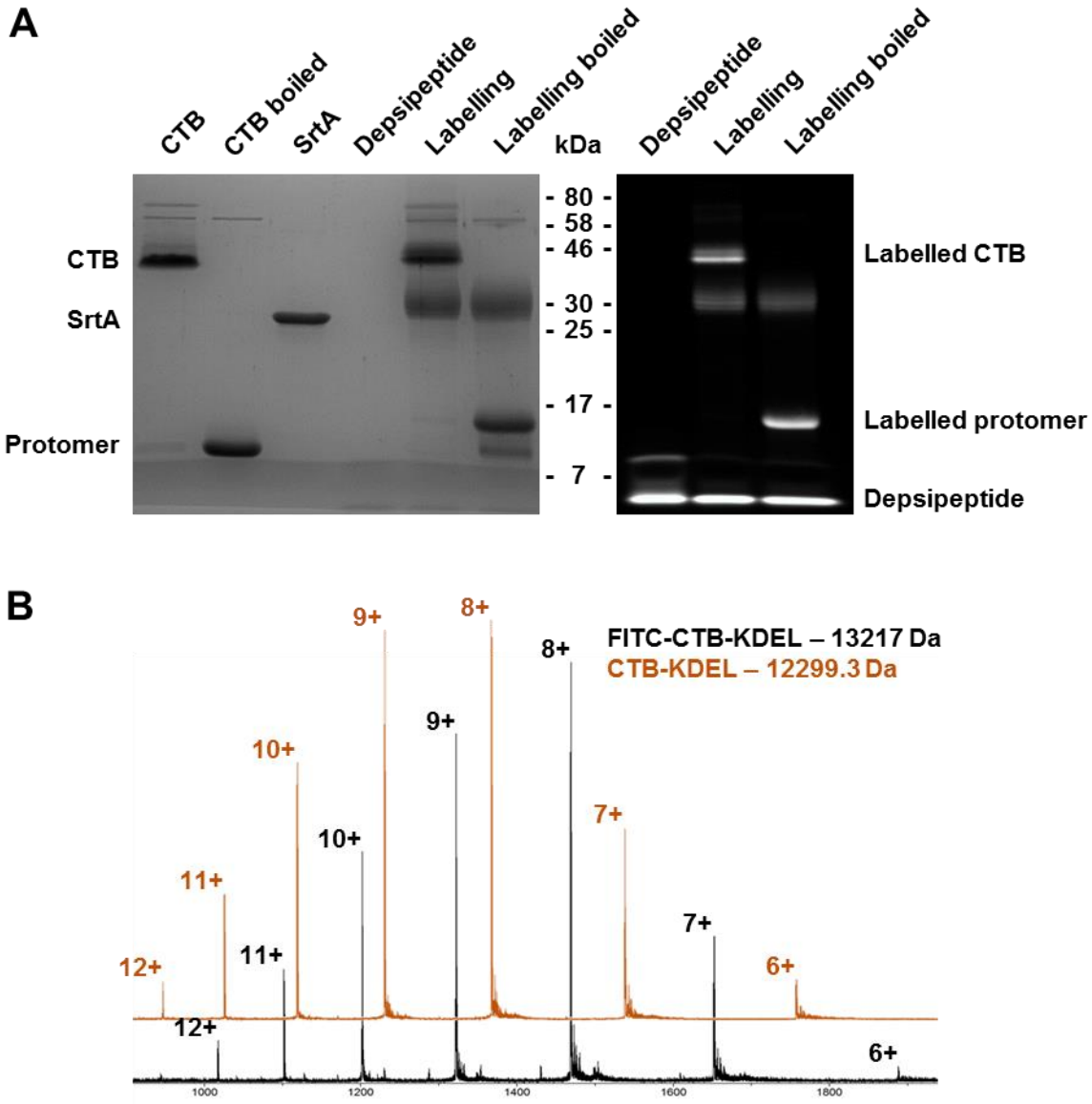

Figure 3.13. SrtA-mediated CTB-KDEL labelling A. Coomassie-stained (left) and UV illuminated (right) SDS-PAGE analysis SrtA-mediated labelling of CTB-KDEL with FITC-depsipeptide. B. Overlaid LC-MS comparing FITC-CTB-KDEL (black) with unlabelled CTB (orange).

3.5. Functional characterisation of labelled CTB-KDEL

3.5.1. GM1 binding characterisation by ITC

The ability of FITC-CTB-KDEL to bind GM1os was assayed by ITC. GM1os was titrated against FITC-CTB-KDEL (figure 3.14; data summarised in table 3.2). The labelled protein bound GM1os with an approximate stoichiometry of 1 GMos residue per binding site and showed an approximate five-fold decrease in affinity for GM1os compared to wt CTB. Again however, FITC-CTB-KDEL retained a relatively high affinity for GM1os.

Protein	[Protein] (μM)	[GM1os] (μM)	K_d (nM)	N
wt CTB	13.5	110	316 ± 76	1.06 ± 0.02

Table 3.1. Summary of ITC to assay modified CTB binding to GM1os

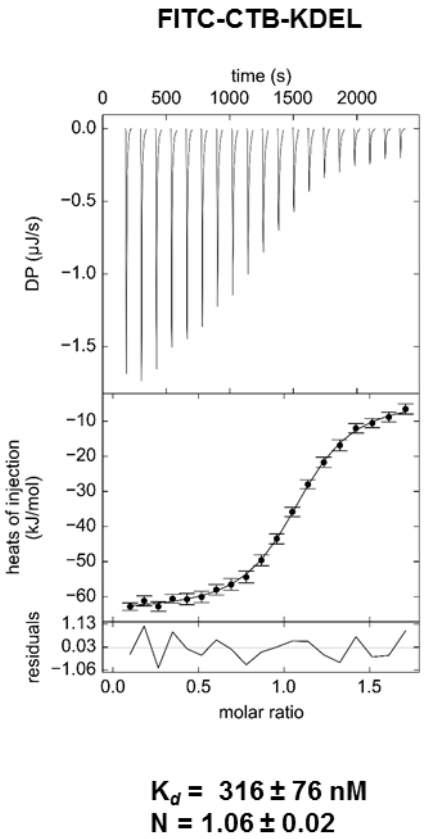

Figure 3.14. ITC of GM1os titrated into FITC-CTB-KDEL Titration of 110 μM GM1os into 13.5 μM FITC-CTB-KDEL. The plot shows the baseline-adjusted raw thermogram (upper), the fitted integral data (middle) and the residual error of the fitting (lower).

3.5.2. Evaluation of the CTB-KDEL endocytic pathway

Vero cells were incubated with FITC-CTB-KDEL (2 μg mL^{-1} protein) in DMEM at 37 °C with 5% CO_2 for 24 h, and fixed with PFA after 15 min, 30 min, 1 h, 2 h, 6 h and 24 h. The cells were mounted with ProLong Gold antifade mounting reagent with DAPI for nuclei staining, and viewed by LSCM (figure 3.15). FITC staining was detectable within the cells at all time points. Similar to FITC-CTB rertrotranslocation, the staining was seen to become increasingly discrete and intense over time, indicating localisation to organelles or other vesicular structures. After 30 min, the foci spread throughout the cytosol began to localise to discrete clumps, Golgi-like in morphology, adjacent to the nucleus. However, at 1 h, the staining became inconsistent with FITC-CTB. The protein began to localise to halo-like regions surrounding the nuclei, consistent with the morphology of the ER. Over time, this localisation increased in intensity, until staining with this morphology was almost exclusively detected after 24 h.

To confirm the identity of the organelle, Vero cells were incubated with FITC-CTB-KDEL (2 μg mL^{-1} protein) for 24 h and co-stained for calnexin, a transmembrane molecular chaperone protein localised to the ER[269], with an anti-calnexin primary Ab to detect the ER. The primary Ab was stained with an AF594-conjugated secondary Ab, and the cells mounted with DAPI. LSCM (figure 3.16) showed morphological match and co-localisation between FITC-CTB-KDEL and the ER, confirming localisation to this organelle. While the co-localisation was not complete, this could be explained by the fact that calnexin is present ubiquitously throughout the ER membrane where ribosomes are present[269-271], while CTB would only localise where vesicles from the trans-Golgi dock with the ER.

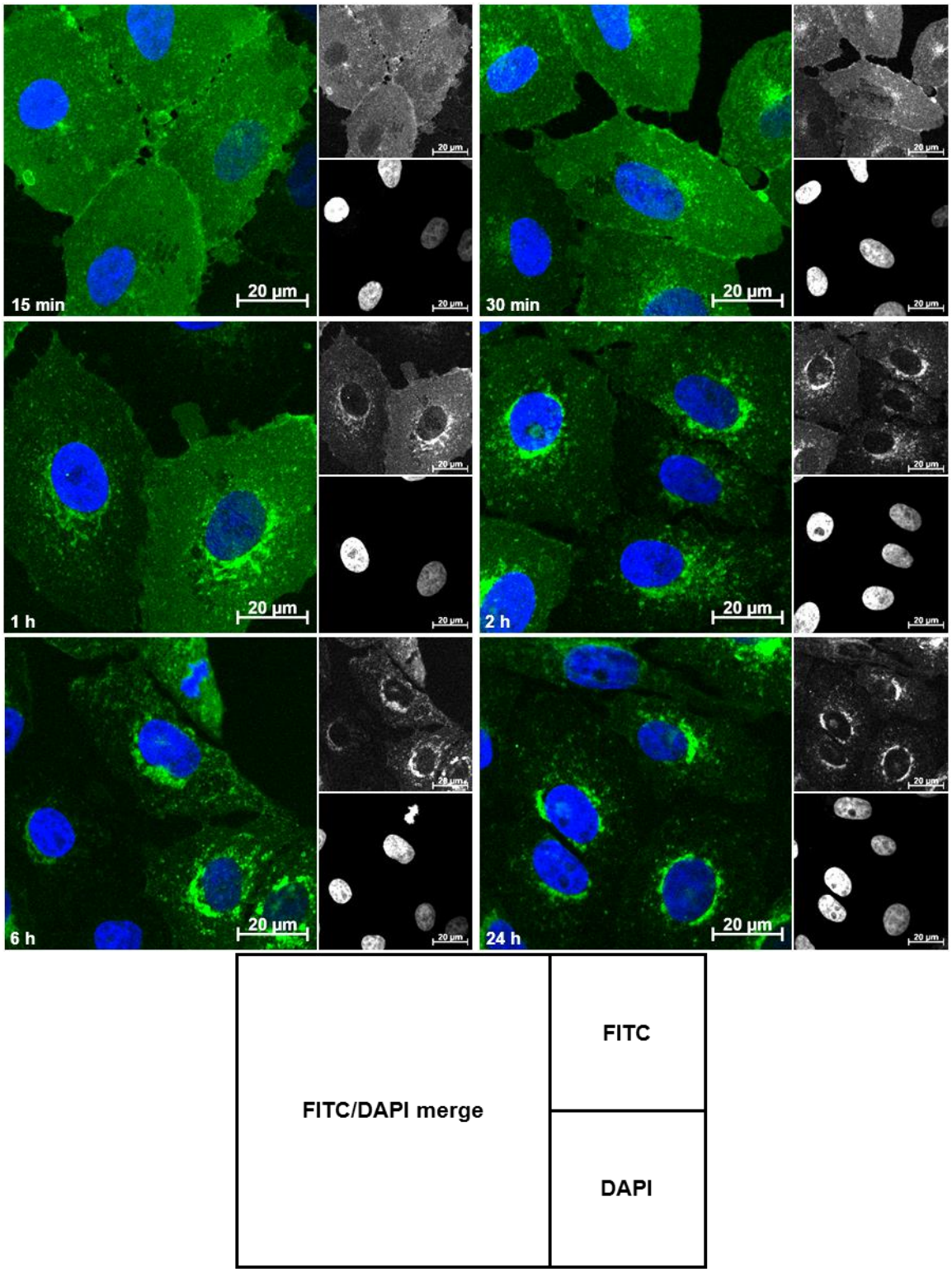

Figure 3.15. Time course of FITC-CTB-KDEL incubation with Vero cells LSCM imaging of Vero cells incubated with FITC-CTB-KDEL (2 µg mL^{-1} protein) and fixed after 15 min, 30 min, 1 h, 2 h, 6 h or 24 h. Each panel shows a false-colour merged image (left) of FITC (CTB; green) and DAPI (nuclei; blue), in addition to individual green (FITC; upper right) and blue (DAPI; lower right) channels.

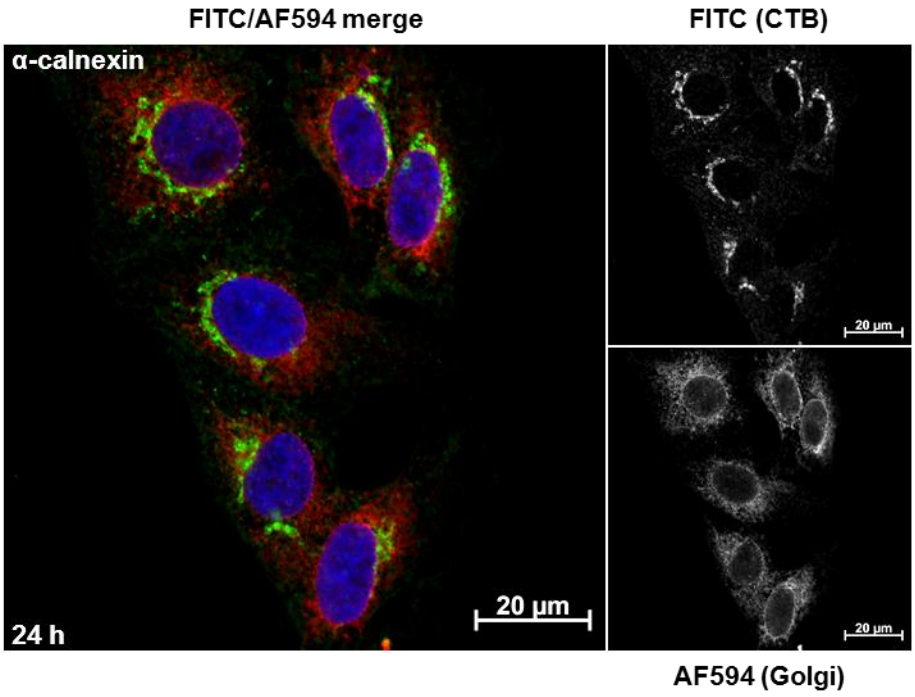

Figure 3.16. ER co-staining of FITC-CTB-KDEL treated Vero cells LSCM imaging of Vero cells incubated with FITC-CTB-KDEL (2 µg mL^{-1} protein) for 24 h and co-stained for the ER with anti-calnexin primary Ab and AF594-conjugated secondary Ab; the panel shows a false-colour merged image (left) of FITC (CTB; green), AF594 (Golgi; red) and DAPI (nuclei; blue), in addition to individual green (FITC; upper right) and red (AF594; lower right) channels.

These results are again consistent with CT retrograde transport pathway. CTB-KDEL, like CTB, would be expected to undergo retrotranslocation to the trans-Golgi, similar to the holotoxin[13]. As a C-terminal KDEL sequence has been shown to promote protein retrieval from the Golgi apparatus and retention in the ER[272,273], it is not unexpected that CTB-KDEL should be targeted to the ER, as seen with similar proteins[110]. It is perhaps surprising that a C-terminal KDEL was able to affect CTB cell localisation at all. The KDEL receptor is a transmembrane protein lacking extensive lumenal domains[274,275]. The KDEL present in the holotoxin is located at the binding face projecting towards the membrane[20], so would be expected to interact with the KDEL receptor, but those present on CTB are located on the opposite face and oriented away from the membrane[22]. This suggests the receptor should be unable to interact with the KDEL sequences present on CTB. However, these results suggest the interaction is occurring, perhaps as CTB is pentameric and so contains five copies of the KDEL sequence per protein, resulting in an amplified effect.

Regardless, the variation in the endocytic pathway of CTB based on the addition of a C-terminal KDEL signal sequence presents an excellent opportunity to control the destination of a conjugated therapeutic molecule. This would allow diseases associated with either the Golgi or ER to be targeted, or alternatively allow access to the various modification pathways associated with the ER, including disulfide formation and reduction, glycosylation, protein folding/unfolding, protein secretion to various parts of the cell and protein degradation.

Chapter 4: CTB oligonucleotide conjugation for cellular delivery

The previous chapter demonstrated that CTB could be labelled with a fluorescent payload and transport it to either the Golgi apparatus or ER, depending on the presence of a simple targeting sequence. However, FITC-depsipeptide is neither therapeutically relevant, nor a good model for such a molecule. A target molecule for delivery by CTB was required. This chapter describes the synthesis of a double-stranded, modified oligonucleotide for conjugation to CTB. Protein labelling and purification are discussed, along with characterisation of receptor binding and cellular oligonucleotide delivery of the CTB-RNA complex.

4.1. Introduction

An ideal molecule for CTB delivery should have the potential to fill a currently unmet treatment need, in addition to lacking a robust delivery system. Therapeutic oligonucleotides represent one such possibility. Oligonucleotides are currently used extensively in the laboratory, predominantly for pre-translational protein knockdown by RNAi using siRNA[3]. Gapmer and steric blocking antisense oligonucleotides offer alternative methods for pre-translational protein knockdown[3]. Steric blocking antisense oligonucleotides have also been adapted to alter pre-mRNA splicing, modifying the sequence of the expressed protein at the pre-mRNA level[3].

All of these oligonucleotides must be protected from nuclease degradation to survive long enough to function in cells. Chemical modifications at the 2′ carbon and to the phosphodiester backbone, as well as alternative scaffold structures to ribose, have been developed for this purpose[3]. Many of these modifications have been combined to improve stability or increase target binding; 2′-OMe, 2′-MOE and LNA oligomers with phosphorothioate backbones are common, as well as morpholino oligomers with phosphorodiamidate backbones[3,124,125,127,131,135,276]. This study focused on the

combination of 2′-OMe and phosphorothioate oligonucleotide modifications, a combination which has been extensively trialled by GlaxoSmithKline (GSK) and one which they are keen to see developed further.

Duchenne muscular dystrophy provides an excellent example of both the potential of oligonucleotide therapies and issues with effective delivery. DMD is a severe, progressive muscle wasting genetic disorder that leads to paralysis and early death[3]. It manifests through mutations in the dystrophin gene, resulting in expression of non-functional protein[3]. GSK have developed a splice altering antisense 2′-OMe phosphorothioate oligonucleotide, drisapersen, for the treatment of a subset of DMD[277]. This functions by inducing skipping of exon 51 during splicing, restoring a correct open reading frame and resulting in the expression of an internally truncated dystrophin protein with partially restored functionality[150,277,278]. The oligonucleotide showed initial promise *in vivo*[149,150,279] and *ex vivo*[280,281], and successfully completed phase I clinical trials[282]; a single 0.8 mg dose given by muscular injection resulted in the production of functional dystrophin in up to 97% of target muscle fibres, restoring up to 12% of control functional dystrophin levels, with no adverse effects. The drug was escalated to phase II clinical trials[156]. Drisapersen was administered by subcutaneous injection for systemic delivery, with no serious adverse effects. The treatment induced functional dystrophin expression in up to 100% of muscle fibres in 83% of the patients, representing up to 16% of healthy muscle expression levels. There was also a slight improvement in patient clinical status, determined by a 6-minute walk test. Unfortunately, drisapersen failed to meet expectations in phase III clinical trials, with patients showing no significant improvement with repeated treatments, and development was halted[283]. However, the oligonucleotide was delivered gymnotically[156]. It was theorised that the oligonucleotide was able to access the dystrophin-deficient muscles primarily due to increased membrane permeability as a result of the disease state[125], so treatment reduced bioavailability. It is therefore feasible that an effective delivery vector could improve treatment results through increased oligonucleotide access to the partially restored dystrophin-deficient muscle cells.

For CTB-mediated oligonucleotide delivery, conjugation required a reliable, bioorthogonal reaction which could be applied to current protein labelling methods. Click chemistry, or Cu(I) catalysed 1,3-dipolar cycloaddition of an azide and alkyne forming a triazole[284,285], represents a rapid, reliable and mild bioorthogonal reaction that could be applied to this study. However, the cytotoxic Cu(I) catalyst could cause problems with downstream cell experiments if not fully removed, so this method was discounted. A

variant of click chemistry, strain-promoted alkyne-azide cycloaddition (SPAAC), negates the need for the Cu(I) catalyst through use of a strained cyclooctyne[286,287]. This reaction has been applied to living systems[286,287], making this a suitable choice of bioorthogonal reaction for oligonucleotide conjugation. Cyclooctynes have also been incorporated into proteins by SrtA-mediated ligation[288], validating the use of this approach.

4.2. Synthesis of modified oligonucleotides for CTB-mediated cell delivery

4.2.1. Strategy

An oligonucleotide was designed for conjugation to CTB in order to test cellular oligonucleotide delivery. As with those developed by GSK, the oligonucleotide was fully modified with 2′-OMe groups and a phosphorothioate backbone. The oligonucleotide sequence, 5′-GCUAUUACCUUAACCCAG-3′ (hereafter termed skipper RNA), was based on a 2′-OMe phosphorothioate oligonucleotide designed by Sazani *et al.*[124,135] for use with a splice-altering assay, similar to the mechanism of action of drisapersen.

The oligonucleotide required both a functional group for CTB conjugation and a fluorophore for visualisation. This presented a problem, as modifying both ends of an oligonucleotide with different molecules can be troublesome. To overcome this, a second oligonucleotide of complementary sequence (5′-CUGGGUUAAGGUAAUAGC-3′; hereafter termed complement RNA) was designed with similar modifications to the skipper RNA. This approach allowed for one oligonucleotide to be modified with a fluorophore while the other could be modified with a functional group for CTB conjugation. Hybridisation of the two would produce a CTB variant labelled with a fluorescent oligonucleotide duplex, which could act as a reporter for oligonucleotide delivery.

Thus, a labelling mechanism (figure 4.1) was designed whereby CTB could be labelled with a cyclooctyne-derivatised depsipeptide, in this case bicyclononyne (BCN), by SrtA-mediated ligation. A duplex of fluorescein-modified skipper RNA hybridised with azide-functionalised complement RNA could subsequently be covalently attached to BCN-CTB by SPAAC.

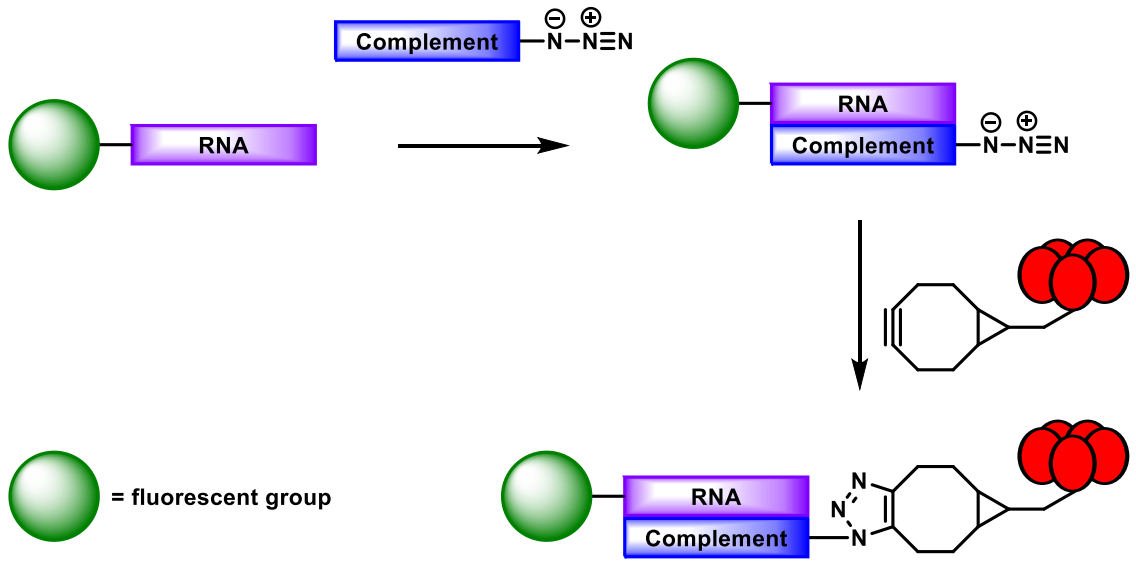

Figure 4.1. Oligonucleotide conjugation strategy Overview of the strategy designed for labelling CTB (red) with a fluorescent oligonucleotide.

4.2.2. Oligonucleotide general characteristics

Oligonucleotides were synthesised as 2′-OMe phosphorothioate RNA, for increased stability and nuclease resistance[3,119,126]. The 5′ end of each oligonucleotide was modified on resin with a primary amine for functionality.

4.2.3. 5′-fluorescein skipper RNA synthesis

The human β-globin intron skipper antisense oligonucleotide designed by Sazani *et al.*[124,135] (5′-GCUAUUACCUUAACCCAG-3′) was synthesised for non-covalent conjugation to CTB. Following solid phase synthesis and purification, the 5′-amino skipper RNA was isolated with 20% yield. The 5′-amino skipper RNA was reacted with 6-carboxyfluorescein NHS ester (figure 4.2) to form 5′-fluorescein skipper RNA with 86% yield.

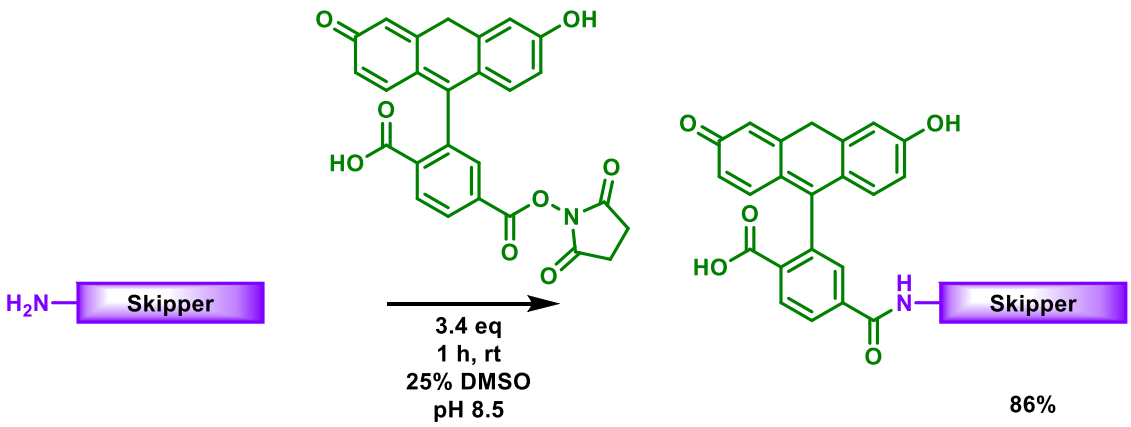

Figure 4.2. Modification of the synthesised 5′-amino skipper with fluorescein Reaction scheme describing the conjugation of the synthesised 5′-amino skipper RNA (purple) to 6-carboxyfluorescein NHS ester (green).

4.2.4. 5′-azido complement RNA synthesis

A 5′-amino oligonucleotide of complementary sequence to the skipper RNA (5′-CUGGGUUAAGGUAAUAGC-3′) was synthesised for covalent attachment to CTB, allowing non-covalent conjugation of the 5′-fluorescein skipper RNA to CTB by hybridisation. Following solid phase synthesis and purification, the 5′-amino skipper RNA was isolated with 20% yield. The oligonucleotide was reacted with azidobutyrate NHS ester (figure 4.3) to form 5′-azido complement RNA with 84% yield.

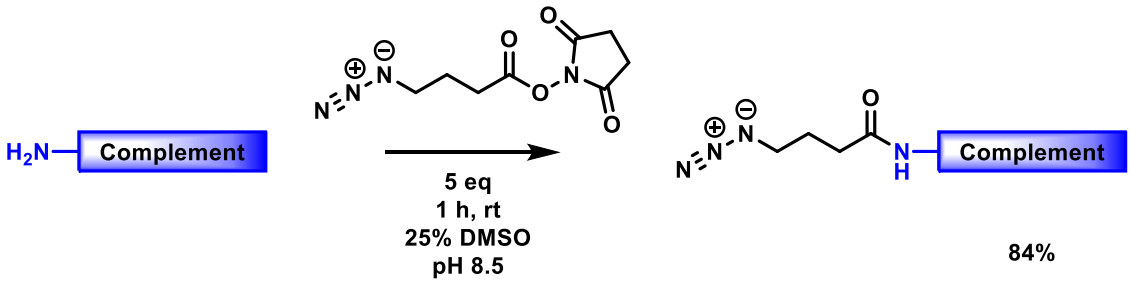

Figure 4.3. Modification of the synthesised 5′-amino complement with an azide Reaction scheme describing the conjugation of the synthesised 5′-amino complement RNA (blue) to azidobutyrate NHS ester.

4.3. Labelling two CTB variants with an oligonucleotide payload for cell delivery

4.3.1. SrtA-mediated labelling with BCN

Both CTB and CTB-KDEL were labelled with oligonucleotides to investigate if altering the endocytic pathway with inclusion of an ER retention sequence was repeated with the alternate payload. Initially, a BCN functional group was conjugated to CTB to allow covalent attachment of the 5′-azido complement RNA by SPAAC. This was achieved through SrtA-mediated ligation of a depsipeptide (LPEToGG) derivatised with a BCN functional group at the N-terminus of the peptide (D. Williamson). Both proteins (120 µM each) in HEPES buffer were labelled with 3 eq BCN-depsipeptide for 3 h at 37 °C (figure 4.4).

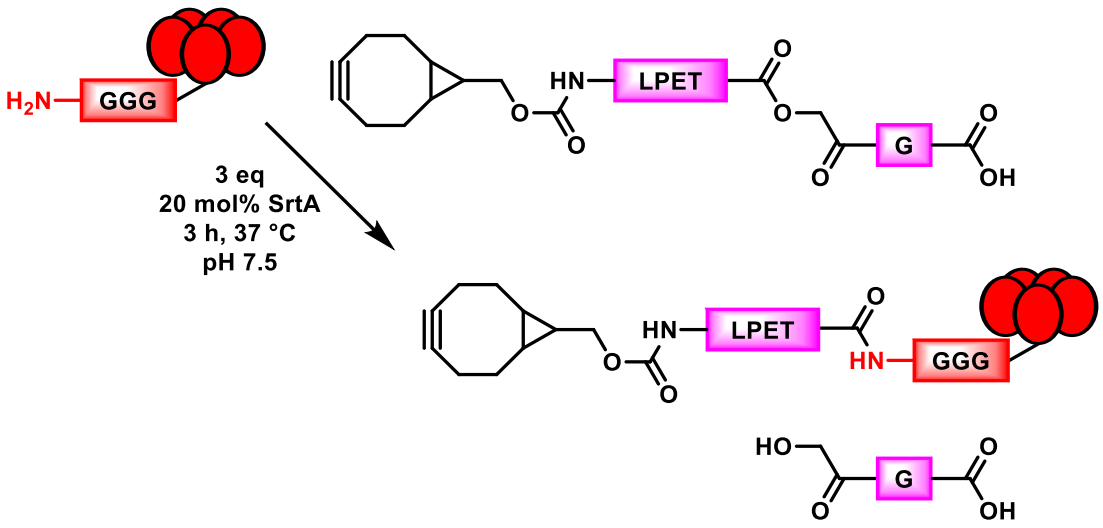

Figure 4.4. Addition of a BCN functional group to CTB and CTB-KDEL Reaction scheme describing SrtA-mediated ligation of a BCN-functionalised depsipeptide (magenta) to CTB (red).

The BCN-labelled proteins were purified by lactose affinity chromatography and analysed by SDS-PAGE (figure 4.5). In both cases, SrtA (~35 kDa band) was removed in the flow through. CTB and CTB-KDEL (~ 45 kDa bands) appeared in the elution fractions, identified as CTB by the replacement of the band with one of approximately 12 kDa on denaturation. Both labelled proteins were concentrated from the elution fractions and new concentrations determined by spectrophotometry as 42 µM (720 µL) for BCN-CTB and 48 µM (770 µL) for BCN-CTB-KDEL. The 64% and 59% product loss was primarily a result of the need to concentrate the samples following purification,

as very little of the protein was lost during purification (figure 4.5). However, this step was unavoidable. Purification was required to remove SrtA, which can gradually remove the conjugated depsipeptide by hydrolysis[249,289,290]. Excess depsipeptide also required removal from the product to conserve the precious modified oligonucleotides, which were required in excess for the subsequent SPAAC reaction. The increase in sample volume following column chromatography purification necessitated concentration of the protein samples to obtain concentrations which would allow SPAAC to proceed efficiently[286,291].

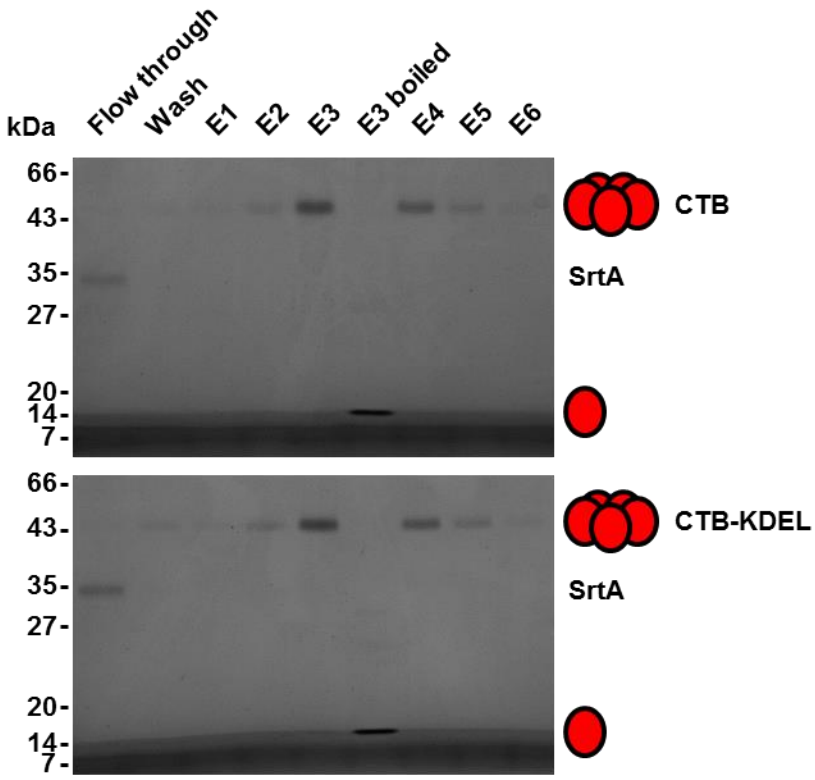

Figure 4.5. Purification of BCN-CTB and BCN-CTB-KDEL SDS-PAGE analysis of BCN-CTB (upper) and BCN-CTB-KDEL (lower) purification by lactose affinity chromatography.

4.3.2. Bioorthogonal conjugation of oligonucleotides

The previously synthesised 5′-azido complement RNA and 5′-fluorescein skipper RNA were hybridised (hereafter termed FdsRNA-azide) at equimolar concentrations. BCN-CTB (35 µM) and BCN-CTB-KDEL (38 µM) in HEPES buffer were reacted with 4.5 eq FdsRNA-azide overnight at room temperature (figure 4.6).

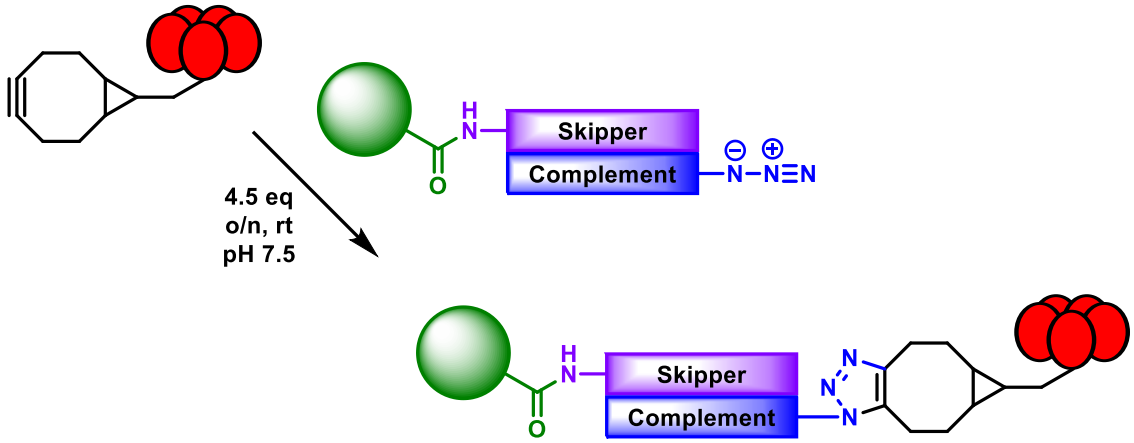

Figure 4.6. SPAAC for bioorthogonal oligonucleotide conjugation to BCN-labelled CTB and CTB-KDEL Reaction scheme describing FdsRNA-azide (green, purple, blue) conjugation to BCN-CTB (red, magenta) by SPAAC.

SDS-PAGE analysis (figure 4.7) showed both CTB variants as non-homogeneously labelled pentamer, appearing as laddered bands spanning approximately 45-75 kDa which were replaced on denaturation with two bands; dsRNA-labelled protomer (~ 25 kDa) and unlabelled protomer (~ 12 kDa) in approximately equal ratios. Under UV illumination, the bands consistent with labelled protein appeared fluorescent, confirming successful FdsRNA labelling.

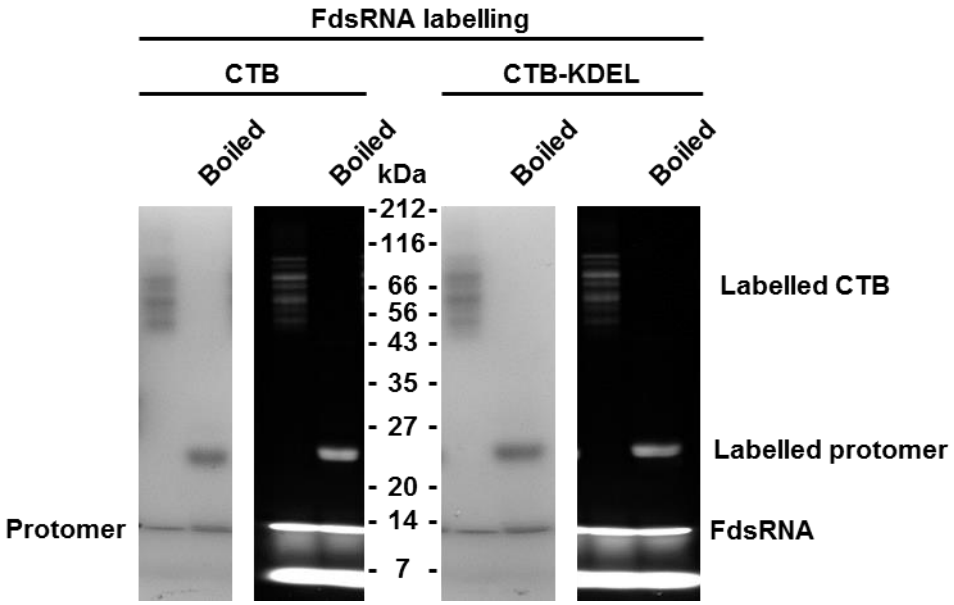

Figure 4.7. BCN-CTB and BCN-CTB-KDEL labelling with FdsRNA SDS-PAGE analysis of BCN-CTB (left panel) and BCN-CTB-KDEL (right panel) labelling reactions with FdsRNA-azide, showing Coomassie-stained (left) UV illuminated (right) gels.

Purification of the labelled proteins was initially attempted by lactose affinity chromatography, but the labelled proteins failed to bind and were eluted in the flow through. Purification was instead achieved by Ni^{2+} affinity chromatography. SDS-PAGE analysis under UV illumination (figure 4.4C) showed both labelled CTB and CTB-KDEL appearing in the elution fractions as laddered fluorescent bands which resolved into a single fluorescent band on denaturation, indicating successful purification. Both labelled proteins were concentrated from the elution fractions, and the new concentrations and labelling efficiencies determined by spectrophotometry. FdsRNA-CTB concentration was calculated as 36 µM (610 µL) with a labelling efficiency of 30%, while FdsRNA-CTB-KDEL concentration was calculated as 40 µM (590 µL) with a labelling efficiency of 34%. The resultant yields of labelled protein were 7% and 9%, respectively, following all reaction, purification and concentration steps. Protein recovery following purification and concentration steps was the primary cause of the low yields, accounting for total losses of 76% for CTB and 74% for CTB-KDEL.

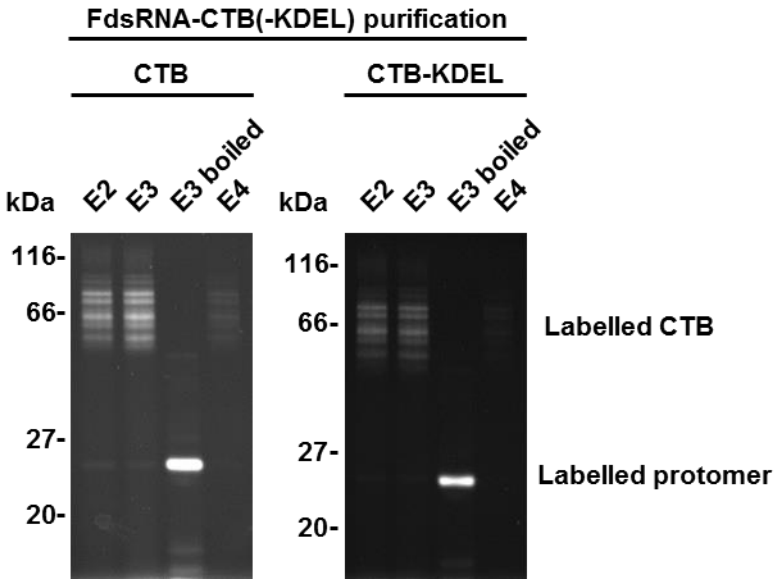

Figure 4.8. Purification of FdsRNA-labelled CTB and CTB-KDEL UV illuminated SDS-PAGE analysis of FdsRNA-CTB (left) and FdsRNA-CTB-KDEL (right) purification by Ni^{2+} affinity chromatography.

The inability of dsRNA-labelled CTB to bind lactose was concerning. One possible explanation was steric hindrance. The galactose residue at the tip of GM1 binds at the deepest point within the binding pocket[18,38,40]. It is possible that the addition of up to five molecules of approximately 15 kDa on the binding face and adjacent to the binding sites, clashing with the agarose resin, resulted in sufficient steric hindrance to prevent the galactose residue of the immobilised lactose reaching the galactose binding region. Another possibility was the addition of dsRNA in close proximity to the binding sites had decreased CTB affinity for lactose such that the interaction was no longer sufficient to immobilise the protein. However, neither of these necessarily presented an insurmountable hurdle. GM1 ganglioside is a longer molecule than lactose, increasing the possibility of the galactose and sialic acid residues critical for binding[38] reaching the correct regions of the binding sites. In addition, the native toxin must descend through the glycocalyx to reach the cell surface[47], which provides significant steric hindrance to passage, yet efficient endocytosis still occurs. Furthermore, CTB conjugated to particles of 14 nm diameter have been shown to bind cell surface GM1[292], so dsRNA should not necessarily negate binding based on size. Regarding affinity, CTB affinity for lactose is over three orders of magnitude weaker than for GM1[293], amongst the highest for carbohydrate-lectin interactions (low nM range)[18,38]. It is feasible that a small loss of affinity for lactose could abrogate binding, an effect that would not be seen with the high

affinity GM1. However, further investigation was required to ensure dsRNA labelling would not abrogate GM1 binding and endocytosis.

4.3.3. Confirmation of GM1 binding

The ability of FdsRNA-CTB and FdsRNA-CTB-KDEL to bind GM1 was investigated by ITC. GM1os (T. McAllister) was titrated against both FdsRNA-CTB and FdsRNA-CTB-KDEL (figure 4.9; data summarised in table 4.1). GM1os binding to both labelled proteins resulted in sigmoidal curves, indicating high affinity binding. The binding interaction with labelled CTB was assigned a K_d of 547 nM and N value of 0.61 per binding site, or 3.05 GM1os per pentamer. The interaction with CTB-KDEL was assigned a K_d of 451 nM and N value of 0.57 per binding site, or 2.85 GM1os per pentamer.

Protein	[Protein] (μM)	[GM1os] (μM)	K_d (nM)	N
FdsRNA-CTB	13.2	132	547 ± 219	0.61 ± 0.03
FdsRNA-CTB-KDEL	13.6	136	451 ± 137	0.57 ± 0.02

Table 4.1. Summary of ITC to assay FdsRNA-CTB and FdsRNA-CTB-KDEL binding to GM1os

The reduced N values for both labelled proteins were unexpected. It is possible that attaching large oligonucleotides to the N-termini of CTB resulted in blocked access to the adjacent binding sites. With two binding sites apparently unavailable and a labelling efficiency of 30-34%, the comparison between N and calculated labelling efficiency is consistent with this theory. An alternative explanation lies with inaccurate calculation of protein concentration, due to the complexity of determining unknown concentrations of protein, nucleic acid and fluorescein in a single sample. In this case, assuming N = 1, the actual concentrations of labelled CTB and CTB-KDEL would have been 8.3 μM and 7.5 μM, respectively. Either way, the thermodynamic parameters of binding were of secondary importance. The ITC data clearly showed high affinity GM1 binding had occurred, which would allow endocytosis to occur.

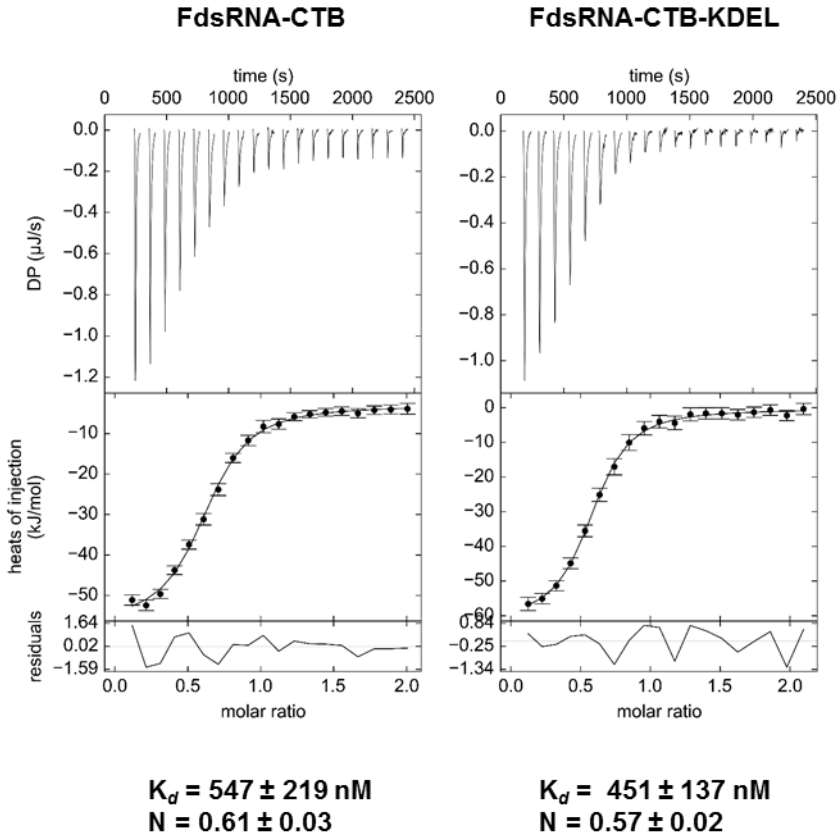

Figure 4.9. Analysis of GM1os binding to dsRNA-labelled CTB and CTB-KDEL by ITC Titrations of GM1os FdsRNA-CTB (left) and FdsRNA-CTB-KDEL (right). Each plot shows the baseline-adjusted raw thermogram (upper), the fitted integral data (middle) and the residual error of the fitting (lower).

4.4. CTB-mediated oligonucleotide delivery

FdsRNA-CTB and FdsRNA-CTB-KDEL were incubated with Vero cells to determine the suitability of both CTB as an oligonucleotide delivery vector and N-terminal SrtA-mediated ligation as a conjugation method. Cells were incubated with either FdsRNA-CTB or FdsRNA-CTB-KDEL (5 µg mL^{-1} protein), or an equivalent concentration of unconjugated FdsRNA, at 37 °C (5% CO_2) over 24 h. The cells were fixed with PFA after 15 min, 30 min, 1 h, 2 h, 4 h, 8 h and 24 h. In addition to conjugated fluorescein for RNA detection, the cells were stained with a rabbit anti-CTB primary Ab followed by a donkey anti-rabbit Alexa Fluor (AF) 555-conjugated secondary Ab to detect CTB. The cells were mounted in ProLong Gold Antifade mounting reagent with DAPI, allowing nuclei detection, and viewed by LSCM.

Cells treated with FdsRNA showed neither fluorescein nor AF555 staining, indicating endocytosis of the RNA had not occurred. In the case of cell treatment with both FdsRNA-CTB (figure 4.10) and FdsRNA-CTB-KDEL (figure 4.11), fluorescein and AF555 were detected within the cells at all time points, indicating endocytosis was successful and RNA was delivered with CTB. The two stains were also closely co-localised, indicating the RNA remained attached to CTB. This is unsurprising, as the complement strand was covalently attached to CTB and the T_m of the duplex sufficiently high as to prevent denaturation at physiological temperature. While the fluorescein staining generally appeared weaker than the AF55 staining, this was explained by the increased brightness and photostability of AFs compared to fluorescein[294-296], along with the amplification effect of secondary antibody staining. With both CTB and CTB-KDEL, the staining became more densely localised to discrete foci over time, indicating the protein-RNA complexes were building up in organelles. Up to 4 h, FdsRNA-CTB appeared to increasingly build up in the Golgi apparatus, forming increasingly discrete clumps adjacent to the nuclei, similar to FITC-CTB. However, the 8 h and 24 h time points showed the staining reverting to increasingly diffuse foci throughout the cells, indicative of complex removal from the Golgi, probably to the lysosome via the autophagosome. The relatively low fluorescein intensity at these two later time points supports this, as fluorescein is quenched at acidic pH[297], as experienced within the lysosome[298]. By comparison, FdsRNA-CTB-KDEL appeared to build up in the ER, forming increasingly discrete halos surrounding the nuclei, similar to FITC-CTB-KDEL. The staining at later time points was less diffuse than FdsRNA-CTB, seeming to remain more heavily localised to the ER than FdsRNA-CTB to the Golgi, indicating a lower degree of complex removal to the lysosome with the presence of a targeting sequence. However, some FdsRNA-CTB-KDEL removal to the lysosome seemed to have occurred.

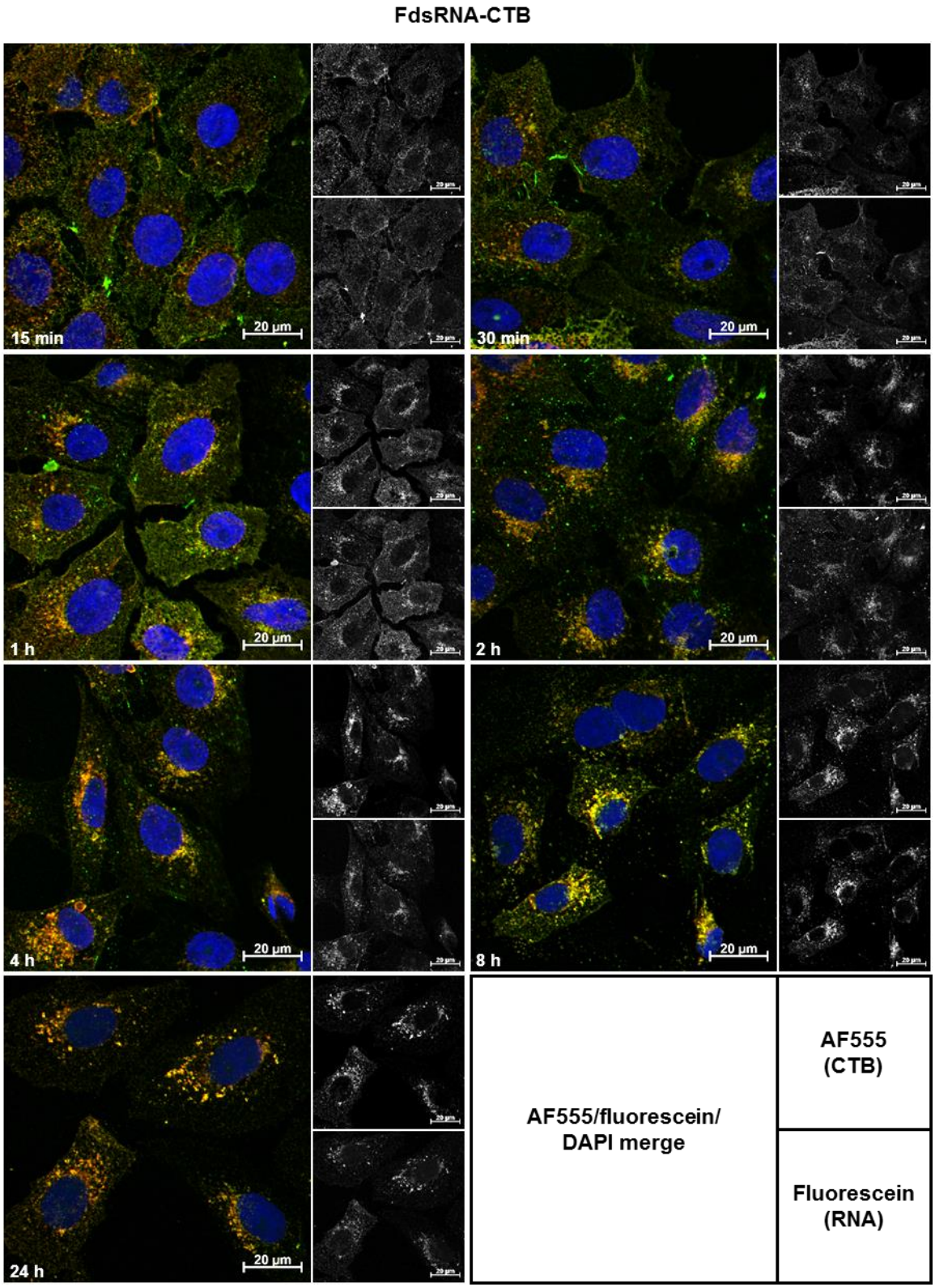

Figure 4.10. Time course of FdsRNA-CTB incubation with Vero cells LSCM imaging of Vero cells incubated with FdsRNA-CTB (5 µg mL^{-1} protein), fixed after 15 min, 30 min, 1 h, 2 h, 4 h, 8 h or 24 h, and stained with anti-CTB primary and AF555-conjugate secondary antibodies. Each panel shows a false-colour merged image (left) of AF555 (α-CTB; red), fluorescein (RNA; green) and DAPI (nuclei; blue), in addition to individual red (AF555; upper right) and green (fluorescein; lower right) channels.

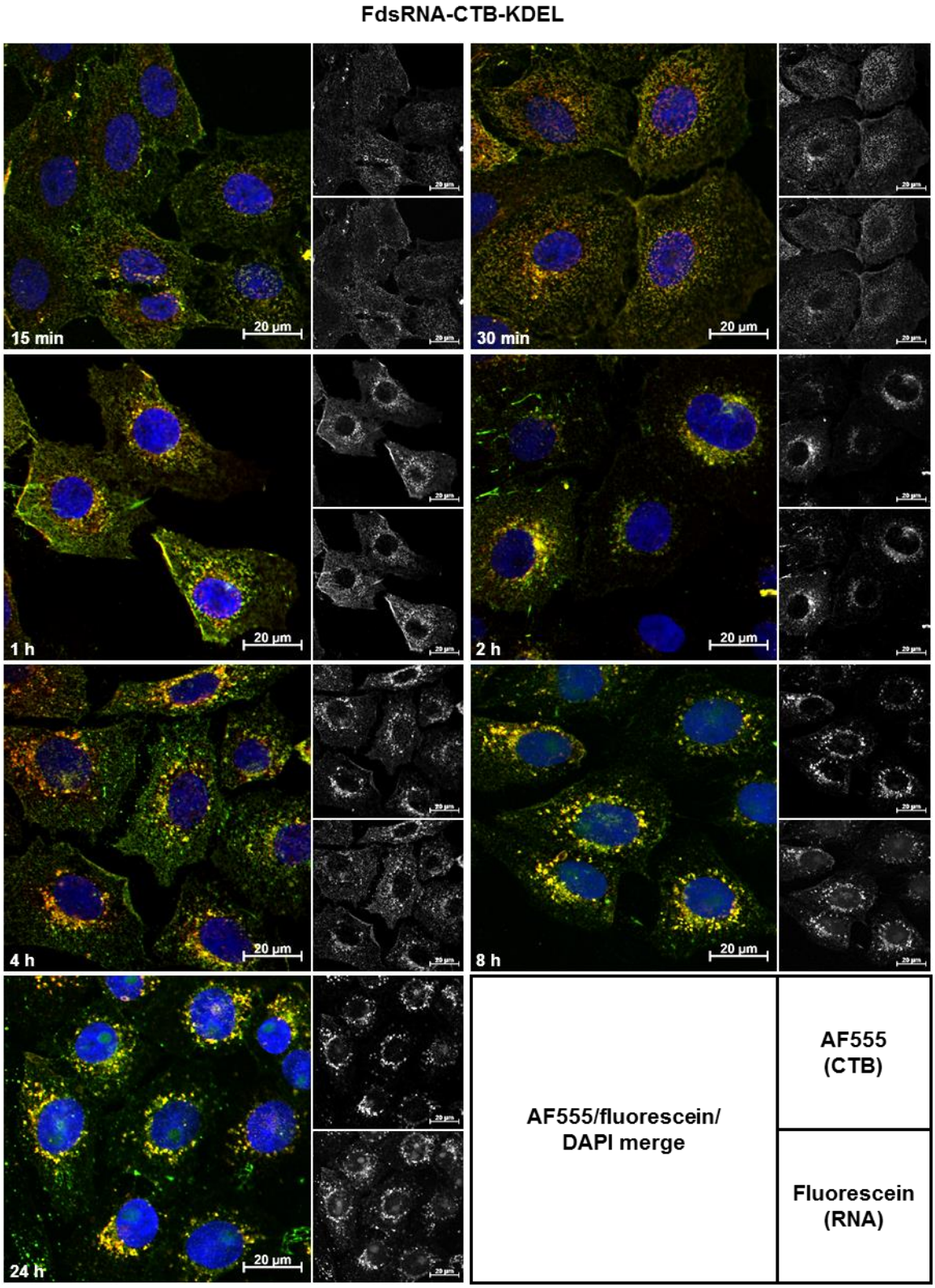

Figure 4.11. Time course of FdsRNA-CTB-KDEL incubation with Vero cells LSCM imaging of Vero cells incubated with FdsRNA-CTB-KDEL (5 µg mL^{-1} protein), fixed after 15 min, 30 min, 1 h, 2 h, 4 h, 8 h or 24 h, and stained with anti-CTB primary and AF555-conjugate secondary antibodies. Each panel shows a false-colour merged image (left) of AF555 (α-CTB; red), fluorescein (RNA; green) and DAPI (nuclei; blue), in addition to individual red (AF555; upper right) and green (fluorescein; lower right) channels.

From the Vero cell time course experiments with FdsRNA-CTB or FdsRNA-CTB-KDEL treatment, it appeared the presence of the KDEL ER retention sequence caused the RNA-protein complex to be more heavily retained in the ER after 24 h, while in its absence the complex was more heavily localised to the lysosome. To confirm this, Vero cells were incubated with FdsRNA-CTB or FdsRNA-CTB-KDEL (5 μg mL^{-1} protein) for 24 h, and the Golgi, ER or lysosome stained for with anti-RCAS1, anti-calnexin or anti-LAMP1 primary Ab, respectively, followed by anti-rabbit AF594-conjugated secondary Ab. The cells were mounted with DAPI and viewed by LSCM. Cells treated with FdsRNA-CTB (figure 4.12) showed some co-localisation between the Golgi and the RNA-CTB complex, although it appeared more circumstantial; the complex was more diffuse and spread beyond the Golgi apparatus, and the staining morphology of the two was poorly matched. The RNA-CTB complex showed better morphological match and co-localisation with the lysosome. This supported the conclusion that the complex was being transported to the Golgi before removal to the lysosome. Cells treated with FdsRNA-CTB-KDEL (figure 4.13) showed good morphological match and co-localisation between the RNA-CTB complex and both the ER and the lysosome, more closely matching the ER. This supported the conclusion that FdsRNA-CTB-KDEL was being transported to the ER and better retained, before some complex removal to the lysosome.

This suggested that in the Golgi apparatus, the conjugated RNA was causing the complex to be targeted to the lysosome, as FITC-CTB travels to the Golgi apparatus but is retained there. However, inclusion of the ER retention sequence caused at least some of the protein-RNA complex to be retained in the ER, preventing its targeting to the lysosome. This was a promising finding. While escaping the Golgi apparatus may be beneficial, the lysosome was not a desirable destination. The lysosome has been shown to degrade various oligonucleotides[299-302], and the lysosomal membrane proteins responsible for nucleotide recognition do so through Arg-rich motifs which are not sequence specific[303], suggesting the oligonucleotide modifications would not prevent recognition. While 2′-OMe phosphorothioate RNA is resistant to circulatory nucleases[3,119,126], there is little data regarding lysosomal degradation and it is doubtful the oligonucleotide would escape intact and still able to perform its function. In contrast, CTB-KDEL showed an increased level of control regarding sub-cellular localisation, although in itself ER localisation is not particularly useful. Therefore, whilst it was clear that oligonucleotides conjugated to the N-termini of CTB could be delivered to cells, validating the conjugation method and

vector choice, it was also clear that an improved conjugation method allowing for oligonucleotide release under defined conditions would be beneficial.

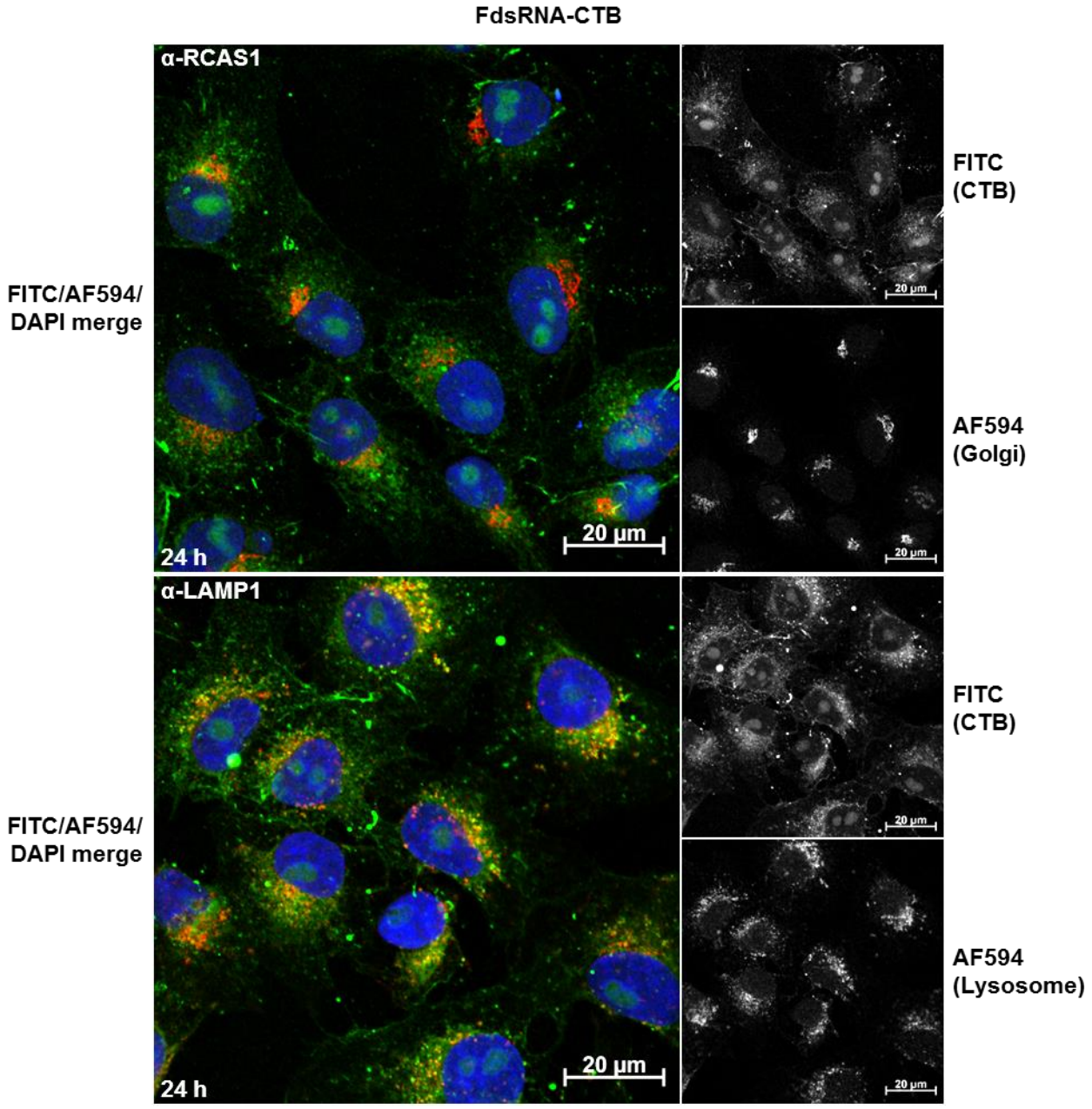

Figure 4.12. Organelle co-staining of FdsRNA-CTB treated Vero cells LSCM imaging of Vero cells incubated with FdsRNA-CTB (5 µg mL^{-1} protein) for 24 h and stained with anti-RCAS1 (Golgi; above) or anti-LAMP1 (lysosome; below) primary Ab followed by AF594-conjugated secondary Ab. Each panel shows a false-colour merged image (left) of AF594 (organelle; red), fluorescein (RNA; green) and DAPI (nuclei; blue), in addition to individual red (AF594; upper right) and green (fluorescein; lower right) channels.

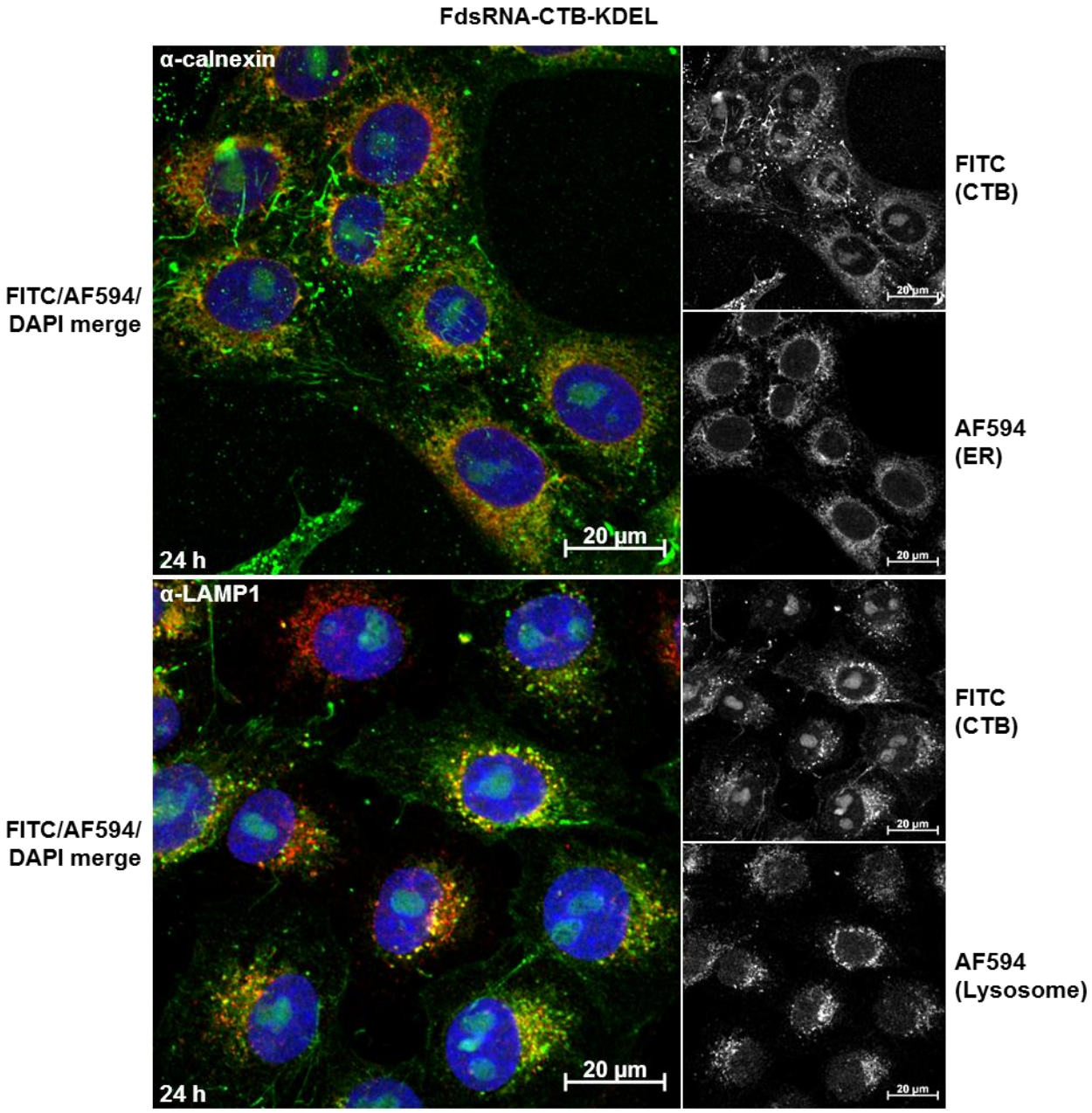

Figure 4.13. Organelle co-staining of FdsRNA-CTB-KDEL treated Vero cells LSCM imaging of Vero cells incubated with FdsRNA-CTB-KDEL (5 µg mL^{-1} protein) for 24 h and stained with anti-calnexin (ER; above) or anti-LAMP1 (lysosome; below) primary Ab followed by AF594-conjugated secondary Ab. Each panel shows a false-colour merged image (left) of AF594 (organelle; red), fluorescein (RNA; green) and DAPI (nuclei; blue), in addition to individual red (AF594; upper right) and green (fluorescein; lower right) channels.

Chapter 5: Towards autonomous oligonucleotide release by disulfide reduction

The previous chapter demonstrated that oligonucleotides conjugated to CTB could be transported into Vero cells. However, it also demonstrated that the oligonucleotides were localising with CTB to the ER or the lysosome, neither ideal locations. A conjugation strategy which would allow controlled oligonucleotide release from CTB was investigated. This chapter outlines the synthesis of a thiolated oligonucleotide capable of protein modification through disulfide formation. The design, production and optimisation of CTB variants containing a free Cys residue, and the subsequent labelling of these proteins with the thiolated oligonucleotide, are discussed. Finally, the retrotranslocation of one of these proteins and its oligonucleotide payload is examined.

5.1. Introduction

Although CTB was shown to carry conjugated oligonucleotides into cells, release of the payload was not achieved. A mechanism of controlled release was required to separate the oligonucleotides from the protein, paving the way for removal of the oligonucleotide to a therapeutically relevant region. Reversibly labelling proteins containing a His-tag with NTA based probes[304] was considered, but studies at the University of Leeds (A. Mercer) have shown that His-tagged B_5 proteins express poorly and are unstable in solution. There are examples of biotin-derivatised photocleavable linkers that have been used for 5′ synthetic oligonucleotide modification[305], and other photocleavable linkers used to conjugate peptides to other species including oligonucleotides[306,307]. However, photocleavable linkers are not amenable to *in vivo* use, so were disregarded. Use of an acid-labile linker shown to be suitable for protein modification and capable of endosomal or lysosomal release[308] was also considered, but the azidomethyl-methylmaleic anhydride linker was non-specifically conjugated via free amine groups, so site-specific labelling of CTB would not be possible without excessive modification of the protein to remove excess surface amines.

A possible alternative mechanism (outlined in figure 5.1) was inspired by the mechanism of action of the holotoxin. On entry to the ER, the toxic A1 subunit is released from the A2 subunit through reduction of the disulfide bond linking the two[37]. It was theorized therefore that anything attached to CTB via a disulfide bond should be carried into a cell with CTB, and on entering the ER the payload would be released through reduction of the disulfide by PDI and glutathione[70]. This design had the benefit that labelled CTB containing a C-terminal KDEL had already been shown to build up in the ER over 24 h, indicating that an oligonucleotide-labelled CTB should act as a suitable delivery vector.

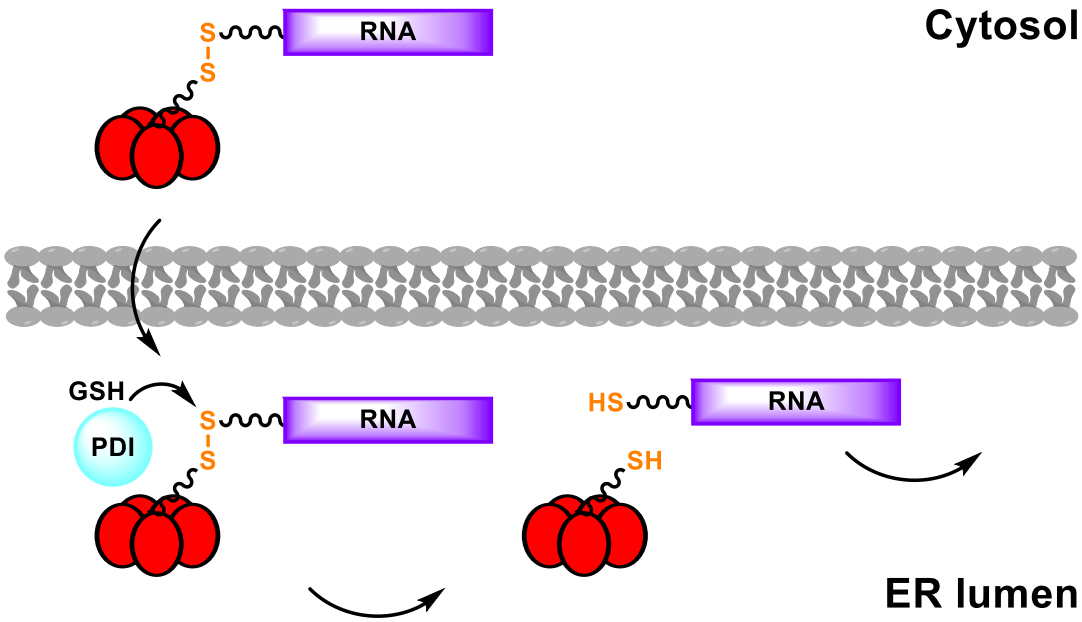

Figure 5.1. Mechanism for CTB-mediated oligonucleotide delivery to, and release from, the ER by disulfide reduction RNA (purple) is attached to CTB (red) via a disulfide bond (orange). CTB is trafficked to ER where the disulfide is reduced by PDI (blue) and glutathione, releasing it from CTB.

Labelling of the Cys-containing CTB variant would require a thiolated oligonucleotide. However, forming disulfides from reduced thiols *in vitro* can be troublesome due to the potential for cross-reactions and lack of catalysts for formation. A method of promoting disulfide formation between CTB and the oligonucleotide whilst preventing symmetrical disulfide formation was required. Previously, proteins have been site-specifically modified at Cys residues to form disulfide bonds using reagents containing bromomaleimide groups[309], methanethiosulfonate groups[310,311], phenylthiosulfonate groups[312] and phenylselenenylsulfide groups[313]. This last category is also able to be reversed such that the protein bears the phenylselenenylsulfide group through chemical

modification of a Cys residue[313], allowing conjugation to other thiol-containing moieties. However, these approaches would require multi-step chemical synthesis to produce the reactive groups, and have never been tested with modified oligonucleotides, where the phosphorothioate group could result in unwanted side-reactions. Pyridylthio groups[314] offer a simpler alternative to those mentioned above. They form disulfides with reduced thiol groups (including Cys residues present in proteins) relatively rapidly (~ 1 h) at room temperature and physiological pH, requiring no catalyst or other reactant, through thiol-disulfide exchange[314] (figure 5.2). They are commercially available (Sigma Aldrich), removing the need to chemically synthesize the reactive group, and are available as bifunctional molecules with an NHS ester to allow easy conjugation to primary amines, removing the need for addition of a thiol group to the oligonucleotides during synthesis. Previous examples of uses of this molecule include protein-protein conjugation[314], production of chemotherapeutic antibody-drug conjugates[315], intramolecular protein crosslinking for structural studies[316], enzyme conjugation to silica nanoparticles for cell delivery[317] and conjugation of peptide nucleic acids to a cationic polymer for cell transfection[318], all reversible under reducing conditions and releasing functional products. This was the method chosen to conjugate the oligonucleotides to a Cys-containing CTB variant.

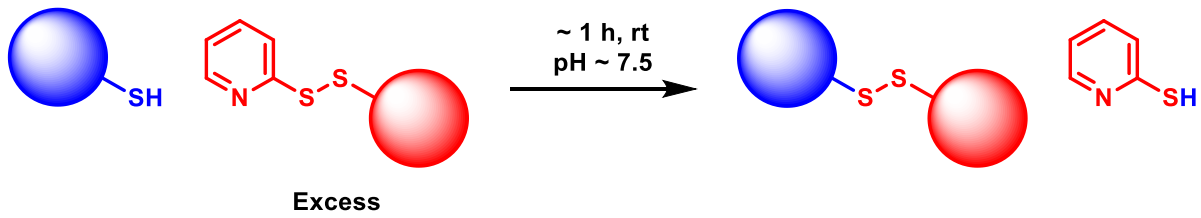

Figure 5.2. Modification of thiol-containing moieties with pyridylthio groups Reaction scheme describing the labelling molecules containing reduced thiols (blue) with molecules containing pyridylthio groups (red) by thiol-disulfide exchange.

5.2. Oligonucleotide synthesis and modification for disulfide labelling

5.2.1. General design characteristics

Oligonucleotides were synthesised as 2′-OMe phosphorothioate RNA, for increased stability and nuclease resistance[3,119,126]. The 5′ end of each oligonucleotide was modified on resin with a primary amine for functionality.

5.2.2. 5′-pyridylthio RNA synthesis

The human β-globin intron skipper antisense oligonucleotide designed by Sazani *et al.*[124,135] (5′-GCUAUUACCUUAACCCAG-3′) was synthesised for conjugation to CTB. Following solid phase synthesis and purification, the 5′-amino skipper RNA was isolated with 42% yield. The 5′-amino oligonucleotide was reacted with 3-(2-pyridyldithio)propionate NHS ester (figure 5.3) to form the 5′-pyridylthio skipper RNA with 86% yield.

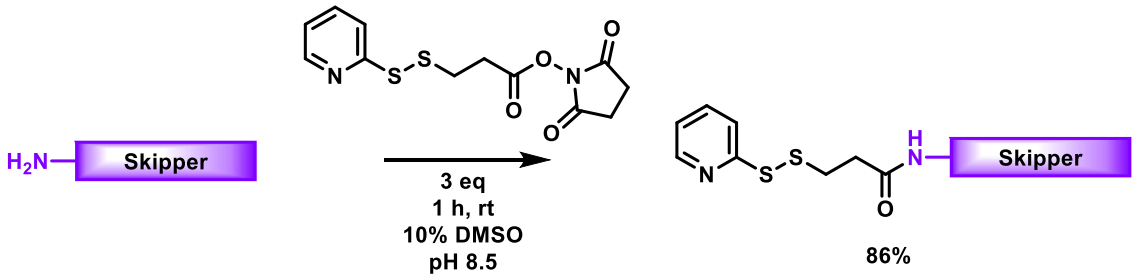

Figure 5.3. Pyridylthio incorporation into synthesised oligonucleotides Reaction scheme describing 5′-amino skipper RNA (purple) labelling with 3-(2-pyridyldithio)propionate NHS ester (red).

5.2.3. Bis-fluorescein and bis-rhodamine complement RNA synthesis

The complementary sequence to the skipper RNA (5′-CUGGGUUAAGGUAAUAGC-3′), hereafter termed complement RNA, was synthesised for recognition and staining of the skipper RNA. It was synthesised with primary amines at both the 5′ and 3′ ends, as double fluorophore labelling of oligonucleotide probes has been shown to improve signal during hybridisation experiments[319]. Following solid phase synthesis and purification, the bis-amino complement RNA was isolated with 20% yield. The lower product yield compared to the previous synthesis probably occurred due to product loss during the requirement of an extra preparatory HPLC purification step. The pure bis-amino oligonucleotide was reacted with either 6-carboxyfluorescein NHS ester (figure 5.4A) or 6-carboxytetramethylrhodamine NHS ester (figure 5.4B) to form bis-fluorescein complement RNA or bis-rhodamine complement RNA, with yields of 51% and 87%, respectively. Both fluorescein and rhodamine probes were formed to allow for more co-staining combinations in later experiments.

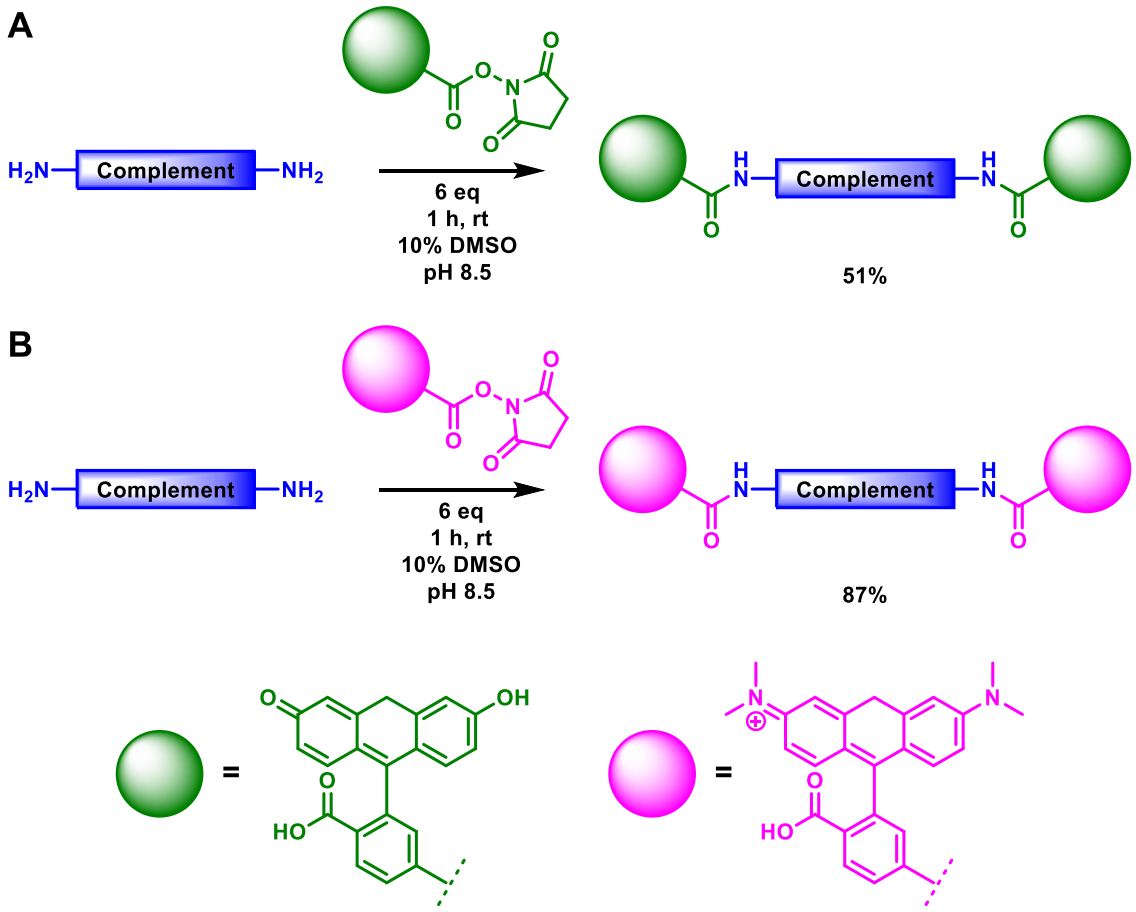

Figure 5.4. Fluorophore incorporation into synthesised bis-amino oligonucleotides Reaction scheme describing bis-amino complement RNA (blue) labelling with A. 6-carboxyfluorescein NHS ester (green) and B. 6-carboxytetramethylrhodamine NHS ester (magenta).

5.3. Production of a Cys-containing CTB variant for disulfide labelling

5.3.1. Initial attempts at Cys introduction

Several means of introducing a free thiol into CTB for disulfide formation were considered. Chemical means were discounted due to the increase in overall complexity, and the decrease in yield due to further reaction and purification steps. The possibility of introducing a non-native Cys residue into a surface-exposed loop of CTB was investigated. Residues K43 and S55 (upper face and binding face, respectively; figure 5.5) were identified as potential sites for mutation due to surface exposure, lack of reported critical interactions, structural similarity to Cys (S55) and distal positioning to the binding sites (K43). Both residues were replaced with Cys by site-directed mutagenesis, but both K43C and S55C resulted in no detectable protein expression. This was presumably due to the non-native Cys residues disrupting the formation of native

disulfides within the protomers, which form between residues C9 and C86 (figure 5.5), during translation.

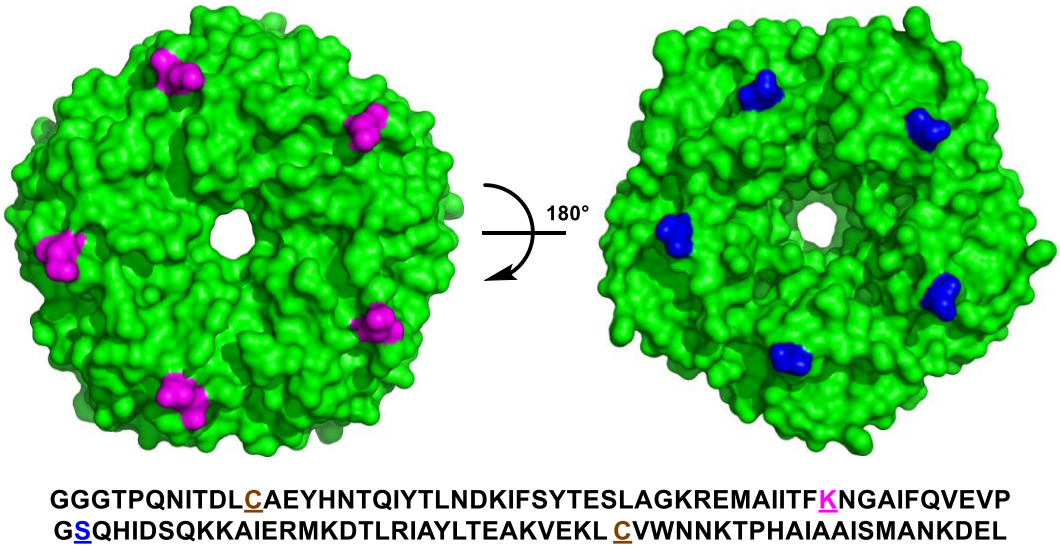

Figure 5.5. Attempted CTB Cys incorporation The upper face (left) and binding face (right) of CTB at 1.25 Å resolution (PDB ref. 3CHB), with the residues at which Cys insertion was attempted highlighted; K43 (magenta) and S55 (blue). The sequence (below) highlights the sequence positions of K43 (magenta) and S55 (blue), in addition to the native disulfide-forming C9 and C86 residues (brown).

5.3.2. Expression and purification of CTB-PkC11

After unsuccessful initial attempts to incorporate Cys residues into CTB, a new approach was required. It has been shown that Cys residues can be incorporated into LTB, which has 80% sequence similarity to CTB, via a C-terminal extension[113]. This consisted of a 14 residue spacer epitope, termed the Pk tag, containing a Cys residue at position 11 (PkC11; sequence GKPIPNPLLGCDST[113]). A CTB variant was designed to include the PkC11 tag immediately following the C-terminal Asn residue. This had the added advantage of keeping the oligonucleotide labels clear of the GM1 binding sites, as the C-termini extend from the opposite face of the protein[22].

The DNA coding sequence was produced by assembly PCR and subcloned into pSAB2.2 using SphI and PstI restriction endonucleases. The protein (CTB-PkC11) was expressed from this plasmid in *E. coli* C41(DE3) cells by IPTG induction overnight at 25 °C and extracted from the growth medium by ammonium sulfate precipitation. The protein was initially purified by Ni^{2+} affinity chromatography. SDS-PAGE analysis (figure 5.5A) showed a protein band of approximately 56 kDa in the elution fractions, which was

replaced with a band of approximately 14 kDa on denaturation, indicating CTB. Impurities left over from Ni^{2+} affinity chromatography were removed by SEC (figure 5.5B). This resulted in a major A_{280} peak at approximately 210 mL, which was identified as CTB-PkC11 by SDS-PAGE (figure 5.5C) and LC-MS, with a mass of 13208.4 Da detected (13208.1 Da calculated).

Whilst expression of CTB-PkC11 was successful, the yield was poor; approximately 0.4 mg pure protein was isolated per 1 L cultured cells. This was possibly, at least partially, due to proteolysis. When expressing LTB-PkC11 in *Vibrio* sp. 60, the authors noted that the PkC11 tag was proteolytically cleaved in the growth medium leading to low yield, which could be improved by addition of EDTA at the point of induction of protein overexpression[113]. However, addition of EDTA during protein overexpression in *E. coli* C41(DE3) cells abrogated expression. This was the only variable besides induction time (which was followed for CTB-PkC11 expression) that was found to positively affect protein yield[113]. Additionally, the incorporation of the C-terminal PkC11 tag also seemed to decrease the stability of the pentamer. This was demonstrated by SDS-PAGE (figure 5.5A and C), in the appearance of protomeric CTB bands in lanes which had not been denatured by heating, which are not seen when running wt CTB. This is perhaps not surprising, as previous CTB C-terminal modifications have been shown to cause pentameric instability[247]. In addition to these issues, CTB-PkC11 also does not possess a C-terminal KDEL signal sequence. Without this, labelled CTB localised to the Golgi apparatus over 24 h, whereas oligonucleotide release was reliant on disulfide bond reduction which would primarily occur in the ER. This analysis indicated a more optimal protein design was required prior to cell experimentation. However, sufficient CTB-PkC11 was produced to test and optimise the oligonucleotide labelling procedure.

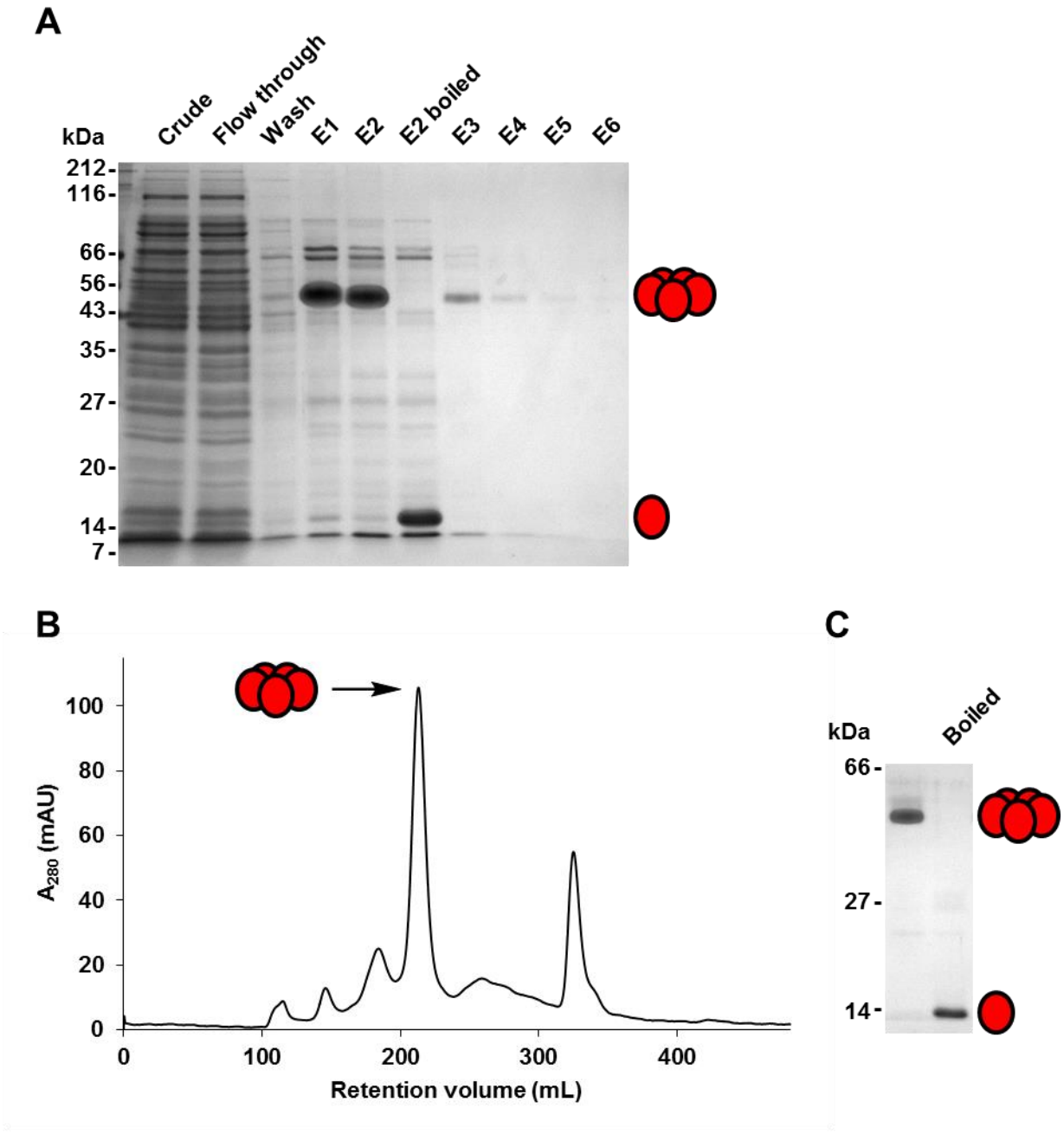

Figure 5.5. Purification of CTB-PkC11 A. SDS-PAGE analysis of CTB-PkC11 purification by Ni^{2+} affinity chromatography. CTB-PkC11 as pentamer and dissociated protomer are indicated. B. A_{280} trace from SEC purification of Ni^{2+}-purified CTB-PkC11, with the desired protein peak indicated. C. SDS-PAGE analysis of the indicated CTB-PkC11 peak.

5.3.3. Labelling CTB-PkC11 with 5′-pyridylthio skipper RNA

CTB-PkC11 (50 mM) in HEPES buffer was initially labelled with 10 eq 5′-pyridylthio skipper RNA at room temperature for 2 h. SDS-PAGE analysis (figure 5.6A) in the absence of reducing agent showed, in place of a single CTB-PkC11 band, the labelled protein appeared as a ladder of several bands spanning approximately 50-80 kDa, indicative of non-homogeneously labelled pentameric protein. When heated to denaturation, the laddered bands were replaced with a single band of approximately 22 kDa, consistent with oligonucleotide-conjugated protomer. This appeared in addition to bands at approximately 14 and 27 kDa, representing unlabelled protomer and protomer-dimer (presumably due to inter-protomer disulfide bond formation due to excessive heat), respectively. Staining the CTB-oligonuceotide complex with bis-fluorescein complement RNA resulted in increased MW of the labelled protein laddered bands, consistent with complement RNA hybridisation to the complex. These bands also appeared fluorescent under UV illumination, confirming complex hybridisation. On denaturation of the stained sample, the labelled pentamer bands were replaced with a protomer band of approximately 25 kDa, which also appeared fluorescent under UV illumination. The RNA-labelled protein (hereafter termed CTB-PkC11(S-S)RNA) was further characterised by analytical SEC (figure 5.6B). The labelled protein presented a lower retention volume and a more intense A_{260} trace compared with unlabelled CTB-PkC11, consistent with the addition of oligonucleotide labels. Product staining with bis-fluorescein complement RNA resulted in a further decrease in retention volume, as well as A_{260} and A_{494} peaks of increased intensity, consistent with fluorescent oligonucleotide addition to the complex. Taken together, these data confirm successful labelling of CTB-PkC11 with 5′-pyridylthio skipper RNA.

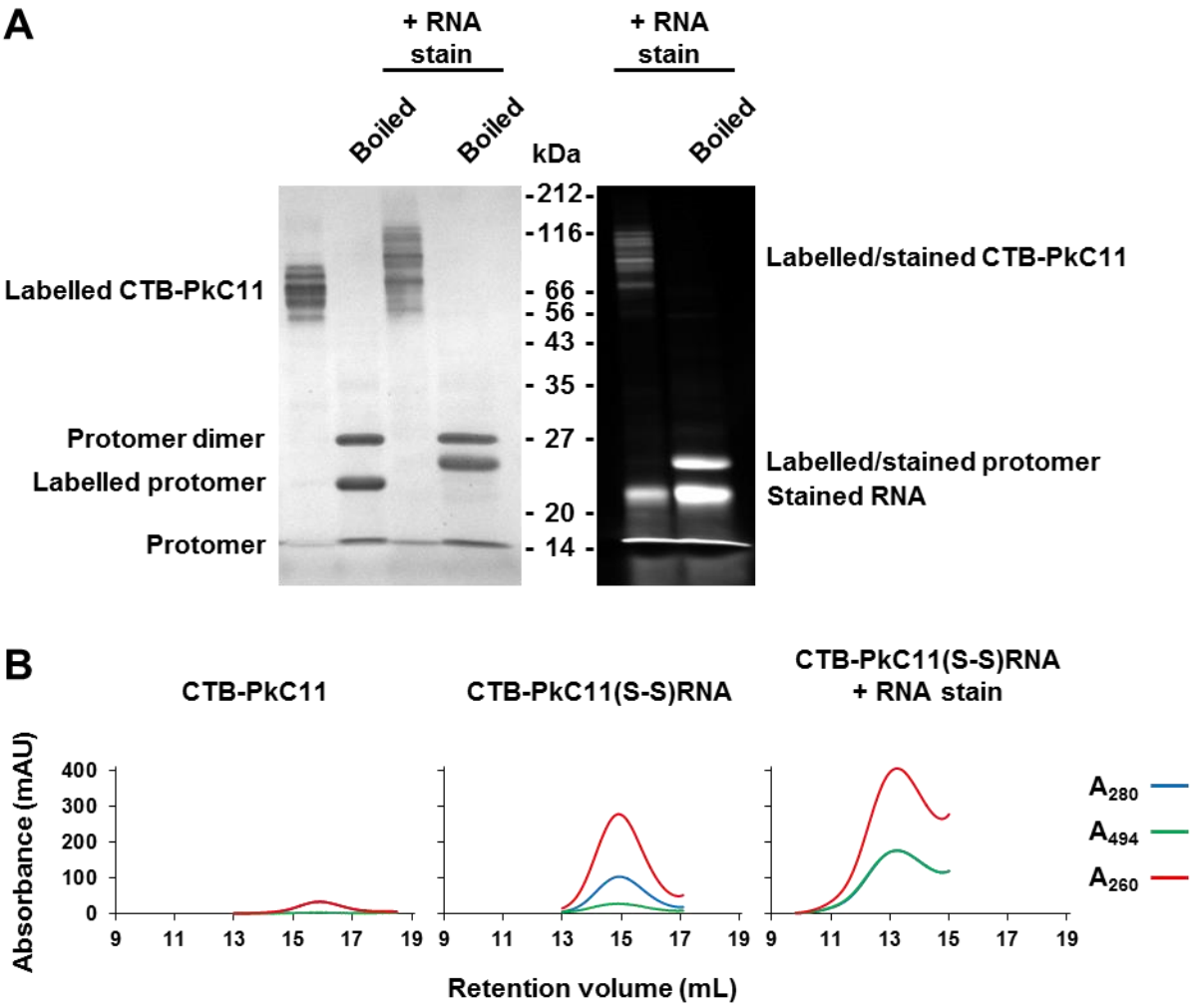

Figure 5.6. Labelling of CTB-PkC11 with 5′-pyridylthio skipper RNA A. Coomassie-stained (left) and UV illuminated (right) SDS-PAGE analysis of CTB-PkC11 labelling with 5′-pyridylthio RNA, in the absence and presence of bis-fluorescein complement RNA staining. B. Analytical SEC comparing the A_{280} (blue), A_{260} (red) and A_{494} (green) traces of untreated (left), 5′-pyridylthio RNA-labelled (centre), and both RNA-labelled and bis-fluorescein complement RNA-stained (right) CTB-PkC11.

5.3.4. Optimising CTB-PkC11 labelling with 5′-pyridylthio skipper RNA

Whilst labelling was successful, supply of the 5′-pyridylthio skipper RNA was limited, and using 10 eq for the reaction probably excessive. Small-scale reactions were conducted on CTB-PkC11 (50 µM) in HEPES buffer with a range of 5′-pyridylthio skipper RNA concentrations (1-10 eq) at room temperature for 2 h. The complete reactions were stained with bis-fluorescein complement RNA for visualisation and analysed by SDS-PAGE (figure 5.7) in the absence of reducing agent. The fluorescent RNA-labelled protomer bands showed an increase in size and intensity between the reactions containing 1 and 1.5 eq 5′-pyridylthio skipper RNA, and again between reactions containing 1.5 and 2 eq, but were more difficult to distinguish thereafter. Therefore, the fluorescence intensity of

the bands was quantitatively determined by densitometry (figure 5.7). These results showed a 66% increase in labelling when using 1.5 eq 5′-pyridylthio skipper RNA compared to 1 eq, 80% when using 2 eq, 83 % when using 3 eq, 85% when using 4 eq, 89% when using 5 eq and 104% when using 10 eq. Balancing the desire for efficient labelling against the desire to minimise use of the oligonucleotide, subsequent labelling reactions were carried out using 5 eq 5′-pyridylthio skipper RNA.

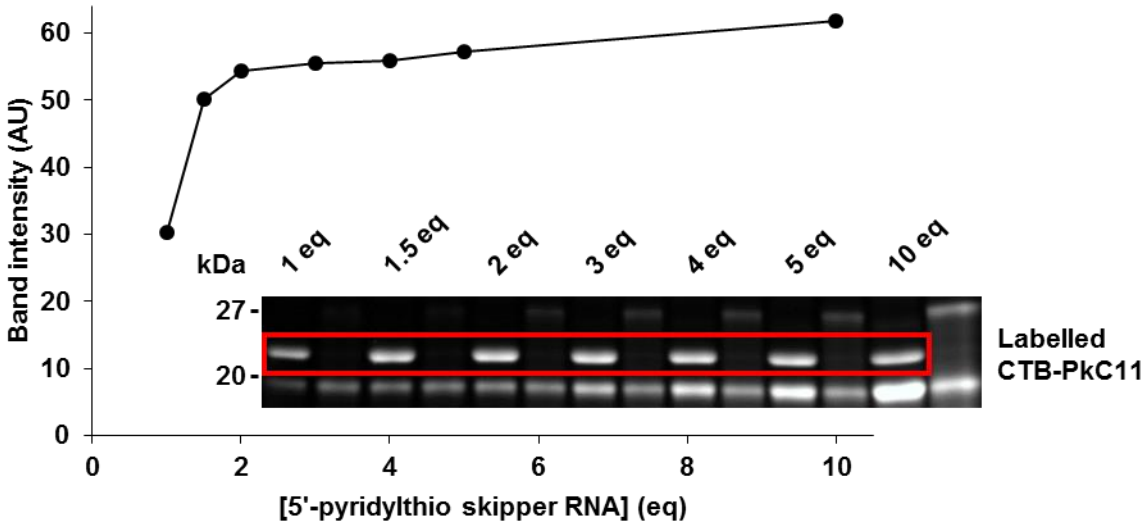

Figure 5.7. Optimisation of CTB-PkC11 labelling with 5′-pyridylthio skipper RNA UV illuminated SDS-PAGE analysis of bis-fluorescein complement RNA-stained CTB-PkC11 labelling reactions conducted with 5′-pyridylthio skipper RNA at increasing concentrations (1, 1.5, 2, 3, 4, 5 and 10 eq). The labelled/stained protein band (red box) intensities were quantified by densitometry and plotted vs 5′-pyridylthio skipper RNA concentration.

5.4. An alternative Cys-containing CTB for oligonucleotide conjugation

5.4.1. Design

Whilst CTB-PkC11 labelling through disulfide formation was successful, the protein itself was sub-optimal due to low expression levels and lack of targeting signal sequence. It was desirable to both improve expression levels and include a C-terminal KDEL signal peptide for ER retention. To this end, a new CTB variant was designed. The protein design was kept simple, consisting of CTB with a C-terminal extension containing a free Cys residue for labelling, a C-terminal KDEL for ER retention, and a five-residue linker region between each for separation and flexibility. The sequence of the designed extension was NGSGNCNGSGNKDEL. The extension was C-terminal so as to avoid disrupting GM1 binding and endocytosis. The linker amino acids were relatively small, neutral and soluble in order to have a minimal effect on the expression and function of the protein. Aromatic and other hydrophobic residues were avoided for solubility reasons, charged residues to avoid disruption of pentamer formation or unintended interactions within the cell, and Pro residues to avoid conformational constraint which could potentially decrease labelling efficiency.

5.4.2. Expression and purification

The DNA coding sequence was produced by assembly PCR, subcloned into pSAB2.2 using SphI and PstI restriction endonucleases and used to transform *E. coli* C41(DE3) cells. The protein (CTB-CKDEL) was expressed by IPTG induction overnight at 25 °C, extracted from the growth medium by ammonium sulfate precipitation and purified by Ni^{2+} affinity chromatography. SDS-PAGE analysis (figure 5.8A) showed a protein band of approximately 56 kDa in the elution fractions, which was replaced with a band of approximately 14kDa on denaturation, indicative of CTB. Remaining impurities following Ni^{2+} affinity chromatography were removed by SEC. This resulted in a major A_{280} peak at approximately 210 mL (figure 5.8B), which was identified as CTB-CKDEL by SDS-PAGE (figure 5.8C) and LC-MS, with a mass of 13261.9 Da detected (13261.9 Da calculated).

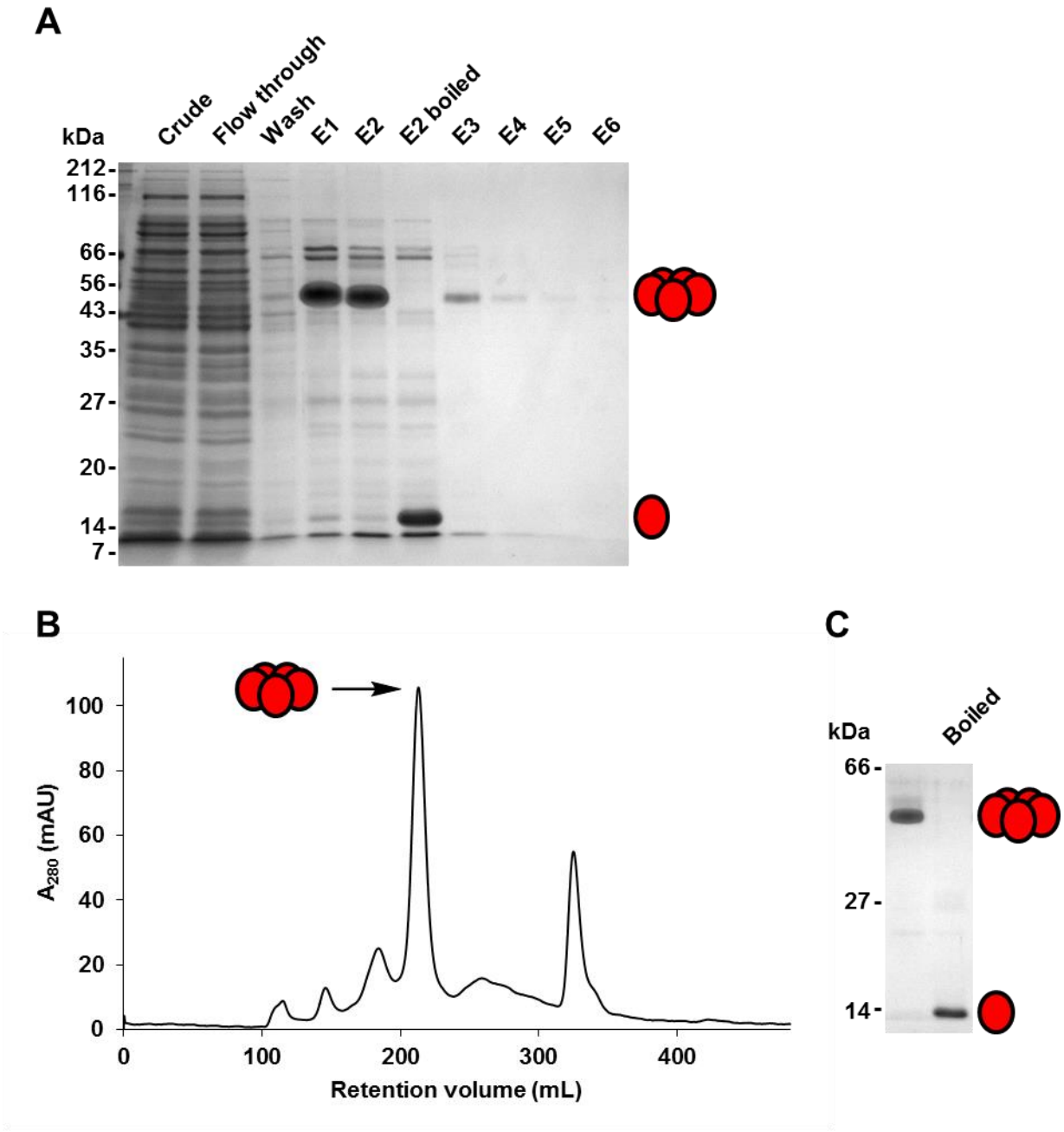

Figure 5.8. Purification of CTB-CKDEL A. SDS-PAGE analysis of CTB-CKDEL purification by Ni^{2+} affinity chromatography. CTB-CKDEL as pentamer and dissociated protomer are indicated. B. A_{280} trace from SEC purification of Ni^{2+}-purified CTB-CKDEL, with the desired protein peak indicated. C. SDS-PAGE analysis of the indicated CTB-CKDEL peak.

5.4.3. Labelling CTB-CKDEL with 5′-pyrdidylthio RNA

CTB-CKDEL was incubated for 1 h with immobilised tris(2-carboxyethyl)phosphine (TCEP) resin to ensure full reduction of disulfides. The reduced protein (215 μM) was labelled with 5 eq 5′-pyridylthio RNA for 2 h at room temperature. SDS-PAGE analysis (figure 5.9) in the absence of reducing agent showed the labelled protein (hereafter termed CTB-CKDEL(S-S)RNA) as a ladder of four discrete bands ranging from approximately 50-65 kDa, indicative of the pentameric protein labelled with 0-3 oligonucleotides. Staining the labelled protein with bis-fluorescein complement RNA caused the bands to separate further and appear fluorescent under UV illumination, allowing traces of 4 and 5 oligonucleotide-labelled CTB-CKDEL to be seen. On denaturation, the laddered bands were replaced with lower MW bands representing labelled and unlabelled protomer, along with protomer dimer. The labelled protomer band was identified by bis-fluorescein complement RNA staining, resulting in increased MW and fluorescent appearance under UV illumination. All of the above samples were also analysed in the presence of DTT (figure 5.9) to identify the presence of a disulfide bond. Under reducing conditions, labelled CTB-CKDEL presents as a single band of similar size to both untreated CTB-CKDEL and the lowest MW band of the laddered labelled protein, while the band present following heat denaturation was of similar size to unlabelled CTB-CKDEL protomer. Moreover, when the labelled protein was stained with bis-fluorescein complement RNA under reducing conditions, the protein bands neither shifted in MW nor appeared fluorescent under UV illumination, showing conclusively that the oligonucleotide label was conjugated via a disulfide bond. Interestingly, the protomer-dimer band of approximately 27 kDa present in boiled samples containing CTB-PkC11 and CTB-CKDEL did not appear under reducing conditions, confirming this species was forming through inter-protomer disulfide bond formation promoted by the excessive heating.

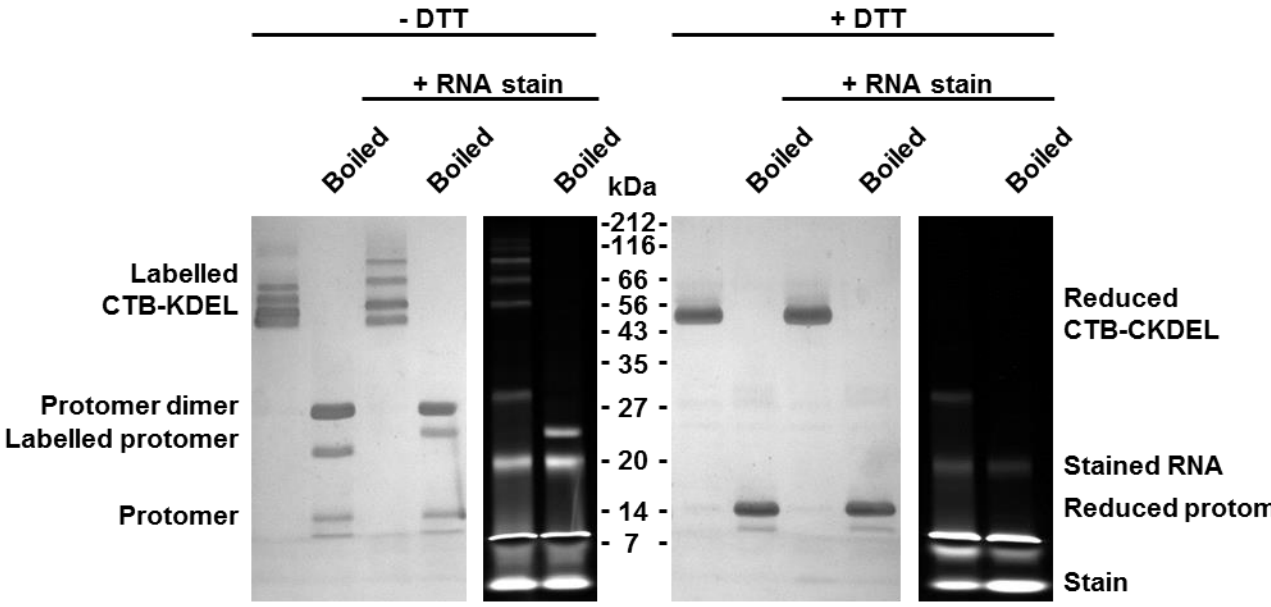

Figure 5.9. Labelling of CTB-CKDEL with 5′-pyridylthio RNA Coomassie-stained (left) and UV illuminated (right) SDS-PAGE analysis of CTB-CKDEL labelling with 5′-pyridylthio RNA, in the absence and presence of both bis-fluorescein complement RNA staining and DTT.

5.4.3. Purification of CTB-CKDEL(S-S)RNA

CTB-CKEL(S-S)RNA was purified into HEPES buffer by SEC (figure 5.10A). Three peaks were identified; one at approximately 55 mL (A_{280}/A_{260} = 0.35), one at approximately 81 mL (A_{280}/A_{260} = 0.23), and one at approximately 97 mL (A_{260} peak saturated). The first peak was identified as CTB-CKDEL(S-S)RNA, with the retention volume consistent with a complex of this size (Superdex prep grade and prepacked HiLoad columns handbook; GE Healthcare). The peak identity was confirmed by SDS-PAGE (figure 5.10B). The second peak was identified as oligonucleotide dimers, with the A_{260}/A_{280} more consistent with oligonucleotides than protein, and the retention volume consistent with a complex of this MW. The third peak was identified as free 5′-pyridylthio RNA.

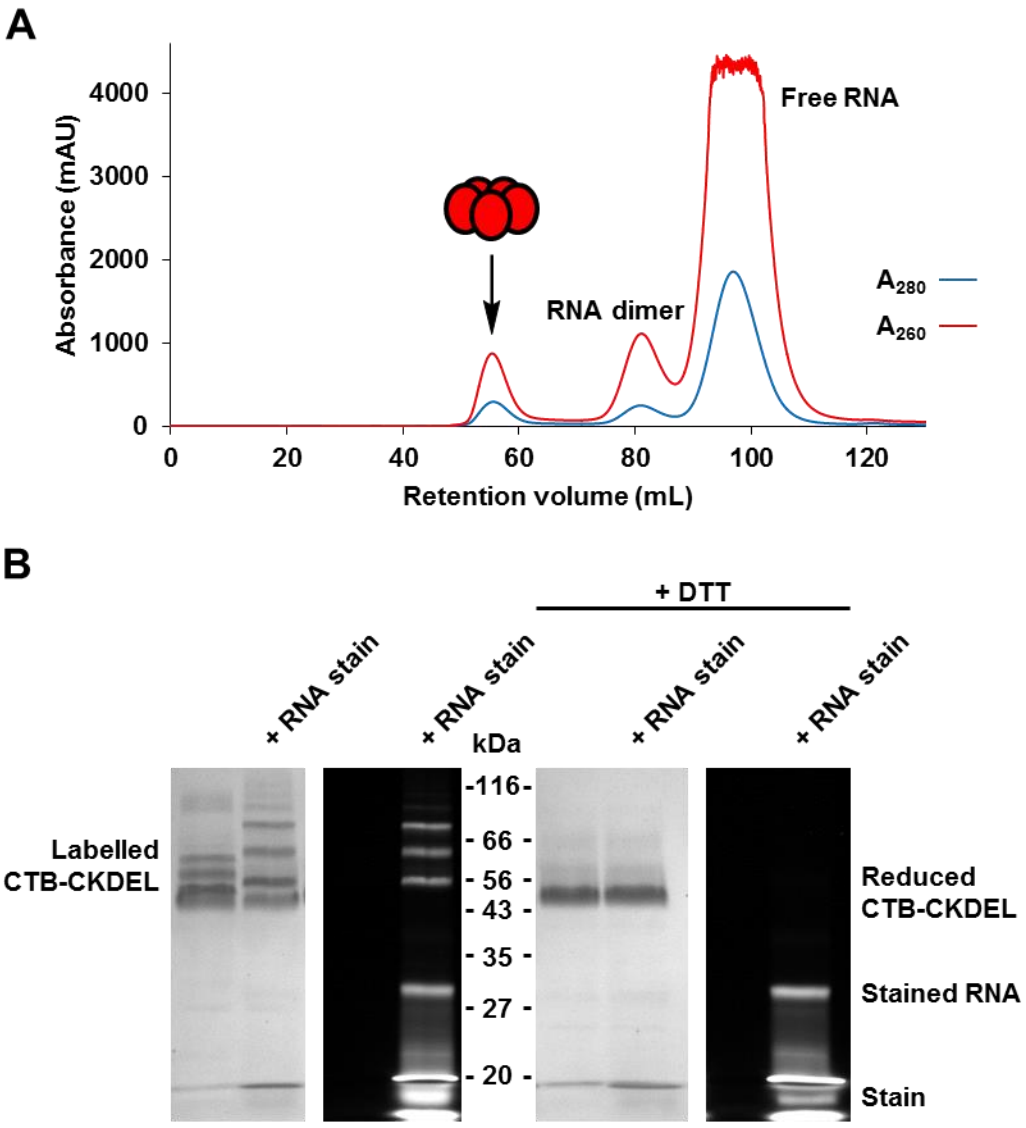

Figure 5.10. Purification of CTB-CKDEL(S-S)RNA A. SEC purification of the CTB-CKDEL labelling reaction with 5′-pyridylthio RNA, showing the A_{280} (blue) and A_{260} (red) traces, with the labelled protein peak indicated with an arrow. B. SDS-PAGE analysis of the labelled protein peak, in the absence and presence of both bis-fluorescein complement RNA staining and DTT.

Following SEC purification, the labelled protein SDS-PAGE bands (figure 5.10) were quantified by densitometry to determine labelling efficiency. An average of 25% labelling was determined; 42% of the protein possessed a single oligonucleotide label, 20% possessed two labels, 12% possessed three labels, 2% possessed four labels and 1% possessed five labels, while 25% of the protein was unlabelled (to the nearest integer). Pure CTB-CKDEL(S-S)RNA was isolated at 210 µM (450 µL).

5.5. Investigating oligonucleotide delivery and release in mammalian cells

5.5.1. Determining cytotoxicity

Prior to cell imaging experiments, cell viability on incubation with CTB-CKDEL(S-S)RNA was assayed to determine if the released oligonucleotides would have a cytotoxic or inhibitory effect on cells. The MTT cell viability assay was performed. In principle, cells are treated with the MTT reagent, a tetrazolium dye which is yellow in solution. In live cells, the dye is reduced by cellular NAD(P)H-dependent oxidoreductase enzymes to a formazan (figure 5.11), an insoluble purple molecule. The formazan crystals are dissolved in an organic solvent, for example DMSO, and the A_{570} recorded; a higher reading is indicative of a greater reduction rate, and thus greater cell viability[320-322].

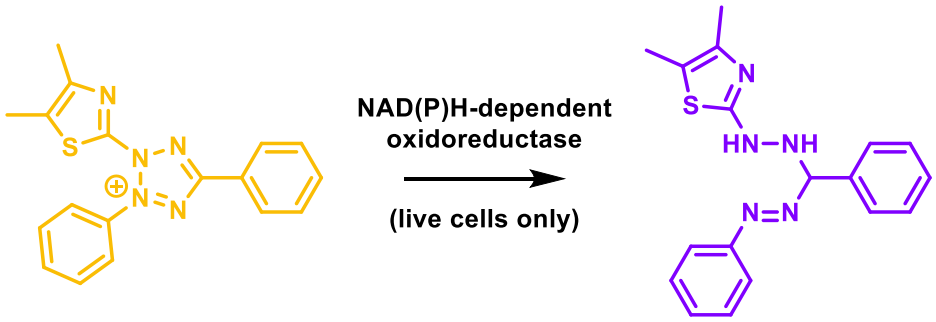

Figure 5.11. Cell viability following CTB-CKDEL(S-S)RNA transfection A. Scheme describing tetrazolium MTT reagent (yellow) reduction to a formazan (purple) during an MTT assay.

Vero cells incubated with CTB-CKDEL(S-S)RNA (10 µg mL^{-1}) for 24 h or 48 h were assayed (figure 5.12). These were compared to mock treated and CTB-KDEL transfected cells as positive viability controls, and staurosporine[323] treated cells as a negative viability control. At both time points, cell viability appeared slightly increased for CTB-treated cells compared to the mock control. It is possible that retrotranslocation and cell processing of CTB, and RNA where applicable, resulted in increased cell metabolism, which can result in increased reduction of the MTT reagent and higher absorbance readings[320-322]. However, overall the assay showed no negative effect on cell viability following incubation with CTB-CKDEL(S-S)RNA.

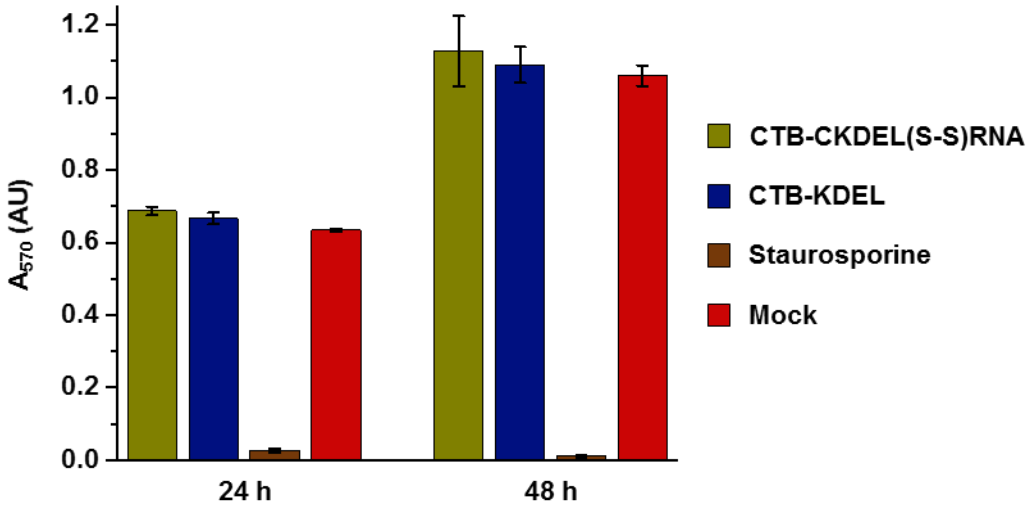

Figure 5.12. Vero cell viability following incubation with CTB-CKDEL(S-S)RNA MTT assay comparing Vero cell viability following incubation for 24 or 48 h with CTB-CKDEL(S-S)RNA (olive), CTB-KDEL (blue) or staurosporine (brown), compared against mock transfected cells (red). Data shown as mean ± standard error of three separate experiments.

5.5.2. Investigating endocytosis

Vero cells were treated with CTB-CKDEL(S-S)RNA to confirm that CTB could carry disulfide-bonded oligonucleotides into cells and release them within the ER. Cells were incubated at 37 °C with CTB-CKDEL(S-S)RNA (5 μg mL^{-1} protein), or an equivalent concentration of pyridylthio-RNA, over 24 h and fixed with PFA after 15 min, 30 min, 1 h, 2 h, 4 h, 8 h and 24 h. The cells were stained for RNA by FISH, using a bis-rhodamine complement RNA probe, then for CTB with a rabbit anti-CTB primary Ab followed by a donkey anti-rabbit AF488-conjugated secondary Ab. LSCM imaging (figure 5.13) showed CTB was able to deliver the oligonucleotide into cells, but in the absence of CTB there was no rhodamine staining following FISH, which would indicate RNA uptake. Initially, the protein and oligonucleotide remained co-localised, following the standard endocytic pathway of CTB-KDEL. However, at 8 h the RNA distribution differentiated from the protein. While CTB-CKDEL remained diffuse across the ER, the previously diffuse RNA coalesced into punctate foci in the region of the ER. At 24 h, the difference in distribution was more pronounced. The RNA appeared increasingly punctate with greater numbers of foci, and spread further throughout the cell. The relative distributions suggested CTB mediated the transport of the oligonucleotide to the ER, where the disulfide bond tethering the two was reduced and the oligonucleotide released from the protein. Subsequently, the oligonucleotide was gathered, packaged and transported away from the ER, possibly to the lysosome for degradation by autophagy[300-303].

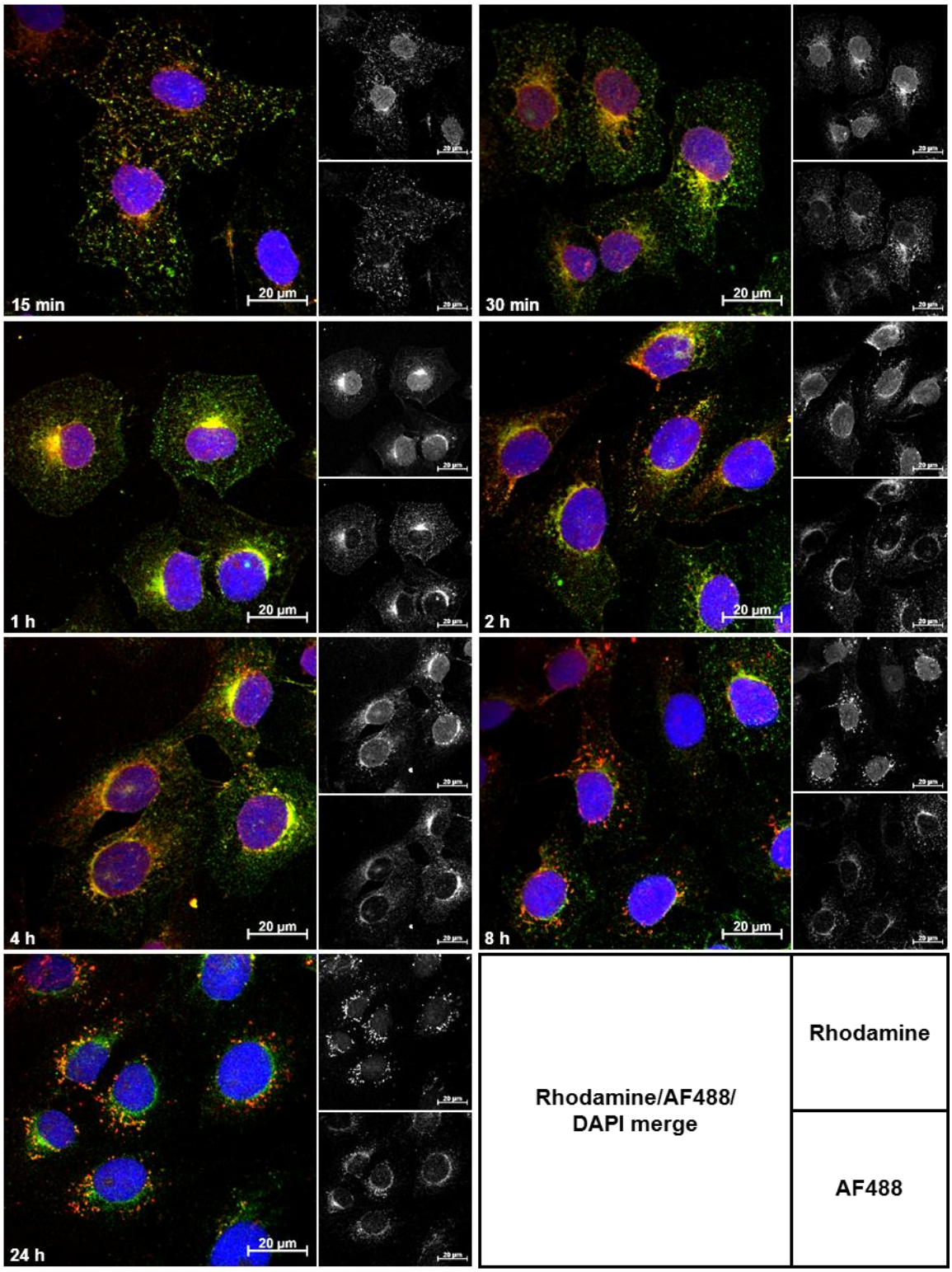

Figure 5.13. Time course of CTB-CKDEL(S-S)RNA incubation with Vero cells LSCM imaging of Vero cells incubated with CTB-CKDEL(S-S)RNA, fixed after 15 min, 30 min, 1 h, 2 h, 4 h, 8 h or 24 h, and stained for RNA by FISH and CTB by IF. Each panel shows a false-colour merged image (left) of rhodamine (RNA; red), AF488 (α-CTB; green) and DAPI (nuclei; blue), in addition to individual red (rhodamine; upper right) and green (AF488; lower right) channels.

To investigate the fate of the oligonucleotides, Vero cells were incubated at 37 °C with CTB-CKDEL(S-S)RNA (5 μg mL^{-1}) for 24 h and stained for RNA by FISH. Cells were co-stained for either PDI, an ER chaperone involved in disulfide formation[324], with an anti-PDI primary Ab, or LAMP1, a lysosomal transmembrane protein involved in regulating lysosome motility[325], with an anti-LAMP1 primary Ab, to detect the ER or the lysosome, respectively. The primary Abs were stained with an AF488-conjugated secondary Ab, mounted with DAPI, and viewed by LSCM (figure 5.14). The RNA showed some co-localisation with both the ER and the lysosome. The distribution of the lysosome staining more closely matched that of the RNA staining, showing a greater degree of co-localisation than with the ER. However, the morphology of the ER staining appeared punctate, more consistent with the morphology of the RNA staining than with the more diffuse lysosome staining. This suggested that RNA was present in both organelles, probably being transported directly from the ER to the lysosome, and had been unable to escape into the cytoplasm. Though this was never a likely possibility, it was unfortunate as the cytosol represents a more therapeutically relevant location. However, it was encouraging that CTB-mediated delivery and release of the disulfide tethered oligonucleotide had been achieved. This also suggested that the modified RNA was targeted for lysosomal degradation whether single- or double-stranded, indicating that an improved targeting method would need to be devised.

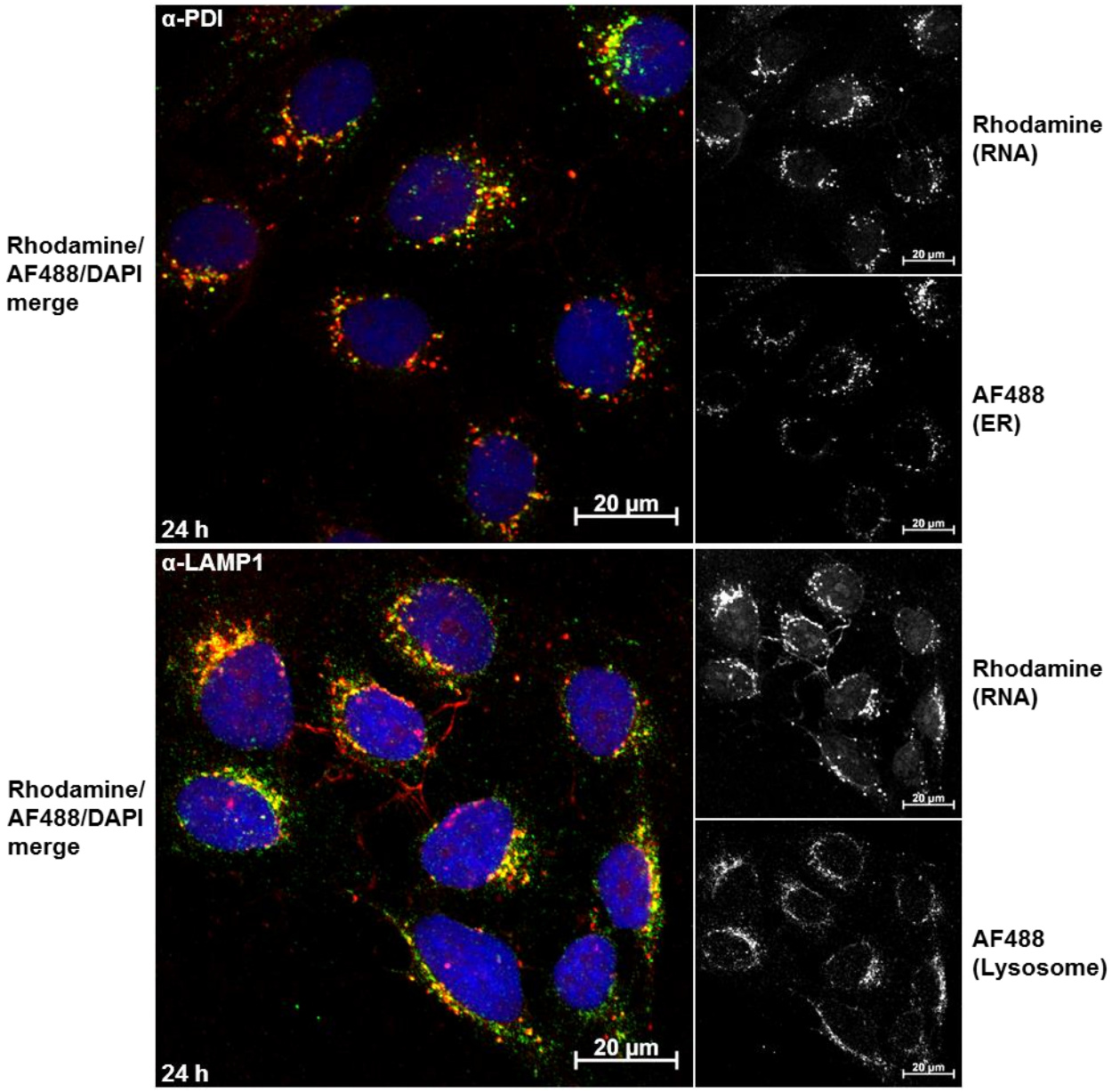

Figure 5.14. Organelle staining of CTB-CKDEL(S-S)RNA treated Vero cells LSCM imaging of Vero cells incubated with CTB-CKDEL(S-S)RNA, fixed after 24 h, and stained for RNA by FISH and either the ER (α-PDI Ab; upper panel) or lysosome (α-LAMP1 Ab; lower panel) by IF. Each panel shows a false-colour merged image (left) of rhodamine (RNA; red), AF488 (organelle; green) and DAPI (nuclei; blue), in addition to individual red (rhodamine; upper right) and green (AF488; lower right) channels.

Chapter 6: Towards autonomous oligonucleotide release by Sec61 recognition

The previous chapter demonstrated that oligonucleotides can be transported into Vero cells with CTB and released in the ER, but cytosolic delivery was not achieved. A method of oligonucleotide conjugation which would allow targeted release of the oligonucleotide from CTB and escape into the cytosol was investigated. This chapter outlines various attempts to form peptide-conjugated oligonucleotides capable of cellular delivery and release by CTB. The synthesis of several unstructured peptide-oligonucleotide conjugates, in addition to a series of truncated complementary oligonucleotides bearing 5′-azide functional groups, and their conjugation to CTB, is discussed. Optimisation of the conjugates for delivery and production of a final set of peptide-RNA-CTB complexes for cellular experimentation is described, along with subsequent cell delivery tests.

6.1. Introduction

Whilst delivering oligonucleotides to the ER and releasing them from the carrier protein represents a step forward towards targeted drug delivery, the mechanism discussed in the previous chapter possessed a potential caveat. Once the oligonucleotide was released, it contained no targeting feature to ensure it was exported from the ER to a location where a therapeutic effect could be delivered, for example to the cytosol or ideally to the nucleus.

A possible mechanism for achieving oligonucleotide recognition and transport from the ER was inspired by another step in the export of CTA1 from the ER; the recognition of the unfolded C-terminus of CTA1 for export from the ER by the Sec61 translocon[75,77]. It has been shown that unstructured peptides, as well as proteins, are exported from the ER by the Sec61 translocon[326]. Conjugating an unstructured peptide to an oligonucleotide could increase the likelihood of export of the oligonucleotide from the ER into the cytosol by the Sec61 translocon, effectively subverting the ER-associated degradation pathway similar to CTA1[73,75]. However, this posed a new problem in the form of the method of attachment to CTB. The previous method of attaching a modified oligonucleotide to CTB,

hybridisation with a complementary strand covalently conjugated to the protein (chapter 4), would not be suitable in this case as there is no mechanism for oligonucleotide release.

Differential dual modification of a single oligonucleotide was considered, combining a pyridylthio group at one end for reversible CTB conjugation with an unstructured peptide at the other for export recognition. Synthesis of an oligonucleotide containing a protected 5′ amine (as previously used) and an unprotected 3′ amine would allow for controlled, site-specific labelling. However, during previous oligonucleotide synthesis the 5′ amine MMT protecting group was found to be unstable at or below neutral pH. During removal of aqueous ammonia following resin cleavage, the resulting pH decrease routinely resulted in the loss of at least 30% of the protecting group (figure 6.1). As a result, the synthesis of a differentially dual labelled oligonucleotide would be complicated, with decreased control over which functional group was appended to which amine. This would lead to a non-homogeneous mix which would be difficult to purify, with a hugely reduced yield, and so this approach was disregarded.

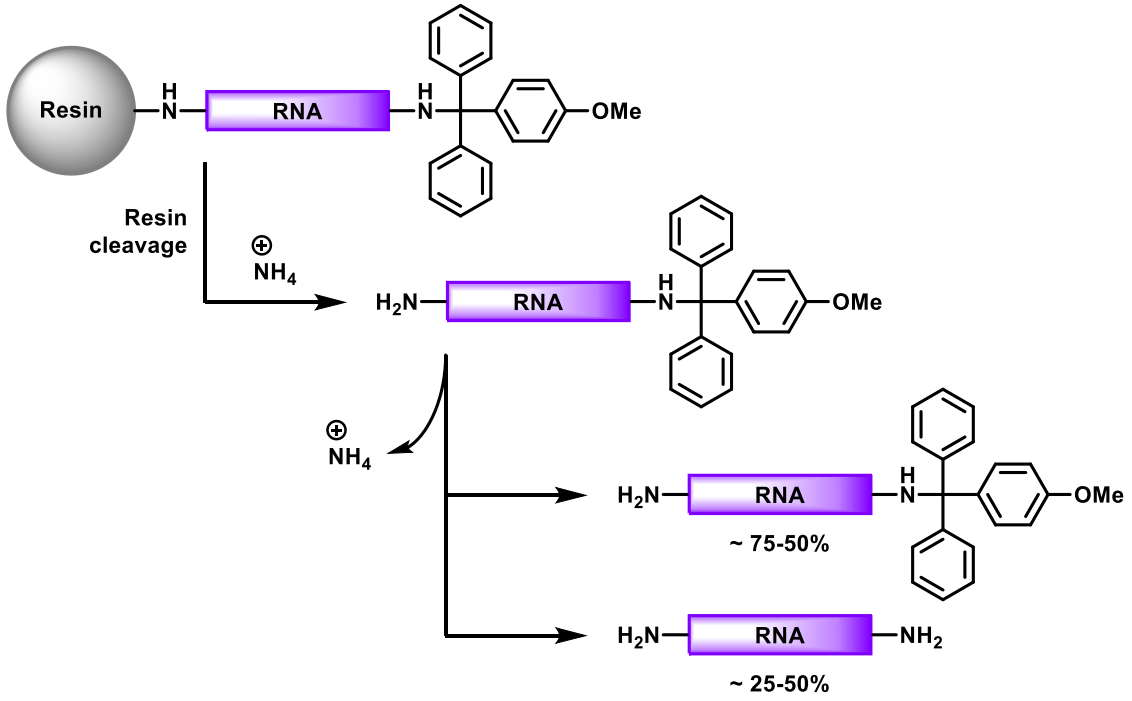

Figure 6.1. Instability of the MMT protecting group Reaction scheme describing MMT protecting group instability. Removal of ammonia, used for resin cleavage of the synthesised oligonucleotide, prior to deprotection or purification resulted in the loss of 25-50% of the MMT protecting group.

A feasible approach for oligonucleotide conjugation and release was inspired by the holotoxin, in addition to a combination of previously successful approaches to oligonucleotide conjugation and release. The CTA1-CTA2 junction, containing the disulfide linking the two domains[20] and the region of the toxin recognised for ER export[73,75,77], could be incorporated into CTB as a fusion. Rather than modifying the oligonucleotide with a peptide and a pyridylthio group, the oligonucleotide could be covalently conjugated to the peptide extension of CTB by SPAAC (as previously, chapter 4). On cleavage of the peptide as in the native holotoxin[20,36], the oligonucleotide would be attached to an unstructured peptide known to promote export from the ER[73] which would be attached to the CTB carrier by a disulfide bond, previously shown to allow payload release in the ER (chapter 5).

As an alternative, the previously successful approach of oligonucleotide hybridisation to a complementary oligonucleotide covalently conjugated to CTB (chapter 4) could be modified to promote oligonucleotide release. The oligonucleotide to be delivered would be conjugated to an unstructured peptide for export recognition. The CTB-conjugated oligonucleotide for hybridisation could be truncated or contain mismatched bases, effectively lowering the T_m of the duplex. If designed correctly, partially dynamic hybridisation would occur at physiological temperature, and on denaturing of the duplex in the ER the peptide-oligonucleotide would be targeted for export to the cytosol by the Sec61 translocon, where the oligonucleotide could potentially show a therapeutic action.

6.2. Towards construction of a peptide-oligonucleotide-CTB conjugate

6.2.1. Design

Covalent oligonucleotide conjugation to CTB by a combination of SrtA-mediated ligation and SPAAC (chapter 4), and by disulfide formation (chapter 5), have been successful. Consequently, the possibility of combining the two approaches for CTB oligonucleotide conjugation, release and targeted delivery was investigated. This approach involved creating an extension to CTB containing an N-terminal tri-Gly for SrtA labelling, a pair of Cys residues for disulfide formation and a proteolytic cleavage site between the two Cys residues. The extension could be covalently labelled with a BCN-depsipeptide using SrtA for oligonucleotide conjugation by SPAAC, and the peptide cleaved between the disulfide, resulting in a short peptide-conjugated oligonucleotide attached to the main body of CTB via a genetically incorporated disulfide (figure 6.2).

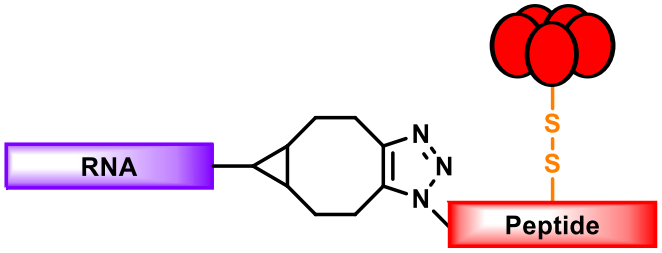

Figure 6.2. A genetically incorporated disulfide for labile oligonucleotide conjugation Outline of a strategy to target an oligonucleotide (purple) to the cytosol, through conjugation to an unstructured peptide (red), for release from CTB in the ER.

Inspiration for the design of the peptide extension was taken from the holotoxin; it consisted of 10 residues of the CTA1 C-terminus followed by the 8 residues of the CTA2 N-terminus[20]. In the wt holotoxin, this section of the protein is cleaved by trypsin following secretion from the bacteria[36,37], transforming the single CTA subunit into separate CTA1 and CTA2 subunits connected by a disulfide bond. On reduction of this disulfide in the ER, the unstructured C-terminus of CTA1 is recognised for transport from the ER by the Sec61 translocon[73,75,77]. This mechanism is highly compatible with oligonucleotide delivery and release, except for the tryptic peptide cleavage. Instead, a TEV protease cleavage site (ENLYFQS)[327] was inserted at the point where the native peptide is cleaved[20], offering increased specificity and control over the cleavage process.

CTB variants were designed with the extension at both the N-terminus (Apep-CTB; figure 6.3A) and the C-terminus (CTB-Apep; figure 6.3B), as their effect on protein expression was unknown. In the case of the N-terminal extension, the tri-Gly for SrtA labelling was located at the N-terminus of the peptide. However with the C-terminal extension, this was not possible. In this case, the tri-Gly for SrtA labelling immediately followed the TEV protease cleavage site, which also allows for a Gly terminal residue in place of Ser (ENLYFQG)[327]. The terminal Gly of the TEV protease cleavage site would become a new N-terminal Gly for SrtA labelling, only made available to SrtA following cleavage.

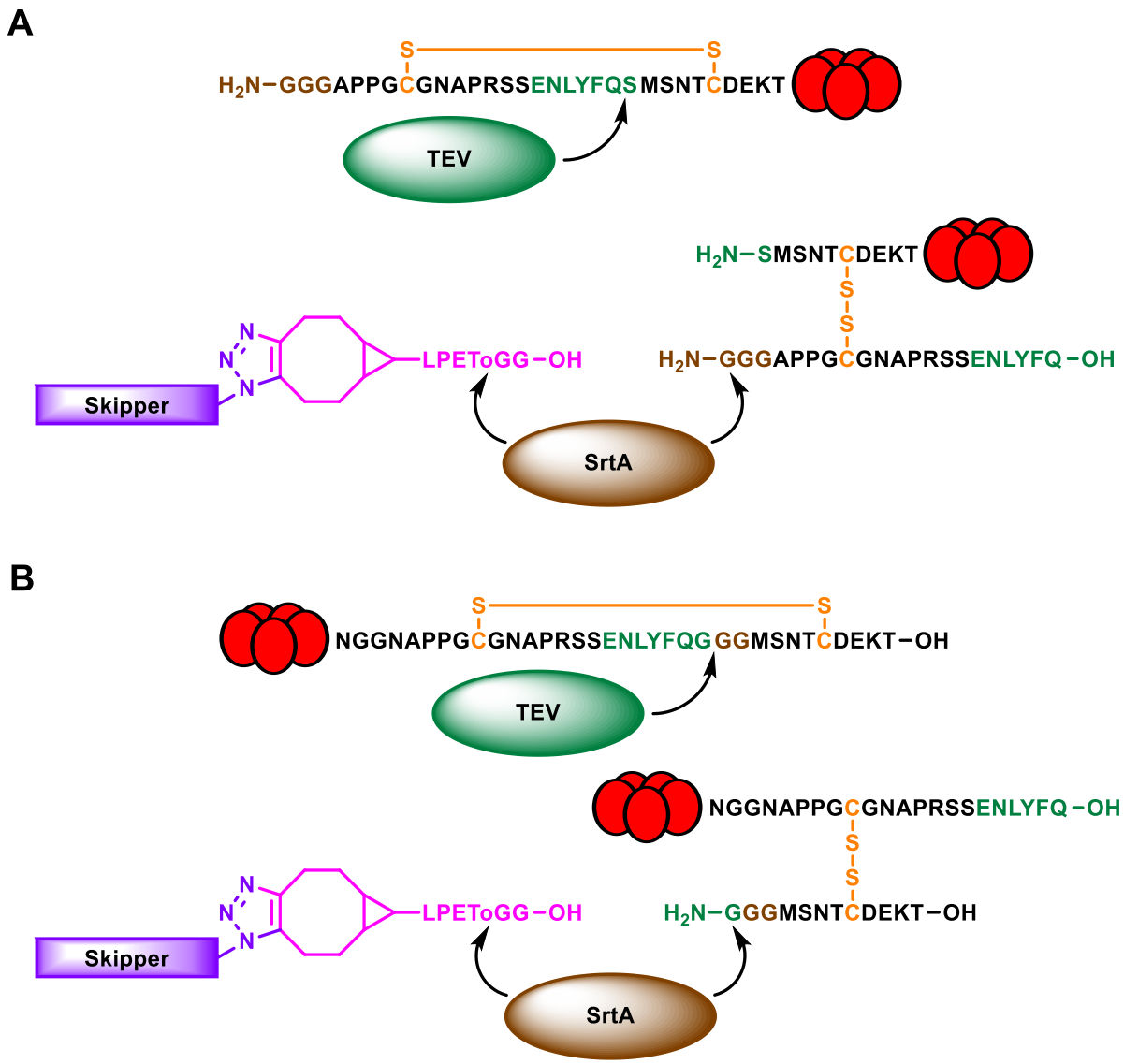

Figure 6.3. Proposed mechanism for oligonucleotide conjugation to a peptide attached to CTB by a disulfide A. CTB (red) with an N-terminal peptide extension containing an N-terminal tri-Gly (brown), and an internal TEV protease cleavage site (green) between two Cys residues forming a disulfide bond (orange). TEV protease (green) cleaves the peptide into two shorter peptides connected by a disulfide, and an oligonucleotide (purple) coupled to a BCN-depsipeptide (magenta) by SPAAC is attached with SrtA (brown). B. CTB with a C-terminal peptide extension containing an internal TEV protease cleavage site immediately followed by a tri-Gly, between two Cys residues forming a disulfide bond (orange). TEV protease cleaves the peptide into two shorter peptides connected by the disulfide, revealing the tri-Gly for SrtA labelling with the oligonucleotide-depsipeptide.

6.2.2. Protein expression and purification

Expression of both the above CTB variants was attempted in *E. coli* C41(DE3) cells by IPTG induction overnight at 25 °C. Following Ni^{2+} affinity chromatography, no Apep-CTB was detectable in either the growth medium or cell lysate. However, expression of CTB-Apep, isolated from the growth medium by ammonium sulfate precipitation, was

successful. Following purification by Ni^{2+} affinity chromatography (figure 6.4A) and SEC (figure 6.4B), the protein was identified by SDS-PAGE (figure 6.4C).

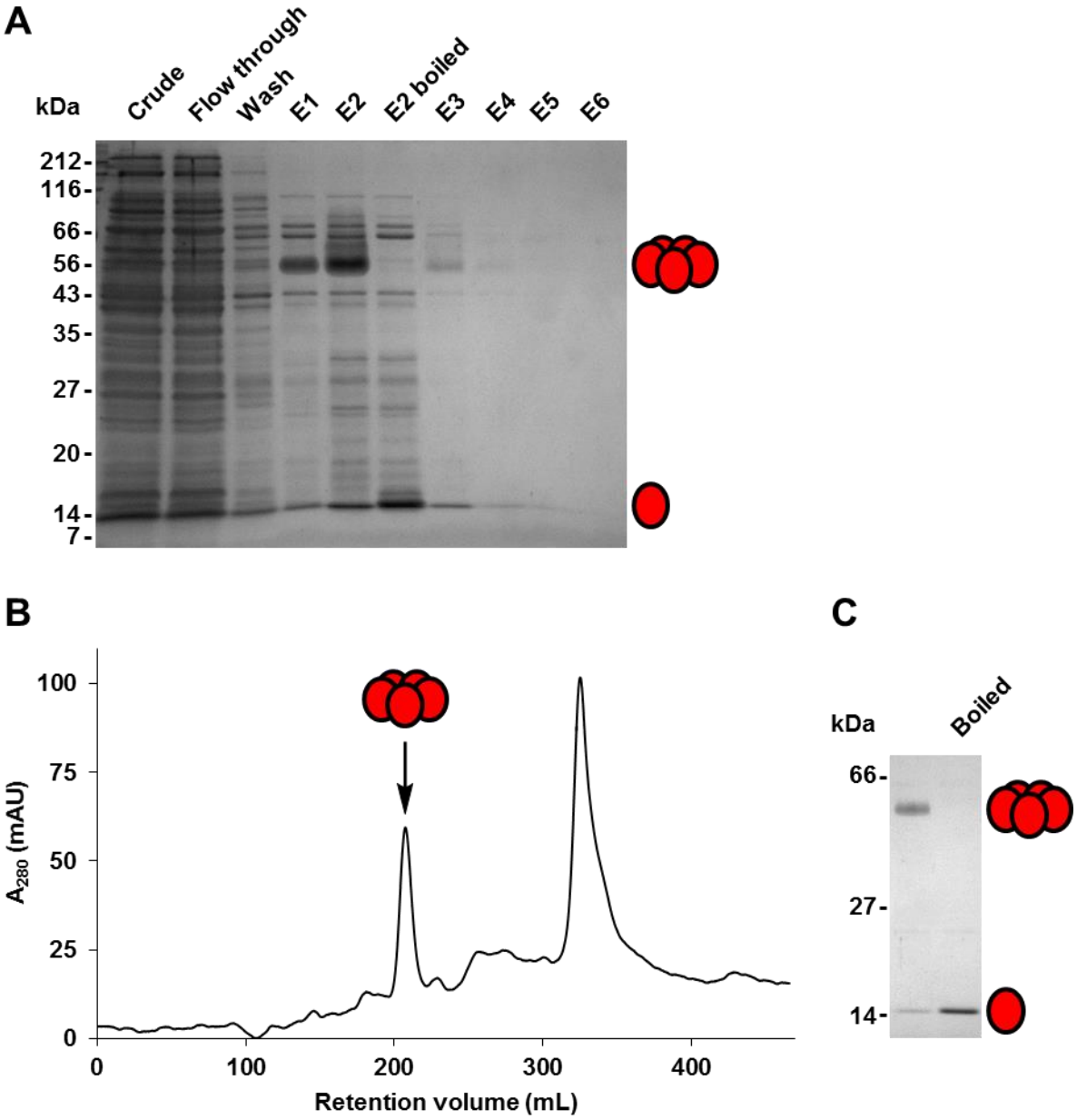

Figure 6.4. Purification of CTB-A A. SDS-PAGE analysis of CTB-Apep purification by Ni^{2+} affinity chromatography. CTB-Apep in pentameric form and dissociated protomer form are indicated. B. A_{280} trace from SEC purification of Ni^{2+}-purified CTB-Apep, with the desired protein peak indicated. C. SDS-PAGE analysis of the indicated CTB-Apep peak.

The pure protein was isolated with a yield of 1.3 mg per 1 L cultured cells. LC-MS analysis resulted in a detected mass of 15054.4 Da (15054.9 Da calculated), which increased to 15056.5 Da on treatment with DTT (15056.9 Da calculated). This indicated that the protein was expressed with an exposed disulfide formed, suggesting the desired intra-protomer disulfide bond had formed correctly. This protein also had the advantage of keeping the labelling sites clear of the GM1 binding sites[22]. However, similar to addition of the C-terminal PkC11 tag, SDS-PAGE (figure 6.3A and C) showed this C-terminal extension appeared to de-stabilise the protein, as evidenced by the appearance of protomeric CTB bands in lanes which had not been denatured by heating. It was also not possible to include a C-terminal KDEL signal sequence in this construct. The only available point for inclusion of a KDEL was the C-terminus of the peptide to be released from CTB on disulfide reduction; a KDEL here would possibly prevent ER escape. The lack of a KDEL sequence could potentially adversely affect the efficiency of disulfide release through decreasing time spent in the ER.

6.2.3. Protein labelling

CTB-Apep was initially cleaved with TEV protease (expressed in *E. coli* BL21-Gold(DE3) cells from glycerol stocks (D. Williamson) without reducing agent) and labelled with FITC-depsipeptide by SrtA-mediated ligation in a one-pot reaction (160 µM CTB-Apep, 1 mol% TEV protease, 20 mol% SrtA, 3 eq FITC-depsipeptide) for 2 h at 37 °C. SDS-PAGE (figure 6.5) showed labelling was successful but inefficient; the UV-illuminated fluorescent SrtA band showed greater intensity than the labelled CTB-Apep band despite being present in five-fold lower concentration. Attempts were made at optimising the reaction by altering the temperature, reaction time and reagent concentrations, as well as performing the TEV protease peptide cleavage and SrtA-mediated ligation separately, but no improvement was observed. TEV protease was shown to cleave the peptide under these conditions, so the apparent labelling inefficiency was likely due to unformed or reduced disulfide bonds within the peptide. This was suggested as the denatured labelled CTB-Apep sample formed several bands spanning approximately 27-75 kDa, with only a trace of fluorescent labelled protomer band (~ 17 kDa), which indicated the protomers possessed free thiols which were able to react under heating to form multiple higher order species. If the disulfide bonds were not formed prior to TEV protease cleavage, the peptide fragment would dissociate from the main protein on cleavage and any labelling would not be detected, as the labelled peptide fragment would be lost with the excess depsipeptide in the gel.

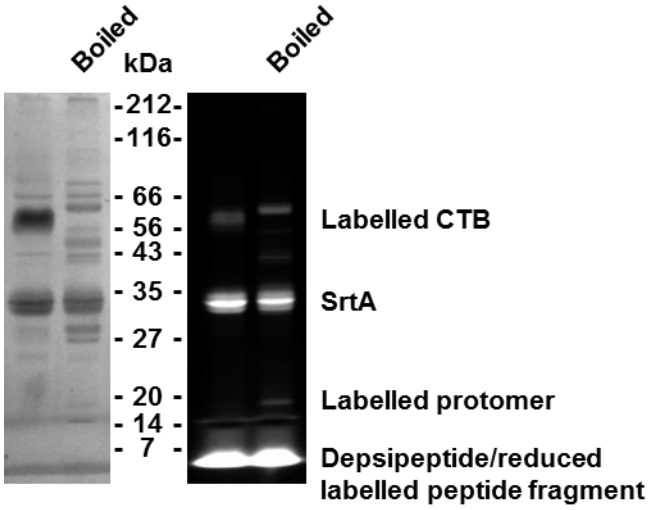

Figure 6.5. One-pot CTB-A TEV cleavage/SrtA labelling Coomassie-stained (left) and UV illuminated (right) SDS-PAGE analysis of the one-pot TEV protease cleavage and SrtA-mediated labelling of CTB-A with FITC-depsipeptide.

The labelled protein was purified by lactose affinity chromatography and concentrated. Analysis by spectrophotometry determined a labelling efficiency of 4% per protomer, or 0.2 depsipeptide labels per pentamer. SDS-PAGE analysis in the absence and presence of TCEP (figure 6.6) confirmed that the FITC-depsipeptide label was attached to CTB-A via a disulfide bond. TCEP treatment did not affect the pentameric (~ 60 kDa) protein band, but resulted in the migration of that fluorescent band to a much lower MW, in addition to the disappearance of the labelled protomer protein band (~ 17 kDa). Unfortunately however, the labelling efficiency was insufficient for oligonucleotide conjugation. Despite multiple attempts at optimisation of the process, including altering reagent concentrations, reaction temperature and time, fresh protein batches, separating the cleavage reaction from the labelling reaction, and altering the number of residues between the bisulfide-forming Cys residues, the labelling efficiency never improved upon the initial 4%. This approach was therefore abandoned.

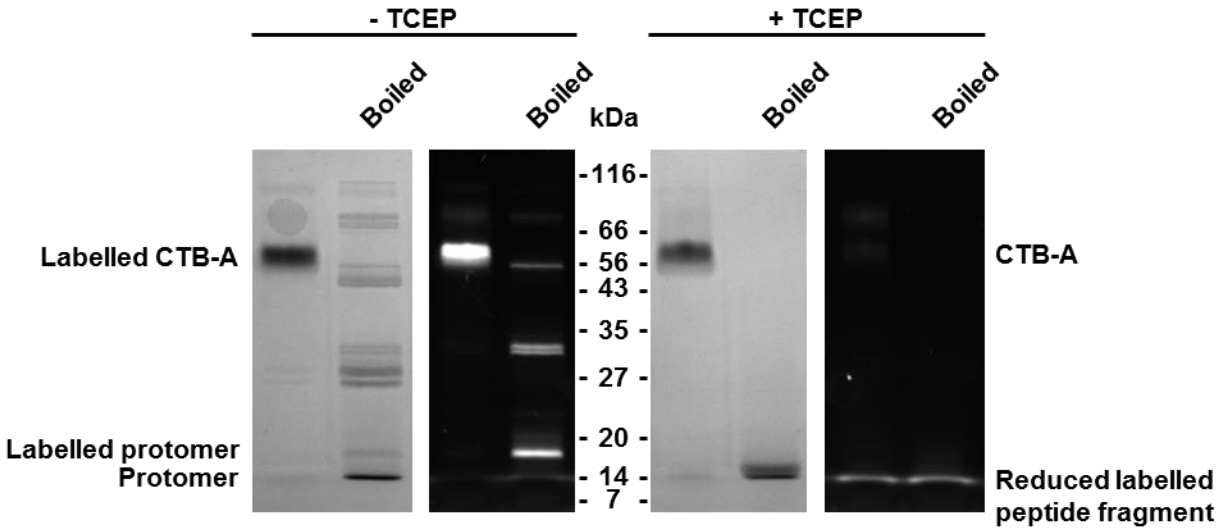

Figure 6.6. Characterisation of labelled CTB-A SDS-PAGE analysis of FITC-labelled CTB-A in the absence (left panel) and presence (right panel) of TCEP, showing Coomassie-stained (left) and UV illuminated (right) gels.

6.3. Oligonucleotide synthesis and modification for mismatched hybridisation

6.3.1. Overall construct design

A new approach to conjugating peptide-oligonucleotides to CTB for cellular delivery and release was developed (outlined in figure 6.7). It had been shown that hybridising oligonucleotides to complementary strands covalently conjugated to CTB was a robust method for cell delivery (chapter 4). This method was adapted toward promoting oligonucleotide release in the ER. Shorter complementary oligonucleotides were designed for covalent attachment to CTB, to be combined with full length oligonucleotides bearing unstructured peptides at one end. Hybridisation between the full-length and truncated complement oligonucleotides would ideally result in a T_m mildly greater than 37 °C, resulting in a small percentage of the peptide-oligonucleotide payload becoming detached from the CTB-oligonucleotide carrier at cellular temperature and oligonucleotide concentration. In the ER, the unstructured peptide would be recognised for export to the cytosol by the Sec61 translocon, similar to CTA[73,75,77]. It is even possible that the attempted export of the peptide by the Sec61 translocon could provide extra energy towards denaturing the hybridised oligonucleotides, effectively lowering the T_m and encouraging detachment of the peptide-oligonucleotide.

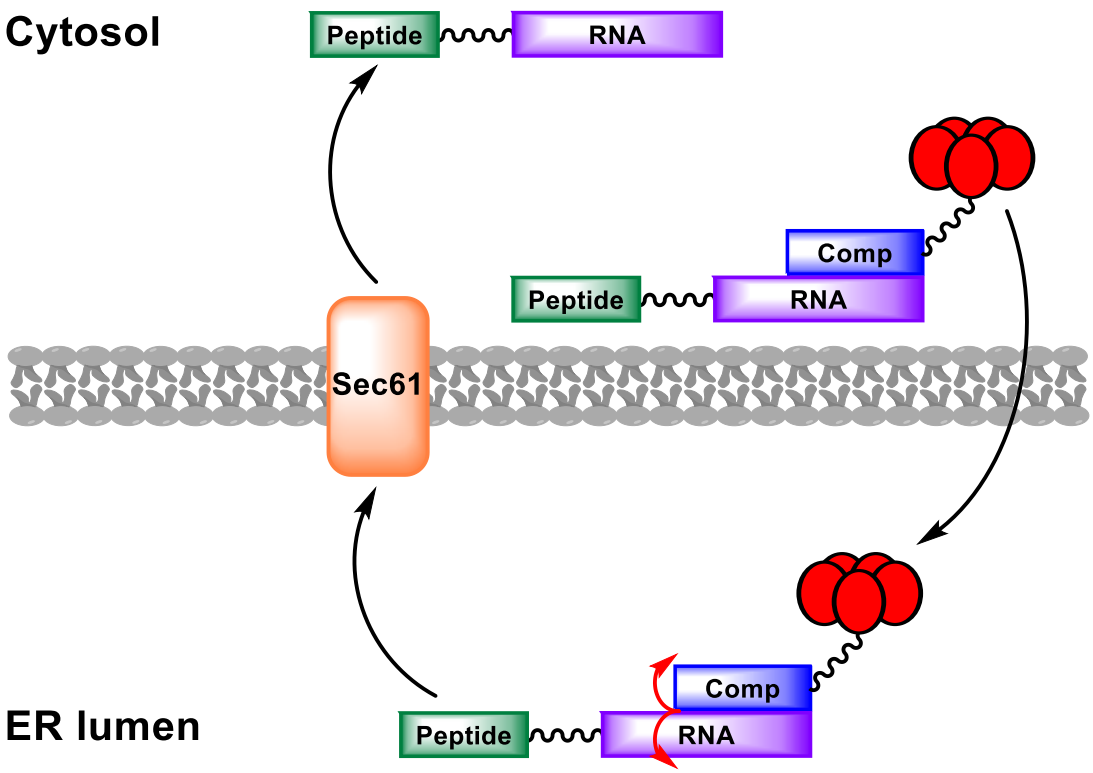

Figure 6.7. Mechanism for CTB-mediated oligonucleotide delivery to, and release from, the ER by mismatched hybridisation and Sec61 translocon recognition RNA-peptide conjugates (purple and green) are attached to CTB (red) via a shortened complementary RNA strand (blue). CTB is trafficked to ER where the peptide is recognised by the Sec61 translocon (orange). On denaturation of the mismatched RNA hybrid (red arrows), the RNA-peptide conjugate is transported by Sec61 across the ER membrane (grey) and into the cytosol.

6.3.2. General oligonucleotide characteristics

Oligonucleotides were synthesised as 2′-OMe phosphorothioate RNA, for increased stability and nuclease resistance[3,119,126]. The 5′ end of each oligonucleotide was modified on resin with a primary amine for functionality.

6.3.3. 5′-azido truncated complement RNA synthesis

The length of the truncated complement RNA molecules synthesised was of critical importance for both hybridisation and release to be possible. A T_m of 45.6 °C was predicted (OligoCalc) for a 12 nucleotide 2′-OMe phosphorothioate RNA molecule of complementary sequence to the 3′ end of the skipper RNA. This T_m correlates approximately with the requirement for partially dynamic hybridisation at 37 °C, but with the majority of the oligonucleotide remaining hybridised. Due to potential inaccuracies with the calculation based on unknown inorganic salt and oligonucleotide concentrations in different organelles at any time, three oligonucleotides were synthesised; the above 12mer, in addition to an 11mer, with a predicted 41.0 °C T_m, and a 13mer, with a predicted

47.6 °C T_m. These three oligonucleotides (hereafter termed 11/12/13mer complement RNA; sequence 5′-CUGGGUUAAGG(U)(A)-3′) were synthesised with 5′ primary amine modifiers. Following solid phase synthesis and purification, the 5′-amino 11mer complement RNA was isolated with a yield of 37%, the 12mer with a yield of 40% and the 13mer with a yield of 25%. The 5′-amino truncated oligonucleotides were reacted with azidobutyrate NHS ester to form 5′-azido truncated complement RNA (figure 6.8). The 5′-azido 11mer complement was isolated with a yield of 67%, the 12mer with a yield of 84% and the 13mer with a yield of 78%.

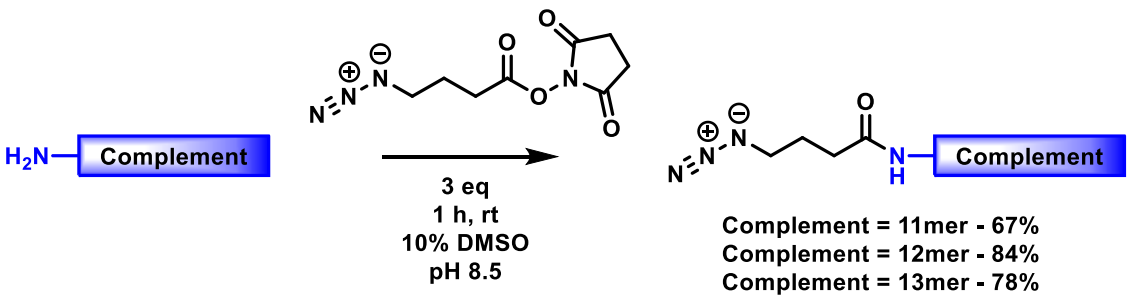

Figure 6.8. 5′-amino truncated complement RNA azide modification Reaction scheme describing the conjugation of the synthesised 5′-amino 11/12/13mer complement RNA (blue) to azidobutyrate NHS ester.

6.3.4. 5′-peptide skipper RNA synthesis

The peptides for attachment to the skipper RNA were carefully selected to maximise the possibility of recognition and transport by Sec61. They were as follows:

- The C-terminal 20 residues of CTA1 (AWREEPWIHHAPPGSGNAPR; hereafter termed CTApep), recognised by the Sec61 translocon for transport on unfolding[73,76,77].
- A 16 residue nuclear localisation signal sequence from the molecular chaperone nucleoplasmin[328,329] (KRPAATKKAGQAKKKK; hereafter termed NLSpep).
- The 19 residue N-terminal leader sequence of the immature α-lactalbumin protein (MRFFVPLFLVGILFPAILA; hereafter termed LACpep), a protein natively targeted to the Sec61 translocon for transport into the ER[330,331].
- A literature-reported 10 residue peptide (RRYIQKSTEL; hereafter termed UNSpep) capable of ER translocation via the Sec61 translocon[326].

The peptides were supplied with an L-azidolysine residue at either the N-terminus (CTApep and NLSpep) or the C-terminus (LACpep and UNSpep; depending on the end required for exposure to Sec61) for oligonucleotide conjugation by SPAAC. The 5′-amino skipper RNA synthesised previously (section 5.2.2) was used for peptide conjugation. The 5′-amino skipper RNA was reacted with bicyclonon-4-yn-9-ylmethyl N-succinimidyl carbonate (BCN NHS ester) to form 5′-BCN skipper RNA (figure 6.9), isolated with a 41% yield.

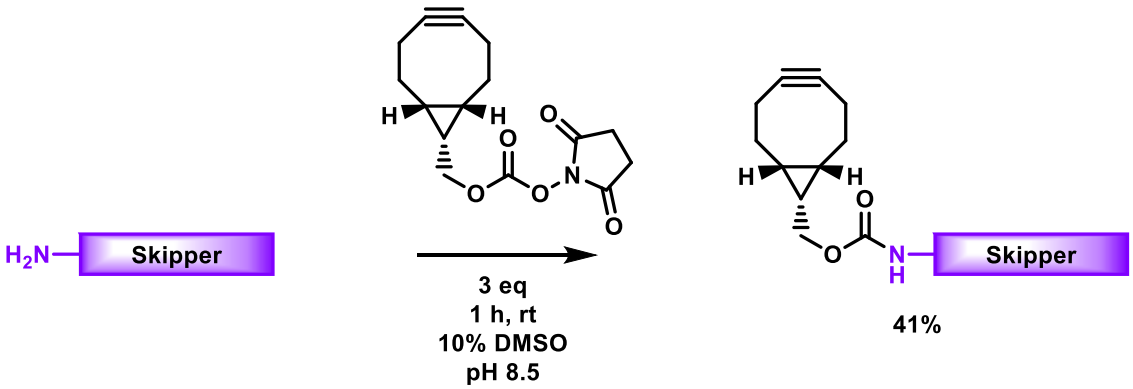

Figure 6.9. 5′-amino skipper RNA BCN modification Reaction scheme describing the conjugation of the synthesised 5′-amino skipper RNA (purple) to bicyclonon-4-yn-9-ylmethyl N-succinimidyl carbonate.

The BCN-skipper RNA was conjugated by SPAAC to either CTApep, NLSpep, UNSpep or LACpep (figure 6.10A). The 5′-CTApep derivative was isolated with a yield of 86%, the 5′-NLSpep derivative with a yield of 84% and the 5′-UNSpep derivative with a yield of 89%. The reaction between the 5′-BCN skipper RNA and LACpep-azide was more troublesome. Under similar reaction conditions to the other three azide-peptides, the LACpep-azide did not fully dissolve and required almost 8-fold greater DMSO concentration, in addition to 25% more of the azide-peptide and increased reaction time and temperature (figure 6.10B) to push the reaction to completion. The final product was eventually isolated with a yield of 84%.

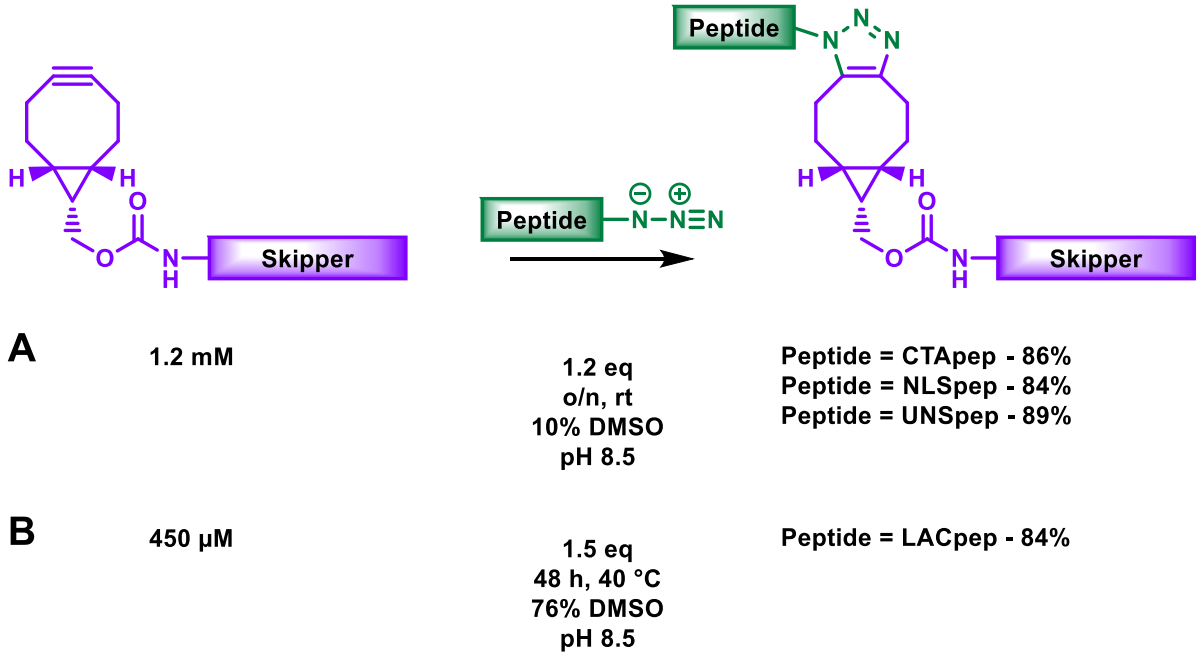

Figure 6.10. 5′-BCN skipper RNA peptide conjugations Reaction scheme describing the conjugation of 5′-BCN skipper RNA (purple) to A. azide-CTApep. Azide-NLSpep, UNSpep-azide, or B. LACpep-azide.

6.4. Characterisation of mismatched oligonucleotide hybridisation

6.4.1. Principle

All oligonucleotides absorb strongly at 260 nm, but the absorbance of double stranded oligonucleotides increases on denaturation to single stranded oligonucleotides[332], in a phenomenon termed hyperchromicity. This is due to a shielding effect caused by the stacking interactions between adjacent nucleotide pairs in double stranded oligonucleotides, which does not occur in single stranded oligonucleotides[332]. This effect can be measured by temperature-resolved spectrophotometry, with the T_m defined as the mid-point in the hyperchromic shift on denaturation[332]. Using this method, the T_m of each of the three truncated complement oligonucleotides with the full-length skipper RNA was determined experimentally prior to protein labelling, both to ensure mismatched hybridisation was possible and to indicate the best candidate for protein labelling.

6.4.2. Mismatched hybridisation T_m determination

The 5′-amino truncated complement oligonucleotides (1.4 µM) were mixed with 5′-amino skipper RNA (1 eq) in water. Samples were heated to 95 °C for 1 min and cooled to room temperature to ensure fully annealed oligonucleotides. Samples were heated from 10-80 °C and the A_{260} recorded. A T_m of 54.7 °C was calculated for the 5′-amino skipper RNA with 5′-amino 11mer complement (figure 6.11A), 58.5 °C with the 5′-amino 12mer complement (figure 6.11B) and 58.8 °C with the 5′-amino 13mer complement (figure 6.11C).

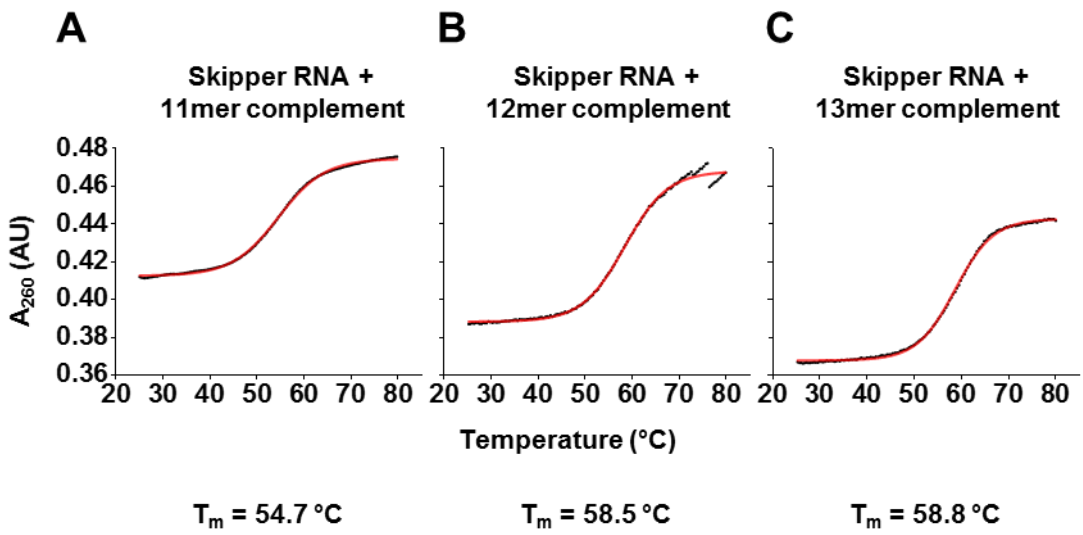

Figure 6.11. Characterisation of skipper-truncated complement RNA hybridisation The hybridisation of the 5′-amino skipper RNA with A. 5′-amino 11mer complement RNA, B. 5′-amino 12mer complement RNA, and C. 5′-amino 13mer complement RNA was characterised by spectrophotometry (A_{260}) to determine T_m.

These results showed all three truncated complement oligonucleotides were capable of hybridising with the full-length skipper RNA. However, the experimental T_m values were greater than the predicted values, indicating denaturation of the hybrid at physiological pH could prove troublesome. It should be noted though that in order to ensure adequate signal the oligonucleotides were tested at higher concentrations than would be used for cell transfection, resulting in anomalously high T_m values, which decrease with concentration[333]. It is also impossible to accurately predict the concentrations and exact behaviour of the oligonucleotides within organelles. However, taking the data into consideration, the 11mer was initially selected for CTB labelling experiments.

6.5. Labelling CTB with a mismatched peptide-oligonucleotide hybrid

6.5.1. CTB-KDEL labelling with 5′-azido 11mer complement RNA

CTB-KDEL, previously shown to localise to the ER over 24 h, was selected for labelling. The protein (150 μM) in HEPES buffer was initially labelled with 3 eq BCN-depsipeptide (Z. Arnott) using 20 mol% SrtA for 3 h at 37 °C. BCN-CTB-KDEL was purified by lactose affinity chromatography, confirmed by SDS-PAGE (figure 6.12). It also suggested SrtA-mediated BCN-depsipeptide labelling of CTB was successful, with the band of slightly higher MW compared to the unlabelled control. The BCN-labelled protein sample was labelled with 1.2 eq 5′-azido 11mer complement RNA (assuming quantitative SrtA labelling and full post-purification recovery) overnight at room temperature. The successful reaction was confirmed by SDS-PAGE (figure 6.12). In place of the single band, labelled CTB-KDEL appeared as a smeared ladder of bands, spanning approximately 50-100 kDa, indicative of non-homogeneously labelled pentamer. More definitively, on denaturation two discrete bands were seen, representing oligonucleotide-labelled CTB (approximately 20 kDa) and unlabelled CTB (approximately 12 kDa), with an approximate ratio of 3:1 in favour of labelled protein. Interestingly, the protomer-dimer band (approximately 26 kDa) previously seen on heating BCN-labelled CTB-KDEL (a trace of which was present in the heat-denatured purified BCN-CTB-KDEL sample) was not seen in this case. This indicated the SPAAC reaction was quantitative, as no BCN groups were available to react under heating, showing SrtA-mediated ligation is the more inefficient labelling step.

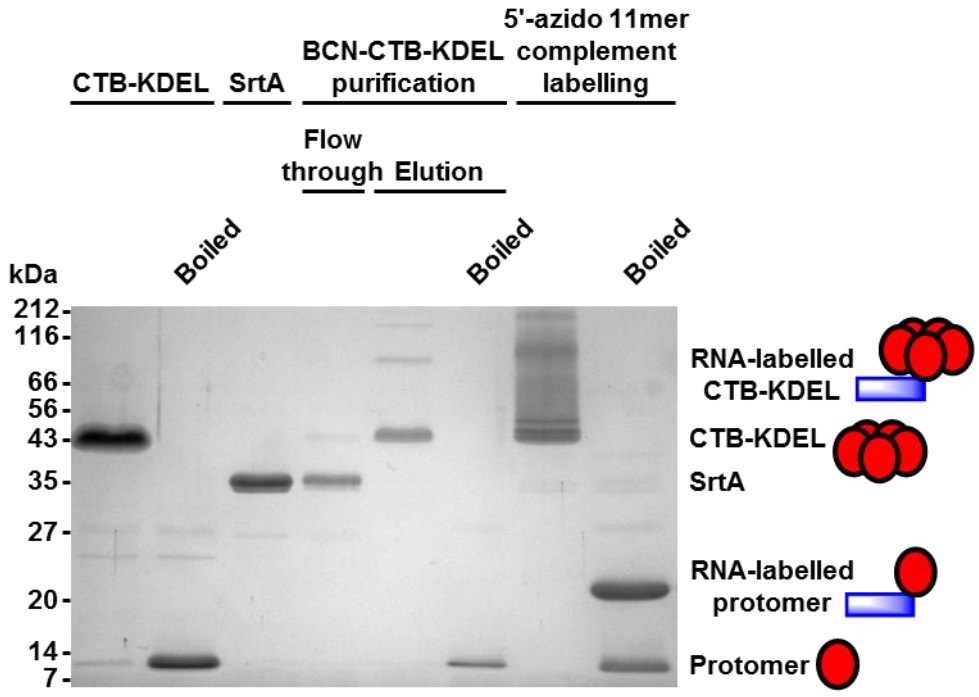

Figure 6.12. BCN-CTB-KDEL labelling with 5′-azido 11mer complement RNA SDS-PAGE analysis of lactose affinity chromatography purification of SrtA-mediated CTB-KDEL labelling with BCN-depsipeptide, and the subsequent conjugation of purified BCN-CTB-KDEL to 5′-azido 11mer complement RNA.

The 11mer complement RNA-labelled CTB-KDEL was split, treated with one of the peptide-skipper conjugates (1.1 eq) for hybridisation and analysed by SEC (figure 6.13). All four peptide-RNA-protein complexes showed a main peak with a lower retention shoulder. The 5′-CTApep skipper-RNA-CTB-KDEL hybrid gave a peak at 13.5 mL along with a 70% shoulder at 12 mL, the 5′-NLSpep hybrid gave a peak at 13.7 mL along with a 25% shoulder at 12 mL, and the 5′-UNSpep hybrid gave a peak at 13.5 mL along with a 50% shoulder at 12 mL. The peak shape of the 5′-LACpep hybrid was inconsistent with the other three, with two adjoining peaks at 9.5 mL and 11 mL of approximately equal intensity. This peak shape could be a result of higher-order complex formation due to interactions between the highly hydrophobic peptides present in the complexes when in aqueous buffer.

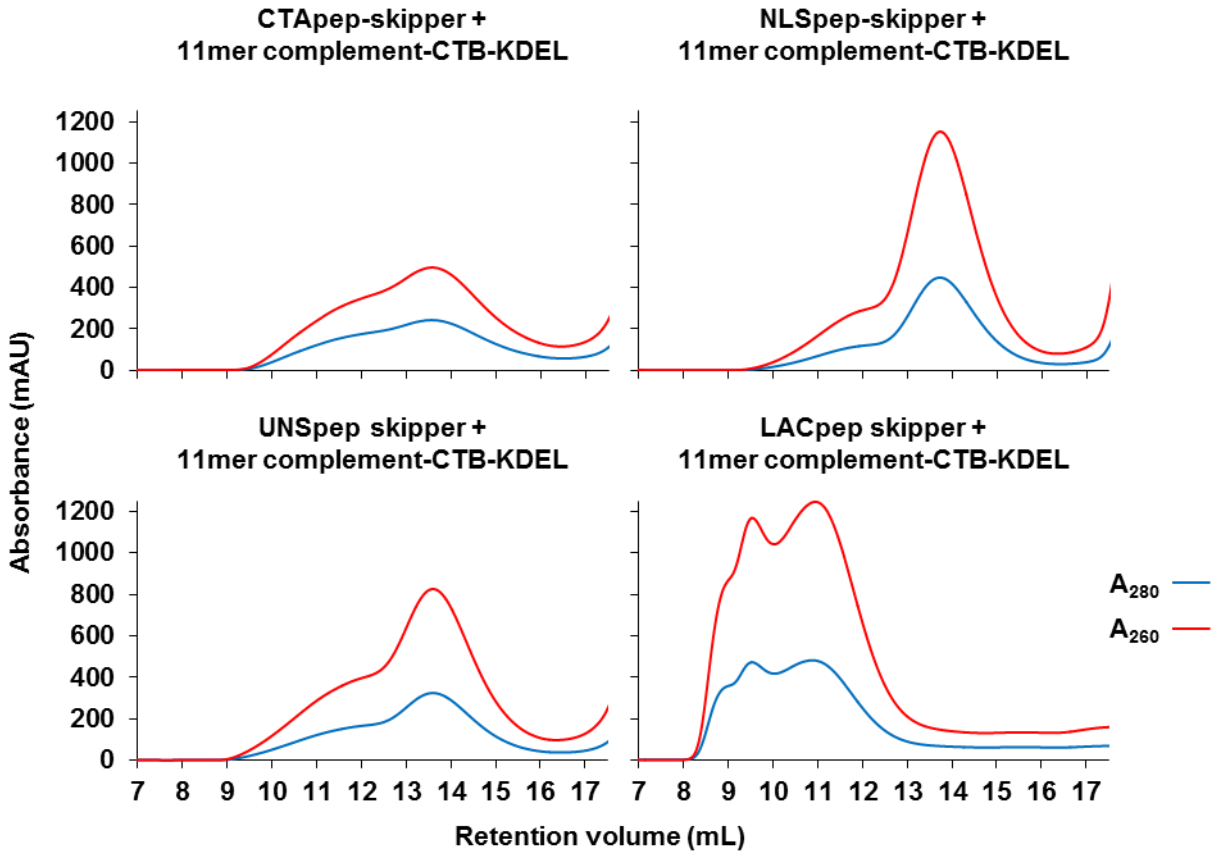

Figure 6.13. SEC characterisation of peptide-RNA-CTB mismatched hybrid complexes Analytical SEC, showing A_{280} (blue) and A_{260} (red) traces, of the 11mer complement RNA-CTB-KDEL complex hybridised with CTApep (top left), NLSpep (top right), UNSpep (bottom left) and LACpep (bottom right) skipper RNA.

In all cases, SEC suggested non-homogeneous labelling. The most likely explanation, based on the efficiency of the 11mer complement labelling reaction, was single-labelled pentamer as the predominant species, with multiply-labelled pentamers comprising less of the population. However, it was also possible that the main peaks represented non-hybridised 11mer RNA-CTB complex. To further characterise the complexes, the elution peaks were analysed by SDS-PAGE (figure 6.14). This showed non-homogeneous labelling in all four cases. The hybridised complex samples appeared as smeared ladders of multiple bands, probably due to unstable, dynamic hybridisation of the peptide-skipper to the truncated complement RNA. This was supported by the denatured samples. All four hybridised complexes showed a labelled/hybridised protein band, of varying MW depending on complexed the peptide-skipper, with a lower MW smear to a band of similar MW for all samples, indicating non-hybridised 11mer complement RNA-CTB-KDEL. The 11mer complement RNA was subsequently discounted for CTB labelling as the hybridised complexes did not display sufficient stability.

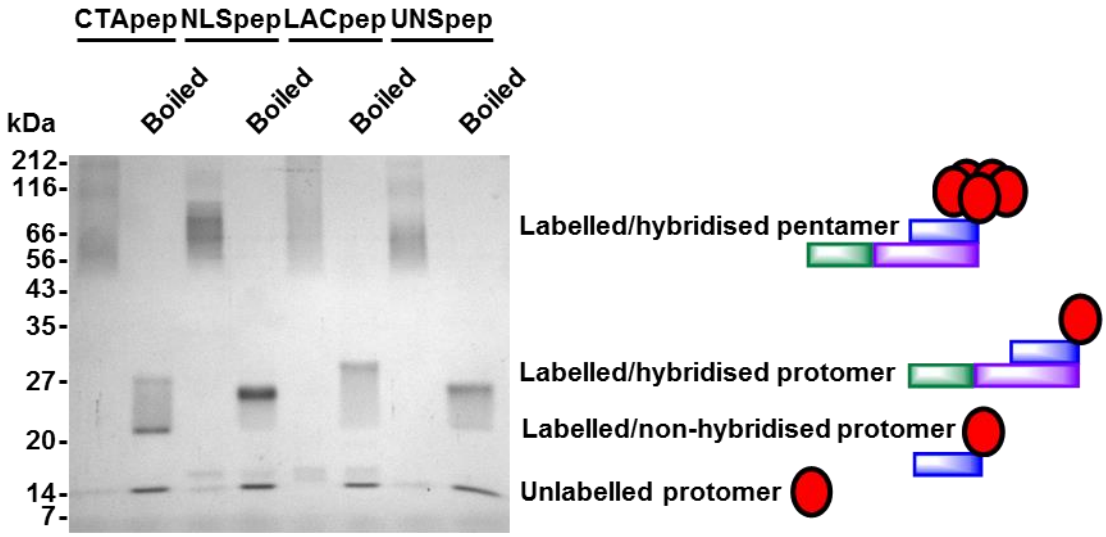

Figure 6.14. SDS-PAGE characterisation of the purified peptide-RNA-CTB mismatched hybrid complexes SDS-PAGE analysis of the SEC elution peaks of 11mer complement RNA-CTB-KDEL complex hybridised with CTApep-, NLSpep-, UNSpep and LACpep-RNA.

6.5.2. Alternative truncated complement RNA for improved hybridisation

Poor hybridisation between the peptide-skipper RNA conjugates and the 11mer complement RNA-labelled CTB-KDEL led to hybridisation tests with the 12mer and 13mer complement RNA. CTB-KDEL (163 µM) in HEPES buffer was labelled with 3 eq BCN-depsipeptide (Z. Arnott) using 20 mol% SrtA for 3 h at 37 °C. BCN-CTB-KDEL was purified by lactose affinity chromatography and samples reacted with 1.2 eq 5′-azido 12mer or 13mer complement RNA (assuming quantitative SrtA labelling and full post-purification recovery) overnight at room temperature. SDS-PAGE analysis (figure 6.15A) showed non-homogeneous, non-quantitative CTB labelling in both cases, with denatured samples showing both labelled and unlabelled CTB with an approximate ratio of 3:1. Very little of the protomer-dimer could be seen on heating, showing SrtA labelling to be the inefficient step. When the CTB-RNA complex was hybridised with CTApep-skipper RNA, which previously showed the least stable hybridisation of the peptide-RNA conjugates, SDS-PAGE analysis (figure 6.15A) showed greater band resolution and less smearing with the 13mer complement complex than the 12mer complex, indicating more stable hybridisation. Analytical SEC of both hybridised complexes (figure 6.15B) showed a more uniform complex peak with the hybridised 13mer complement complex compared to the hybridised 12mer complement complex, indicating more efficient hybridisation. The 13mer complement RNA seemed to offer the greatest possibility of carrying a peptide-RNA conjugate into cells at physiological temperature through hybridisation.

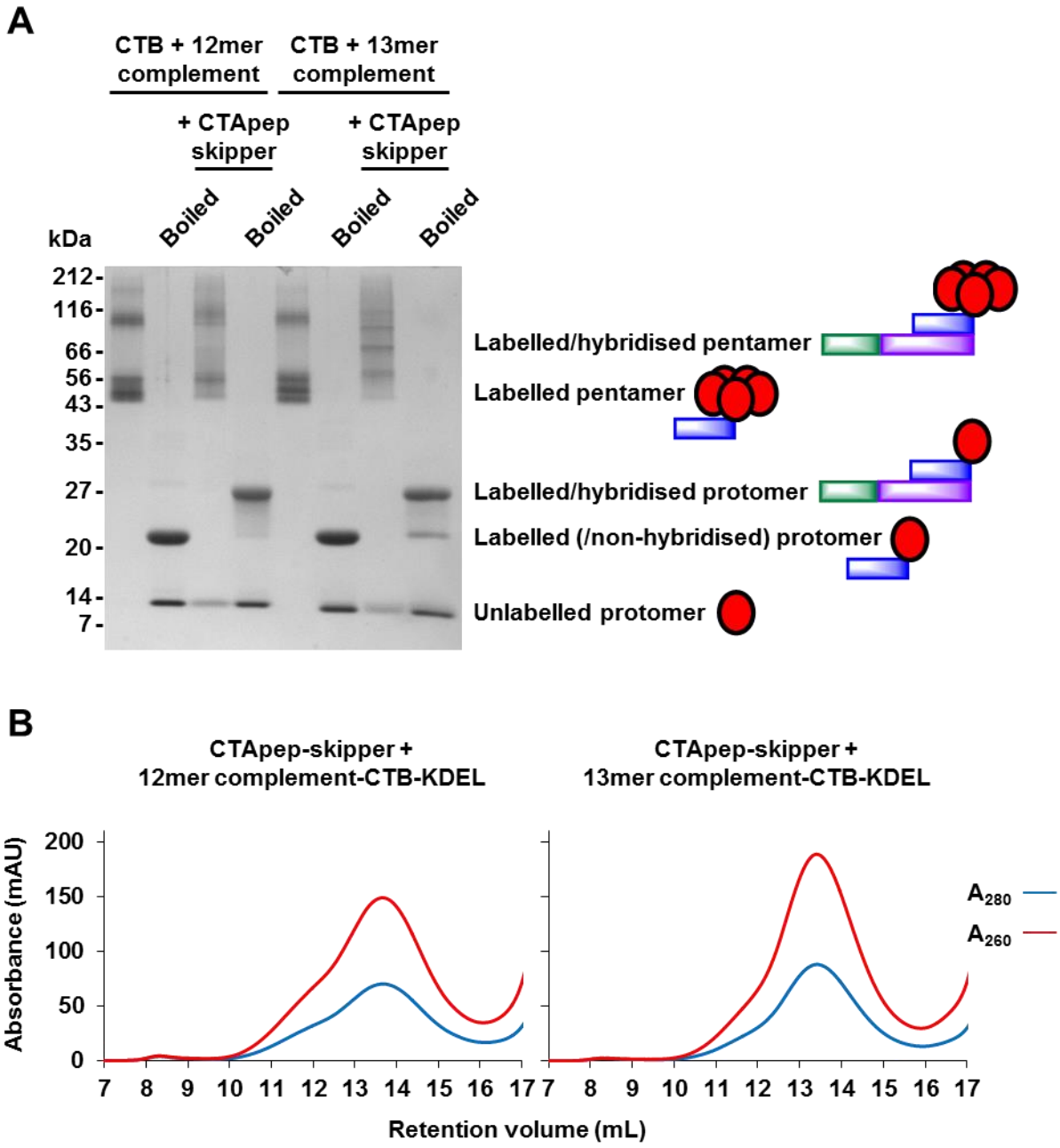

Figure 6.15. Characterisation of mismatched hybridisation between 12mer and 13mer complement RNA-CTB complexes and full length CTApep-RNA A. SDS-PAGE analysis of BCN-CTB labelled with 5′-azido 12mer or 13mer complement RNA and subsequent hybridisation with CTApep-skipper RNA. B. Analytical SEC, showing A_{280} (blue) and A_{260} (red) traces, of CTApep-skipper RNA hybridised with the 12mer (left) and 13mer (right) complement RNA-CTB-KDEL complex.

6.5.3. Four peptide-oligonucleotide conjugates for cell delivery by CTB

BCN-CTB-KDEL (150 µM) in HEPES buffer was labelled with 1.2 eq 5′-azido 13mer complement RNA overnight at room temperature. The reaction was split and each sample treated with one of the four peptide-skipper RNA conjugates for hybridisation. Each hybridisation reaction was then purified by SEC (figure 6.16). All four complexes

resulted in elution peaks of greater uniformity compared to previous hybridisations with shorter complement RNA. The CTApep-, NLSpep- and UNSpep-skipper RNA hybridisations gave peaks at 13.5 mL, while the LACpep-skipper RNA hybridisation resulted in a peak at 10.5 mL, with a lower retention 75% shoulder.

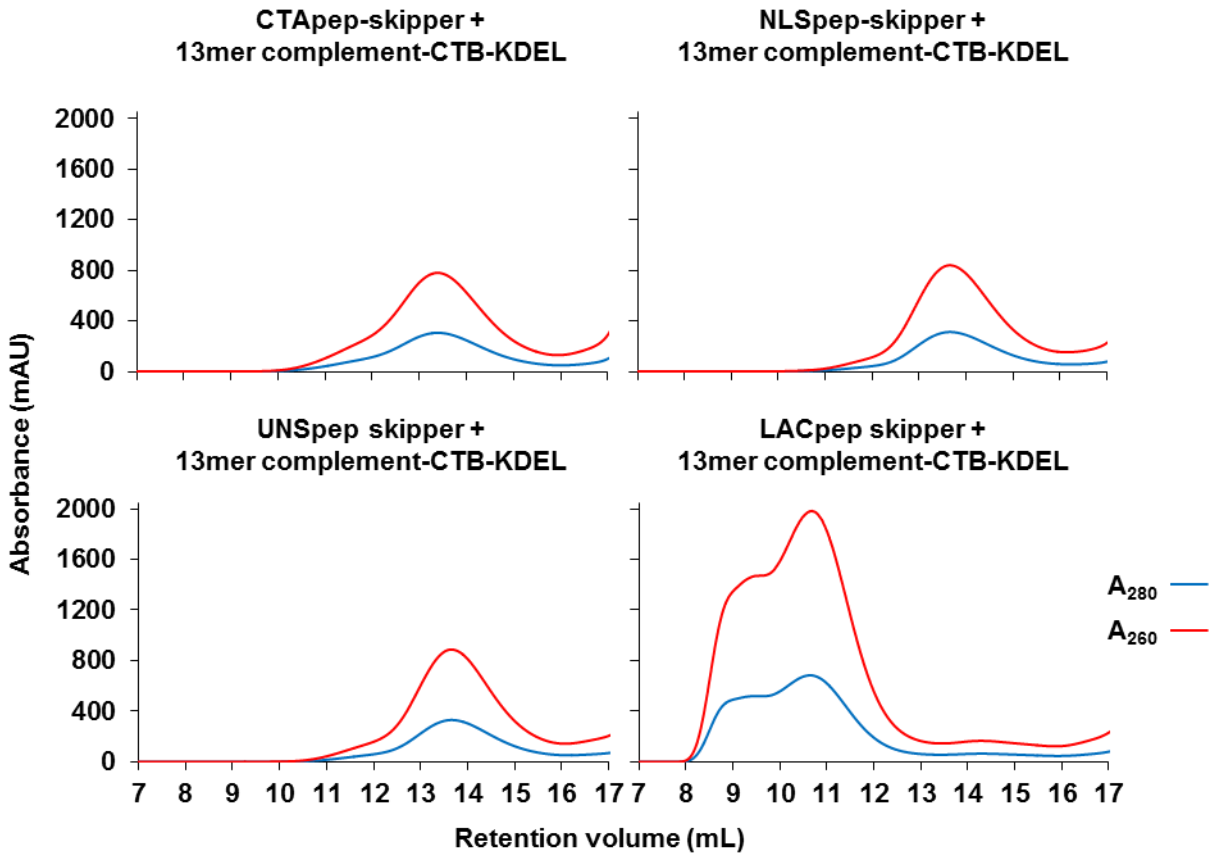

Figure 6.16. SEC characterisation of 13mer complement RNA-CTB conjugate hybridised to CTApep-, NLSpep-, UNSpep- and LACpep-skipper RNA SEC purification, showing A_{280} (blue) and A_{260} (red) traces, of 13mer complement RNA-labelled CTB-KDEL hybridised with either CTApep-skipper RNA (top left), NLSpep-skipper RNA (top right), UNSpep-skipper RNA (bottom left) and LACpep-skipper RNA (bottom right).

All four hybridised complex purification peaks were analysed by SDS-PAGE (figure 6.17). Labelled/hybridised complex predominated over unlabelled protein in all cases. The non-hybridised 13mer complement RNA-CTB-KDEL species was only detected with the CTApep-skipper RNA hybridisation (approximately 3:1 in favour of the hybridised species), with none present in the other samples. Considering the CTApep-skipper RNA-CTB-KDEL complex SEC peak showed less uniformity than the NLSpep or UNSpep complexes, this could indicate that increased peak uniformity indicates

increased hybridisation stability. Due to the complexity of the samples, concentration and labelling efficiency could not be determined by spectrophotometry and were determined by densitometry. Concentrations of 97 µM (53% labelled; 300 µL), 89 µM (63% labelled; 250 µL), 66 µM (61% labelled; 260 µL) and 41 µM (50% labelled; 250 µL) were determined for CTB-KDEL complexes with the CTApep-skipper RNA, NLSpep-skipper RNA, UNSpep-skipper RNA and LACpep-skipper RNA, respectively.

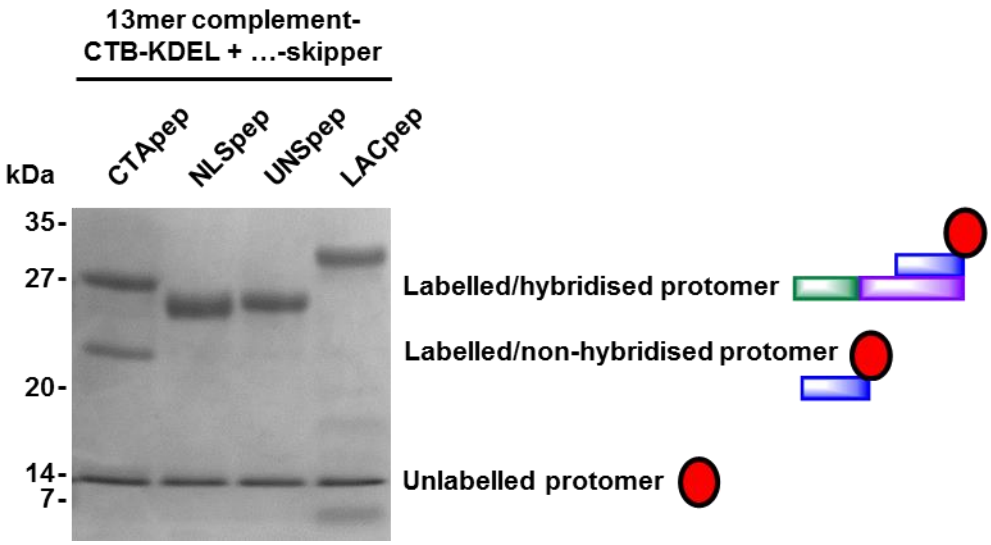

Figure 6.17. SDS-PAGE characterisation of purified 13mer complement RNA-CTB conjugate hybridised to CTApep-, NLSpep-, UNSpep- and LACpep-skipper RNA SDS-PAGE analysis purified, denatured 13mer complement RNA-CTB-KDEL hybridised to CTApep-, NLSpep-, UNSpep- and LACpep-skipper RNA.

6.6. Investigating oligonucleotide delivery and release in mammalian cells

6.6.1. Determining cytotoxicity

Prior to cell imaging experiments, an MTT assay was performed to determine any cytotoxic effects of the four peptide-RNA-CTB complexes. Vero cells incubated with the complexes (10 µg mL^{-1} protein) for 24 or 48 h were assayed (figure 6.18), and compared to mock treated, CTB-KDEL transfected and staurosporine[323] treated cells. As with CTB-CKDEL(S-S)RNA transfection, at both time points cell viability appeared increased following protein transfection compared to the mock control, particularly after 48 h. This again suggested protein transfection resulted in increased cell metabolism, but overall showed the complexes had no inhibitory or cytotoxic effects on cell viability.

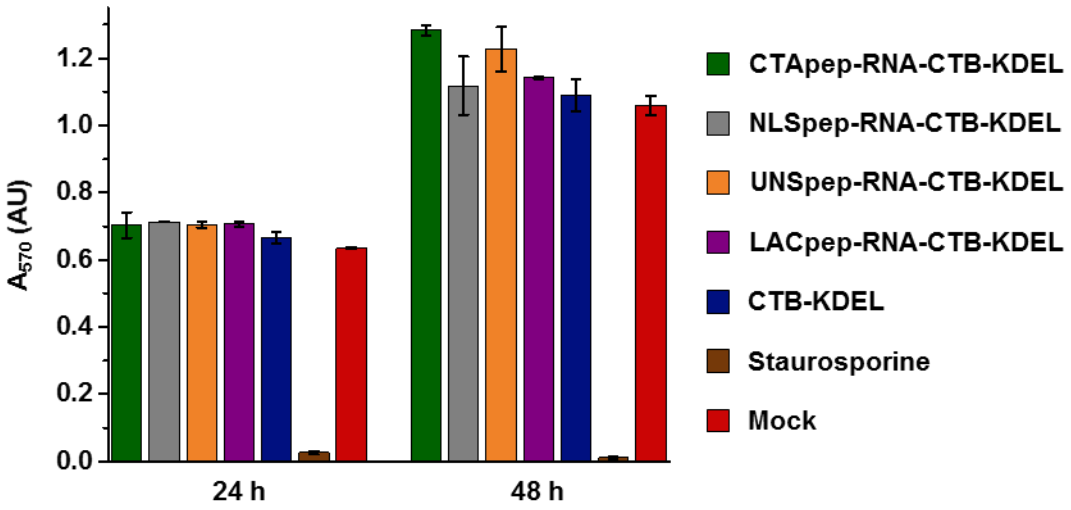

Figure 6.18. Cell viability following peptide-RNA-CTB-KDEL transfection MTT assay comparing Vero cell viability following incubation for 24 or 48 h with CTApep-RNA-CTB-KDEL (green), NLSpep-RNA-CTB-KDEL (grey), UNSpep-RNA-CTB-KDEL (orange), LACpep-RNA-CTB-KDEL (purple), CTB-KDEL (blue) or staurosporine (brown), compared against mock transfected cells (red). Data shown as mean ± standard error of three separate experiments.

6.6.2. Investigating endocytosis

Vero cells were treated with the four peptide-RNA-CTB-KDEL complexes to determine if the mismatched hybridisation conjugation technique was suitable for RNA delivery, if the hybridised peptide-RNA could be released from the RNA-CTB-KDEL complex, and if the different peptides conjugated to the RNA would affect cell localisation. Cells were incubated at 37 °C with each peptide-RNA-CTB-KDEL complex (5 µg mL^{-1} protein), or an equivalent concentration of each peptide-RNA conjugate, for 24 h and fixed with PFA. The cells were stained for RNA by FISH with a bis-rhodamine complement RNA probe, then for CTB with rabbit anti-CTB Ab followed by donkey anti-rabbit AF488-conjugate Ab. LSCM imaging (figure 6.19) showed no uptake of peptide-RNA in the absence of CTB, shown by a lack of rhodamine staining following FISH. However, CTB was able to deliver the peptide-oligonucleotides into the cells in all cases. The CTApep-RNA, NLSpep-RNA and UNSpep-RNA all appeared as diffuse staining in small, discrete, halo-like regions adjacent to the nuclei, indicative of ER staining. They also showed excellent co-localisation with CTB. This suggested the peptide-RNA was not released from the truncated complement RNA, and that the protein complex was unable to escape the ER.

The LACpep-RNA staining, however, showed different morphology to the other three peptide-RNA conjugates. It appeared in punctate foci, primarily surrounding the nuclei but more spread throughout the cell than would be expected for either Golgi or ER

staining. The RNA again showed excellent co-localisation with CTB, indicating the peptide-RNA was not released from the protein complex, but the whole complex was able to escape the ER. This clearly showed that the 13mer complement RNA-skipper RNA duplex was too stable to be denatured to a detectable degree under physiological conditions in the ER. It also suggests that the unstructured N-terminal α-lactalbumin leader sequence was able to function as a targeting sequence mediating ER escape where the other three peptides did not.

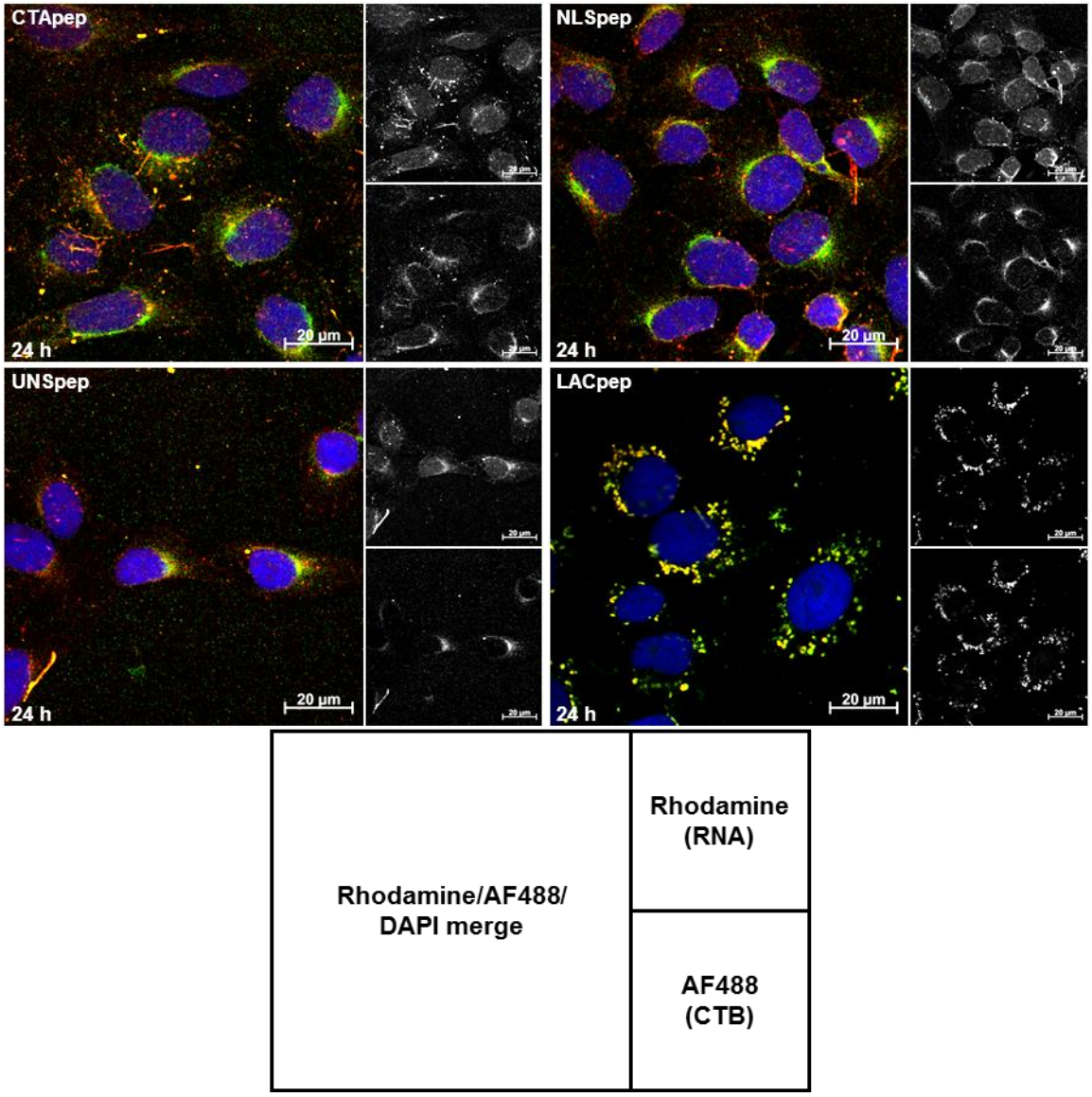

Figure 6.19. Peptide-RNA-CTB-KDEL incubation with Vero cells LSCM imaging of Vero cells incubated with CTApep- (upper left panel), NLSpep- (upper right panel), UNSpep- (lower left panel) or LACpep-RNA-CTB-KDEL (lower right panel), fixed after 24 h, and stained for RNA by FISH and CTB by IF. Each panel shows a false-colour merged image (left) of rhodamine (RNA; red), AF488 (α-CTB; green) and DAPI (nuclei; blue), in addition to individual red (rhodamine; upper right) and green (AF488; lower right) channels.

To determine the location of the LACpep-RNA-CTB-KDEL complex after 24 h, transfected cells were stained for RNA by FISH with a bis-rhodamine complement RNA probe. Cells were co-stained with an anti-PDI or anti-LAMP1 primary Ab to detect the ER or the lysosome, respectively. The primary Abs were stained with an AF488-conjugated secondary Ab, and mounted with DAPI. LSCM imaging (figure 6.20) showed good but incomplete co-localisation of both the ER and the lysosome with the RNA. This suggests that the LACpep-RNA-CTB-KDEL complex was trafficked initially to the ER before removal to the lysosome. This in turn suggests that the peptide was able to mediate ER escape in some manner. The exact mechanism was unclear from the available data, but it seems plausible that direct transport from the ER to the lysosome occurred, for degradation by autophagy via the autophagosome[334-336]. This possibility was supported by the lack of cytosolic staining seen. While this is not good news in terms of delivering RNA for therapeutic purposes, the fact that the complex is able to both reach and escape from the ER intact is promising.

It is interesting that of the four peptides, only LACpep seemed to promote removal from the ER. This is possibly because while the other three peptides are largely polar, LACpep is highly hydrophobic. One of the mechanisms for the detection of misfolded proteins in the ER, and their targeting for degradation, is exposed hydrophobic residues[337,338]. The hydrophobic nature of LACpep could lead to its identification as a misfolded protein and subsequent targeting for degradation by the ERAD pathway[337,338]. This would lead to removal of the complex initially to the cytosol, and though cytosolic complex distribution was not seen, it cannot be ruled out either based on the available data. Transport to the cytosol is obviously a desirable outcome, so a further assay to accurately detect entry to the cytosol[55] is required.

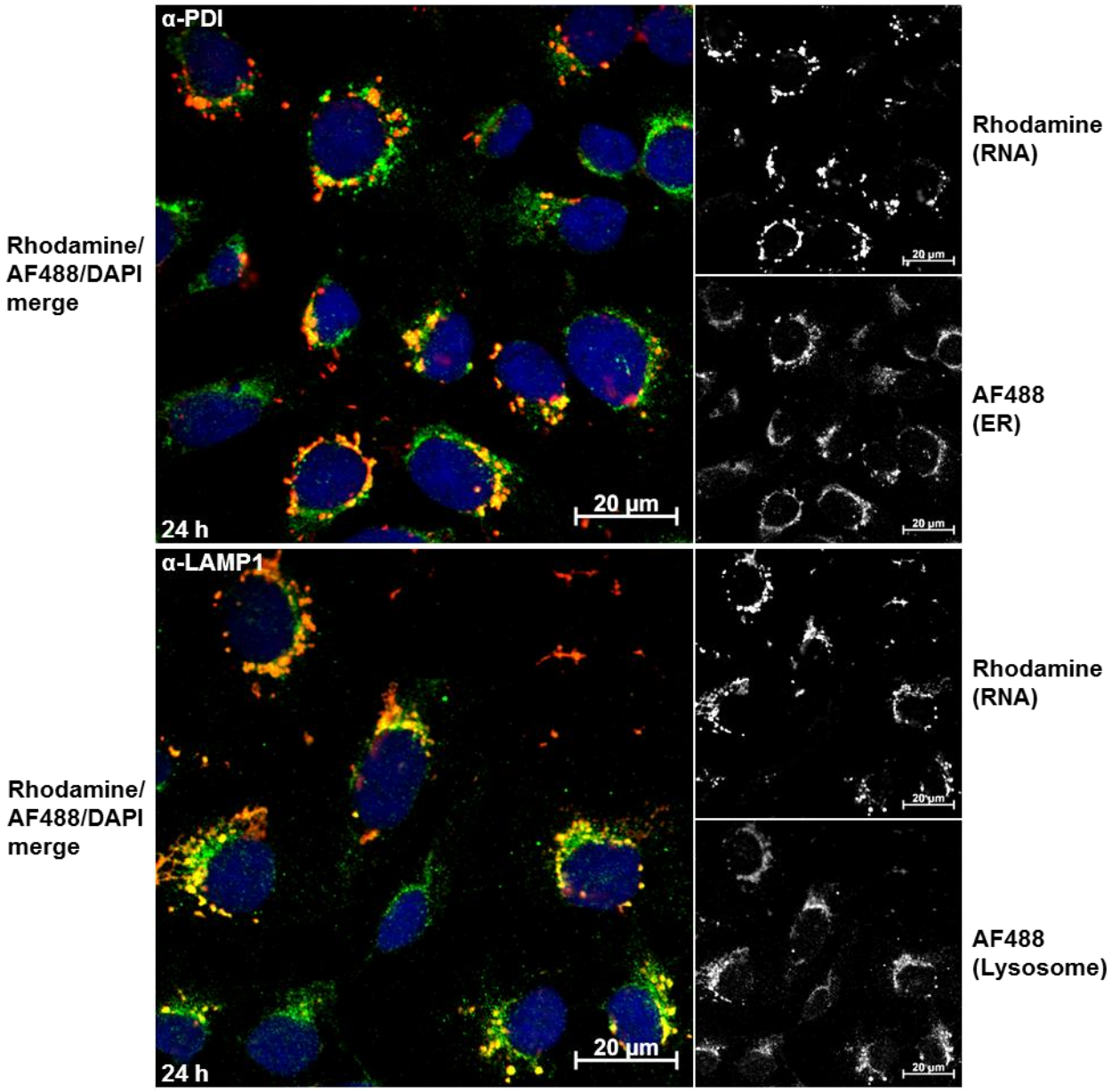

Figure 6.20. Organelle staining of LACpep-RNA-CTB-KDEL treated Vero cells LSCM imaging of Vero cells incubated with LACpep-RNA-CTB-KDEL, fixed after 24 h, and stained for RNA by FISH and either the ER (α-PDI Ab; left) or the lysosome (α-LAMP1 Ab; right) by IF. Each panel shows a false-colour merged image (left) of rhodamine (RNA; red), AF488 (organelle; green) and DAPI (nuclei; blue), in addition to individual red (rhodamine; upper right) and green (AF488; lower right) channels.

Chapter 7: Discussion

7.1. Summary and conclusions

The potential of the non-toxic B subunit of cholera toxin, which is responsible for endocytosis on GM1 binding, as a vector for targeted oligonucleotide delivery was probed. Initially, CTB was efficiently and site-specifically labelled at the N-terminus with a fluorescent depsipeptide by SrtA-mediated ligation. CTB was shown to transport the payload into Vero cells, localising to the Golgi apparatus after 24 h. With the addition of a C-terminal KDEL ER retention sequence, a similarly labelled CTB variant instead localised to the ER over a 24 h period. This validated CTB as a potential delivery vector, confirming its capability to deliver a payload to a defined and controllable cellular location.

The FITC-depsipeptide label was replaced with modified dsRNA, of consistent structure and size with therapeutic oligomers, to determine if CTB was capable of therapeutic oligonucleotide delivery. The oligonucleotide was conjugated to CTB by SrtA-mediated ligation and SPAAC. CTB was able to transport the RNA into Vero cells, with the RNA-protein complex remaining intact over 24 h. The complex was initially transported to the Golgi apparatus, before removal of most of the complex to the lysosome. With the addition of a C-terminal KDEL to CTB, transport to the ER occurred, and while there was some removal to the lysosome a greater proportion remained localised to the ER after 24 h. This opened the possibility of oligonucleotide release and escape from the vesicular system through processing mechanisms within the ER.

Strategies for oligonucleotide release were investigated. Initially, a CTB variant was produced with a C-terminal extension containing a Cys residue for disulfide formation and a KDEL for ER targeting, and labelled with a pyridylthio-conjugated modified oligonucleotide. CTB was able to transport the oligonucleotide into Vero cells, with the complex showing no cytotoxic effect after 48 h. CTB initially delivered the oligonucleotide to the ER. After 8 h the oligonucleotide had been released from CTB within the ER, with some exported to the lysosome after 24 h. This validated the strategy

for oligonucleotide release, but also highlighted the need for a targeting mechanism to promote cytosolic or nuclear delivery.

An alternative payload release delivery system was designed based on recognition of unstructured peptides for translocation to the cytosol by Sec61. Building on the success of the disulfide release strategy, a CTB construct was designed which would allow oligonucleotide conjugation to a short, unstructured peptide which was attached to CTB by a genetically incorporated disulfide. However, labelling was inefficient and this strategy abandoned.

An alternative method for labelling CTB with peptide-conjugated oligonucleotides was developed. CTB-KDEL was labelled with modified RNA attached to one of four unstructured peptides, all predicted to mediate ER translocation by Sec61. The peptide-RNA conjugates were attached to CTB through hybridisation to a shortened complementary oligonucleotide, covalently conjugated to the N-termini by SrtA-mediated ligation and SPAAC. A 13mer was shown as the shortest oligonucleotide to provide efficient hybridisation. All of the peptide-RNA-protein complexes were able to travel intact to the ER, and none showed a cytotoxic effect on Vero cells over 48 h. Unfortunately, none of the complexes released the hybridised oligonucleotide. Only the α-lactalbumin leader sequence peptide promoted export from the ER, partially localising to the lysosome after 24 h, possibly because it was recognised as a misfolded protein by the ERAD system due to its hydrophobicity and targeted for degradation.

This study validated the potential use of CTB as a vector for targeted oligonucleotide delivery, but further optimisation of the oligonucleotide release mechanism is required before it could be adapted for clinical use.

7.2. Discussion and future perspectives

7.2.1. Comments on the methodologies employed during this study

Cultured Vero cells were used for CTB payload delivery experiments, primarily because they are easy to handle[263], naturally display abundant GM1 on their cell surface[264] and have been previously used for CT-based endocytosis experiments[72,264,265]. While this provided an adequate proof of concept system, Vero cells are not a good model for human disease. Apart from obviously not being a human cell line, they have a 9 Mb genome deletion resulting in the loss of cyclin-dependent kinase (CDK) inhibitor genes and the type I interferon genes[339]. The loss of the interferon response, an innate immune response against viral infections[340], means their response to foreign oligonucleotides may not be consistent with the response *in vivo*, particularly as oligonucleotides are known to activate innate immune pathways (RNAi[1] for example). The loss of CDK inhibitors is predicted to play a role in the immortality of the cell line[339], as CDKs promote cell cycle progression[341]. The immortality of the cell also casts potential doubt over results obtained in the cell line. Most of the targets for disease treatment in humans involve senescent cells[3], and dividing cells behave differently to senescent cells. In particular, access to the nucleus is significantly increased in dividing cells due to the breakdown of the nuclear membrane during mitosis, significant for oligonucleotides which require nuclear access to function. One notable exception to this is oligonucleotide-based cancer treatments[4], but there are many tumorigenic cell lines available. In addition, they are a kidney-derived cell line, and there are no reports of the kidney currently being targeted for oligonucleotide therapy.

Separate to the specific cell line, cell culture in general is not a good model for human disease states. The cells are grown on plastic or glass in a non-contiguous monolayer, sustained by non-native media possessing few of the signalling molecules present in the native environment of the cell. The large number of cell divisions undergone mean mutations are likely to be picked up which could have unpredictable consequences on results. In addition, Cell behaviour as part of tissues and organs is likely to differ from that displayed in culture as other cell types are present which can affect their behaviour. For example, the common type II diabetes drug Metformin was found to completely halt replication of hepatitis C virus in cultured Huh-7 cells, allowing the cells to clear the infection[342], but had no effect during clinical trials. So while a good proof of concept model for the reasons previously stated, results using cultured Vero cells should be treated with caution with regard to human disease.

Fluorescence *in situ* hybridisation with fixed cells provided an efficient method for detecting oligonucleotides, clearly showing the location of the oligonucleotides at defined time points. However, the method does not provide sufficient resolution to determine if the delivery and release mechanism provided by CTB was partially successful. For example, if between time-points the oligonucleotide was exported from the ER to the cytoplasm, but then sequestered and transported to the lysosome, it would remain undetected and would therefore be assumed not to have occurred. In this case, live cell imaging represents an improved method for time-resolved visualisation. Live cell imaging requires the oligonucleotides to be visible, requiring the introduction of a fluorescent probe into the cells. Methods for introduction of nucleic acid probes into live cells include microinjection[343], cationic transfection reagents[344], electroporation[345] and toxin-based membrane permeabilisation[346]. However, all have the potential to damage the cells or alter their behaviour, and all require time between the addition of the probe and visualising hybridisation. If the oligonucleotides remain compartmentalised within organelles, the probe would not have access to them. This would provide an excellent indication of oligonucleotide export to the cytosol from organelles, but if they were not released then no information would be obtained. Binding of a probe would also likely alter the behaviour of the oligonucleotides, with the pathway requiring subsequent validation by fixed-cell FISH.

A reporter assay represents an alternative method for detecting the export of oligonucleotides to the cytosol. A reporter assay could determine oligonucleotide efficacy, as well as detecting any minor or transient oligonucleotide delivery to the cytosol undetectable with fixed, stained cells. One such assay, SNAP-trap, has been developed by Geiger *et al.*[55]. The SNAP-tag protein was expressed in cells from a transfected plasmid, targeted to the relevant sub-cellular location (the ER and cytosol were demonstrated). Proteins to be probed were labelled with benzylguanine, a group which covalently and irreversibly binds to SNAP-tag. If the labelled protein was transported to the location SNAP-tag was expressed, binding could occur and SNAP-tag was detected on the isolated protein. This method could be adapted to probe cytosolic oligonucleotide delivery by labelling the oligonucleotide with benzylguanine.

The SNAP-trap assay is an excellent detection system for oligonucleotide delivery, but it cannot detect function. Another assay capable of probing both delivery and function has been designed by Sazani *et al.*[124] (figure 7.1), based on alternative splicing. The EGFP coding sequence of a pEGFP expression vector was interrupted with a mutated version of

the human β-globin intron containing a C654T mutation, one of the causes of thalassemia[124]. This created preferential 5′ and 3′ aberrant splice sites within the intron, resulting in retention of a portion of the intron in the mRNA and expression of non-fluorescent protein. Hybridisation of an antisense oligonucleotide to the region of the intron containing the mutation prevented recognition of the aberrant 3′ splice site, restoring correct pre-mRNA splicing and functional protein expression. Assay results can be qualitative, using fluorescence microscopy to determine the presence or absence of functional EGFP, and quantitative, using fluorescence-activated cell sorting (FACS) to quantify cell fluorescence, as required.

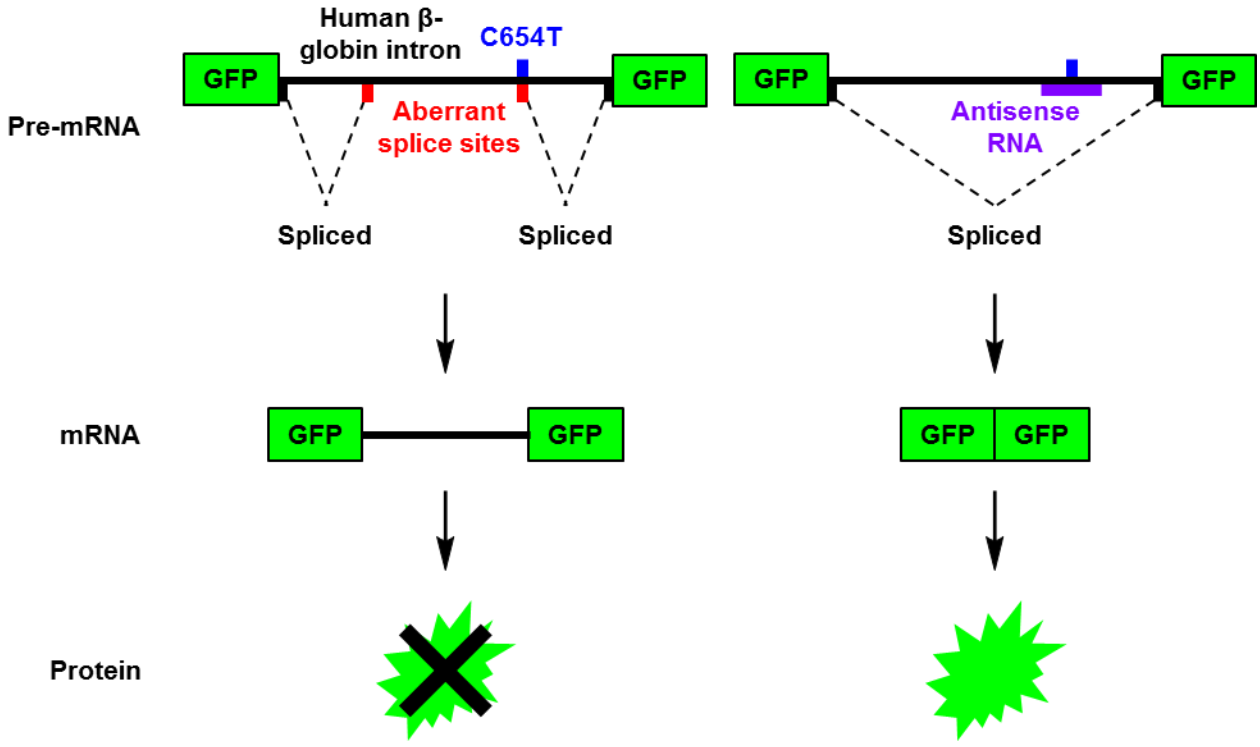

Figure 7.1. Antisense intron skipper reporter assay Overview of the antisense intron skipper reporter assay designed by Sazani *et al.* in the absence (left) and presence (right) of an antisense oligonucleotide (purple) binding to the 3′ aberrant splice site (red).

The C654T mutated intron (hereafter termed I654) was produced by assembly PCR from 18 internal parts (figure 7.2A), and inserted into the pEGFP-C1 vector between nucleotides 89 and 90 of the EGFP coding sequence by exponential megapriming PCR. In brief, a 17 nt 3′ extension, complementary to the region of the plasmid immediately downstream of the insertion site (EGFP nt 90-106), was added to I654 by PCR

(figure 7.2B). This "megaprimer" was used as the forward primer for extension of pEGFP-C1 by PCR, inserting the sequence into the vector (hereafter termed pEGFP-I654; figure 7.2C). A version of the vector containing the functional wt intron in the same position (hereafter termed pEGFP-I) was produced by site-directed mutagenesis as a positive control.

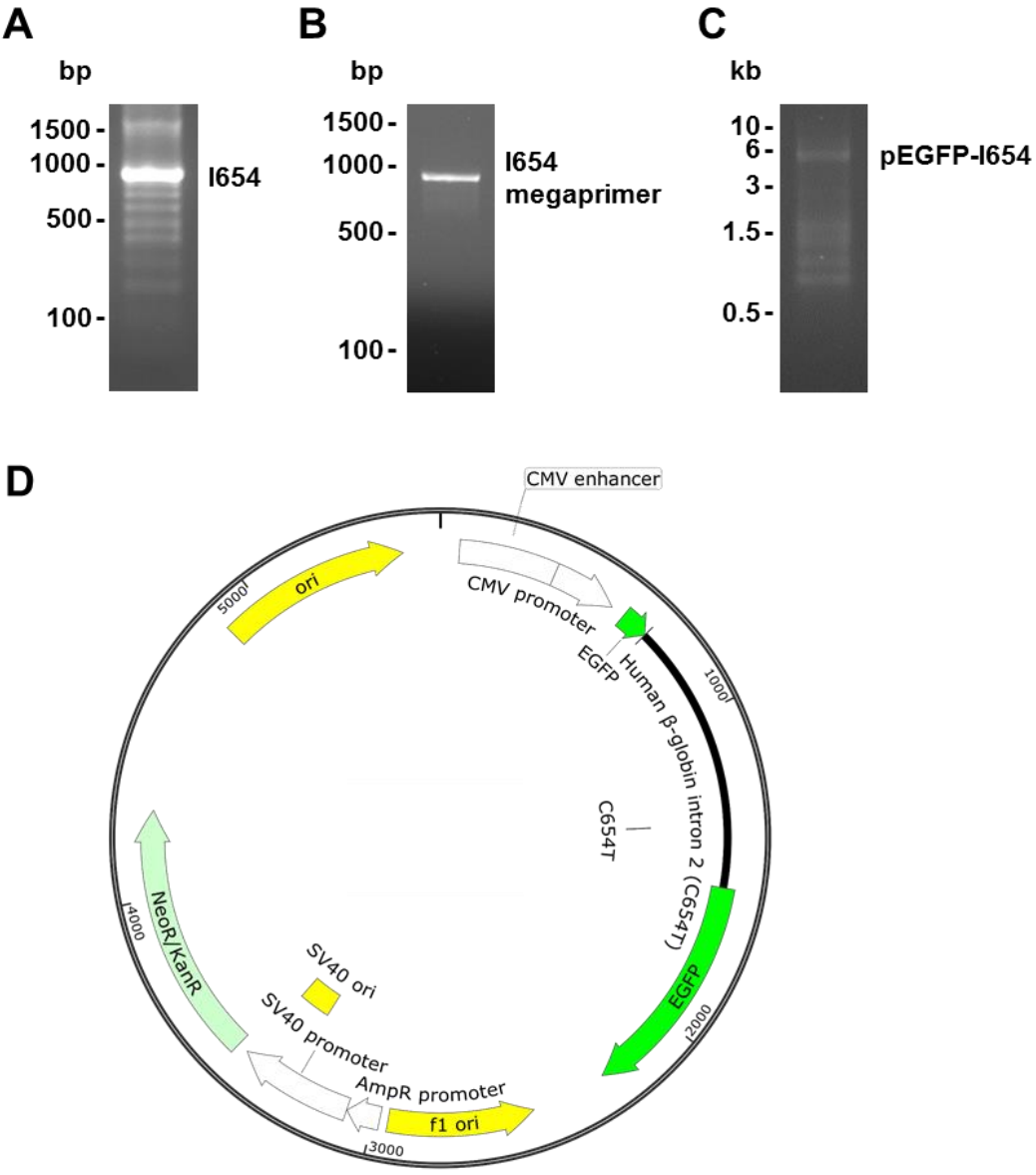

Figure 7.2. An EGFP-based reporter assay for oligonucleotide delivery A. Production of the I654 insert by assembly PCR. B. Production of the extended I654 megaprimer by PCR. C. Insertion of I654 into the EGFP coding sequence of pEGFP-C1 by PCR. D. Plasmid map of the pEGFP-I654 reporter construct, with EGFP shown in green and the β-globin intron in black. The position of the C654T mutation is highlighted. Plasmid map generated with SnapGene Viewer software version 3.1.4.

To test the construct, pEGFP-I, pEGFP-I654 and unmodified pEGFP were used to transfect Vero cells. After 18 h, cells transfected with the two positive controls had produced functional EGFP while cells transfected with pEGFP-I654 had not. However, the mutated intron also had a cytotoxic effect on the cells. This was probably a result of the constitutive, high-level expression of a misfolded protein, shown to cause cytotoxicity[347], due to the transfection of multiple copies of the vector into each cell. The developers of the assay created stable cell lines containing the plasmid for use in their assays[124]. It is possible that a single copy of the DNA in the cells did not lead to high enough expression for cytotoxicity, whereas transient transfection resulted in multiple copies of the plasmid in each cell, leading to higher expression levels. In addition, stable cell lines present the opportunity for accurate quantification of oligonucleotide function and determination of dose dependencies, as every cell contains a consistent number of copies of the DNA coding sequence under the same regulation. Therefore, creation of a stable reporter Vero cell line was attempted. Three attempts were made, with increasing concentrations of G418 (a neomycin analogue) for selection. The greatest concentration of G418, 1 mg mL^{-1}, resulted in complete control cell death after 14 days, but the vector-treated cells continued to exhibit G418 resistance 21 days after control cell death. The time scale of the study did not allow further attempts. Development of this assay would be a matter of priority for future CTB-mediated oligonucleotide delivery studies.

7.2.2. Alternative methods for payload delivery

Disulfide-conjugated RNA was shown to be released from CTB on within the ER, and the conjugated LACpep was shown to promote export from the ER, although the peptide-RNA remained hybridised to the RNA-CTB complex. Combining these two approaches, conjugating LACpep-skipper RNA to CTB by a disulfide bond, could offer a solution whereby LACpep could promote export of the freed oligonucleotide to the cytosol. If a Cys residue were incorporated into LACpep at the C-terminus (it requires a free N-terminus), it could be conjugated to the skipper RNA by SPAAC as previously (chapter 6). The LACpep Cys would allow conjugation to CTB-CKDEL through disulfide formation (figure 7.3), using the phenylselenenylsulfide-based method developed by Gamblin *et al.*[313].

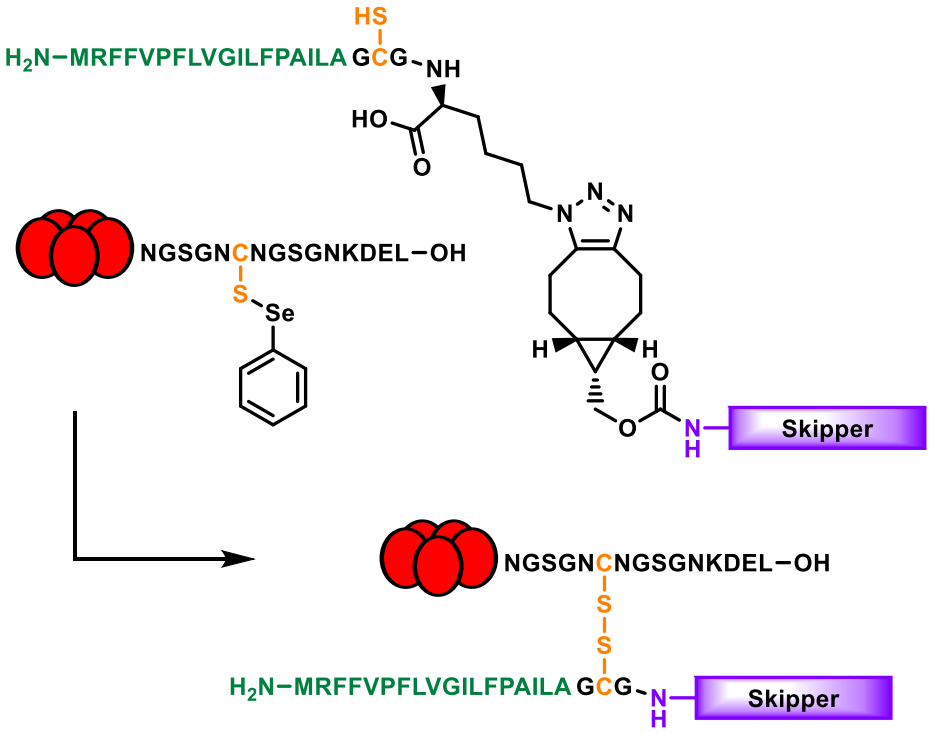

Figure 7.3. An alternative mechanism of targeted delivery and release of LAC-pep-skipper RNA Reaction scheme describing conjugation of CTB (red) containing a phenylselenenylsulfide group to a peptide-skipper RNA (purple) conjugate via a disulfide bond (orange). The peptide consists of LAC-pep (green) and a Cys residue (orange) for disulfide formation, separated by Gly linker residues.

To promote oligonucleotide targeting to the nucleus, the peptide conjugated to the skipper RNA could be further modified (figure 7.4) to contain a free N-terminal α-lactalbumin leader sequence, a nuclear localisation sequence (which does not require presence at a terminus but just surface exposure[328,329]), a Cys for disulfide formation and a C-terminal L-azidolysine for RNA conjugation. This could combine export from the ER with nuclear targeting, potentially improving the alternative splice activity of the oligonucleotide.

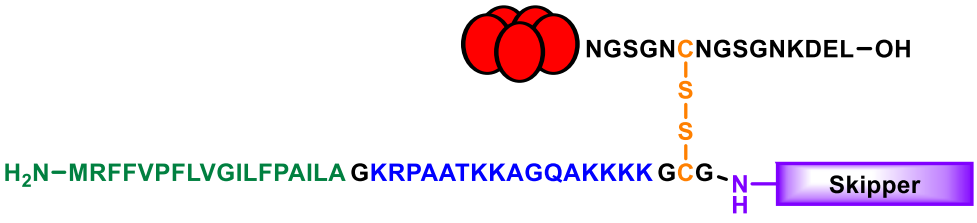

Figure 7.4. A peptide-RNA-CTB complex for improved targeting upon release A complex of CTB (red) linked to a peptide-skipper RNA (purple) conjugate via a disulfide bond (orange). The peptide consists of LACpep (green), an NLS (blue) and a Cys residue (orange) for disulfide formation, separated by Gly linker residues.

Endosomal escape offers an alternative potential method for release of payloads to the cytosol. Fusogenic peptides mediating endosomal escape have been designed based on membrane-disrupting domains of the influenza virus hemagglutinin HA-2 subunit[348], the TAT protein of human immunodeficiency virus[349], glycoprotein H of herpes simplex virus[350] and the minor capsid protein of papillomavirus[351]. In all of these cases, the lower pH of the endosome results in conformational changes to the peptides, resulting in fusion with and disruption of the endosomal membrane. Polypeptides derived from bacterial sources have also been used to promote endosomal escape, including listeriolysin O from *Listeria monocytogenes*[352], domain II of exotoxin A from *Pseudomonas aeruginosa*[353] and the T domain of diphtheria toxin from *Corynebacterium diphtheria*[354]. This last example is also a pH-dependent fusogenic polypeptide, while the other two are pH-dependent pore-forming polypeptides. This is not an exhaustive list and many other examples exist, derived from plants and animals in addition to microorganisms[355]. All of these examples have been shown to facilitate the delivery of large biologic molecules of therapeutic potential, including proteins, DNA and oligonucleotides. Fusions of these peptides with CTB could combine the cell-specific targeting and efficient endocytic properties of CTB with endosome-specific membrane disruption, allowing the release of therapeutic payloads into the cytosol. However, due to the high affinity, multi-valent association of CTB with GM1[18,38], it is likely CTB would not be released from the endosomal membrane without severe membrane disruption. In this case, an acid-labile linker would have to be considered to allow delivery to the cytosol.

7.2.3. Suitability of CTB for clinical use

There are several unmet treatment requirements for diseases which affect cells presenting GM1 on their surface. Amyotrohic lateral sclerosis[356] and lysosomal storage disorders[357] are both highly debilitating diseases, with no current cure and limited treatment options, which affect cells displaying high levels of GM1[358]. This marks CTB as an excellent choice for highly targeted delivery of therapeutics against these diseases. In terms of safety, recombinant CTB represents a promising delivery vector, having shown no systemic toxic effects compared to commercial preparations of CTB[241], known to contain 0.1-2% holotoxin contaminant[359]. In addition, during this study no obvious cytotoxicity of Vero cells was detected over 48 h, supporting the designation of recombinant CTB as non-toxic. However, the effects of long-term exposure to CTB are unclear. If the protein is not degraded or exported and continues to accumulate with subsequent doses, it may have a deleterious effect on the organelle in which it accumulates, preventing efficient

function. Alternatively, the resources required by the cell for processing the protein may have an inhibitory effect on their native function, either sequestering resources for other functions or inducing an unsustainably high metabolic state. The apparent increase in cell viability over 48 h on treatment with RNA-CTB complexes, as determined by MTT assay, may be an indication of an increased metabolic rate[321,322], lending some support the latter possibility. As such, in its current state CTB remains unsuitable for transferral to clinical use. Further, longer-term *in vivo* studies are required to elucidate the fate of CTB following endocytosis and the effect this has on the cells.

The methods for protein expression and payload conjugation used for this study require refinement prior to any clinical use. The protein yields obtained are too low to make production commercially viable. While the yields could be improved through alternative cell lines[89,230,231,235] and conditions, for example use of a fermentor[231], CTB is primarily secreted into the growth media on overexpression. Extracting the protein from such a high volume of liquid would be impractical. Similarly, the number and complexity of steps required for protein labelling mean the transition to production on a scale suitable for a drug is unlikely at present. Significant improvements in these areas are required for CTB to be transferrable to the clinic.

Finally, and perhaps most importantly, CTB administration has the potential to cause an immune response, both against itself and against the therapeutic molecule it carries. It has been known since the 1930s that conjugating small molecules to a non-native carrier protein can illicit an immune response in animals[360-362]. Additionally, there are many examples of protein-based therapeutics resulting in an undesirable immune response[363-365], both endangering the patient and rendering the protein less effective as a therapeutic. Both CTB[92,359,366-368] and the holotoxin[359,369-371] have been used as adjuvants in vaccines, although contradictory evidence suggests recombinant CTB is considerably less effective[359,369,372] and cite CTA impurity as the cause of any adjuvant effects. However, CTB coupled to foreign antigens either chemically or genetically have been shown to induce an immune response against the attached antigen[92,94,359], so reducing or negating any immune response is key to the use of CTB as a delivery vector.

Suppression or modulation of the immune system has shown some promise in improving gene therapy by preventing the destruction of immunogenic vectors[373]. However, this carries the risk of opportunistic infection and should be avoided if alternative methods are available. N-terminal extensions to CTB have been shown to mitigate

immunogenicity[88], convenient as current methods for efficient SrtA-mediated ligation require N-terminal labelling[261].

Creation of hybrid molecules which contain groups that promote immune evasion have shown some promise. Conjugation of polyethylene glycol (PEG; figure 7.5A) has been shown to mitigate the immune response to proteins[374], adenoviral vectors[375] and nanoparticles[376], without loss of function, by masking antigenic features with the non-immunogenic PEG. This could be adapted for CTB, using PEG containing NHS ester or isothiocyanate functional groups to non-specifically coat the protein at surface-exposed Lys residues. Other methods of immune evasion without loss of function include the fusion of immunogenic proteins to the Gly-Ala repeat (GAr) domain from the Epstein-Barr virus nuclear antigen-1, which prevents epitope generation in T-lymphocytes[377], or conjugation to mannosamine-biotin adducts through exposed Lys residues[378] (figure 7.5B), resulting in a masking effect similar to PEG. Both could potentially be applied to CTB, either through genetic incorporation in the case of the former, or conjugation to surface-exposed Lys residues for the latter. However, expression of a CTB-GAr fusion protein is unlikely due to the size of the GAr domain (239 residues). While antigen masking has been very successful, PEG and mannosamine-biotin masking both require high degrees of surface coverage to provide immune protection. This could prove problematic if there are insufficient available residues for conjugation on CTB.

Perhaps the most elegant method for immune evasion involves the display of CD22 receptor ligands[379] (figure 7.5C). These synthetic glycans were displayed on the surface of liposomes bearing antigenic peptides, and induced apoptosis in B-cells recognising the antigens through binding to the CD22 coreceptor, which regulates B-cell activity. This resulted in antigen-specific tolerance to protein antigens *in vitro* and *in vivo*, preventing an immune response on re-administration of similar antigens. If this could be adapted for use with CTB, it could solve any potential problems with immunogenicity and enable its effective use in clinical applications using the methods described in this study.

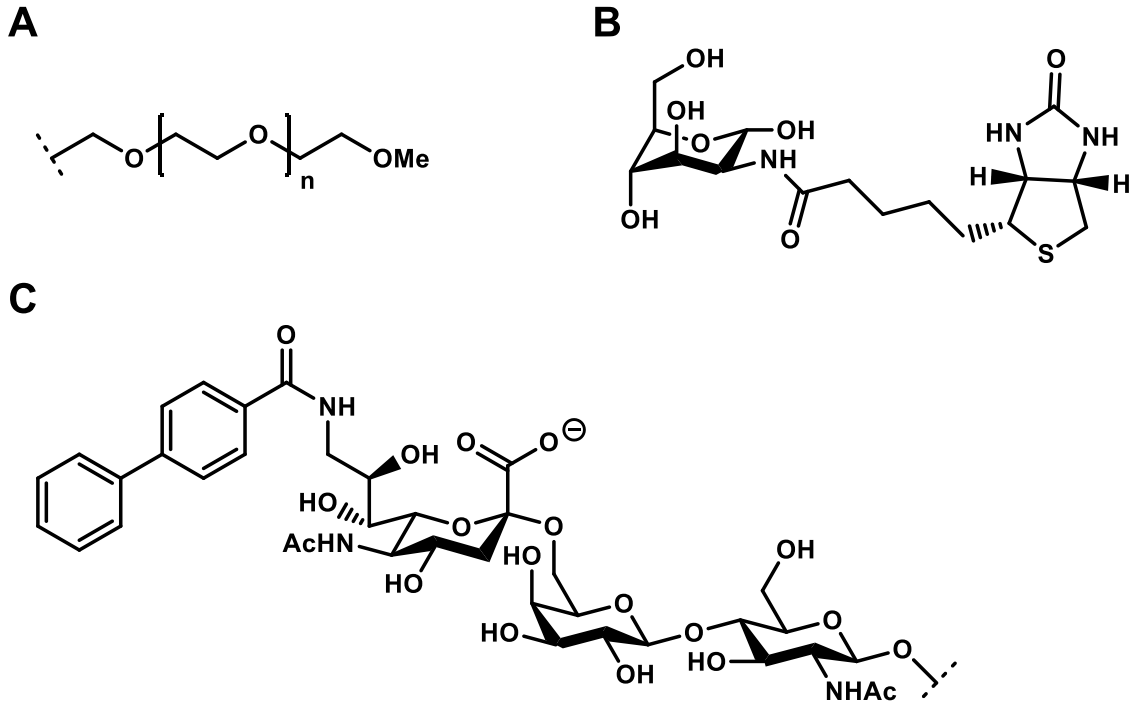

Figure 7.5. Molecules adapted for immune evasion Chemical structures of A. PEG, B. mannosamine-biotin adduct, and C. the CD22 receptor ligand.

Chapter 8: Appendix

8.1. Oligonucleotides

The following oligonucleotides were used during this study (m = 2′-OMe; * = phosphorothioate backbone).

Nomenclature (protein)	**Sequence (5′ – 3′)**
Y5 (Apep-CTB)	CTGTTCAGGCGCATGCAGGAGGTGGCGCACCGCCGGGTTGTGGGAATGCTCCAAGATCATCGGAAAAC
Z5 (Apep-CTB)	CCACCTCCGGTTTTTTCATCGCAAGTATTACTCATGCTCTGAAAGTACAGGTTTTCCGATGATCTTGG
A1 (GGG-CTB, CTB-KDEL, CTB-PkC11, CTB-CKDEL, CTB-Apep)	CTGTTCAGGCGCATGCAGGAGGTGGCACTCCTCAAAATATTACTGATTTGTGCGCAGAATACCACAACAC
A5 (Apep-CTB)	GAAAAAACCGGAGGTGGCGCTCCTCAAAATATTACTGATTTGTGCGCAGAATACCACAACAC
B1 (GGG-CTB, CTB-KDEL, CTB-PkC11, CTB-CKDEL, Apep-CTB, CTB-Apep)	CTCTTTTTCCCGCTAGCGATTCTGTATACGAAAAGATCTTATCATTTAGCGTATATATTTTGTGTGTTGTGGTATTCTGCG
C1 (GGG-CTB, CTB-KDEL, CTB-PkC11, CTB-CKDEL, Apep-CTB, CTB-Apep)	GCTAGCGGGAAAAAGAGAGATGGCTATCATTACTTTTAAGAATGGTGCAATTTTTCAAGTAGAGGTACCAGGTAGTC

D1 (GGG-CTB, CTB-KDEL, CTB-PkC11, CTB-CKDEL, Apep-CTB, CTB-Apep)	GCAATCCTCAGGGTATCCTTCATACGTTCGATTGCCTTTTTTTGTGAATCTATATGTTGACTACCTGGTACCTCTACTTG
E1 (GGG-CTB, CTB-KDEL, CTB-PkC11, CTB-CKDEL, Apep-CTB, CTB-Apep)	GATACCCTGAGGATTGCATATCTTACTGAAGCTAAAGTCGAAAAGTTATGTGTATGGAATAATAAA
F1 (GGG-CTB)	CCTGCAGGGAAAACTTAGTTTGCCATACTAATTGCGGCGATCGCATGAGGCGTTTTATTATTCCATACACATAA
F2 (CTB-KDEL, Apep-CTB)	CCTGCAGGGAAAACTTACAGTTCATCTTTGTTTGCCATACTAATTGCGGCGATCGCATGAGGCGTTTTATTATTCCATACACATAA
F3 (CTB-PkC11, CTB-CKDEL)	CTAATTGCGGCGATCGCATGAGGCGTTTTATTATTCCATACACATAA
F6 (CTB-Apep)	GTGCGTTACCGCCATTGTTTGCCATACTAATTGCGGCGATCGCATGAGGCGTTTTATTATTCCATACACATAA
G3 (CTB-PkC11)	CGATCGCCGCAATTAGTATGGCAAACGGAAAGCCGATCCCAAACCCTTTG
G4 (CTB-CKDEL)	CGATCGCCGCAATTAGTATGGCAAACAACGGCAGCGGGAACTGCAACGGC
G6 (CTB-Apep)	CAATGGCGGTAACGCACCGCCGGGTTGTGGGAATGCTCCAAGATCATCGGAAAACCTGTACTTTCAGG
H3 (CTB-PkC11)	CCTGCAGGGAAAACTTAGGTGGAGTCGCATCCCAGCAAAGGGTTTGGGATCG
H4 (CTB-CKDEL)	CCTGCAGGGAAAACTTACAGTTCATCTTTATTGCCACTGCCGTTGCAGTTCCC
H6 (CTB-Apep)	CCTGCAGGGAAAACTTAGGTTTTTTCATCGCAAGTATTACTCATGCCACCTCCCTGAAAGTACAGGTTTTC

FT1 (GGG-CTB, CTB-KDEL, CTB-PkC11, CTB-CKDEL, Apep-CTB, CTB-Apep)	CATGCGCCTGAACAG
RT1 (GGG-CTB, CTB-PkC11, CTB-Apep)	CCTGCAGGGAAAACTTAG
RT2 (CTB-KDEL, CTB-CKDEL, Apep-CTB)	CCTGCAGGGAAAACTTAC
A5 (I654)	CTGACCCTTAAGTGAGTCTATGGGACCCTTGATGTTTTCTTTCCCCTTCTTTTCTATG
B5 (I654)	TAAACTGTACCCTGTTACTTCTCCCCTTCCTATGACATGAACTTAACCATAGAAAAG AAGGGGAAA
C5 (I654)	GTAACAGGGTACAGTTTAGAATGGGAAACAGACGAATGATTGCATCAGTGTGGAAG TCTCAGGATC
D5 (I654)	TAAACAAAAGAAAACAATTGTTATGAACAGCAAATAAAAGAAACTAAAACGATCCT GAGACTTCCAC
E5 (I654)	ACAATTGTTTTCTTTTGTTTAATTCTTGCTTTCTTTTTTTTTCTTCTCCGCAATTTTTAC TATTATAC
F5 (I654)	GTATCTCAGAGATATTTCCTTTTGTTATACACAATGTTAAGGCATTAAGTATAATAG TAAAAATTGCG
G5 (I654)	GGAAATATCTCTGAGATACATTAAGTAACTTAAAAAAAAACTTTACACAGTCTGCCT AGTACATTA
H5 (I654)	AGTAGGGAGATTATGAATATGCAAATAAGCACACATATATTCCAAATAGTAATGTA CTAGGCAGACT
I5 (I654)	TATTCATAATCTCCCTACTTTATTTTCTTTTATTTTTAATTGATACATAATCATTATAC ATATTTATG

J5 (I654)	TGATTTGGTCAATATGTGTACACATATTAAAACATTACACTTTAACCCATAAATATG TATAATGATTAT
K5 (I654)	ACACATATTGACCAAATCAGGGTAATTTTGCATTTGTAATTTTAAAAAATGCTTTCTT CTTTTAATAT
L5 (I654)	AAGAAAGAGATTAGGGAAAGTATTAGAAATAAGATAAACAAAAAAGTATATTAAA AGAAGAAAGCATT
M5 (I654)	TTTCCCTAATCTCTTTCTTTCAGGGCAATAATGATACAATGTATCATGCCTCTTTGCA CCATTCTA
N5 (I654)	GCAGAAATATTGCTATTACCTTAACCCAGAAATTATCACTGTTATTCTTTAGAATGG TGCAAAGAGG
O5 (I654)	GTAATAGCAATATTTCTGCATATAAATATTTCTGCATATAAATTGTAACTGATGTAA GAGGTTTCA
P5 (I654)	ATAAAATAAAAGCAGAATGGTAGCTGGATTGTAGCTGCTATTAGCAATATGAAACC TCTTACATCAG
Q5 (I654)	CCATTCTGCTTTTATTTTATGGTTGGGATAAGGCTGGATTATTCTGAGTCCAAGCTAG GCCCTTTTG
R5 (I654)	GATGAACTTAAGCTGTGGGAGGAAGATAAGAGGTATGAACATGATTAGCAAAAGG GCCTAGCTTG
FT5 (I654)	CTGACCCTTAAGTGAGT
RT5 (I654)	GATGAACTTAAGCTGTGG
OEP F1 (I654)	GTGAGTCTATGGGACCCTTG
OEP R1 (I654)	CCTCGCCCTCGCCGGACCTGTGGGAGGAAGATAAGAGG

OEP R2 (I654)	ACGCTGAACTTGTGGCCGTTTAC
SDM T654C F (I654)	CAGTGATAATTTCTGGGTTAAGGCAATAGCAATATTTCTGC
SDM T654C R (I654)	GCAGAAATATTGCTATTGCCTTAACCCAGAAATTATCACTG
Seq1 (pSAB2.2)	GGCAAATATTCTGAAATGAGC
Seq2 F (pEGFP-C1)	CGTGTACGGTGGGAGGTC
Seq2 R (pEGFP-C1)	CAGGTTCAGGGGGAGGTG
Intron skipper RNA	mG*mC*mU*mA*mU*mU*mA*mC*mC*mU*mU*mA*mA*mC*mC*mC*mA*mG
Complement RNA	mC*mU*mG*mG*mG*mU*mU*mA*mA*mG*mG*mU*mA*mA*mU*mA*mG*mC
11mer complement RNA	mC*mU*mG*mG*mG*mU*mU*mA*mA*mG*mG
12mer complement RNA	mC*mU*mG*mG*mG*mU*mU*mA*mA*mG*mG*mU
13mer complement RNA	mC*mU*mG*mG*mG*mU*mU*mA*mA*mG*mG*mU*mA

8.2. Plasmid sequences

8.2.1. pSAB2.2 (including wt CTB)

The pSAB2.2 plasmid containing wt CTB was provided by J. Ross (University of Leeds), derived from the pMAL-p5x plasmid available from NEB. This plasmid was used to express all CTB variants. CTB is shown with red text, the periplasmic leader sequence with purple text, and the SphI and PstI restriction sites used for sub-cloning by yellow and green highlighting, respectively.

CCGACACCATCGAATGGTGCAAAACCTTTCGCGGTATGGCATGATAGCGCCCGGAA
GAGAGTCAATTCAGGGTGGTGAATGTGAAACCAGTAACGTTATACGATGTCGCAGA
GTATGCCGGTGTCTCTTATCAGACCGTTTCCCGCGTGGTGAACCAGGCCAGCCACGT
TTCTGCGAAAACGCGGGAAAAAGTGGAAGCGGCGATGGCGGAGCTGAATTACATT
CCCAACCGCGTGGCACAACAACTGGCGGGCAAACAGTCGTTGCTGATTGGCGTTGC
CACCTCCAGTCTGGCCCTGCACGCGCCGTCGCAAATTGTCGCGGCGATTAAATCTC
GCGCCGATCAACTGGGTGCCAGCGTGGTGGTGTCGATGGTAGAACGAAGCGGCGTC
GAAGCCTGTAAAGCGGCGGTGCACAATCTTCTCGCGCAACGCGTCAGTGGGCTGAT
CATTAACTATCCGCTGGATGACCAGGATGCCATTGCTGTGGAAGCTGCCTGCACTA
ATGTTCCGGCGTTATTTCTTGATGTCTCTGACCAGACACCCATCAACAGTATTATTT
TCTCCCATGAAGACGGTACGCGACTGGGCGTGGAGCATCTGGTCGCATTGGGTCAC
CAGCAAATCGCGCTGTTAGCGGGCCCATTAAGTTCTGTCTCGGCGCGTCTGCGTCTG
GCTGGCTGGCATAAATATCTCACTCGCAATCAAATTCAGCCGATAGCGGAACGGGA
AGGCGACTGGAGTGCCATGTCCGGTTTTCAACAAACCATGCAAATGCTGAATGAGG
GCATCGTTCCCACTGCGATGCTGGTTGCCAACGATCAGATGGCGCTGGGCGCAATG
CGCGCCATTACCGAGTCCGGGCTGCGCGTTGGTGCGGATATTTCGGTAGTGGGATA
CGACGATACCGAAGACAGCTCATGTTATATCCCGCCGTTAACCACCATCAAACAGG
ATTTTCGCCTGCTGGGGCAAACCAGCGTGGACCGCTTGCTGCAACTCTCTCAGGGC
CAGGCGGTGAAGGGCAATCAGCTGTTGCCCGTCTCACTGGTGAAAAGAAAAACCA
CCCTGGCGCCCAATACGCAAACCGCCTCTCCCCGCGCGTTGGCCGATTCATTAATGC
AGCTGGCACGACAGGTTTCCCGACTGGAAAGCGGGCAGTGAGCGCAACGCAATTA
ATGTAAGTTAGCTCACTCATTAGGCACAATTCTCATGTTTGACAGCTTATCATCGAC
TGCACGGTGCACCAATGCTTCTGGCGTCAGGCAGCCATCGGAAGCTGTGGTATGGC
TGTGCAGGTCGTAAATCACTGCATAATTCGTGTCGCTCAAGGCGCACTCCCGTTCTG
GATAATGTTTTTTGCGCCGACATCATAACGGTTCTGGCAAATATTCTGAAATGAGCT
GTTGACAATTAATCATCGGCTCGTATAATGTGTGGAATTGTGAGCGGATAACAATT
TCACACAGGAAACAGCCAGTCCGTTTAGGTGTTTTCACGAGCAATTGACCAACAAG
GACCATAGATTATGAGCTTTAAGAAAATTATCAAGGCATTTGTTATCATGGCTGCTT
TGGTATCTGTTCAGGCGCATGCAGGAGGTGGCACTCCTCAAAATATTACTGATTTGT
GCGCAGAATACCACAACACACAAATATATACGCTAAATGATAAGATCTTTTCGTAT
ACAGAATCGCTAGCGGGAAAAAGAGAGATGGCTATCATTACTTTTAAGAATGGTGC
AATTTTTCAAGTAGAGGTACCAGGTAGTCAACATATAGATTCACAAAAAAAAGCGA
TTGAAAGGATGAAGGATACCCTGAGGATTGCATATCTTACTGAAGCTAAAGTCGAA
AAGTTATGTGTATGGAATAATAAAACGCCTCATGCGATCGCCGCAATTAGTATGGC
AAACTAAGTTTTCCCTGCAGGTAATTAAATAAGCTTCAAATAAAACGAAAGGCTCA
GTCGAAAGACTGGGCCTTTCGTTTTATCTGTTGTTTGTCGGTGAACGCTCTCCTGAG
TAGGACAAATCCGCCGGGAGCGGATTTGAACGTTGCGAAGCAACGGCCCGGAGGG
TGGCGGGCAGGACGCCCGCCATAAACTGCCAGGCATCAAATTAAGCAGAAGGCCA

TCCTGACGGATGGCCTTTTTGCGTTTCTACAAACTCTTTCGGTCCGTTGTTTATTTTT
CTAAATACATTCAAATATGTATCCGCTCATGAGACAATAACCCTGATAAATGCTTC
AATAATATTGAAAAAGGAAGAGTATGAGTATTCAACATTTCCGTGTCGCCCTTATT
CCCTTTTTTGCGGCATTTTGCCTTCCTGTTTTTGCTCACCCAGAAACGCTGGTGAAA
GTAAAAGATGCTGAAGATCAGTTGGGTGCACGAGTGGGTTACATCGAACTGGATCT
CAACAGCGGTAAGATCCTTGAGAGTTTTCGCCCCGAAGAACGTTTCCCAATGATGA
GCACTTTTAAAGTTCTGCTATGTGGCGCGGTATTATCCCGTGTTGACGCCGGGCAAG
AGCAACTCGGTCGCCGCATACACTATTCTCAGAATGACTTGGTTGAGTACTCACCA
GTCACAGAAAAGCATCTTACGGATGGCATGACAGTAAGAGAATTATGCAGTGCTGC
CATAACCATGAGTGATAACACTGCGGCCAACTTACTTCTGACAACGATCGGAGGAC
CGAAGGAGCTAACCGCTTTTTTGCACAACATGGGGGATCATGTAACTCGCCTTGAT
CGTTGGGAACCGGAGCTGAATGAAGCCATACCAAACGACGAGCGTGACACCACGA
TGCCTGTAGCAATGGCAACAACGTTGCGCAAACTATTAACTGGCGAACTACTTACT
CTAGCTTCCCGGCAACAATTAATAGACTGGATGGAGGCGGATAAAGTTGCAGGACC
ACTTCTGCGCTCGGCCCTTCCGGCTGGCTGGTTTATTGCTGATAAATCTGGAGCCGG
TGAGCGTGGGTCTCGCGGTATCATTGCAGCACTGGGGCCAGATGGTAAGCCCTCCC
GTATCGTAGTTATCTACACGACGGGGAGTCAGGCAACTATGGATGAACGAAATAGA
CAGATCGCTGAGATAGGTGCCTCACTGATTAAGCATTGGTAACTGTCAGACCAAGT
TTACTCATATATACTTTAGATTGATTTCCTTAGGACTGAGCGTCAACCCCGTAGAAA
AGATCAAAGGATCTTCTTGAGATCCTTTTTTTCTGCGCGTAATCTGCTGCTTGCAAA
CAAAAAAACCACCGCTACCAGCGGTGGTTTGTTTGCCGGATCAAGAGCTACCAACT
CTTTTTCCGAAGGTAACTGGCTTCAGCAGAGCGCAGATACCAAATACTGTCCTTCTA
GTGTAGCCGTAGTTAGGCCACCACTTCAAGAACTCTGTAGCACCGCCTACATACCT
CGCTCTGCTAATCCTGTTACCAGTGGCTGCTGCCAGTGGCGATAAGTCGTGTCTTAC
CGGGTTGGACTCAAGACGATAGTTACCGGATAAGGCGCAGCGGTCGGGCTGAACG
GGGGGTTCGTGCACACAGCCCAGCTTGGAGCGAACGACCTACACCGAACTGAGAT
ACCTACAGCGTGAGCTATGAGAAAGCGCCACGCTTCCCGAAGGGAGAAAGGCGGA
CAGGTATCCGGTAAGCGGCAGGGTCGGAACAGGAGAGCGCACGAGGGAGCTTCCA
GGGGGAAACGCCTGGTATCTTTATAGTCCTGTCGGGTTTCGCCACCTCTGACTTGAG
CGTCGATTTTTGTGATGCTCGTCAGGGGGGCGGAGCCTATGGAAAAACGCCAGCAA
CGCGGCCTTTTTACGGTTCCTGGCCTTTTGCTGGCCTTTTGCTCACATGTTCTTTCCT
GCGTTATCCCCTGATTCTGTGGATAACCGTATTACCGCCTTTGAGTGAGCTGATACC
GCTCGCCGCAGCCGAACGACCGAGCGCAGCGAGTCAGTGAGCGAGGAAGCGGAAG
AGCGCCTGATGCGGTATTTTCTCCTTACGCATCTGTGCGGTATTTCACACCGCATAT
AAGGTGCACTGTGACTGGGTCATGGCTGCGCCCCGACACCCGCCAACACCCGCTGA
CGCGCCCTGACGGGCTTGTCTGCTCCCGGCATCCGCTTACAGACAAGCTGTGACCG
TCTCCGGGAGCTGCATGTGTCAGAGGTTTTCACCGTCATCACCGAAACGCGCGAGG
CAGCTGCGGTAAAGCTCATCAGCGTGGTCGTGCAGCGATTCACAGATGTCTGCCTG
TTCATCCGCGTCCAGCTCGTTGAGTTTCTCCAGAAGCGTTAATGTCTGGCTTCTGAT
AAAGCGGGCCATGTTAAGGGCGGTTTTTTCCTGTTTGGTCACTGATGCCTCCGTGTA
AGGGGGATTTCTGTTCATGGGGGTAATGATACCGATGAAACGAGAGAGGATGCTCA
CGATACGGGTTACTGATGATGAACATGCCCGGTTACTGGAACGTTGTGAGGGTAAA
CAACTGGCGGTATGGATGCGGCGGGACCAGAGAAAAATCACTCAGGGTCAATGCC
AGCGCTTCGTTAATACAGATGTAGGTGTTCCACAGGGTAGCCAGCAGCATCCTGCG
ATGCAGATCCGGAACATAATGGTGCAGGGCGCTGACTTCCGCGTTTCCAGACTTTA
CGAAACACGGAAACCGAAGACCATTCATGTTGTTGCTCAGGTCGCAGACGTTTTGC
AGCAGCAGTCGCTTCACGTTCGCTCGCGTATCGGTGATTCATTCTGCTAACCAGTAA
GGCAACCCCGCCAGCCTAGCCGGGTCCTCAACGACAGGAGCACGATCATGCGCACC
CGTGGCCAGGACCCAACGCTGCCCGAAATT

8.2.2. pET28a (including SrtA)

The pET28a plasmid containing SrtA was provided by D. Williamson (University of Leeds), derived from the pET28a plasmid available from NEB. This plasmid was used to express SrtA-His_6. SrtA-His_6 is shown with red text and the NdeI and EcoRI restriction sites used for sub-cloning by yellow and green highlighting, respectively.

TGGCGAATGGGACGCGCCCTGTAGCGGCGCATTAAGCGCGGCGGGTGTGGTGGTTA
CGCGCAGCGTGACCGCTACACTTGCCAGCGCCCTAGCGCCCGCTCCTTTCGCTTTCT
TCCCTTCCTTTCTCGCCACGTTCGCCGGCTTTCCCCGTCAAGCTCTAAATCGGGGGC
TCCCTTTAGGGTTCCGATTTAGTGCTTTACGGCACCTCGACCCCAAAAAACTTGATT
AGGGTGATGGTTCACGTAGTGGGCCATCGCCCTGATAGACGGTTTTTCGCCCTTTGA
CGTTGGAGTCCACGTTCTTTAATAGTGGACTCTTGTTCCAAACTGGAACAACACTCA
ACCCTATCTCGGTCTATTCTTTTGATTTATAAGGGATTTTGCCGATTTCGGCCTATTG
GTTAAAAAATGAGCTGATTTAACAAAAATTTAACGCGAATTTTAACAAAATATTAA
CGTTTACAATTTCAGGTGGCACTTTTCGGGGAAATGTGCGCGGAACCCCTATTTGTT
TATTTTTCTAAATACATTCAAATATGTATCCGCTCATGAATTAATTCTTAGAAAAAC
TCATCGAGCATCAAATGAAACTGCAATTTATTCATATCAGGATTATCAATACCATAT
TTTTGAAAAAGCCGTTTCTGTAATGAAGGAGAAAACTCACCGAGGCAGTTCCATAG
GATGGCAAGATCCTGGTATCGGTCTGCGATTCCGACTCGTCCAACATCAATACAAC
CTATTAATTTCCCCTCGTCAAAAATAAGGTTATCAAGTGAGAAATCACCATGAGTG
ACGACTGAATCCGGTGAGAATGGCAAAAGTTTATGCATTTCTTTCCAGACTTGTTCA
ACAGGCCAGCCATTACGCTCGTCATCAAAATCACTCGCATCAACCAAACCGTTATT
CATTCGTGATTGCGCCTGAGCGAGACGAAATACGCGATCGCTGTTAAAAGGACAAT
TACAAACAGGAATCGAATGCAACCGGCGCAGGAACACTGCCAGCGCATCAACAAT
ATTTTCACCTGAATCAGGATATTCTTCTAATACCTGGAATGCTGTTTTCCCGGGGAT
CGCAGTGGTGAGTAACCATGCATCATCAGGAGTACGGATAAAATGCTTGATGGTCG
GAAGAGGCATAAATTCCGTCAGCCAGTTTAGTCTGACCATCTCATCTGTAACATCAT
TGGCAACGCTACCTTTGCCATGTTTCAGAAACAACTCTGGCGCATCGGGCTTCCCAT
ACAATCGATAGATTGTCGCACCTGATTGCCCGACATTATCGCGAGCCCATTTATACC
CATATAAATCAGCATCCATGTTGGAATTTAATCGCGGCCTAGAGCAAGACGTTTCC
CGTTGAATATGGCTCATAACACCCCTTGTATTACTGTTTATGTAAGCAGACAGTTTT
ATTGTTCATGACCAAAATCCCTTAACGTGAGTTTTCGTTCCACTGAGCGTCAGACCC
CGTAGAAAAGATCAAAGGATCTTCTTGAGATCCTTTTTTTCTGCGCGTAATCTGCTG
CTTGCAAACAAAAAAACCACCGCTACCAGCGGTGGTTTGTTTGCCGGATCAAGAGC
TACCAACTCTTTTTCCGAAGGTAACTGGCTTCAGCAGAGCGCAGATACCAAATACT
GTCCTTCTAGTGTAGCCGTAGTTAGGCCACCACTTCAAGAACTCTGTAGCACCGCCT
ACATACCTCGCTCTGCTAATCCTGTTACCAGTGGCTGCTGCCAGTGGCGATAAGTCG
TGTCTTACCGGGTTGGACTCAAGACGATAGTTACCGGATAAGGCGCAGCGGTCGGG
CTGAACGGGGGGTTCGTGCACACAGCCCAGCTTGGAGCGAACGACCTACACCGAA
CTGAGATACCTACAGCGTGAGCTATGAGAAAGCGCCACGCTTCCCGAAGGGAGAA
AGGCGGACAGGTATCCGGTAAGCGGCAGGGTCGGAACAGGAGAGCGCACGAGGG
AGCTTCCAGGGGGAAACGCCTGGTATCTTTATAGTCCTGTCGGGTTTCGCCACCTCT
GACTTGAGCGTCGATTTTTGTGATGCTCGTCAGGGGGGCGGAGCCTATGGAAAAAC
GCCAGCAACGCGGCCTTTTTACGGTTCCTGGCCTTTTGCTGGCCTTTTGCTCACATG
TTCTTTCCTGCGTTATCCCCTGATTCTGTGGATAACCGTATTACCGCCTTTGAGTGAG
CTGATACCGCTCGCCGCAGCCGAACGACCGAGCGCAGCGAGTCAGTGAGCGAGGA
AGCGGAAGAGCGCCTGATGCGGTATTTTCTCCTTACGCATCTGTGCGGTATTTCACA
CCGCATATATGGTGCACTCTCAGTACAATCTGCTCTGATGCCGCATAGTTAAGCCAG

TATACACTCCGCTATCGCTACGTGACTGGGTCATGGCTGCGCCCCGACACCCGCCA
ACACCCGCTGACGCGCCCTGACGGGCTTGTCTGCTCCCGGCATCCGCTTACAGACA
AGCTGTGACCGTCTCCGGGAGCTGCATGTGTCAGAGGTTTTCACCGTCATCACCGA
AACGCGCGAGGCAGCTGCGGTAAAGCTCATCAGCGTGGTCGTGAAGCGATTCACA
GATGTCTGCCTGTTCATCCGCGTCCAGCTCGTTGAGTTTCTCCAGAAGCGTTAATGT
CTGGCTTCTGATAAAGCGGGCCATGTTAAGGGCGGTTTTTTCCTGTTTGGTCACTGA
TGCCTCCGTGTAAGGGGGATTTCTGTTCATGGGGGTAATGATACCGATGAAACGAG
AGAGGATGCTCACGATACGGGTTACTGATGATGAACATGCCCGGTTACTGGAACGT
TGTGAGGGTAAACAACTGGCGGTATGGATGCGGCGGGACCAGAGAAAAATCACTC
AGGGTCAATGCCAGCGCTTCGTTAATACAGATGTAGGTGTTCCACAGGGTAGCCAG
CAGCATCCTGCGATGCAGATCCGGAACATAATGGTGCAGGGCGCTGACTTCCGCGT
TTCCAGACTTTACGAAACACGGAAACCGAAGACCATTCATGTTGTTGCTCAGGTCG
CAGACGTTTTGCAGCAGCAGTCGCTTCACGTTCGCTCGCGTATCGGTGATTCATTCT
GCTAACCAGTAAGGCAACCCCGCCAGCCTAGCCGGGTCCTCAACGACAGGAGCAC
GATCATGCGCACCCGTGGGGCCGCCATGCCGGCGATAATGGCCTGCTTCTCGCCGA
AACGTTTGGTGGCGGGACCAGTGACGAAGGCTTGAGCGAGGGCGTGCAAGATTCC
GAATACCGCAAGCGACAGGCCGATCATCGTCGCGCTCCAGCGAAAGCGGTCCTCGC
CGAAAATGACCCAGAGCGCTGCCGGCACCTGTCCTACGAGTTGCATGATAAAGAAG
ACAGTCATAAGTGCGGCGACGATAGTCATGCCCCGCGCCCACCGGAAGGAGCTGA
CTGGGTTGAAGGCTCTCAAGGGCATCGGTCGAGATCCCGGTGCCTAATGAGTGAGC
TAACTTACATTAATTGCGTTGCGCTCACTGCCCGCTTTCCAGTCGGGAAACCTGTCG
TGCCAGCTGCATTAATGAATCGGCCAACGCGCGGGGAGAGGCGGTTTGCGTATTGG
GCGCCAGGGTGGTTTTTCTTTTCACCAGTGAGACGGGCAACAGCTGATTGCCCTTCA
CCGCCTGGCCCTGAGAGAGTTGCAGCAAGCGGTCCACGCTGGTTTGCCCCAGCAGG
CGAAAATCCTGTTTGATGGTGGTTAACGGCGGGATATAACATGAGCTGTCTTCGGT
ATCGTCGTATCCCACTACCGAGATATCCGCACCAACGCGCAGCCCGGACTCGGTAA
TGGCGCGCATTGCGCCCAGCGCCATCTGATCGTTGGCAACCAGCATCGCAGTGGGA
ACGATGCCCTCATTCAGCATTTGCATGGTTTGTTGAAAACCGGACATGGCACTCCA
GTCGCCTTCCCGTTCCGCTATCGGCTGAATTTGATTGCGAGTGAGATATTTATGCCA
GCCAGCCAGACGCAGACGCGCCGAGACAGAACTTAATGGGCCCGCTAACAGCGCG
ATTTGCTGGTGACCCAATGCGACCAGATGCTCCACGCCCAGTCGCGTACCGTCTTCA
TGGGAGAAAATAATACTGTTGATGGGTGTCTGGTCAGAGACATCAAGAAATAACGC
CGGAACATTAGTGCAGGCAGCTTCCACAGCAATGGCATCCTGGTCATCCAGCGGAT
AGTTAATGATCAGCCCACTGACGCGTTGCGCGAGAAGATTGTGCACCGCCGCTTTA
CAGGCTTCGACGCCGCTTCGTTCTACCATCGACACCACCACGCTGGCACCCAGTTG
ATCGGCGCGAGATTTAATCGCCGCGACAATTTGCGACGGCGCGTGCAGGGCCAGAC
TGGAGGTGGCAACGCCAATCAGCAACGACTGTTTGCCCGCCAGTTGTTGTGCCACG
CGGTTGGGAATGTAATTCAGCTCCGCCATCGCCGCTTCCACTTTTTCCCGCGTTTTC
GCAGAAACGTGGCTGGCCTGGTTCACCACGCGGGAAACGGTCTGATAAGAGACAC
CGGCATACTCTGCGACATCGTATAACGTTACTGGTTTCACATTCACCACCCTGAATT
GACTCTCTTCCGGGCGCTATCATGCCATACCGCGAAAGGTTTTGCGCCATTCGATGG
TGTCCGGGATCTCGACGCTCTCCCTTATGCGACTCCTGCATTAGGAAGCAGCCCAGT
AGTAGGTTGAGGCCGTTGAGCACCGCCGCCGCAAGGAATGGTGCATGCAAGGAGA
TGGCGCCCAACAGTCCCCCGGCCACGGGGCCTGCCACCATACCCACGCCGAAACAA
GCGCTCATGAGCCCGAAGTGGCGAGCCCGATCTTCCCCATCGGTGATGTCGGCGAT
ATAGGCGCCAGCAACCGCACCTGTGGCGCCGGTGATGCCGGCCACGATGCGTCCGG
CGTAGAGGATCGAGATCTCGATCCCGCGAAATTAATACGACTCACTATAGGGGAAT
TGTGAGCGGATAACAATTCCCCTCTAGAAATAATTTTGTTTAACTTTAAGAAGGAG
ATATACCATGGGCAGCAGCCATCATCATCATCATCACAGCAGCGGCCTGGTGCCGC

GCGGCAGCCATATGAAACCACATATCGATAATTATCTTCACGATAAAGATAAAGAT
GAAAAGATTGAACAATATGATAAAAATGTAAAAGAACAGGCGAGTAAAGATAAAA
AGCAGCAAGCTAAACCTCAAATTCCGAAAGATAAATCGAAAGTGGCAGGCTATATT
GAAATTCCAGATGCTGATATTAAAGAACCAGTATATCCAGGACCAGCAACACCTGA
ACAATTAAATAGAGGTGTAAGCTTTGCAGAAGAAAATGAATCACTAGATGATCAA
AATATTTCAATTGCAGGACACACTTTCATTGACCGTCCGAACTATCAATTTACAAAT
CTTAAAGCAGCCAAAAAAGGTAGTATGGTGTACTTTAAAGTTGGTAATGAAACACG
TAAGTATAAAATGACAAGTATAAGAGATGTTAAGCCTACAGATGTAGGAGTTCTAG
ATGAACAAAAAGGTAAAGATAAACAATTAACATTAATTACTTGTGATGATTACAAT
GAAAAGACAGGCGTTTGGGAAAAACGTAAAATCTTTGTAGCTACAGAAGTCAAAT
AATCGAATTCGAGCTCCGTCGACAAGCTTGCGGCCGCACTCGAGCACCACCACCAC
CACCACTGAGATCCGGCTGCTAACAAAGCCCGAAAGGAAGCTGAGTTGGCTGCTGC
CACCGCTGAGCAATAACTAGCATAACCCCTTGGGGCCTCTAAACGGGTCTTGAGGG
GTTTTTTGCTGAAAGGAGGAACTATATCCGGAT

8.2.3. pET28a (including SrtA-CBD)

The pET28a plasmid containing SrtA was provided by M. Balmforth (University of Leeds), derived from the pET28a plasmid available from NEB. This plasmid was used to express SrtA-CBD. SrtA-CBD is shown with red text.

TGGCGAATGGGACGCGCCCTGTAGCGGCGCATTAAGCGCGGCGGGTGTGGTGGTTA
CGCGCAGCGTGACCGCTACACTTGCCAGCGCCCTAGCGCCCGCTCCTTTCGCTTTCT
TCCCTTCCTTTCTCGCCACGTTCGCCGGCTTTCCCCGTCAAGCTCTAAATCGGGGGC
TCCCTTTAGGGTTCCGATTTAGTGCTTTACGGCACCTCGACCCCAAAAAACTTGATT
AGGGTGATGGTTCACGTAGTGGGCCATCGCCCTGATAGACGGTTTTTCGCCCTTTGA
CGTTGGAGTCCACGTTCTTTAATAGTGGACTCTTGTTCCAAACTGGAACAACACTCA
ACCCTATCTCGGTCTATTCTTTTGATTTATAAGGGATTTTGCCGATTTCGGCCTATTG
GTTAAAAAATGAGCTGATTTAACAAAAATTTAACGCGAATTTTAACAAAATATTAA
CGTTTACAATTTCAGGTGGCACTTTTCGGGGAAATGTGCGCGGAACCCCTATTTGTT
TATTTTTCTAAATACATTCAAATATGTATCCGCTCATGAATTAATTCTTAGAAAAAC
TCATCGAGCATCAAATGAAACTGCAATTTATTCATATCAGGATTATCAATACCATAT
TTTTGAAAAAGCCGTTTCTGTAATGAAGGAGAAAACTCACCGAGGCAGTTCCATAG
GATGGCAAGATCCTGGTATCGGTCTGCGATTCCGACTCGTCCAACATCAATACAAC
CTATTAATTTCCCCTCGTCAAAAATAAGGTTATCAAGTGAGAAATCACCATGAGTG
ACGACTGAATCCGGTGAGAATGGCAAAAGTTTATGCATTTCTTTCCAGACTTGTTCA
ACAGGCCAGCCATTACGCTCGTCATCAAAATCACTCGCATCAACCAAACCGTTATT
CATTCGTGATTGCGCCTGAGCGAGACGAAATACGCGATCGCTGTTAAAAGGACAAT
TACAAACAGGAATCGAATGCAACCGGCGCAGGAACACTGCCAGCGCATCAACAAT
ATTTTCACCTGAATCAGGATATTCTTCTAATACCTGGAATGCTGTTTTCCCGGGGAT
CGCAGTGGTGAGTAACCATGCATCATCAGGAGTACGGATAAAATGCTTGATGGTCG
GAAGAGGCATAAATTCCGTCAGCCAGTTTAGTCTGACCATCTCATCTGTAACATCAT
TGGCAACGCTACCTTTGCCATGTTTCAGAAACAACTCTGGCGCATCGGGCTTCCCAT
ACAATCGATAGATTGTCGCACCTGATTGCCCGACATTATCGCGAGCCCATTTATACC
CATATAAATCAGCATCCATGTTGGAATTTAATCGCGGCCTAGAGCAAGACGTTTCC
CGTTGAATATGGCTCATAACACCCCTTGTATTACTGTTTATGTAAGCAGACAGTTTT
ATTGTTCATGACCAAAATCCCTTAACGTGAGTTTTCGTTCCACTGAGCGTCAGACCC
CGTAGAAAAGATCAAAGGATCTTCTTGAGATCCTTTTTTTCTGCGCGTAATCTGCTG
CTTGCAAACAAAAAAACCACCGCTACCAGCGGTGGTTTGTTTGCCGGATCAAGAGC
TACCAACTCTTTTTCCGAAGGTAACTGGCTTCAGCAGAGCGCAGATACCAAATACT

GTCCTTCTAGTGTAGCCGTAGTTAGGCCACCACTTCAAGAACTCTGTAGCACCGCCT
ACATACCTCGCTCTGCTAATCCTGTTACCAGTGGCTGCTGCCAGTGGCGATAAGTCG
TGTCTTACCGGGTTGGACTCAAGACGATAGTTACCGGATAAGGCGCAGCGGTCGGG
CTGAACGGGGGGTTCGTGCACACAGCCCAGCTTGGAGCGAACGACCTACACCGAA
CTGAGATACCTACAGCGTGAGCTATGAGAAAGCGCCACGCTTCCCGAAGGGAGAA
AGGCGGACAGGTATCCGGTAAGCGGCAGGGTCGGAACAGGAGAGCGCACGAGGG
AGCTTCCAGGGGGAAACGCCTGGTATCTTTATAGTCCTGTCGGGTTTCGCCACCTCT
GACTTGAGCGTCGATTTTTGTGATGCTCGTCAGGGGGGCGGAGCCTATGGAAAAAC
GCCAGCAACGCGGCCTTTTTACGGTTCCTGGCCTTTTGCTGGCCTTTTGCTCACATG
TTCTTTCCTGCGTTATCCCCTGATTCTGTGGATAACCGTATTACCGCCTTTGAGTGAG
CTGATACCGCTCGCCGCAGCCGAACGACCGAGCGCAGCGAGTCAGTGAGCGAGGA
AGCGGAAGAGCGCCTGATGCGGTATTTTCTCCTTACGCATCTGTGCGGTATTTCACA
CCGCATATATGGTGCACTCTCAGTACAATCTGCTCTGATGCCGCATAGTTAAGCCAG
TATACACTCCGCTATCGCTACGTGACTGGGTCATGGCTGCGCCCCGACACCCGCCA
ACACCCGCTGACGCGCCCTGACGGGCTTGTCTGCTCCCGGCATCCGCTTACAGACA
AGCTGTGACCGTCTCCGGGAGCTGCATGTGTCAGAGGTTTTCACCGTCATCACCGA
AACGCGCGAGGCAGCTGCGGTAAAGCTCATCAGCGTGGTCGTGAAGCGATTCACA
GATGTCTGCCTGTTCATCCGCGTCCAGCTCGTTGAGTTTCTCCAGAAGCGTTAATGT
CTGGCTTCTGATAAAGCGGGCCATGTTAAGGGCGGTTTTTTCCTGTTTGGTCACTGA
TGCCTCCGTGTAAGGGGGATTTCTGTTCATGGGGGTAATGATACCGATGAAACGAG
AGAGGATGCTCACGATACGGGTTACTGATGATGAACATGCCCGGTTACTGGAACGT
TGTGAGGGTAAACAACTGGCGGTATGGATGCGGCGGGACCAGAGAAAAATCACTC
AGGGTCAATGCCAGCGCTTCGTTAATACAGATGTAGGTGTTCCACAGGGTAGCCAG
CAGCATCCTGCGATGCAGATCCGGAACATAATGGTGCAGGGCGCTGACTTCCGCGT
TTCCAGACTTTACGAAACACGGAAACCGAAGACCATTCATGTTGTTGCTCAGGTCG
CAGACGTTTTGCAGCAGCAGTCGCTTCACGTTCGCTCGCGTATCGGTGATTCATTCT
GCTAACCAGTAAGGCAACCCCGCCAGCCTAGCCGGGTCCTCAACGACAGGAGCAC
GATCATGCGCACCCGTGGGGCCGCCATGCCGGCGATAATGGCCTGCTTCTCGCCGA
AACGTTTGGTGGCGGGACCAGTGACGAAGGCTTGAGCGAGGGCGTGCAAGATTCC
GAATACCGCAAGCGACAGGCCGATCATCGTCGCGCTCCAGCGAAAGCGGTCCTCGC
CGAAAATGACCCAGAGCGCTGCCGGCACCTGTCCTACGAGTTGCATGATAAAGAAG
ACAGTCATAAGTGCGGCGACGATAGTCATGCCCCGCGCCCACCGGAAGGAGCTGA
CTGGGTTGAAGGCTCTCAAGGGCATCGGTCGAGATCCCGGTGCCTAATGAGTGAGC
TAACTTACATTAATTGCGTTGCGCTCACTGCCCGCTTTCCAGTCGGGAAACCTGTCG
TGCCAGCTGCATTAATGAATCGGCCAACGCGCGGGGAGAGGCGGTTTGCGTATTGG
GCGCCAGGGTGGTTTTTCTTTTCACCAGTGAGACGGGCAACAGCTGATTGCCCTTCA
CCGCCTGGCCCTGAGAGAGTTGCAGCAAGCGGTCCACGCTGGTTTGCCCCAGCAGG
CGAAAATCCTGTTTGATGGTGGTTAACGGCGGGATATAACATGAGCTGTCTTCGGT
ATCGTCGTATCCCACTACCGAGATATCCGCACCAACGCGCAGCCCGGACTCGGTAA
TGGCGCGCATTGCGCCCAGCGCCATCTGATCGTTGGCAACCAGCATCGCAGTGGGA
ACGATGCCCTCATTCAGCATTTGCATGGTTTGTTGAAAACCGGACATGGCACTCCA
GTCGCCTTCCCGTTCCGCTATCGGCTGAATTTGATTGCGAGTGAGATATTTATGCCA
GCCAGCCAGACGCAGACGCGCCGAGACAGAACTTAATGGGCCCGCTAACAGCGCG
ATTTGCTGGTGACCCAATGCGACCAGATGCTCCACGCCCAGTCGCGTACCGTCTTCA
TGGGAGAAAATAATACTGTTGATGGGTGTCTGGTCAGAGACATCAAGAAATAACGC
CGGAACATTAGTGCAGGCAGCTTCCACAGCAATGGCATCCTGGTCATCCAGCGGAT
AGTTAATGATCAGCCCACTGACGCGTTGCGCGAGAAGATTGTGCACCGCCGCTTTA
CAGGCTTCGACGCCGCTTCGTTCTACCATCGACACCACCACGCTGGCACCCAGTTG
ATCGGCGCGAGATTTAATCGCCGCGACAATTTGCGACGGCGCGTGCAGGGCCAGAC

TGGAGGTGGCAACGCCAATCAGCAACGACTGTTTGCCCGCCAGTTGTTGTGCCACG
CGGTTGGGAATGTAATTCAGCTCCGCCATCGCCGCTTCCACTTTTTCCCGCGTTTTC
GCAGAAACGTGGCTGGCCTGGTTCACCACGCGGGAAACGGTCTGATAAGAGACAC
CGGCATACTCTGCGACATCGTATAACGTTACTGGTTTCACATTCACCACCCTGAATT
GACTCTCTTCCGGGCGCTATCATGCCATACCGCGAAAGGTTTTGCGCCATTCGATGG
TGTCCGGGATCTCGACGCTCTCCCTTATGCGACTCCTGCATTAGGAAGCAGCCCAGT
AGTAGGTTGAGGCCGTTGAGCACCGCCGCCGCAAGGAATGGTGCATGCAAGGAGA
TGGCGCCCAACAGTCCCCCGGCCACGGGGCCTGCCACCATACCCACGCCGAAACAA
GCGCTCATGAGCCCGAAGTGGCGAGCCCGATCTTCCCCATCGGTGATGTCGGCGAT
ATAGGCGCCAGCAACCGCACCTGTGGCGCCGGTGATGCCGGCCACGATGCGTCCGG
CGTAGAGGATCGAGATCTCGATCCCGCGAAATTAATACGACTCACTATAGGGGAAT
TGTGAGCGGATAACAATTCCCCTCTAGAAATAATTTTGTTTAACTTTAAGAAGGAG
ATATACATATGCACCATCATCATCATCATTCTTCTGGTACCGAGAACTTgtACTTCCA
ATCCATGACAAATCCTGGTgtATCCGCTTGGCAGGTCAACACAGCTTATACTGCGGG
ACAATTGGTCACATATAACGGCAAGACGTATAAATGTTTGCAGCCCCACACCTCCT
TGGCAGGATGGGAACCATCCAACGTTCCTGCCTTGTGGCAGCTTCAAGGTAACAAT
AACAACAACAATAACAATGGCAAACCACATATCGATAATTATCTTCACGATAAAGA
TAAAGATGAAAAGATTGAACAATATGATAAAAATGTAAAAGAACAGGCGAGTAAA
GATAAAAAGCAGCAAGCTAAACCTCAAATTCCGAAAGATAAATCGAAAGTGGCAG
GCTATATTGAAATTCCAGATGCTGATATTAAAGAACCAGTATATCCAGGACCAGCA
ACACCTGAACAATTAAATAGAGGTGTAAGCTTTGCAGAAGAAAATGAATCACTAG
ATGATCAAAATATTTCAATTGCAGGACACACTTTCATTGACCGTCCGAACTATCAAT
TTACAAATCTTAAAGCAGCCAAAAAAGGTAGTATGGTGTACTTTAAAGTTGGTAAT
GAAACACGTAAGTATAAAATGACAAGTATAAGAGATGTTAAGCCTACAGATGTAG
GAGTTCTAGATGAACAAAAAGGTAAAGATAAACAATTAACATTAATTACTTGTGAT
GATTACAATGAAnAGACAGGCGTTTGGGAAAAACGTAAAATCTTTGTAGCTACAGA
AGTCAAATAACAGTAAAGGTGGATACGGATCCGAATTCGAGCTCCGTCGACAAGCT
TGCGGCCGCACTCGAGCACCACCACCACCACCACTGAGATCCGGCTGCTAACAAAG
CCCGAAAGGAAGCTGAGTTGGCTGCTGCCACCGCTGAGCAATAACTAGCATAACCC
CTTGGGGCCTCTAAACGGGTCTTGAGGGGTTTTTTGCTGAAAGGAGGAACTATATC
CGGAT

8.2.4. pMAL-c5x (containing TEV protease)

The pMAL-c5x plasmid containing TEV protease was provided by D. Williamson (University of Leeds), derived from the pMAL-c5x plasmid available from NEB. This plasmid was used to express MBP-TEV protease. MBP-TEV protease is shown with red text and the BamHI and PstI restriction sites used for sub-cloning by yellow and green highlighting, respectively.

CCGACACCATCGAATGGTGCAAAACCTTTCGCGGTATGGCATGATAGCGCCCGGAA
GAGAGTCAATTCAGGGTGGTGAATGTGAAACCAGTAACGTTATACGATGTCGCAGA
GTATGCCGGTGTCTCTTATCAGACCGTTTCCCGCGTGGTGAACCAGGCCAGCCACGT
TTCTGCGAAAACGCGGGAAAAAGTGGAAGCGGCGATGGCGGAGCTGAATTACATT
CCCAACCGCGTGGCACAACAACTGGCGGGCAAACAGTCGTTGCTGATTGGCGTTGC
CACCTCCAGTCTGGCCCTGCACGCGCCGTCGCAAATTGTCGCGGCGATTAAATCTC
GCGCCGATCAACTGGGTGCCAGCGTGGTGGTGTCGATGGTAGAACGAAGCGGCGTC
GAAGCCTGTAAAGCGGCGGTGCACAATCTTCTCGCGCAACGCGTCAGTGGGCTGAT
CATTAACTATCCGCTGGATGACCAGGATGCCATTGCTGTGGAAGCTGCCTGCACTA

ATGTTCCGGCGTTATTTCTTGATGTCTCTGACCAGACACCCATCAACAGTATTATTT
TCTCCCATGAAGACGGTACGCGACTGGGCGTGGAGCATCTGGTCGCATTGGGTCAC
CAGCAAATCGCGCTGTTAGCGGGCCCATTAAGTTCTGTCTCGGCGCGTCTGCGTCTG
GCTGGCTGGCATAAATATCTCACTCGCAATCAAATTCAGCCGATAGCGGAACGGGA
AGGCGACTGGAGTGCCATGTCCGGTTTTCAACAAACCATGCAAATGCTGAATGAGG
GCATCGTTCCCACTGCGATGCTGGTTGCCAACGATCAGATGGCGCTGGGCGCAATG
CGCGCCATTACCGAGTCCGGGCTGCGCGTTGGTGCGGATATTTCGGTAGTGGGATA
CGACGATACCGAAGACAGCTCATGTTATATCCCGCCGTTAACCACCATCAAACAGG
ATTTTCGCCTGCTGGGGCAAACCAGCGTGGACCGCTTGCTGCAACTCTCTCAGGGC
CAGGCGGTGAAGGGCAATCAGCTGTTGCCCGTCTCACTGGTGAAAAGAAAAACCA
CCCTGGCGCCCAATACGCAAACCGCCTCTCCCCGCGCGTTGGCCGATTCATTAATGC
AGCTGGCACGACAGGTTTCCCGACTGGAAAGCGGGCAGTGAGCGCAACGCAATTA
ATGTAAGTTAGCTCACTCATTAGGCACAATTCTCATGTTTGACAGCTTATCATCGAC
TGCACGGTGCACCAATGCTTCTGGCGTCAGGCAGCCATCGGAAGCTGTGGTATGGC
TGTGCAGGTCGTAAATCACTGCATAATTCGTGTCGCTCAAGGCGCACTCCCGTTCTG
GATAATGTTTTTTGCGCCGACATCATAACGGTTCTGGCAAATATTCTGAAATGAGCT
GTTGACAATTAATCATCGGCTCGTATAATGTGTGGAATTGTGAGCGGATAACAATT
TCACACAGGAAACAGCCAGTCCGTTTAGGTGTTTTCACGAGCAATTGACCAACAAG
GACCATAGATTATGAAAATCGAAGAAGGTAAACTGGTAATCTGGATTAACGGCGAT
AAAGGCTATAACGGTCTCGCTGAAGTCGGTAAGAAATTCGAGAAAGATACCGGAA
TTAAAGTCACCGTTGAGCATCCGGATAAACTGGAAGAGAAATTCCCACAGGTTGCG
GCAACTGGCGATGGCCCTGACATTATCTTCTGGGCACACGACCGCTTTGGTGGCTA
CGCTCAATCTGGCCTGTTGGCTGAAATCACCCCGGACAAAGCGTTCCAGGACAAGC
TGTATCCGTTTACCTGGGATGCCGTACGTTACAACGGCAAGCTGATTGCTTACCCGA
TCGCTGTTGAAGCGTTATCGCTGATTTATAACAAAGATCTGCTGCCGAACCCGCCA
AAAACCTGGGAAGAGATCCCGGCGCTGGATAAAGAACTGAAAGCGAAAGGTAAGA
GCGCGCTGATGTTCAACCTGCAAGAACCGTACTTCACCTGGCCGCTGATTGCTGCTG
ACGGGGGTTATGCGTTCAAGTATGAAAACGGCAAGTACGACATTAAAGACGTGGG
CGTGGATAACGCTGGCGCGAAAGCGGGTCTGACCTTCCTGGTTGACCTGATTAAAA
ACAAACACATGAATGCAGACACCGATTACTCCATCGCAGAAGCTGCCTTTAATAAA
GGCGAAACAGCGATGACCATCAACGGCCCGTGGGCATGGTCCAACATCGACACCA
GCAAAGTGAATTATGGTGTAACGGTACTGCCGACCTTCAAGGGTCAACCATCCAAA
CCGTTCGTTGGCGTGCTGAGCGCAGGTATTAACGCCGCCAGTCCGAACAAAGAGCT
GGCAAAAGAGTTCCTCGAAAACTATCTGCTGACTGATGAAGGTCTGGAAGCGGTTA
ATAAAGACAAACCGCTGGGTGCCGTAGCGCTGAAGTCTTACGAGGAAGAGTTGGT
GAAAGATCCGCGTATTGCCGCCACTATGGAAAACGCCCAGAAAGGTGAAATCATG
CCGAACATCCCGCAGATGTCCGCTTTCTGGTATGCCGTGCGTACTGCGGTGATCAAC
GCCGCCAGCGGTCGTCAGACTGTCGATGAAGCCCTGAAAGACGCGCAGACTAATTC
GAGCTCGAACAACAACAACAATAACAATAACAACAACCTCGGGATCGAGGGAAGG
ATTTCACATATGTCCATGGGCGGCCGCGATATCGTCGACGGATCCGGAAAAAGCTT
GTTTAAGGGGCCGCGTGATTACAACCCGATATCGAGCACCATTTGTCATTTGACGA
ATGAATCTGATGGGCACACAACATCGTTGTATGGTATTGGATTTGGTCCCTTCATCA
TTACAAACAAGCACTTGTTTAGAAGAAATAATGGAACACTGTTGGTCCAATCACTA
CATGGTGTATTCAAGGTCAAGAACACCACGACTTTGCAACAACACCTCATTGATGG
GAGGGACATGATAATTATTCGCATGCCTAAGGATTTCCCACCATTTCCTCAAAAGCT
GAAATTTAGAGAGCCACAAAGGGAAGAACGCATATGTCTTGTTACAACCAACTTCC
AAACTAAGAGCATGTCTAGCATGGTGTCAGACACTAGTTGCACATTCCCTTCATCTG
ATGGCATATTCTGGAAGCATTGGATTCAAACCAAGGATGGGCAGTGTGGCAGTCCA
TTAGTATCAACTAGAGATGGGTTCATTGTTGGTATACACTCAGCATCGAATTTCACC

AACACAAACAATTATTTCACAAGCGTGCCGAAAAACTTCATGGAATTGTTGACAAA
TCAGGAGGCGCAGCAGTGGGTTAGTGGTTGGCGATTAAATGCTGACTCAGTATTGT
GGGGGGGCCATAAAGTTTTCATGCCGAAACCTGAAGAGCCTTTTCAGCCAGTTAAG
GAAGCGACTCAACTCATGAATCGTCGTCGCCGTCGCTAATAAGGACTGCAGGTAAT
TAAATAAGCTTCAAATAAAACGAAAGGCTCAGTCGAAAGACTGGGCCTTTCGTTTT
ATCTGTTGTTTGTCGGTGAACGCTCTCCTGAGTAGGACAAATCCGCCGGGAGCGGA
TTTGAACGTTGCGAAGCAACGGCCCGGAGGGTGGCGGGCAGGACGCCCGCCATAA
ACTGCCAGGCATCAAATTAAGCAGAAGGCCATCCTGACGGATGGCCTTTTTGCGTT
TCTACAAACTCTTTCGGTCCGTTGTTTATTTTTCTAAATACATTCAAATATGTATCCG
CTCATGAGACAATAACCCTGATAAATGCTTCAATAATATTGAAAAAGGAAGAGTAT
GAGTATTCAACATTTCCGTGTCGCCCTTATTCCCTTTTTTGCGGCATTTTGCCTTCCT
GTTTTTGCTCACCCAGAAACGCTGGTGAAAGTAAAAGATGCTGAAGATCAGTTGGG
TGCACGAGTGGGTTACATCGAACTGGATCTCAACAGCGGTAAGATCCTTGAGAGTT
TTCGCCCCGAAGAACGTTTCCCAATGATGAGCACTTTTAAAGTTCTGCTATGTGGCG
CGGTATTATCCCGTGTTGACGCCGGGCAAGAGCAACTCGGTCGCCGCATACACTAT
TCTCAGAATGACTTGGTTGAGTACTCACCAGTCACAGAAAAGCATCTTACGGATGG
CATGACAGTAAGAGAATTATGCAGTGCTGCCATAACCATGAGTGATAACACTGCGG
CCAACTTACTTCTGACAACGATCGGAGGACCGAAGGAGCTAACCGCTTTTTTGCAC
AACATGGGGGATCATGTAACTCGCCTTGATCGTTGGGAACCGGAGCTGAATGAAGC
CATACCAAACGACGAGCGTGACACCACGATGCCTGTAGCAATGGCAACAACGTTGC
GCAAACTATTAACTGGCGAACTACTTACTCTAGCTTCCCGGCAACAATTAATAGAC
TGGATGGAGGCGGATAAAGTTGCAGGACCACTTCTGCGCTCGGCCCTTCCGGCTGG
CTGGTTTATTGCTGATAAATCTGGAGCCGGTGAGCGTGGGTCTCGCGGTATCATTGC
AGCACTGGGGCCAGATGGTAAGCCCTCCCGTATCGTAGTTATCTACACGACGGGGA
GTCAGGCAACTATGGATGAACGAAATAGACAGATCGCTGAGATAGGTGCCTCACTG
ATTAAGCATTGGTAACTGTCAGACCAAGTTTACTCATATATACTTTAGATTGATTTC
CTTAGGACTGAGCGTCAACCCCGTAGAAAAGATCAAAGGATCTTCTTGAGATCCTT
TTTTTCTGCGCGTAATCTGCTGCTTGCAAACAAAAAAACCACCGCTACCAGCGGTG
GTTTGTTTGCCGGATCAAGAGCTACCAACTCTTTTTCCGAAGGTAACTGGCTTCAGC
AGAGCGCAGATACCAAATACTGTCCTTCTAGTGTAGCCGTAGTTAGGCCACCACTT
CAAGAACTCTGTAGCACCGCCTACATACCTCGCTCTGCTAATCCTGTTACCAGTGGC
TGCTGCCAGTGGCGATAAGTCGTGTCTTACCGGGTTGGACTCAAGACGATAGTTAC
CGGATAAGGCGCAGCGGTCGGGCTGAACGGGGGGTTCGTGCACACAGCCCAGCTT
GGAGCGAACGACCTACACCGAACTGAGATACCTACAGCGTGAGCTATGAGAAAGC
GCCACGCTTCCCGAAGGGAGAAAGGCGGACAGGTATCCGGTAAGCGGCAGGGTCG
GAACAGGAGAGCGCACGAGGGAGCTTCCAGGGGGAAACGCCTGGTATCTTTATAG
TCCTGTCGGGTTTCGCCACCTCTGACTTGAGCGTCGATTTTTGTGATGCTCGTCAGG
GGGGCGGAGCCTATGGAAAAACGCCAGCAACGCGGCCTTTTTACGGTTCCTGGCCT
TTTGCTGGCCTTTTGCTCACATGTTCTTTCCTGCGTTATCCCCTGATTCTGTGGATAA
CCGTATTACCGCCTTTGAGTGAGCTGATACCGCTCGCCGCAGCCGAACGACCGAGC
GCAGCGAGTCAGTGAGCGAGGAAGCGGAAGAGCGCCTGATGCGGTATTTTCTCCTT
ACGCATCTGTGCGGTATTTCACACCGCATATAAGGTGCACTGTGACTGGGTCATGG
CTGCGCCCCGACACCCGCCAACACCCGCTGACGCGCCCTGACGGGCTTGTCTGCTC
CCGGCATCCGCTTACAGACAAGCTGTGACCGTCTCCGGGAGCTGCATGTGTCAGAG
GTTTTCACCGTCATCACCGAAACGCGCGAGGCAGCTGCGGTAAAGCTCATCAGCGT
GGTCGTGCAGCGATTCACAGATGTCTGCCTGTTCATCCGCGTCCAGCTCGTTGAGTT
TCTCCAGAAGCGTTAATGTCTGGCTTCTGATAAAGCGGGCCATGTTAAGGGCGGTT
TTTTCCTGTTTGGTCACTGATGCCTCCGTGTAAGGGGGATTTCTGTTCATGGGGGTA
ATGATACCGATGAAACGAGAGAGGATGCTCACGATACGGGTTACTGATGATGAAC

ATGCCCGGTTACTGGAACGTTGTGAGGGTAAACAACTGGCGGTATGGATGCGGCGG
GACCAGAGAAAAATCACTCAGGGTCAATGCCAGCGCTTCGTTAATACAGATGTAGG
TGTTCCACAGGGTAGCCAGCAGCATCCTGCGATGCAGATCCGGAACATAATGGTGC
AGGGCGCTGACTTCCGCGTTTCCAGACTTTACGAAACACGGAAACCGAAGACCATT
CATGTTGTTGCTCAGGTCGCAGACGTTTTGCAGCAGCAGTCGCTTCACGTTCGCTCG
CGTATCGGTGATTCATTCTGCTAACCAGTAAGGCAACCCCGCCAGCCTAGCCGGGT
CCTCAACGACAGGAGCACGATCATGCGCACCCGTGGCCAGGACCCAACGCTGCCCG
AAATT

8.3. Protein sequences

All DNA sequences are given in the 5′ – 3′ direction, beginning with the 5′ restriction site and ending with the 3′ restriction site. The coding sequence for the protein is shown with red text. All amino acid sequences are given in the N-terminal – C-terminal direction, showing the expressed protein sequence.

8.3.1. GGG-CTB

8.3.1.1. DNA insert sequence

GCATGCAGGAGGTGGCACTCCTCAAAATATTACTGATTTGTGCGCAGAATACCACA
ACACACAAATATATACGCTAAATGATAAGATCTTTTCGTATACAGAATCGCTAGCG
GGAAAAAGAGAGATGGCTATCATTACTTTTAAGAATGGTGCAATTTTTCAAGTAGA
GGTACCAGGTAGTCAACATATAGATTCACAAAAAAAAAGCGATTGAAAGGATGAAG
GATACCCTGAGGATTGCATATCTTACTGAAGCTAAAGTCGAAAAGTTATGTGTATG
GAATAATAAAACGCCTCATGCGATCGCCGCAATTAGTATGGCAAACTAAGTTTTCC
CTGCAG

8.3.1.2. Expressed amino acid sequence

GGGTPQNITDLCAEYHNTQIYTLNDKIFSYTESLAGKREMAIITFKNGAIFQVEVPGSQHI
DSQKKAIERMKDTLRIAYLTEAKVEKLCVWNNKTPQAIAAISMAN

8.3.2. CTB-KDEL

8.3.2.1. DNA insert sequence

GCATGCAGGAGGTGGCACTCCTCAAAATATTACTGATTTGTGCGCAGAATACCACA
ACACACAAATATATACGCTAAATGATAAGATCTTTTCGTATACAGAATCGCTAGCG
GGAAAAAGAGAGATGGCTATCATTACTTTTAAGAATGGTGCAATTTTTCAAGTAGA
GGTACCAGGTAGTCAACATATAGATTCACAAAAAAAAAGCGATTGAAAGGATGAAG
GATACCCTGAGGATTGCATATCTTACTGAAGCTAAAGTCGAAAAGTTATGTGTATG
GAATAATAAAACGCCTCATGCGATCGCCGCAATTAGTATGGCAAACAAAGATGAA
CTGTAAGTTTTCCCTGCAG

8.3.2.2. Expressed amino acid sequence

GGGTPQNITDLCAEYHNTQIYTLNDKIFSYTESLAGKREMAIITFKNGAIFQVEVPGSQHI
DSQKKAIERMKDTLRIAYLTEAKVEKLCVWNNKTPHAIAAISMANKDEL

8.3.3. CTB(K43C)

8.3.3.1. DNA insert sequence

GCATGCAGGAGGTGGCACTCCTCAAAATATTACTGATTTGTGCGCAGAATACCACA
ACACACAAATATATACGCTAAATGATAAGATCTTTTCGTATACAGAATCGCTAGCG
GGAAAAAGAGAGATGGCTATCATTACTTTTTGCAATGGTGCAATTTTTCAAGTAGA
GGTACCAGGTAGTCAACATATAGATTCACAAAAAAAGGCAATCGAACGTATGAAG
GATACCCTGAGGATTGCATATCTTACTGAAGCTAAAGTCGAAAAGTTATGTGTATG
GAATAATAAAACGCCTCATGCGATCGCCGCAATTAGTATGGCAAACAAAGATGAA
CTGTAAGTTTTCCCTGCAG

8.3.3.2. Expressed amino acid sequence

GGGTPQNITDLCAEYHNTQIYTLNDKIFSYTESLAGKREMAIITFCNGAIFQVEVPGSQHI
DSQKKAIERMKDTLRIAYLTEAKVEKLCVWNNKTPHAIAAISMANKDEL

8.3.4. CTB(S55C)

8.3.4.1. DNA insert sequence

GCATGCAGGAGGTGGCACTCCTCAAAATATTACTGATTTGTGCGCAGAATACCACA
ACACACAAATATATACGCTAAATGATAAGATCTTTTCGTATACAGAATCGCTAGCG
GGAAAAAGAGAGATGGCTATCATTACTTTTAAGAATGGTGCAATTTTTCAAGTAGA
GGTACCAGGTTGCCAACATATAGATTCACAAAAAAAGGCAATCGAACGTATGAAG
GATACCCTGAGGATTGCATATCTTACTGAAGCTAAAGTCGAAAAGTTATGTGTATG
GAATAATAAAACGCCTCATGCGATCGCCGCAATTAGTATGGCAAACAAAGATGAA
CTGTAAGTTTTCCCTGCAG

8.3.4.2. Expressed amino acid sequence

GGGTPQNITDLCAEYHNTQIYTLNDKIFSYTESLAGKREMAIITFKNGAIFQVEVPGCQH
IDSQKKAIERMKDTLRIAYLTEAKVEKLCVWNNKTPHAIAAISMANKDEL

8.3.5. CTB-PkC11

8.3.5.1. DNA insert sequence

GCATGCAGGAGGTGGCACTCCTCAAAATATTACTGATTTGTGCGCAGAATACCACA
ACACACAAATATATACGCTAAATGATAAGATCTTTTCGTATACAGAATCGCTAGCG
GGAAAAAGAGAGATGGCTATCATTACTTTTAAGAATGGTGCAATTTTTCAAGTAGA
GGTACCAGGTAGTCAACATATAGATTCACAAAAAAAGGCAATCGAACGTATGAAG
GATACCCTGAGGATTGCATATCTTACTGAAGCTAAAGTCGAAAAGTTATGTGTATG
GAATAATAAAACGCCTCATGCGATCGCCGCAATTAGTATGGCAAACGGAAAGCCG
ATCCCAAACCCTTTGCTGGGATGCGACTCCACCTAAGTTTTCCCTGCAG

8.3.5.2. Expressed amino acid sequence

GGGTPQNITDLCAEYHNTQIYTLNDKIFSYTESLAGKREMAIITFKNGAIFQVEVPGSQHI
DSQKKAIERMKDTLRIAYLTEAKVEKLCVWNNKTPHAIAAISMANGKPIPNPLLGCDST

8.3.6. CTB-CKDEL

8.3.6.1. DNA insert sequence

GCATGCAGGAGGTGGCACTCCTCAAAATATTACTGATTTGTGCGCAGAATACCACA
ACACACAAATATATACGCTAAATGATAAGATCTTTTCGTATACAGAATCGCTAGCG
GGAAAAAGAGAGATGGCTATCATTACTTTTAAGAATGGTGCAATTTTTCAAGTAGA
GGTACCAGGTAGTCAACATATAGATTCACAAAAAAAGGCAATCGAACGTATGAAG
GATACCCTGAGGATTGCATATCTTACTGAAGCTAAAGTCGAAAAGTTATGTGTATG
GAATAATAAAACGCCTCATGCGATCGCCGCAATTAGTATGGCAAACAACGGCGGG
AACTGCAACGGCGGCAATAAAGATGAACTGTAAGTTTTCCCTGCAG

8.3.6.2. Expressed amino acid sequence

GGGTPQNITDLCAEYHNTQIYTLNDKIFSYTESLAGKREMAIITFKNGAIFQVEVPGSQHI
DSQKKAIERMKDTLRIAYLTEAKVEKLCVWNNKTPHAIAAISMANNGSGNCNGSGNK
DEL

8.3.7. Apep-CTB

8.3.7.1. DNA insert sequence

GCATGCAGGAGGTGGCGCACCGCCGGGTTGTGGGAATGCTCCAAGATCATCGGAA
AACCTGTACTTTCAGAGCATGAGTAATACTTGCGATGAAAAAACCGGAGGTGGCGC
TCCTCAAAATATTACTGATTTGTGCGCAGAATACCACAACACACAAATATATACGC
TAAATGATAAGATCTTTTCGTATACAGAATCGCTAGCGGGAAAAAGAGAGATGGCT
ATCATTACTTTTAAGAATGGTGCAATTTTTCAAGTAGAGGTACCAGGTAGTCAACAT
ATAGATTCACAAAAAAAAGCGATTGAAAGGATGAAGGATACCCTGAGGATTGCAT
ATCTTACTGAAGCTAAAGTCGAAAAGTTATGTGTATGGAATAATAAAACGCCTCAT
GCGATCGCCGCAATTAGTATGGCAAACAAAGATGAACTGTAAGTTTTCCCTGCAG

8.3.7.2. Expressed amino acid sequence

GGGAPPGCGNAPRSSENLYFQSMSNTCDEKTGGGAPQNITDLCAEYHNTQIYTLNDKIF
SYTESLAGKREMAIITFKNGAIFQVEVPGSQHIDSQKKAIERMKDTLRIAYLTEAKVEKL
CVWNNKTPHAIAAISMANKDEL

8.3.8. CTB-Apep

8.3.8.1. DNA insert sequence

GCATGCAACTCCTCAAAATATTACTGATTTGTGCGCAGAATACCACAACACACAAA
TATATACGCTAAATGATAAGATCTTTTCGTATACAGAATCGCTAGCGGGAAAAAGA
GAGATGGCTATCATTACTTTTAAGAATGGTGCAATTTTTCAAGTAGAGGTACCAGG
TAGTCAACATATAGATTCACAAAAAAAGGCAATCGAACGTATGAAGGATACCCTG
AGGATTGCATATCTTACTGAAGCTAAAGTCGAAAAGTTATGTGTATGGAATAATAA
AACGCCTCATGCGATCGCCGCAATTAGTATGGCAAACAATGGCGGTAACGCACCGC
CGGGTTGTGGGAATGCTCCAAGATCATCGGAAAACCTGTACTTTCAGGGAGGTGGC
ATGAGTAATACTTGCGATGAAAAAACCTAAGTTTTCCCTGCAG

8.3.8.2. Expressed amino acid sequence

TPQNITDLCAEYHNTQIYTLNDKIFSYTESLAGKREMAIITFKNGAIFQVEVPGSQHIDSQ
KKAIERMKDTLRIAYLTEAKVEKLCVWNNKTPHAIAAISMANNGGNAPPGCGNAPRSS
ENLYFQGGGMSNTCDEKT

8.3.9. SrtA-His_6

8.3.9.1. DNA insert sequence

CATATGAAACCACATATCGATAATTATCTTCACGATAAAGATAAAGATGAAAAGAT
TGAACAATATGATAAAAATGTAAAAGAACAGGCGAGTAAAGATAAAAAGCAGCAA
GCTAAACCTCAAATTCCGAAAGATAAATCGAAAGTGGCAGGCTATATTGAAATTCC
AGATGCTGATATTAAAGAACCAGTATATCCAGGACCAGCAACACCTGAACAATTAA
ATAGAGGTGTAAGCTTTGCAGAAGAAAATGAATCACTAGATGATCAAAATATTTCA
ATTGCAGGACACACTTTCATTGACCGTCCGAACTATCAATTTACAAATCTTAAAGCA
GCCAAAAAAGGTAGTATGGTGTACTTTAAAGTTGGTAATGAAACACGTAAGTATAA
AATGACAAGTATAAGAGATGTTAAGCCTACAGATGTAGGAGTTCTAGATGAACAA
AAAGGTAAAGATAAACAATTAACATTAATTACTTGTGATGATTACAATGAAAAGAC
AGGCGTTTGGGAAAAACGTAAAATCTTTGTAGCTACAGAAGTCAAATAATCGAATT
C

8.3.9.2. Expressed amino acid sequence

GSSHHHHHHSSGLVPRGSHMKPHIDNYLHDKDKDEKIEQYDKNVKEQASKDKKQQAK
PQIPKDKSKVAGYIEIPDADIKEPVYPGPATPEQLNRGVSFAEENESLDDQNISIAGHTFI
DRPNYQFTNLKAAKKGSMVYFKVGNETRKYKMTSIRDVKPTDVGVLDEQKGKDKQL
TLITCDDYNEKTGVWEKRKIFVATEVK

8.3.10. SrtA-CBD

8.3.10.1. DNA insert sequence

CATATGCACCATCATCATCATCATTCTTCTGGTACCGAGAACTTGTACTTCCAATCC
ATGACAAATCCTGGTGTATCCGCTTGGCAGGTCAACACAGCTTATACTGCGGGACA
ATTGGTCACATATAACGGCAAGACGTATAAATGTTTGCAGCCCCACACCTCCTTGG
CAGGATGGGAACCATCCAACGTTCCTGCCTTGTGGCAGCTTCAAGGTAACAATAAC
AACAACAATAACAATGGCAAACCACATATCGATAATTATCTTCACGATAAAGATAA
AGATGAAAAGATTGAACAATATGATAAAAATGTAAAAGAACAGGCGAGTAAAGAT
AAAAAGCAGCAAGCTAAACCTCAAATTCCGAAAGATAAATCGAAAGTGGCAGGCT
ATATTGAAATTCCAGATGCTGATATTAAAGAACCAGTATATCCAGGACCAGCAACA
CCTGAACAATTAAATAGAGGTGTAAGCTTTGCAGAAGAAAATGAATCACTAGATGA
TCAAAATATTTCAATTGCAGGACACACTTTCATTGACCGTCCGAACTATCAATTTAC
AAATCTTAAAGCAGCCAAAAAAGGTAGTATGGTGTACTTTAAAGTTGGTAATGAAA
CACGTAAGTATAAAATGACAAGTATAAGAGATGTTAAGCCTACAGATGTAGGAGTT
CTAGATGAACAAAAAGGTAAAGATAAACAATTAACATTAATTACTTGTGATGATTA
CAATGAAAAGACAGGCGTTTGGGAAAAACGTAAAATCTTTGTAGCTACAGAAGTC
AAATAACAGTAAAGGTGGATACGGATCC

8.3.10.2. Expressed amino acid sequence

MHHHHHHSSGTENLYFQSMTNPGVSAWQVNTAYTAGQLVTYNGKTYKCLQPHTSLA
GWEPSNVPALWQLQGNNNNNNNNGKPHIDNYLHDKDKDEKIEQYDKNVKEQASKDK
KQQAKPQIPKDKSKVAGYIEIPDADIKEPVYPGPATPEQLNRGVSFAEENESLDDQNISI
AGHTFIDRPNYQFTNLKAAKKGSMVYFKVGNETRKYKMTSIRDVKPTDVGVLDEQKG
KDKQLTLITCDDYNEKTGVWEKRKIFVATEVK

8.3.11. MBP-TEV protease

8.3.11.1. DNA insert sequence

GGATCCGGAAAAAGCTTGTTTAAGGGGCCGCGTGATTACAACCCGATATCG
AGCACCATTTGTCATTTGACGAATGAATCTGATGGGCACACAACATCGTTGT
ATGGTATTGGATTTGGTCCCTTCATCATTACAAACAAGCACTTGTTTAGAAG
AAATAATGGAACACTGTTGGTCCAATCACTACATGGTGTATTCAAGGTCAA
GAACACCACGACTTTGCAACAACACCTCATTGATGGGAGGGACATGATAAT
TATTCGCATGCCTAAGGATTTCCCACCATTTCCTCAAAAGCTGAAATTTAGA
GAGCCACAAAGGGAAGAACGCATATGTCTTGTTACAACCAACTTCCAAACT
AAGAGCATGTCTAGCATGGTGTCAGACACTAGTTGCACATTCCCTTCATCTG
ATGGCATATTCTGGAAGCATTGGATTCAAACCAAGGATGGGCAGTGTGGCA
GTCCATTAGTATCAACTAGAGATGGGTTCATTGTTGGTATACACTCAGCATC
GAATTTCACCAACACAAACAATTATTTCACAAGCGTGCCGAAAAACTTCAT
GGAATTGTTGACAAATCAGGAGGCGCAGCAGTGGGTTAGTGGTTGGCGATT
AAATGCTGACTCAGTATTGTGGGGGGGCCATAAAGTTTTCATGCCGAAACC
TGAAGAGCCTTTTCAGCCAGTTAAGGAAGCGACTCAACTCATGAATCGTCG
TCGCCGTCGCTAATAAGGACTGCAG

8.3.11.2. Expressed amino acid sequence

MKIEEGKLVIWINGDKGYNGLAEVGKKFEKDTGIKVTVEHPDKLEEKFPQVAA
TGDGPDIIFWAHDRFGGYAQSGLLAEITPDKAFQDKLYPFTWDAVRYNGKLIA
YPIAVEALSLIYNKDLLPNPPKTWEEIPALDKELKAKGKSALMFNLQEPYFTWP
LIAADGGYAFKYENGKYDIKDVGVDNAGAKAGLTFLVDLIKNKHMNADTDYS
IAEAAFNKGETAMTINGPWAWSNIDTSKVNYGVTVLPTFKGQPSKPFVGVLSA
GINAASPNKELAKEFLENYLLTDEGLEAVNKDKPLGAVALKSYEEELVKDPRIA
ATMENAQKGEIMPNIPQMSAFWYAVRTAVINAASGRQTVDEALKDAQTNSSS
NNNNNNNNNNLGIEGRISHMSMGGRDIVDGSGKSLFKGPRDYNPISSTICHLTN
ESDGHTTSLYGIGFGPFIITNKHLFRRNNGTLLVQSLHGVFKVKNTTTLQQHLID
GRDMIIIRMPKDFPPFPQKLKFREPQREERICLVTTNFQTKSMSSMVSDTSCTFPS
SDGIFWKHWIQTKDGQCGSPLVSTRDGFIVGIHSASNFTNTNNYFTSVPKNFME
LLTNQEAQQWVSGWRLNADSVLWGGHKVFMPKPEEPFQPVKEATQLMNRRR
RR

Chapter 9: Bibliography

1. O. Bagasra and K. R. Prilliman, *J. Mol. Histol.*, 2004, **35**, 545.
2. J. P. DeVincenzo, *Antivir. Ther.*, 2012, **17**, 213.
3. R. Kole, A. R. Krainer and S. Altman, *Nat. Rev. Drug Discov.*, 2012, **11**, 125.
4. K. Okamoto and Y. Murawaki, *Curr. Pharm. Biotechnol.*, 2012, **13**, 2235.
5. S. Rivera and F. Yuan, *Curr. Pharm. Biotechnol.*, 2012, **13**, 1279.
6. S. Duarte, G. Carle, H. Faneca, M. C. P. de Lima and V. Pierrefite-Carle, *Cancer Lett.*, 2012, **324**, 160.
7. C. X. Liu and N. Zhang, *Angiogenesis*, 2012, **15**, 521.
8. M. A. Firer and G. Gellerman, *J. Hematol. Oncol.*, 2012, **5**, 16.
9. J. Park, K. Singha, S. Son, J. Kim, R. Namgung, C. O. Yun and W. J. Kim, *Cancer Gene Ther.*, 2012, **19**, 741.
10. J. T. Schiffer, M. Aubert, N. D. Weber, E. Mintzer, D. Stone and K. R. Jerome, *J. Virol.*, 2012, **86**, 8920.
11. L. de Haan and T. R. Hirst, *Mol. Membr. Biol.*, 2004, **21**, 77.
12. J. Sanchez and J. Holmgren, *Indian J. Med. Res.*, 2011, **133**, 153.
13. N. L. B. Wernick, D. J. F. Chinnapen, J. A. Cho and W. I. Lencer, *Toxins*, 2010, **2**, 310.
14. S. N. De, *Nature*, 1959, **183**, 1533.
15. R. A. Finkelstein and J. J. LoSpalluto, *J. Exp. Med.*, 1969, **130**, 185.
16. I. Lonnroth and J. Holmgren, *J. Gen. Microbiol.*, 1973, **76**, 417.
17. J. Holmgren, I. Lonnroth and Svennerh.L, *Infect. Immun.*, 1973, **8**, 208.
18. E. A. Merritt, S. Sarfaty, F. Vandenakker, C. L'hoir, J. A. Martial and W. G. J. Hol, *Protein Sci.*, 1994, **3**, 166.
19. R. G. Zhang, M. L. Westbrook, E. M. Westbrook, D. L. Scott, Z. Otwinowski, P. R. Maulik, R. A. Reed and G. G. Shipley, *J. Mol. Biol.*, 1995, **251**, 550.
20. R. G. Zhang, D. L. Scott, M. L. Westbrook, S. Nance, B. D. Spangler, G. G. Shipley and E. M. Westbrook, *J. Mol. Biol.*, 1995, **251**, 563.
21. C. J. O'Neal, E. I. Amaya, M. G. Jobling, R. K. Holmes and W. G. J. Hol, *Biochemistry*, 2004, **43**, 3772.
22. E. A. Merritt, P. Kuhn, S. Sarfaty, J. L. Erbe, R. K. Holmes and W. G. J. Hol, *J. Mol. Biol.*, 1998, **282**, 1043.
23. W. I. Lencer, C. Constable, S. Moe, M. G. Jobling, H. M. Webb, S. Ruston, J. L. Madara, T. R. Hirst and R. K. Holmes, *J. Cell Biol.*, 1995, **131**, 951.
24. T. S. Galloway and S. Vanheyningen, *Biochem. J.*, 1987, **244**, 225.
25. J. K. Tinker, J. L. Erbe and R. K. Holmes, *Infect. Immun.*, 2005, **73**, 3627.
26. E. R. Green and J. Mecsas, *Microbiol. Spectr.*, 2016, **4**, VMBF.0012.2015.
27. T. R. Hirst, J. Sanchez, J. B. Kaper, S. J. S. Hardy and J. Holmgren, *Proc. Natl. Acad. Sci. U. S. A.*, 1984, **81**, 7752.
28. J. K. Tinker, J. L. Erbe, W. G. J. Hol and R. K. Holmes, *Infect. Immun.*, 2003, **71**, 4093.
29. M. G. Jobling and R. K. Holmes, *Mol. Microbiol.*, 1991, **5**, 1755.

30. S. J. S. Hardy, J. Holmgren, S. Johansson, J. Sanchez and T. R. Hirst, *Proc. Natl. Acad. Sci. U. S. A.*, 1988, **85**, 7109.
31. F. van den Akker, S. Sarfaty, E. M. Twiddy, T. D. Connell, R. K. Holmes and W. G. J. Hol, *Structure*, 1996, **4**, 665.
32. M. Sandkvist, L. O. Michel, L. P. Hough, V. M. Morales, M. Bagdasarian, M. Koomey and V. J. DiRita, *J. Bacteriol.*, 1997, **179**, 6994.
33. T. L. Johnson, J. Abendroth, W. G. J. Hol and M. Sandkvist, *FEMS Microbiol. Lett.*, 2006, **255**, 175.
34. K. V. Korotkov, M. Sandkvist and W. G. J. Hol, *Nat. Rev. Microbiol.*, 2012, **10**, 336.
35. S. L. Reichow, K. V. Korotkov, W. G. J. Hol and T. Gonen, *Nat. Struct. Mol. Biol.*, 2010, **17**, 1226.
36. J. J. Mekalanos, R. J. Collier and W. R. Romig, *J. Biol. Chem.*, 1979, **254**, 5855.
37. B. Tsai, C. Rodighiero, W. I. Lencer and T. A. Rapoport, *Cell*, 2001, **104**, 937.
38. W. B. Turnbull, B. L. Precious and S. W. Homans, *J. Am. Chem. Soc.*, 2004, **126**, 1047.
39. J. H. Seo, C. S. Kim and H. J. Cha, *Analyst*, 2013, **138**, 6924.
40. E. A. Merritt, T. K. Sixma, K. H. Kalk, B. A. M. Vanzanten and W. G. J. Hol, *Mol. Microbiol.*, 1994, **13**, 745.
41. T. R. Branson, T. E. McAllister, J. Garcia-Hartjes, M. A. Fascione, J. F. Ross, S. L. Warriner, T. Wennekes, H. Zuilhof and W. B. Turnbull, *Angew. Chem. Int. Ed. (English)*, 2014, **53**, 8323.
42. Y. Fujinaga, A. A. Wolf, C. Rodighiero, H. Wheeler, B. Tsai, L. Allen, M. G. Jobling, T. Rapoport, R. K. Holmes and W. I. Lencer, *Mol. Biol. Cell*, 2003, **14**, 4783.
43. H. Pang, P. U. Le and I. R. Nabi, *J. Cell Sci.*, 2004, **117**, 1421.
44. W. I. Lencer and D. Saslowsky, *Biochim. Biophys. Acta*, 2005, **1746**, 314.
45. M. W.-L. Popp, R. A. Karssemeijer and H. L. Ploegh, *PLoS Pathog.*, 2012, **8**, e1002604.
46. A. A. Wolf, Y. Fujinaga and W. I. Lencer, *J. Biol. Chem.*, 2002, **277**, 16249.
47. G. H. Hansen, S. M. Dalskov, C. R. Rasmussen, L. Immerdal, L. L. Niels-Christiansen and E. M. Danielsen, *Biochemistry*, 2005, **44**, 873.
48. D. V. Broeck, A. R. Lagrou and M. J. S. De Wolf, *Acta Biochim. Pol.*, 2007, **54**, 757.
49. M. L. Torgersen, G. Skretting, B. van Deurs and K. Sandvig, *J. Cell Sci.*, 2001, **114**, 3737.
50. R. G. Parton, *J. Histochem. Cytochem.*, 1994, **42**, 155.
51. R. D. Singh, V. Puri, J. T. Valiyaveettil, D. L. Marks, R. Bittman and R. E. Pagano, *Mol. Biol. Cell*, 2003, **14**, 3254.
52. R. H. Massol, J. E. Larsen, Y. Fujinaga, W. I. Lencer and T. Kirchhausen, *Mol. Biol. Cell*, 2004, **15**, 3631.
53. M. Kirkham, A. Fujita, R. Chadda, S. J. Nixon, T. V. Kurzchalia, D. K. Sharma, R. E. Pagano, J. F. Hancock, S. Mayor and R. G. Parton, *J. Cell Biol.*, 2005, **168**, 465.
54. O. O. Glebov, N. A. Bright and B. J. Nichols, *Nat. Cell Biol.*, 2006, **8**, 46.
55. R. Geiger, S. Luisoni, K. Johnsson, U. F. Greber and A. Helenius, *Traffic*, 2013, **14**, 36.
56. Y.-W. Liu, V. Lukiyanchuk and S. L. Schmid, *Traffic*, 2011, **12**, 1620.
57. E. Macia, M. Ehrlich, R. Massol, E. Boucrot, C. Brunner and T. Kirchhausen, *Dev. Cell*, 2006, **10**, 839.
58. A. A. Wolf, M. G. Jobling, D. E. Saslowsky, E. Kern, K. R. Drake, A. K. Kenworthy, R. K. Holmes and W. I. Lencer, *Infect. Immun.*, 2008, **76**, 1476.

59. M. G. Jobling, Z. J. Yang, W. R. Kam, W. I. Lencer and R. K. Holmes, *Mbio*, 2012, **3**, 9.
60. D. J. F. Chinnapen, W.-T. Hsieh, Y. M. te Welscher, D. E. Saslowsky, L. Kaoutzani, E. Brandsma, L. D'Auria, H. Park, J. S. Wagner, K. R. Drake, M. Kang, T. Benjamin, M. D. Ullman, C. E. Costello, A. K. Kenworthy, T. Baumgart, R. H. Massol and W. I. Lencer, *Dev. Cell*, 2012, **23**, 573.
61. K. Simons and R. Ehehalt, *J. Clin. Invest.*, 2002, **110**, 597.
62. H. Ewers, W. Roemer, A. E. Smith, K. Bacia, S. Dmitrieff, W. Chai, R. Mancini, J. Kartenbeck, V. Chambon, L. Berland, A. Oppenheim, G. Schwarzmann, T. Feizi, P. Schwille, P. Sens, A. Helenius and L. Johannes, *Nat. Cell Biol.*, 2010, **12**, 11.
63. M. G. Jobling, Z. Yang, W. R. Kam, W. I. Lencer and R. K. Holmes, *mBio*, 2012, **3**, e00401.
64. Y. Feng, A. P. Jadhav, C. Rodighiero, Y. Fujinaga, T. Kirchhausen and W. I. Lencer, *EMBO Rep.*, 2004, **5**, 596.
65. D. J. F. Chinnapen, H. Chinnapen, D. Saslowsky and W. I. Lencer, *FEMS Microbiol. Lett.*, 2007, **266**, 129.
66. G. Tai, L. Lu, T. L. Wang, B. L. Tang, B. Goud, L. Johannes and W. Hong, *Mol. Biol. Cell*, 2004, **15**, 4011.
67. M. Amessou, A. Fradagrada, T. Falguieres, J. M. Lord, D. C. Smith, L. M. Roberts, C. Lamaze and L. Johannes, *J. Cell Sci.*, 2007, **120**, 1457.
68. P. Cosson and F. Letourneur, *Curr. Opin. Cell Biol.*, 1997, **9**, 484.
69. M. Stornaiuolo, L. V. Lotti, N. Borgese, M.-R. Torrisi, G. Mottola, G. Martire and S. Bonatti, *Mol. Biol. Cell*, 2003, **14**, 889.
70. I. Majoul, D. Ferrari and H.-D. Söling, *FEBS Lett.*, 1997, **401**, 104.
71. C. Hwang, A. J. Sinskey and H. F. Lodish, *Science*, 1992, **257**, 1496.
72. I. V. Majoul, P. I. H. Bastiaens and H. D. Soling, *J. Cell Biol.*, 1996, **133**, 777.
73. R. S. Ampapathi, A. L. Creath, D. I. Lou, J. W. Craft, Jr., S. R. Blanke and G. B. Legge, *J. Mol. Biol.*, 2008, **377**, 748.
74. A. H. Pande, P. Scaglione, M. Taylor, K. N. Nemec, S. Tuthill, D. Moe, R. K. Holmes, S. A. Tatulian and K. Teter, *J. Mol. Biol.*, 2007, **374**, 1114.
75. B. Hazes and R. J. Read, *Biochemistry*, 1997, **36**, 11051.
76. B. Tsai and T. A. Rapoport, *J. Cell Biol.*, 2002, **159**, 207.
77. A. Schmitz, H. Herrgen, A. Winkeler and V. Herzog, *J. Cell Biol.*, 2000, **148**, 1203.
78. B. Tsai, Y. H. Ye and T. A. Rapoport, *Nat. Rev. Mol. Cell Biol.*, 2002, **3**, 246.
79. N. L. B. Wernick, H. De Luca, W. R. Kam and W. I. Lencer, *J. Biol. Chem.*, 2010, **285**, 6145.
80. C. Rodighiero, B. Tsai, T. A. Rapoport and W. I. Lencer, *EMBO Rep.*, 2002, **3**, 1222.
81. C. J. O'Neal, M. G. Jobling, R. K. Holmes and W. G. J. Hol, *Science*, 2005, **309**.
82. C. P. Guimaraes, J. E. Carette, M. Varadarajan, J. Antos, M. W. Popp, E. Spooner, T. R. Brummelkamp and H. L. Ploegh, *J. Cell Biol.*, 2011, **195**, 751.
83. W. W. Navarre and O. Schneewind, *Mol. Microbiol.*, 1994, **14**, 115.
84. K. Bacia, I. V. Majoul and P. Schwille, *Biophys. J.*, 2002, **83**, 1184.
85. S. O. Hatic, J. A. McCann and W. D. Picking, *Anal. Biochem.*, 2001, **292**, 171.
86. M. G. Jobling and R. K. Holmes, *Infect. Immun.*, 1992, **60**, 4915.
87. M. T. Dertzbaugh, D. L. Peterson and F. L. Macrina, *Infect. Immun.*, 1990, **58**, 70.
88. M. T. Dertzbaugh and C. O. Elson, *Infect. Immun.*, 1993, **61**, 384.
89. Y. Yuki, C. Hara-Yakoyama, A. A. E. Guadiz, S. Udaka, H. Kiyono and S. Chatterjee, *Biotechnol. Bioeng.*, 2005, **92**, 803.

90. T. Arakawa, J. Yu, D. K. X. Chong, J. Hough, P. C. Engen and W. H. R. Langridge, *Nat. Biotechnol.*, 1998, **16**, 934.
91. Z. Gong, X. e. Long, L. Pan, Y. Le, Q. Liu, S. Wang, J. Guo, B. Xiao, M. Zhou and D. Mei, *Protein Expression Purif.*, 2009, **66**, 191.
92. S. Li, Z. Wei, J. Chen, Y. Chen, Z. Lv, W. Yu, Q. Meng and Y. Jin, *PLoS One*, 2014, **9**, e113585.
93. M. Sun, K. Qian, N. Su, H. Chang, J. Liu and G. Shen, *Biotechnol. Lett.*, 2003, **25**, 1087.
94. N. Olivera, C. E. Castuma, D. Hozbor, M. E. Gaillard, M. Rumbo and R. M. Gomez, *BioMed Res. Int.*, 2014, **2014**, 421486.
95. Y. Hiramatsu, M. Yamamoto, T. Satho, K. Irie, A. Kai, S. Uyeda, Y. Fukumitsu, A. Toda, T. Miyata, F. Miake, T. Arakawa and N. Kashige, *BMC Biotechnol.*, 2014, **14**, 1.
96. N. Schroeder, C.-S. Chung, C.-H. Chen, C.-L. Liao and W. Chang, *J. Virol.*, 2012, **86**, 4868.
97. W. L. Conte, H. Kamishina and R. L. Reep, *Nat. Protocols*, 2009, **4**, 1157.
98. C. Ren, M. Pu, Q. Cui and K.-F. So, *PLoS One*, 2014, **9**, e103306.
99. S. K. Chakraborty, J. A. J. Fitzpatrick, J. A. Phillippi, S. Andreko, A. S. Waggoner, M. P. Bruchez and B. Ballou, *Nano Lett.*, 2007, **7**, 2618.
100. N. Zhou, Z. Y. Hao, X. H. Zhao, S. Maharjan, S. J. Zhu, Y. B. Song, B. Yang and L. J. Lu, *Nanoscale*, 2015, **7**, 15635.
101. A. Keppler, S. Gendreizig, T. Gronemeyer, H. Pick, H. Vogel and K. Johnsson, *Nat. Biotechnol.*, 2003, **21**, 86.
102. E. Harokopakis, N. K. Childers, S. M. Michalek, S. S. Zhang and M. Tomasi, *J. Immunol. Methods*, 1995, **185**, 31.
103. C. Czerkinsky, M. W. Russell, N. Lycke, M. Lindblad and J. Holmgren, *Infect. Immun.*, 1989, **57**, 1072.
104. B. S. Fox, K. M. Kantak, M. A. Edwards, K. M. Black, B. K. Bollinger, A. J. Botka, T. L. French, T. L. Thompson, V. C. Schad, J. L. Greenstein, M. L. Gefter, M. A. Exley, P. A. Swain and T. J. Briner, *Nat. Med.*, 1996, **2**, 1129.
105. M. K. Kantak, L. S. Collins, G. E. Lipman, J. Bond, K. Giovanoni and S. B. Fox, *Psychopharmacology*, 2000, **148**, 251.
106. T. R. Kosten, C. B. Domingo, D. Shorter, F. Orson, C. Green, E. Somoza, R. Sekerka, F. R. Levin, J. J. Mariani, M. Stitzer, D. A. Tompkins, J. Rotrosen, V. Thakkar, B. Smoak and K. Kampman, *Drug Alcohol Depend.*, 2014, **140**, 42.
107. J. M. Antos, G.-L. Chew, C. P. Guimaraes, N. C. Yoder, G. M. Grotenbreg, M. W.-L. Popp and H. L. Ploegh, *J. Am. Chem. Soc.*, 2009, **131**, 10800.
108. K. Rose, J. Chen, M. Dragovic, W. Zeng, D. Jeannerat, P. Kamalaprija and U. Burger, *Bioconj. Chem.*, 1999, **10**, 1038.
109. J. Chen, W. Zeng, R. Offord and K. Rose, *Bioconj. Chem.*, 2003, **14**, 614.
110. L. Johannes, D. Tenza, C. Antony and B. Goud, *J. Biol. Chem.*, 1997, **272**, 19554.
111. E. A. Merritt and W. G. J. Hol, *Curr. Opin. Struct. Biol.*, 1995, **5**, 165.
112. E. A. Green, C. Botting, H. M. Webb, T. R. Hirst and R. E. Randall, *Vaccine*, 1996, **14**, 949.
113. A. M. O'Dowd, C. H. Botting, B. Precious, R. Shawcross and R. E. Randall, *Vaccine*, 1999, **17**, 1442.
114. C. W. Lindsley, *ACS Chem. Neurosci.*, 2015, **6**, 505.
115. F. Eckstein, *Expert Opin. Biol. Ther.*, 2007, **7**, 1021.
116. J. C. Burnett and J. J. Rossi, *Chem. Biol.*, 2012, **19**, 60.
117. S. T. Crooke, *Antisense Nucleic Acid Drug Dev.*, 1998, **8**, VII.
118. E. Wong and T. Goldberg, *P. T.*, 2014, **39**, 119.
119. M. A. Behlke, *Oligonucleotides*, 2008, **18**, 305.

120. S. Shukla, C. S. Sumaria and P. I. Pradeepkumar, *ChemMedChem*, 2010, **5**, 328.
121. R. L. Juliano, *Nucleic Acids Res.*, 2016, **44**, 6518.
122. F. T. M. d. C. Vicentini, L. N. Borgheti-Cardoso, L. V. Depieri, D. de Macedo Mano, T. F. Abelha, R. Petrilli and M. V. L. B. Bentley, *Pharm. Res.*, 2013, **30**, 915.
123. J. Zhou, K.-T. Shum, J. C. Burnett and J. J. Rossi, *Pharmaceuticals*, 2013, **6**, 85.
124. P. Sazani, S. H. Kang, M. A. Maier, C. F. Wei, J. Dillman, J. Summerton, M. Manoharan and R. Kole, *Nucleic Acids Res.*, 2001, **29**, 3965.
125. H. Heemskerk, C. de Winter, P. van Kuik, N. Heuvelmans, P. Sabatelli, P. Rimessi, P. Braghetta, G.-J. B. van Ommen, S. de Kimpe, A. Ferlini, A. Aartsma-Rus and J. C. T. van Deutekom, *Mol. Ther.*, 2010, **18**, 1210.
126. B. P. Monia, J. F. Johnston, H. Sasmor and L. L. Cummins, *J. Biol. Chem.*, 1996, **271**, 14533.
127. R. S. Geary, T. A. Watanabe, L. Truong, S. Freier, E. A. Lesnik, N. B. Sioufi, H. Sasmor, M. Manoharan and A. A. Levin, *J. Pharmacol. Exp. Ther.*, 2001, **296**, 890.
128. S. K. Singh, A. A. Koshkin, J. Wengel and P. Nielsen, *Chem. Commun.*, 1998, **1998**, 455.
129. B. Vester and J. Wengel, *Biochemistry*, 2004, **43**, 13233.
130. M. Matsukura, K. Shinozuka, G. Zon, H. Mitsuya, M. Reitz, J. S. Cohen and S. Broder, *Proc. Natl. Acad. Sci. U. S. A.*, 1987, **84**, 7706.
131. L. J. Popplewell, C. Trollet, G. Dickson and I. R. Graham, *Mol. Ther.*, 2009, **17**, 554.
132. E. P. Stirchak, J. E. Summerton and D. D. Weller, *Nucleic Acids Res.*, 1989, **17**, 6129.
133. P. Nielsen, M. Egholm, R. Berg and O. Buchardt, *Science*, 1991, **254**, 1497.
134. N. Dias, S. Dheur, P. E. Nielsen, S. Gryaznov, A. Van Aerschot, P. Herdewijn, C. Hélène and T. E. Saison-Behmoaras, *J. Mol. Biol.*, 1999, **294**, 403.
135. P. Sazani, F. Gemignani, S. H. Kang, M. A. Maier, M. Manoharan, M. Persmark, D. Bortner and R. Kole, *Nat. Biotechnol.*, 2002, **20**, 1228.
136. E. Bernstein, A. A. Caudy, S. M. Hammond and G. J. Hannon, *Nature*, 2001, **409**, 363.
137. A. Vermeulen, L. Behlen, A. Reynolds, A. Wolfson, W. S. Marshall, J. O. N. Karpilow and A. Khvorova, *RNA*, 2005, **11**, 674.
138. C. Matranga, Y. Tomari, C. Shin, D. P. Bartel and P. D. Zamore, *Cell*, 2005, **123**, 607.
139. P. J. F. Leuschner, S. L. Ameres, S. Kueng and J. Martinez, *EMBO Rep.*, 2006, **7**, 314.
140. S. M. Hammond, E. Bernstein, D. Beach and G. J. Hannon, *Nature*, 2000, **404**, 293.
141. J. Martinez, A. Patkaniowska, H. Urlaub, R. Lührmann and T. Tuschl, *Cell*, 2002, **110**, 563.
142. G. Meister, M. Landthaler, A. Patkaniowska, Y. Dorsett, G. Teng and T. Tuschl, *Mol. Cell*, 2004, **15**, 185.
143. T. A. Rand, K. Ginalski, N. V. Grishin and X. Wang, *Proc. Natl. Acad. Sci. U. S. A.*, 2004, **101**, 14385.
144. S. M. Elbashir, J. Harborth, W. Lendeckel, A. Yalcin, K. Weber and T. Tuschl, *Nature*, 2001, **411**, 494.
145. J. K. Watts, G. F. Deleavey and M. J. Damha, *Drug Discov. Today*, 2008, **13**, 842.
146. R. M. Hudziak, J. Summerton, D. D. Weller and P. L. Iversen, *Antisense Nucleic Acid Drug Dev.*, 2000, **10**, 163.
147. C. L. Will and R. Lührmann, *Cold Spring Harb. Perspect. Biol.*, 2011, **3**, a003707.

148. B. Bestas, P. M. D. Moreno, K. E. M. Blomberg, D. K. Mohammad, A. F. Saleh, T. Sutlu, J. Z. Nordin, P. Guterstam, M. O. Gustafsson, S. Kharazi, B. Piatosa, T. C. Roberts, M. A. Behlke, M. J. A. Wood, M. J. Gait, K. E. Lundin, S. El Andaloussi, R. Mansson, A. Berglof, J. Wengel and C. I. E. Smith, *J. Clin. Invest.*, 2014, **124**, 4067.
149. S. D. Wilton, F. Lloyd, K. Carville, S. Fletcher, K. Honeyman, S. Agrawal and R. Kole, *Neuromuscul. Disord.*, 1999, **9**, 330.
150. Q. L. Lu, C. J. Mann, F. Lou, G. Bou-Gharios, G. E. Morris, S.-a. Xue, S. Fletcher, T. A. Partridge and S. D. Wilton, *Nat. Med.*, 2003, **9**, 1009.
151. S. M. Hammond, G. McClorey, J. Z. Nordin, C. Godfrey, S. Stenler, K. A. Lennox, C. I. E. Smith, A. M. Jacobi, M. A. Varela, Y. Lee, M. A. Behlke, M. J. A. Wood and S. E. L. Andaloussi, *Mol. Ther. Nucleic Acids*, 2014, **3**, e212.
152. F. Debart, S. Abes, G. Deglane, H. M. Moulton, P. Clair, M. J. Gait, J.-J. Vasseur and B. Lebleu, *Curr. Top. Med. Chem.*, 2007, **7**, 727.
153. J. Hoyer and I. Neundorf, *Acc. Chem. Res.*, 2012, **45**, 1048.
154. J. DeVincenzo, J. E. Cehelsky, R. Alvarez, S. Elbashir, J. Harborth, I. Toudjarska, L. Nechev, V. Murugaiah, A. V. Vliet, A. K. Vaishnaw and R. Meyers, *Antiviral Res.*, 2008, **77**, 225.
155. F. J. Raal, R. D. Santos, D. J. Blom, A. D. Marais, M.-J. Charng, W. C. Cromwell, R. H. Lachmann, D. Gaudet, J. L. Tan, S. Chasan-Taber, D. L. Tribble, J. D. Flaim and S. T. Crooke, *Lancet*, 2010, **375**, 998.
156. N. M. Goemans, M. Tulinius, J. T. van den Akker, B. E. Burm, P. F. Ekhart, N. Heuvelmans, T. Holling, A. A. Janson, G. J. Platenburg, J. A. Sipkens, J. M. A. Sitsen, A. Aartsma-Rus, G.-J. B. van Ommen, G. Buyse, N. Darin, J. J. Verschuuren, G. V. Campion, S. J. de Kimpe and J. C. van Deutekom, *New Engl. J. Med.*, 2011, **364**, 1513.
157. D. A. Braasch, Z. Paroo, A. Constantinescu, G. Ren, O. K. Öz, R. P. Mason and D. R. Corey, *Bioorg. Med. Chem. Lett.*, 2004, **14**, 1139.
158. C. Lorenz, P. Hadwiger, M. John, H.-P. Vornlocher and C. Unverzagt, *Bioorg. Med. Chem. Lett.*, 2004, **14**, 4975.
159. K. Nishina, T. Unno, Y. Uno, T. Kubodera, T. Kanouchi, H. Mizusawa and T. Yokota, *Mol. Ther.*, 2008, **16**, 734.
160. P. Järver, T. Coursindel, S. E. L. Andaloussi, C. Godfrey, M. J. A. Wood and M. J. Gait, *Mol. Ther. Nucleic Acids*, 2012, **1**, e27.
161. F. Madani, S. Lindberg, U. Langel, S. Futaki and A. Graslund, *J. Biophys.*, 2011, **2011**, 414729.
162. J. P. Bongartz, A. M. Aubertin, P. G. Milhaud and B. Lebleu, *Nucleic Acids Res.*, 1994, **22**, 4681.
163. M. Pooga, U. Soomets, M. Hallbrink, A. Valkna, K. Saar, K. Rezaei, U. Kahl, J.-X. Hao, X.-J. Xu, Z. Wiesenfeld-Hallin, T. Hokfelt, T. Bartfai and U. Langel, *Nat. Biotechnol.*, 1998, **16**, 857.
164. N. Jearawiriyapaisarn, H. M. Moulton, B. Buckley, J. Roberts, P. Sazani, S. Fucharoen, P. L. Iversen and R. Kole, *Mol. Ther.*, 2008, **16**, 1624.
165. S. El-Andaloussi, P. Järver, Henrik J. Johansson and Ü. Langel, *Biochem. J.*, 2007, **407**, 285.
166. D. Sarko, B. Beijer, R. G. Boy, E.-M. Nothelfer, K. Leotta, M. Eisenhut, A. Altmann, U. Haberkorn and W. Mier, *Mol. Pharm.*, 2010, **7**, 2224.
167. T. Geib and K. J. Hertel, *PLoS One*, 2009, **4**, e8204.
168. H. Sumimoto, S. Yamagata, A. Shimizu, H. Miyoshi, H. Mizuguchi, T. Hayakawa, M. Miyagishi, K. Taira and Y. Kawakami, *Gene Ther.*, 2004, **12**, 95.
169. X. W. Zhang, T. Kon, H. Wang, F. Li, Q. Huang, Z. N. Rabbani, J. P. Kirkpatrick, Z. Vujaskovic, M. W. Dewhirst and C. Y. Li, *Cancer Res.*, 2004, **64**, 8139.

170. D. B. Kohn, M. Sadelain and J. C. Glorioso, *Nat. Rev. Cancer*, 2003, **3**, 477.
171. S. Hacein-Bey-Abina, A. Garrigue, G. P. Wang, J. Soulier, A. Lim, E. Morillon, E. Clappier, L. Caccavelli, E. Delabesse, K. Beldjord, V. Asnafi, E. Macintyre, L. Dal Cortivo, I. Radford, N. Brousse, F. Sigaux, D. Moshous, J. Hauer, A. Borkhardt, B. H. Belohradsky, U. Wintergerst, M. C. Velez, L. Leiva, R. Sorensen, N. Wulffraat, S. Blanche, F. D. Bushman, A. Fischer and M. Cavazzana-Calvo, *J. Clin. Invest.*, 2008, **118**, 3132.
172. D. B. Fenske, A. Chonn and P. R. Cullis, *Toxicol. Pathol.*, 2008, **36**, 21.
173. Y.-C. Tseng, S. Mozumdar and L. Huang, *Adv. Drug Del. Rev.*, 2009, **61**, 721.
174. S. C. Semple, S. K. Klimuk, T. O. Harasym, N. Dos Santos, S. M. Ansell, K. F. Wong, N. Maurer, H. Stark, P. R. Cullis, M. J. Hope and P. Scherrer, *Biochim. Biophys. Acta*, 2001, **1510**, 152.
175. P. Y. Chien, J. K. Wang, D. Carbonaro, S. Lei, B. Miller, S. Sheikh, S. M. Ali, M. U. Ahmad and I. Ahmad, *Cancer Gene Ther.*, 2005, **12**, 321.
176. A. Pal, A. Ahmad, S. Khan, I. Sakabe, C. B. Zhang, U. N. Kasid and I. Ahmad, *Int. J. Oncol.*, 2005, **26**, 1087.
177. A. de Fougerolles, H.-P. Vornlocher, J. Maraganore and J. Lieberman, *Nat. Rev. Drug Discov.*, 2007, **6**, 443.
178. T. S. Zimmermann, A. C. H. Lee, A. Akinc, B. Bramlage, D. Bumcrot, M. N. Fedoruk, J. Harborth, J. A. Heyes, L. B. Jeffs, M. John, A. D. Judge, K. Lam, K. McClintock, L. V. Nechev, L. R. Palmer, T. Racie, I. Rohl, S. Seiffert, S. Shanmugam, V. Sood, J. Soutschek, I. Toudjarska, A. J. Wheat, E. Yaworski, W. Zedalis, V. Koteliansky, M. Manoharan, H. P. Vornlocher and I. MacLachlan, *Nature*, 2006, **441**, 111.
179. H. Nakamura, S. S. Siddiqui, X. Shen, A. B. Malik, J. S. Pulido, N. M. Kumar and B. Yue, *Mol. Vis.*, 2004, **10**, 703.
180. D. Palliser, D. Chowdhury, Q. Y. Wang, S. J. Lee, R. T. Bronson, D. M. Knipe and J. Lieberman, *Nature*, 2006, **439**, 89.
181. T. W. Geisbert, L. E. Hensley, E. Kagan, E. Z. Yu, J. B. Geisbert, K. Daddario-DiCaprio, E. A. Fritz, P. B. Jahrling, K. McClintock, J. R. Phelps, A. C. H. Lee, A. Judge, L. B. Jeffs and I. MacLachlan, *J. Infect. Dis.*, 2006, **193**, 1650.
182. M.-C. Luo, D.-Q. Zhang, S.-W. Ma, Y.-Y. Huang, S. J. Shuster, F. Porreca and J. Lai, *Mol. Pain*, 2005, **1**, 29.
183. M. Khoury, P. Louis-Plence, V. Escriou, D. Noel, C. Largeau, C. Cantos, D. Scherman, C. Jorgensen and F. Apparailly, *Arthritis Rheum.*, 2006, **54**, 1867.
184. U. N. Verma, R. M. Surabhi, A. Schmaltieg, C. Becerra and R. B. Gaynor, *Clin. Cancer. Res.*, 2003, **9**, 1291.
185. J. Yano, K. Hirabayashi, S.-i. Nakagawa, T. Yamaguchi, M. Nogawa, I. Kashimori, H. Naito, H. Kitagawa, K. Ishiyama, T. Ohgi and T. Irimura, *Clin. Cancer. Res.*, 2004, **10**, 7721.
186. M. Nogawa, T. Yuasa, S. Kimura, M. Tanaka, J. Kuroda, K. Sato, A. Yokota, H. Segawa, Y. Toda, S. Kageyama, T. Yoshiki, Y. Okada and T. Maekawa, *J. Clin. Invest.*, 2005, **115**, 978.
187. S. Akhtar, *Expert Opin. Drug Metab. Toxicol.*, 2010, **6**, 1347.
188. J. H. Jeong, T. G. Park and S. H. Kim, *Pharm. Res.*, 2011, **28**, 2072.
189. H. Y. Xue, S. Liu and H. L. Wong, *Nanomedicine*, 2014, **9**, 295.
190. Z. Ma, J. Li, F. He, A. Wilson, B. Pitt and S. Li, *Biochem. Biophys. Res. Commun.*, 2005, **330**, 755.
191. M. Sioud, *J. Mol. Biol.*, 2005, **348**, 1079.
192. M. A. Robbins, M. J. Li, I. Leung, H. T. Li, D. V. Boyer, Y. Song, M. A. Behlke and J. J. Rossi, *Nat. Biotechnol.*, 2006, **24**, 566.

193. J. D. Heidel, S. Hu, X. F. Liu, T. J. Triche and M. E. Davis, *Nat. Biotechnol.*, 2004, **22**, 1579.
194. H. de Martimprey, C. Vauthier, C. Malvy and P. Couvreur, *Eur. J. Pharm. Biopharm.*, 2009, **71**, 490.
195. L.-R. Tsai, M.-H. Chen, C.-T. Chien, M.-K. Chen, F.-S. Lin, K. M.-C. Lin, Y.-K. Hwu, C.-S. Yang and S.-Y. Lin, *Biomaterials*, 2011, **32**, 3647.
196. S. Biswas, P. P. Deshpande, G. Navarro, N. S. Dodwadkar and V. P. Torchilin, *Biomaterials*, 2013, **34**, 1289.
197. C. Chavany, T. Saison-Behmoaras, T. L. Doan, F. Puisieux, P. Couvreur and C. Hélène, *Pharm. Res.*, 1994, **11**, 1370.
198. Y. Zhang, A. Satterlee and L. Huang, *Mol. Ther.*, 2012, **20**, 1298.
199. S. Lindberg, J. Regberg, J. Eriksson, H. Helmfors, A. Muñoz-Alarcón, A. Srimanee, R. A. Figueroa, E. Hallberg, K. Ezzat and Ü. Langel, *J. Control. Release*, 2015, **206**, 58.
200. A. A. Eltoukhy, G. Sahay, J. M. Cunningham and D. G. Anderson, *ACS Nano*, 2014, **8**, 7905.
201. I.-D. Kim, C.-M. Lim, J.-B. Kim, H. Y. Nam, K. Nam, S.-W. Kim, J.-S. Park and J.-K. Lee, *J. Control. Release*, 2010, **142**, 422.
202. J. Zhou, C. P. Neff, X. Liu, J. Zhang, H. Li, D. D. Smith, P. Swiderski, T. Aboellail, Y. Huang, Q. Du, Z. Liang, L. Peng, R. Akkina and J. J. Rossi, *Mol. Ther.*, 2011, **19**, 2228.
203. M. Nakamura, J.-i. Jo, Y. Tabata and O. Ishikawa, *Am. J. Pathol.*, 2008, **172**, 650.
204. R. M. Schiffelers, A. Ansari, J. Xu, Q. Zhou, Q. Tang, G. Storm, G. Molema, P. Y. Lu, P. V. Scaria and M. C. Woodle, *Nucleic Acids Res.*, 2004, **32**, e149.
205. X. Zhu, Y. Xu, L. M. Solis, W. Tao, L. Wang, C. Behrens, X. Xu, L. Zhao, D. Liu, J. Wu, N. Zhang, I. I. Wistuba, O. C. Farokhzad, B. R. Zetter and J. Shi, *Proc. Natl. Acad. Sci. U. S. A.*, 2015, **112**, 7779.
206. M. E. Davis, J. E. Zuckerman, C. H. J. Choi, D. Seligson, A. Tolcher, C. A. Alabi, Y. Yen, J. D. Heidel and A. Ribas, *Nature*, 2010, **464**, 1067.
207. S. M. Moghimi, P. Symonds, J. C. Murray, A. C. Hunter, G. Debska and A. Szewczyk, *Mol. Ther.*, 2005, **11**, 990.
208. G. Grandinetti, N. P. Ingle and T. M. Reineke, *Mol. Pharm.*, 2011, **8**, 1709.
209. J. A. Wolff and D. B. Rozema, *Mol. Ther.*, 2007, **16**, 8.
210. J. E. Zuckerman, I. Gritli, A. Tolcher, J. D. Heidel, D. Lim, R. Morgan, B. Chmielowski, A. Ribas, M. E. Davis and Y. Yen, *Proc. Natl. Acad. Sci. U. S. A.*, 2014, **111**, 11449.
211. C. E. Nelson, J. R. Kintzing, A. Hanna, J. M. Shannon, M. K. Gupta and C. L. Duvall, *ACS Nano*, 2013, **7**, 8870.
212. J. C. Burnett, J. J. Rossi and K. Tiemann, *Biotechnology Journal*, 2011, **6**, 1130.
213. S. H. Kim, J. H. Jeong, S. H. Lee, S. W. Kim and T. G. Park, *Bioconj. Chem.*, 2008, **19**, 2156.
214. T. Kanazawa, F. Akiyama, S. Kakizaki, Y. Takashima and Y. Seta, *Biomaterials*, 2013, **34**, 9220.
215. H. He, N. Zheng, Z. Song, K. H. Kim, C. Yao, R. Zhang, C. Zhang, Y. Huang, F. M. Uckun, J. Cheng, Y. Zhang and L. Yin, *ACS Nano*, 2016, **10**, 1859.
216. A. Ohyama, T. Higashi, K. Motoyama and H. Arima, *Bioconj. Chem.*, 2016, **27**, 521.
217. H. O. Smith, C. A. Hutchison, C. Pfannkoch and J. C. Venter, *Proc. Natl. Acad. Sci. U. S. A.*, 2003, **100**.
218. A. S. Xiong, R. H. Peng, J. Zhuang, F. Gao, Y. Li, Z. M. Cheng and Q. H. Yao, *FEMS Microbiol. Rev.*, 2008, **32**, 522.

219. R. Perozzo, G. Folkers and L. Scapozza, *J. Recept. Signal Transduct.*, 2004, **24**, 1.
220. S. Nunez, J. Venhorst and C. G. Kruse, *Drug Discov. Today*, 2012, **17**, 10.
221. D. E. Wolf, *Methods Cell Biol.*, 2003, **72**, 157.
222. V. Prasad, D. Semwogerere and E. R. Weeks, *J. Phys.: Condens. Matter*, 2007, **19**, 113102.
223. R. Rydzanicz, X. S. Zhao and P. E. Johnson, *Nucleic Acids Res.*, 2005, **33**, W521.
224. W. A. Kibbe, *Nucleic Acids Res.*, 2007, **35**, W43.
225. M. P. Weiner, G. L. Costa, W. Schoettlin, J. Cline, E. Mathur and J. C. Bauer, *Gene*, 1994, **151**, 119.
226. C. Papworth, J. C. Bauer and J. Braman, *Strategies*, 1996, **9**, 3.
227. A. Ulrich, K. R. Andersen and T. U. Schwartz, *PLoS One*, 2012, **7**, e53360.
228. H. C. Birnboim and J. Doly, *Nucleic Acids Res.*, 1979, **7**, 1513.
229. S. Keller, C. Vargas, H. Zhao, G. Piszczek, C. A. Brautigam and P. Schuck, *Anal. Chem.*, 2012, **84**, 5066.
230. C. L'hoir, A. Renard and J. A. Martial, *Gene*, 1990, **89**, 47.
231. P. Slos, D. Speck, N. Accart, H. V. J. Kolbe, D. Schubnel, B. Bouchon, R. Bischoff and M. P. Kieny, *Protein Expression Purif.*, 1994, **5**, 518.
232. A. Paula de Mattos Arêas, M. Leonor Sarno de Oliveira, C. Raul Romero Ramos, M. E. Sbrogio-Almeida, I. a. Raw and P. L. Ho, *Protein Expression Purif.*, 2002, **25**, 481.
233. H. Zeighami, M. Sattari and M. Rezayat, *Ann. Microbiol.*, 2010, **60**, 451.
234. J. Sanchez and J. Holmgren, *Proc. Natl. Acad. Sci. U. S. A.*, 1989, **86**, 481.
235. M. van de Walle, R. Fass and J. Shiloach, *Appl. Microbiol. Biotechnol.*, 1990, **33**, 389.
236. C. Rodighiero, A. T. Aman, M. J. Kenny, J. Moss, W. I. Lencer and T. R. Hirst, *J. Biol. Chem.*, 1999, **274**, 3962.
237. A. T. Aman, S. Fraser, E. A. Merritt, C. Rodigherio, M. Kenny, M. Ahn, W. G. J. Hol, N. A. Williams, W. I. Lencer and T. R. Hirst, *Proc. Natl. Acad. Sci. U. S. A.*, 2001, **98**, 8536.
238. C. M. Richards, A. T. Aman, T. R. Hirst, T. J. Hill and N. A. Williams, *J. Virol.*, 2001, **75**, 1664.
239. C. Rodighiero, Y. Fujinaga, T. R. Hirst and W. I. Lencer, *J. Biol. Chem.*, 2001, **276**, 36939.
240. P. Slos, P. Dutot, J. Reymund, P. Kleinpeter, D. Prozzi, M.-P. Kieny, J. Delcour, A. Mercenier and P. Hols, *FEMS Microbiol. Lett.*, 1998, **169**, 29.
241. N. Goto, J.-i. Maeyama, Y. Yasuda, M. Isaka, K. Matano, S. Kozuka, T. Taniguchi, Y. Miura, K. Ohkuma and K. Tochikubo, *Vaccine*, 2000, **18**, 2164.
242. J.-G. Lim and H.-S. Jin, *Biotechnol. Bioprocess. Eng.*, 2008, **13**, 598.
243. H. Daniell, S.-B. Lee, T. Panchal and P. O. Wiebe, *J. Mol. Biol.*, 2001, **311**, 1001.
244. Y.-S. Kim, M.-Y. Kim, T.-G. Kim and M.-S. Yang, *Mol. Biotechnol.*, 2009, **41**, 8.
245. S. Karaman, J. Cunnick and K. Wang, *Plant Cell Rep.*, 2012, **31**, 527.
246. Z. H. Gong, H. Q. Jin, Y. F. Jin and Y. Z. Zhang, *J. Biochem. Mol. Biol.*, 2005, **38**, 717.
247. M. Sandkvist, T. R. Hirst and M. Bagdasarian, *J. Bacteriol.*, 1987, **169**, 4570.
248. S. K. Mazmanian, G. Liu, T. T. Hung and O. Schneewind, *Science*, 1999, **285**, 760.
249. S. Tsukiji and T. Nagamune, *ChemBioChem*, 2009, **10**, 787.
250. M. W.-L. Popp and H. L. Ploegh, *Angew. Chem. Int. Ed. (English)*, 2011, **50**, 5024.

251. L. Chan, H. F. Cross, J. K. She, G. Cavalli, H. F. P. Martins and C. Neylon, *PLoS One*, 2007, **2**, e1164.
252. R. Parthasarathy, S. Subramanian and E. T. Boder, *Bioconj. Chem.*, 2007, **18**, 469.
253. M. W. Popp, J. M. Antos, G. M. Grotenbreg, E. Spooner and H. L. Ploegh, *Nat. Chem. Biol.*, 2007, **3**, 707.
254. J. M. Antos, G. M. Miller, G. M. Grotenbreg and H. L. Ploegh, *J. Am. Chem. Soc.*, 2008, **130**, 16338.
255. F. Clow, J. D. Fraser and T. Proft, *Biotechnol. Lett.*, 2008, **30**, 1603.
256. T. Tanaka, T. Yamamoto, S. Tsukiji and T. Nagamune, *ChemBioChem*, 2008, **9**, 802.
257. X. Guo, Z. Wu and Z. Guo, *Bioconj. Chem.*, 2012, **23**, 650.
258. R. D. Row, T. J. Roark, M. C. Philip, L. L. Perkins and J. M. Antos, *Chem. Commun.*, 2015, **51**, 12548.
259. J. W. Nelson, A. G. Chamessian, P. J. McEnaney, R. P. Murelli, B. I. Kazmiercak and D. A. Spiegel, *ACS Chem. Biol.*, 2010, **5**, 1147.
260. S. Pritz, Y. Wolf, O. Kraetke, J. Klose, M. Bienert and M. Beyermann, *J. Org. Chem.*, 2007, **72**, 3909.
261. D. J. Williamson, M. A. Fascione, M. E. Webb and W. B. Turnbull, *Angew. Chem. Int. Ed. (English)*, 2012, **51**, 9377.
262. M. T. Dertzbaugh and L. M. Cox, *Protein Eng.*, 1998, **11**, 577.
263. N. C. Ammerman, M. Beier-Sexton and A. F. Azad, *Curr. Protoc. Microbiol.*, 2008, **Appendix 4**, 4E.
264. I. Majoul, T. Schmidt, M. Pomasanova, E. Boutkevich, Y. Kozlov and H.-D. Söling, *J. Cell Sci.*, 2002, **115**, 817.
265. P. I. Bastiaens, I. V. Majoul, P. J. Verveer, H. D. Söling and T. M. Jovin, *The EMBO Journal*, 1996, **15**, 4246.
266. A. Chen, T. Hu, C. Mikoryak and R. K. Draper, *Biochim. Biophys. Acta*, 2002, **1589**, 124.
267. A. Engelsberg, R. Hermosilla, U. Karsten, R. Schülein, B. Dörken and A. Rehm, *J. Biol. Chem.*, 2003, **278**, 22998.
268. M. E. Fraser, M. M. Chernaia, Y. V. Kozlov and M. N. G. James, *Nat. Struct. Biol.*, 1994, **1**, 59.
269. J. J. M. Bergeron, M. B. Brenner, D. Y. Thomas and D. B. Williams, *Trends Biochem. Sci.*, 1994, **19**, 124.
270. N. Ahluwalia, J. J. M. Bergeron, I. Wada, E. Degen and D. B. Williams, *J. Biol. Chem.*, 1992, **267**, 10914.
271. D. B. Williams, *J. Cell Sci.*, 2006, **119**, 615.
272. G. Griffiths, M. Ericsson, J. Krijnselocker, T. Nilsson, B. Goud, H. D. Soling, B. L. Tang, S. H. Wong and W. J. Hong, *J. Cell Biol.*, 1994, **127**, 1557.
273. M. Cabrera, M. Muniz, J. Hidalgo, L. Vega, M. E. Martin and A. Velasco, *Mol. Biol. Cell*, 2003, **14**, 4114.
274. F. M. Townsley, D. W. Wilson and H. R. Pelham, *EMBO J.*, 1993, **12**, 2821.
275. M. J. Lewis and H. R. B. Pelham, *Nature*, 1990, **348**, 162.
276. P. L. Iversen, *Curr. Opin. Mol. Ther.*, 2001, **3**, 235.
277. S. M. Hammond and M. J. A. Wood, *Curr. Opin. Mol. Ther.*, 2010, **12**, 478.
278. S. D. Wilton, A. M. Fall, P. L. Harding, G. McClorey, C. Coleman and S. Fletcher, *Mol. Ther.*, 2007, **15**, 1288.
279. Q. L. Lu, A. Rabinowitz, Y. C. Chen, T. Yokota, H. Yin, J. Alter, A. Jadoon, G. Bou-Gharios and T. Partridge, *Proc. Natl. Acad. Sci. U. S. A.*, 2005, **102**, 198.
280. J. C. T. van Deutekom, M. Bremmer-Bout, A. A. M. Janson, I. B. Ginjaar, F. Baas, J. T. den Dunnen and G.-J. B. van Ommen, *Hum. Mol. Genet.*, 2001, **10**, 1547.

281. Y. Takeshima, H. Wada, M. Yagi, Y. Ishikawa, Y. Ishikawa, R. Minami, H. Nakamura and M. Matsuo, *Brain Dev.*, 2001, **23**, 788.
282. J. C. van Deutekom, A. A. Janson, I. B. Ginjaar, W. S. Frankhuizen, A. Aartsma-Rus, M. Bremmer-Bout, J. T. den Dunnen, K. Koop, A. J. van der Kooi, N. M. Goemans, S. J. de Kimpe, P. F. Ekhart, E. H. Venneker, G. J. Platenburg, J. J. Verschuuren and G.-J. B. van Ommen, *New Engl. J. Med.*, 2007, **357**, 2677.
283. Q.-l. Lu, S. Cirak and T. Partridge, *Mol. Ther. Nucleic Acids*, 2014, **3**, e152.
284. C. W. Tornøe, C. Christensen and M. Meldal, *J. Org. Chem.*, 2002, **67**, 3057.
285. V. V. Rostovtsev, L. G. Green, V. V. Fokin and K. B. Sharpless, *Angew. Chem. Int. Ed. (English)*, 2002, **41**, 2596.
286. N. J. Agard, J. A. Prescher and C. R. Bertozzi, *J. Am. Chem. Soc.*, 2004, **126**, 15046.
287. J. M. Baskin, J. A. Prescher, S. T. Laughlin, N. J. Agard, P. V. Chang, I. A. Miller, A. Lo, J. A. Codelli and C. R. Bertozzi, *Proc. Natl. Acad. Sci. U. S. A.*, 2007, **104**, 16793.
288. M. D. Witte, C. Theile, T. Wu, C. P. Guimaraes, A. E. M. Blom and H. L. Ploegh, *Nat. Protoc.*, 2013, **8**, 1808.
289. X. Y. Huang, A. Aulabaugh, W. D. Ding, B. Kapoor, L. Alksne, K. Tabei and G. Ellestad, *Biochemistry*, 2003, **42**, 11307.
290. H. Y. Mao, S. A. Hart, A. Schink and B. A. Pollok, *J. Am. Chem. Soc.*, 2004, **126**.
291. E. M. Sletten and C. R. Bertozzi, *Angew. Chem. Int. Ed. (English)*, 2009, **48**, 6974.
292. A. Frey, K. T. Giannasca, R. Weltzin, P. J. Giannasca, H. Reggio, W. I. Lencer and M. R. Neutra, *J. Exp. Med.*, 1996, **184**, 1045.
293. J. A. Mertz, J. A. McCann and W. D. Picking, *Biochem. Biophys. Res. Commun.*, 1996, **226**, 140.
294. N. Panchuk-Voloshina, R. P. Haugland, J. Bishop-Stewart, M. K. Bhalgat, P. J. Millard, F. Mao, W.-Y. Leung and R. P. Haugland, *J. Histochem. Cytochem.*, 1999, **47**, 1179.
295. J. E. Berlier, A. Rothe, G. Buller, J. Bradford, D. R. Gray, B. J. Filanoski, W. G. Telford, S. Yue, J. Liu, C.-Y. Cheung, W. Chang, J. D. Hirsch, J. M. Beechem Rosaria P. Haugland and R. P. Haugland, *J. Histochem. Cytochem.*, 2003, **51**, 1699.
296. J. Mahmoudian, R. Hadavi, M. Jeddi-Tehrani, A. R. Mahmoudi, A. A. Bayat, E. Shaban, M. Vafakhah, M. Darzi, M. Tarahomi and R. Ghods, *Cell J.*, 2011, **13**, 169.
297. R. Hayward, K. J. Saliba and K. Kirk, *J. Cell Sci.*, 2006, **119**, 1016.
298. J. A. Mindell, *Annu. Rev. Physiol.*, 2012, **74**, 69.
299. C. Arsenis, J. S. Gordon and O. Touster, *J. Biol. Chem.*, 1970, **245**, 205.
300. Y. Fujiwara, A. Furuta, H. Kikuchi, S. Aizawa, Y. Hatanaka, C. Konya, K. Uchida, A. Yoshimura, Y. Tamai, K. Wada and T. Kabuta, *Autophagy*, 2013, **9**, 403.
301. Y. Fujiwara, H. Kikuchi, S. Aizawa, A. Furuta, Y. Hatanaka, C. Konya, K. Uchida, K. Wada and T. Kabuta, *Autophagy*, 2013, **9**, 1167.
302. K. Hase, Y. Fujiwara, H. Kikuchi, S. Aizawa, F. Hakuno, S.-I. Takahashi, K. Wada and T. Kabuta, *Nucleic Acids Res.*, 2015, **43**, 6439.
303. Y. Fujiwara, K. Hase, K. Wada and T. Kabuta, *Biochem. Biophys. Res. Commun.*, 2015, **460**, 281.
304. E. G. Guignet, R. Hovius and H. Vogel, *Nat. Biotechnol.*, 2004, **22**, 440.
305. J. Olejnik, E. Krzymańska-Olejnik and K. J. Rothschild, *Nucleic Acids Res.*, 1996, **24**, 361.
306. G. Zhou, X. Yan, D. Wu and S. J. Kron, *Bioconj. Chem.*, 2010, **21**, 1917.

307. G. Zhou, F. Khan, Q. Dai, J. E. Sylvester and S. J. Kron, *Mol. Biosyst.*, 2012, **8**, 2395.
308. K. Maier and E. Wagner, *J. Am. Chem. Soc.*, 2012, **134**, 10169.
309. R. I. Nathani, V. Chudasama, C. P. Ryan, P. R. Moody, R. E. Morgan, R. J. Fitzmaurice, M. E. B. Smith, J. R. Baker and S. Caddick, *Org. Biomol. Chem.*, 2013, **11**, 2408.
310. B. G. Davis, R. C. Lloyd and J. B. Jones, *J. Org. Chem.*, 1998, **63**, 9614.
311. B. G. Davis, M. A. T. Maughan, M. P. Green, A. Ullman and J. B. Jones, *Tetrahedron: Asymmetry*, 2000, **11**, 245.
312. D. P. Gamblin, P. Garnier, S. J. Ward, N. J. Oldham, A. J. Fairbanks and B. G. Davis, *Org. Biomol. Chem.*, 2003, **1**, 3642.
313. D. P. Gamblin, P. Garnier, S. van Kasteren, N. J. Oldham, A. J. Fairbanks and B. G. Davis, *Angew. Chem. Int. Ed. (English)*, 2004, **43**, 828.
314. J. Carlsson, H. Drevin and R. Axen, *Biochem. J.*, 1978, **173**, 723.
315. T. Weber, A. Mavratzas, S. Kiesgen, S. Haase, B. Botticher, E. Exner, W. Mier, L. Grosse-Hovest, D. Jager, M. A. E. Arndt and J. Krauss, *J. Immunol. Res.*, 2015, **2015**, 561814.
316. M. Ciano, M. Fuszard, H. Heide, C. H. Botting and A. Galkin, *FEBS Lett.*, 2013, **587**, 867.
317. J. Mendez, A. Monteagudo and K. Griebenow, *Bioconj. Chem.*, 2012, **23**, 698.
318. P. R. Berthold, T. Shiraishi and P. E. Nielsen, *Bioconj. Chem.*, 2010, **21**, 1933.
319. K. Stoecker, C. Dorninger, H. Daims and M. Wagner, *Appl. Environ. Microbiol.*, 2010, **76**, 922.
320. T. Mosmann, *J. Immunol. Methods*, 1983, **65**, 55.
321. M. V. Berridge and A. S. Tan, *Arch. Biochem. Biophys.*, 1993, **303**, 474.
322. M. V. Berridge, P. M. Herst and A. S. Tan, *Biotechnol. Annu. Rev.*, 2005, **11**, 127.
323. C. A. Belmokhtar, J. Hillion and E. Segal-Bendirdjian, *Oncogene*, 2001, **20**, 3354.
324. L. Ellgaard and L. W. Ruddock, *EMBO Rep.*, 2005, **6**, 28.
325. E. L. Eskelinen, Y. Tanaka and P. Saftig, *Trends Cell Biol.*, 2003, **13**, 137.
326. J. O. Koopmann, J. Albring, E. Huter, N. Bulbuc, P. Spee, J. Neefjes, G. J. Hammerling and F. Momburg, *Immunity*, 2000, **13**, 117.
327. J. C. Carrington and W. G. Dougherty, *Proc. Natl. Acad. Sci. U. S. A.*, 1988, **85**, 3391.
328. D. Kalderon, B. L. Roberts, W. D. Richardson and A. E. Smith, *Cell*, 1984, **39**, 499.
329. C. Dingwall, J. Robbins, S. M. Dilworth, B. Roberts and W. D. Richardson, *J. Cell Biol.*, 1988, **107**, 841.
330. P. Gaye and J. C. Mercier, *Reprod. Nutr. Dev.*, 1981, **21**, 199.
331. L. Hall and P. N. Campbell, *Essays Biochem.*, 1986, **22**, 1.
332. J. L. Mergny, J. Li, L. Lacroix, S. Amrane and J. B. Chaires, *Nucleic Acids Res.*, 2005, **33**, e138.
333. S. M. Freier, R. Kierzek, J. A. Jaeger, N. Sugimoto, M. H. Caruthers, T. Neilson and D. H. Turner, *Proc. Natl. Acad. Sci. U. S. A.*, 1986, **83**, 9373.
334. D. M. Benbrook and A. Long, *Exp. Oncol.*, 2012, **34**, 286.
335. S. T. Shibutani and T. Yoshimori, *Cell Res.*, 2014, **24**, 58.
336. J. Sanchez-Wandelmer, N. T. Ktistakis and F. Reggiori, *J. Cell Sci.*, 2015, **128**, 185.
337. S. S. Vembar and J. L. Brodsky, *Nat. Rev. Mol. Cell Biol.*, 2008, **9**, 944.
338. S. A. Houck, S. Singh and D. M. Cyr, *Methods Mol. Biol.*, 2012, **832**, 455.
339. N. Osada, A. Kohara, T. Yamaji, N. Hirayama, F. Kasai, T. Sekizuka, M. Kuroda and K. Hanada, *DNA Res.*, 2014, **21**, 673.
340. A. K. Perry, G. Chen, D. Zheng, H. Tang and G. Cheng, *Cell Res.*, 2005, **15**, 407.

341. M. Malumbres, *Genome Biol.*, 2014, **15**, 122.
342. J. Mankouri, P. R. Tedbury, S. Gretton, M. E. Hughes, S. D. C. Griffin, M. L. Dallas, K. A. Green, D. G. Hardie, C. Peers and M. Harris, *Proc. Natl. Acad. Sci. U. S. A.*, 2010, **107**, 11549.
343. G. Bao, W. J. Rhee and A. Tsourkas, *Annu. Rev. Biomed. Eng.*, 2009, **11**, 25.
344. X.-H. Peng, Z.-H. Cao, J.-T. Xia, G. W. Carlson, M. M. Lewis, W. C. Wood and L. Yang, *Cancer Res.*, 2005, **65**, 1909.
345. A. K. Chen, M. A. Behlke and A. Tsourkas, *Nucleic Acids Res.*, 2008, **36**, e69.
346. M. A. Barry and A. Eastman, *Arch. Biochem. Biophys.*, 1993, **300**, 440.
347. K. A. Geiler-Samerotte, M. F. Dion, B. A. Budnik, S. M. Wang, D. L. Hartl and D. A. Drummond, *Proc. Natl. Acad. Sci. U. S. A.*, 2011, **108**, 680.
348. E. Mastrobattista, G. A. Koning, L. van Bloois, A. C. S. Filipe, W. Jiskoot and G. Storm, *J. Biol. Chem.*, 2002, **277**, 27135.
349. S. L. Lo and S. Wang, *Biomaterials*, 2008, **29**, 2408.
350. Y. Tu and J.-s. Kim, *J. Gene Med.*, 2008, **10**, 646.
351. N. Kämper, P. M. Day, T. Nowak, H.-C. Selinka, L. Florin, J. Bolscher, L. Hilbig, J. T. Schiller and M. Sapp, *J. Virol.*, 2006, **80**, 759.
352. M. Kullberg, J. L. Owens and K. Mann, *J. Drug Target.*, 2010, **18**, 313.
353. D. Bruell, M. Stocker, M. Huhn, N. Redding, M. Kupper, P. Schumacher, A. Paetz, C. J. Bruns, H. J. Haisma, R. Fischer, R. Finnern and S. Barth, *Int. J. Oncol.*, 2003, **23**, 1179.
354. S. Kakimoto, T. Hamada, Y. Komatsu, M. Takagi, T. Tanabe, H. Azuma, S. Shinkai and T. Nagasaki, *Biomaterials*, 2009, **30**, 402.
355. A. K. Varkouhi, M. Scholte, G. Storm and H. J. Haisma, *J. Control. Release*, 2011, **151**, 220.
356. W. Robberecht and T. Philips, *Nat. Rev. Neurosci.*, 2013, **14**, 248.
357. R. U. Onyenwoke and J. E. Brenman, *J. Exp. Neurosci.*, 2015, **9**, 81.
358. R. W. Ledeen and G. Wu, *Trends Biochem. Sci.*, 2015, **40**, 407.
359. J. Holmgren, N. Lycke and C. Czerkinsky, *Vaccine*, 1993, **11**, 1179.
360. R. Schneerson, O. Barrera, A. Sutton and J. B. Robbins, *J. Exp. Med.*, 1980, **152**, 361.
361. D. F. Kelly, E. R. Moxon and A. J. Pollard, *Immunology*, 2004, **113**, 163.
362. M. E. Pichichero, *Hum. Vaccin. Immunother.*, 2013, **9**, 2505.
363. A. S. De Groot and D. W. Scott, *Trends Immunol.*, 2007, **28**, 482.
364. M. P. Baker, H. M. Reynolds, B. Lumicisi and C. J. Bryson, *Self Nonself*, 2010, **1**, 314.
365. C. Yanover, N. Jain, G. Pierce, T. E. Howard and Z. E. Sauna, *Nat. Biotechnol.*, 2011, **29**, 870.
366. M. T. Dertzbaugh and C. O. Elson, *Infect. Immun.*, 1993, **61**, 48.
367. M. Isaka, T. Komiya, M. Takahashi, Y. Yasuda, T. Taniguchi, Y. Zhao, K. Matano, H. Matsui, J.-i. Maeyama, K. Morokuma, K. Ohkuma, N. Goto and K. Tochikubo, *Vaccine*, 2004, **22**, 3061.
368. H. J. Kim, J.-K. Kim, S. B. Seo, H. J. Lee and H.-J. Kim, *Arch. Pharmacal Res.*, 2007, **30**, 366.
369. M. Vajdy and N. Y. Lycke, *Immunology*, 1992, **75**, 488.
370. M. Marinaro, H. F. Staats, T. Hiroi, R. J. Jackson, M. Coste, P. N. Boyaka, N. Okahashi, M. Yamamoto, H. Kiyono, H. Bluethmann, K. Fujihashi and J. R. McGhee, *J. Immunol.*, 1995, **155**, 4621.
371. K. Eriksson, M. Fredriksson, I. Nordström and J. Holmgren, *Infect. Immun.*, 2003, **71**, 1740.
372. T. G. Blanchard, N. Lycke, S. J. Czinn and J. G. Nedrud, *Immunology*, 1998, **94**, 22.

373. B. K. Sack and R. W. Herzog, *Curr. Opin. Mol. Ther.*, 2009, **11**, 493.
374. T. So, H. O. Ito, T. Koga, T. Ueda and T. Imoto, *Immunol. Lett.*, 1996, **49**, 91.
375. M. A. Croyle, N. Chirmule, Y. Zhang and J. M. Wilson, *J. Virol.*, 2001, **75**, 4792.
376. Q. Yang, S. W. Jones, C. L. Parker, W. C. Zamboni, J. E. Bear and S. K. Lai, *Mol. Pharm.*, 2014, **11**, 1250.
377. M. Ossevoort, B. M. J. Visser, D. J. M. van den Wollenberg, E. I. H. van der Voort, R. Offringa, C. J. M. Melief, R. E. M. Toes and R. C. Hoeben, *Gene Ther.*, 2003, **10**, 2020.
378. J. Vaya, E. Aizenshtein, S. Khatib, T. Gefen, M. Fassler, R. Musa, S. Krispel and J. Pitcovski, *Vaccine*, 2009, **27**, 6869.
379. M. S. Macauley, F. Pfrengle, C. Rademacher, C. M. Nycholat, A. J. Gale, A. von Drygalski and J. C. Paulson, *J. Clin. Invest.*, 2013, **123**, 3074.